LEABHARLANN CHOLÁISTE NA TRÍONÓIDE, BAILE ÁTHA CLIATH | TRINITY COLLEGE LIBRARY DUBLIN
Ollscoil Átha Cliath | The University of Dublin

Terms and Conditions of Use of Digitised Theses from Trinity College Library Dublin

Copyright statement

All material supplied by Trinity College Library is protected by copyright (under the Copyright and Related Rights Act, 2000 as amended) and other relevant Intellectual Property Rights. By accessing and using a Digitised Thesis from Trinity College Library you acknowledge that all Intellectual Property Rights in any Works supplied are the sole and exclusive property of the copyright and/or other IPR holder. Specific copyright holders may not be explicitly identified. Use of materials from other sources within a thesis should not be construed as a claim over them.

A non-exclusive, non-transferable licence is hereby granted to those using or reproducing, in whole or in part, the material for valid purposes, providing the copyright owners are acknowledged using the normal conventions. Where specific permission to use material is required, this is identified and such permission must be sought from the copyright holder or agency cited.

Liability statement

By using a Digitised Thesis, I accept that Trinity College Dublin bears no legal responsibility for the accuracy, legality or comprehensiveness of materials contained within the thesis, and that Trinity College Dublin accepts no liability for indirect, consequential, or incidental, damages or losses arising from use of the thesis for whatever reason. Information located in a thesis may be subject to specific use constraints, details of which may not be explicitly described. It is the responsibility of potential and actual users to be aware of such constraints and to abide by them. By making use of material from a digitised thesis, you accept these copyright and disclaimer provisions. Where it is brought to the attention of Trinity College Library that there may be a breach of copyright or other restraint, it is the policy to withdraw or take down access to a thesis while the issue is being resolved.

Access Agreement

By using a Digitised Thesis from Trinity College Library you are bound by the following Terms & Conditions. Please read them carefully.

I have read and I understand the following statement: All material supplied via a Digitised Thesis from Trinity College Library is protected by copyright and other intellectual property rights, and duplication or sale of all or part of any of a thesis is not permitted, except that material may be duplicated by you for your research use or for educational purposes in electronic or print form providing the copyright owners are acknowledged using the normal conventions. You must obtain permission for any other use. Electronic or print copies may not be offered, whether for sale or otherwise to anyone. This copy has been supplied on the understanding that it is copyright material and that no quotation from the thesis may be published without proper acknowledgement.

An Investigation of the Physiological and Pathological Role of Uncoupling Proteins

Lars Manzke
Dipl. Biol.



A thesis submitted to

Trinity College Dublin

For the degree
of
Doctor of Philosophy

Supervisor: Dr. Richard K. Porter
Energy Metabolism Group
Trinity Biomedical Sciences Institute
School of Biochemistry and Immunology
Trinity College Dublin
2012

TRINITY COLLEGE
2 4 MAY 2013
LIBRARY DUBLIN

Thesis 9825

Declaration of Authorship

I hereby declare and confirm that this thesis is entirely the result of my own work and has not been submitted anywhere else. I gratefully acknowledge supervision and guidance I have received from Dr. Richard K. Porter. The author gives permission for the library to lend or copy this thesis upon request.

Keep on going and the chances are you will stumble on something, perhaps when you are least expecting it. I have never heard of anyone stumbling on something sitting down.

- Charles F. Kettering -

Abstract

Uncoupling proteins (UCPs) are found in numerous different tissues and have been associated with many physiological and pathological conditions. After decades of research on uncoupling proteins, there is still only a modest understanding of how the uncoupling protein function is regulated. Furthermore, the functions of the "new" uncoupling proteins 2 and 3 are still unknown, although there is some evidence that they catalyze a proton leak similar to UCP1. The present work characterizes the role of uncoupling proteins 1, 2 and 3 in physiological and pathological models.

Firstly, I set out to determine the role of UCPs 1, 2 and 3 on T-cell profiles, in thymus and spleen of 6-8 week old mice. I was able to demonstrate that ablation of UCP1 increases frequencies of single positive CD4 cells and decreases frequencies of CD4 CD8 double positive cells in the thymus. In the spleen, UCP1 ablation results in an increase in frequencies of double positive CD4 CD8 cells and a decrease in frequencies of double negative CD4 CD8 cells. Ablation of UCP2 had no effect on T-cell profiles in thymus, spleen or lymph nodes whereas UCP3 ablation resulted in reduced frequencies of CD4 CD8 double positive cells, reduced frequencies of CD4 CD8 double negative cells and increased frequencies of CD4 single positive cells in thymus. UCP3 ablation also increased frequencies of CD8 single positive and reduced frequencies of CD4 CD8 double positive cells in spleen. Clearly, UCP1 and UCP3 play a role in T-cell maturation and selection.

Secondly, I set out to further investigate the role of UCP2 in the murine model of multiple sclerosis (experimental autoimmune encephalomyelitis, EAE), based on the fact that a single nucleotide polymorphism (G866A) in the promoter region of UCP2 increases susceptibility to multiple sclerosis and based on a previous report that UCP2 has a protective role in EAE. I found that UCP2 knock-out mice had a delayed onset of clinical symptoms. In addition, I saw no difference in the final stage severity of the condition, nor did I observe any differences in frequencies of infiltrating T-cells in the brain, lymph nodes and spleen, nor in cytokine profiles of lymph nodes and spleen.

Thirdly, as part of a project investigating the role of UCPs in regulating ROS production by mitochondria, I discovered increased glycerol-3-phosphate supported oxygen consumption in liver and kidney mitochondria isolated from UCP2 knock-out mice

compared to wild type controls. This increased oxygen consumption was due to increased glycerol-3-phosphate dehydrogenase abundance and enzyme complex specific activity. In support of these observations, a parallel project in our laboratory found increased glycerol-3-phosphate dehydrogenase activity and increased glycerol-3-phosphate supported oxygen consumption in BAT mitochondria of UCP1 knock-out animals compared to wild-type controls, and I was able to demonstrate that glycerol-3-phosphate dehydrogenase abundance was increased (publication in progress).

Furthermore, based on our previous report that MDMA leads to phosphorylation and activation of UCP3 in skeletal muscle mitochondria, I set out to investigate whether physiological conditions such as starvation and cold acclimation, which are known to increase UCP3 abundance, also affect UCP3 phosphorylation state and activity. I also did some preliminary work on determining whether noradrenaline administration (i.p.) affects UCP3 activity. The results indicate that neither noradrenaline administration nor the aforementioned physiological conditions result in UCP3 phosphorylation or UCP3 proton leak activity.

Lastly, I was able to demonstrate a reduction of oxygen consumption by resveratrol treatment and a moderate exercise regime in brown adipose tissue mitochondria. Moreover, resveratrol treatment increased the responsiveness to noradrenaline in mature BAT cells, while skeletal muscle oxygen consumption remained unchanged by resveratrol treatment or exercise on a cellular and on a mitochondrial level. The effects of resveratrol and exercise in BAT were not attributable to UCP1 abundance, but more work needs to be done to clarify the mechanism behind these observations.

Publications and Courses

Kieran J. Clarke, Alison E. Adams, **Lars H. Manzke**, Terry W. Pearson, Christoph H. Borchers, Richard K. Porter (2012) "A role for ubiquitinylation and the cytosolic proteasome in turnover of mitochondrial uncoupling protein 1 (UCP1)". Biochim Biophys Acta. 2012 Apr 16.

Kelly OM, McNamara YM, **Manzke LH**, Meegan MJ, Porter RK. (2011) "The preservation of in vivo phosphorylated and activated uncoupling protein 3 (UCP3) in isolated skeletal muscle mitochondria following administration of 3,4-methylenedioxymethamphetamine (MDMA aka ecstasy) to rats/mice". Mitochondrion. 2012 Jan;12(1):110-9. Epub 2011 Mar 29

Kieran J. Clark, **Lars H. Manzke**, Richard K. Porter (2012) "Reactive oxygen species production by forward and reverse electron flow in brown adipose tissue mitochondria" (in preparation)

Lars H. Manzke, Kieran J. Clark, Richard K. Porter (2012) "Knock-out of uncoupling protein 1 in BAT and uncoupling protein 2 in kidney and liver causes upregulation of mitochondrial glycerol-3-phopshate dehydrogenase" (in preparation)

Conferences

EBEC 2010 Poster presentation

Manzke, L.H. and R. K. Porter (2010). "Reduced cytotoxic CD8+ lymphocytes in heterozygous UCP2-KO mice in experimental autoimmune encephalomyelitis." Biochimica et Biophysica Acta (BBA) - Bioenergetics 1797, Supplement(0): 89.

EBEC 2012 Poster presentation

Manzke, L.H. and R. K. Porter (2012) "Upregulation of mitochondrial glycerol-3-phosphate dehydrogenase abundance in brown adipose tissue mitochondria from UCP1 knock-out mice" Biochimica et Biophysica Acta (BBA) – Bioenergetics 1817, Supplement

Courses

Successfully completed Graduate Course in Immunology in 2010

Successfully completed Oroboros Oxygraph-2k advanced course (MiP60) in 2010

Contents

Abstract i

Publications and Courses iii

Abbreviations ix

1 Introduction 1

1.1 General Introduction 1

1.2 The Mitochondrion 2

1.3 Oxidative Phosphorylation 4

1.4 Mitochondrial Glycerol-3-Phosphate Dehydrogenase (mGPDH) 6

1.5 Mitochondrial proton leak 9

1.6 Protein mediated proton leak 9

1.7 Uncoupling protein 1 10

1.7.1 Regulation of UCP1 11

1.7.2 Expression of UCP1 12

1.8 Uncoupling protein 2 13

1.9 Uncoupling protein 3 16

1.10 UCPs and Obesity 19

1.11 ROS and UCPs 19

1.12 Cold Acclimation 21

1.13 Noradrenaline signalling in brown adipose tissue cells and muscle fibres 22

1.14 Resveratrol 23

1.15 Changes in nutrition of mammals pre and post weaning 27

1.16 The Immune System 27

1.16.1 The innate immune system 29

1.16.2 The Adaptive immune system 31

1.16.3 Apoptosis in Thymus 33

1.16.4 Apoptosis in general 35

1.16.5 Multiple sclerosis and experimental autoimmune encephalomyelitis (EAE) 37

2 Materials and Methods 43
2.1 Materials 43
2.2 Animals 44
2.3 Wild Type (WT) and UCP1-/- (KO) mice 44
2.4 Wild Type (WT) and UCP2-/- (KO) mice 44
2.5 Wild Type (WT) and UCP3-/- (KO) mice 45
2.6 Isolation of genomic DNA for genotyping 45
2.7 PCR for genotyping of WT and UCP2-/- mice 45
2.8 PCR for genotyping of WT and UCP3-/- mice 47
2.9 Agarose gel DNA electrophoresis 48
2.10 Spectrophotometric quantification of nucleic acids 49
2.11 Nanodrop quantification of isolated DNA 49
2.12 Isolation of Brown Adipose Tissue mitochondria (BAT) 50
2.13 Isolation of Liver mitochondria 51
2.14 Isolation of Kidney mitochondria 52
2.15 Isolation of skeletal muscle mitochondria 53
2.16 Protection of phosphorylation state in isolated mitochondria 54
2.17 Mitochondrial protein determination using the Bicinchoninic Acid Assay 54
2.18 Sodium Dodecyl Sulphate Polyacrylamide Gel Electrophoresis (SDS-PAGE) 55
2.19 Western Blotting 56
2.20 Immunodetection of proteins 56
2.21 Calculation of free calcium concentration in assay buffer 57
2.22 Measurement of mitochondrial Oxygen consumption 58
2.23 Measurement of mitochondrial ROS generation 59
2.24 Complex II activity assay 60
2.25 Glycerol-3-phosphate dehydrogenase activity assay 61
2.26 Resveratrol treatment and exercise regime on rats 61
2.26.1 Animals 61
2.26.2 Drug and dosing regime 62
2.26.3 Exercise programme 62
2.26.4 Harvest of tissue samples 62
2.27 Isolation of mature brown adipose tissue cells 63
2.28 Isolation and seeding of intact muscle fibres 64

2.29 Measurement of cellular oxygen consumption in brown adipose tissue cells.....65
2.30 Measurement of oxygen consumption rate and extracellular acidification rate in intact muscle fibres.....65
2.31 Isolation of Thymocytes.....66
2.32 Isolation of Splenocytes.....66
2.33 Myelin oligodendrocyte glycoprotein induced Experimental Autoimmune Encephalomyelitis.....67
2.34 Cell Counting.....67
2.35 Mononuclear Cell Isolation from CNS Tissue.....68
2.36 In vivo Restimulation and FACS Analysis.....68
2.37 Stimulation of Spleen and Lymph Node Cells *Ex Vivo*.....69
2.38 Statistical analysis.....69
3 Effects of the absence of UCP1, 2 and 3 on the T-cell profile in murine thymus and spleen.....73
3.1 Introduction.....73
3.2 Results.....74
3.2.1 Effects of UCP1 ablation on T-cell subset composition in thymus and spleen.....74
3.2.2 No Effect of UCP2 ablation on T-cell subsets in thymus, spleen and inguinal lymph nodes.....77
3.2.3 No effect of UCP2 ablation on the apoptotic potential of thymocytes and splenocytes.....81
3.2.4 UCP3 ablation affects T-cell subsets in thymus and spleen.....86
3.3 Discussion.....89
4 UCP2 in Experimental Autoimmune Encephalomyelitis (EAE) – a murine model of Multiple Sclerosis (MS).....93
4.1 Introduction.....93
4.2 Experimental.....94
4.3 Results.....95
4.3.1 Time course of clinical symptoms and body weight in EAE.....95
4.3.2 FACS analysis of T-cell subsets in EAE mice 21 days post immunization.....97
4.3.3 T-cell subsets of WT and UCP2-/- mice in Experimental Autoimmune Encephalomyelitis.....99

4.3.4 IL-17 positive T-cells in brain, spleen and ILN of WT and UCP2-/- EAE mice 102
4.3.5 IFNγ positive T-cells in brain, spleen and ILN of WT and UCP2-/- mice in EAE . 106
4.3.6 IL-17 and IFNγ cytokine profile in EAE 110
4.4 Discussion 115
5 UCP2 bioenergetics 121
5.1 Introduction 121
5.2 Results 123
5.2.1 Increased abundance of mitochondrial glycerol-3-phosphate dehydrogenase in brown adipose tissue mitochondria of UCP1-/- mice 123
5.2.2 Increased Glycerol-3-phosphate supported oxygen consumption in liver and kidney mitochondria of UCP2-/- mice 126
5.2.3 Increased mitochondrial glycerol-3-phosphate dehydrogenase specific activity in liver and kidney mitochondria of UCP2-/- mice 131
5.2.4 Increased mGPDH expression in liver and kidney mitochondria of UCP2 ablated mice 134
5.2.5 No effect of UCP2 ablation on ROS production by liver and kidney mitochondria 138
5.3 Discussion 143
6 UCP3 bioenergetics 151
6.1 Introduction 151
6.2 Results 153
6.2.1 No effect of Noradrenaline treatment on SKM mitochondria 153
6.2.2 Effects of short term starvation on SKM mitochondria 155
6.2.3 Effects of cold acclimation on SKM and BAT mitochondria in WT and UCP1-KO mice 161
6.3 Discussion 167
7 Resveratrol and Exercise 175
7.1 Introduction 175
7.2 Results 176
7.2.1 Effects of Resveratrol and Exercise on BAT cell oxygen consumption 176
7.2.2 Resveratrol and Exercise do not affect skeletal muscle fibre oxygen consumption and extracellular acidification 179

7.2.3 Effects of Resveratrol and Exercise on oxygen consumption in BAT and SKM mitochondria 184

7.2.4 Resveratrol treatment or Exercise do not affect UCP1 expression in BAT or UCP3 expression in SKM mitochondria 188

7.3 Discussion 191

8 General Discussion 197

9 Future work 209

Acknowledgements 210

10 References I

A. Appendix I

Abbreviations

aCD3 – anti CD3 antibody

ADP - Adenosine 5′-diphosphate

AMP – Adenosine 5′-monophosphate

AMPK – AMP-kinase

BAT – brown adipose tissue

bp – base pairs

cAMP – 3'-5'-cyclic Adenosine monophosphate

CD – Cluster of Differentiation

CFA – Complete Freund's Adjuvant

cGPDH – cytosolic Glycerol-3-phosphate dehydrogenase

DC – Dendritic Cell

DCPIP – Dichlorophenolindophenol

DNP – Dinitrophenol

EAE – Experimental Autoimmune Encephalomyelitis

EtBr – Ethidium Bromide

ETC – electron transport chain

EtOH – Ethanol

FACS – Fluorescence Assisted Cell Sorting

FCCP – Carbonyl cyanide 4-(trifluoromethoxy)phenylhydrazone

GAPDH – Glyceraldehyde-3-phopshate dehydrogenase

GDP – Guanosine 5′-diphosphate

G3P – Glycerol-3-Phosphate

IFNγ – Interferon gamma

IGF-1 – Insulin-like growth factor 1

IGFBP-1 – Insulin-like growth factor-binding protein 1

IL-17 – Interleukin 17

ILN – Inguinal Lymph Nodes

IMS – inter membrane space

KCl – Potassium Chloride

KHE – KCl , HEPES, EGTA (mitochondrial respiration buffer)

MetOH – Methanol

mGPDH – mitochondrial Glycerol-3-phosphate dehydrogenase

MilliQ – MilliQ water purification system

MS – Multiple Sclerosis

NST – non-shivering thermogenesis

O_2 – Dioxide

OxPhos – Oxidative Phosphorylation

PGC-1α – peroxisome proliferator-activated receptor coactivator 1α

PI – Phosphatase inhibitors

P_i – inorganic phosphate

PMA - Phorbol mysteric acid

PMF – proton motive force

PMN – polymorphonuclear leukocytes

PT – Pertussis toxin

RORγt – retinoic acid-related orphan receptor gamma t

ROS – Reactive Oxygen Species

RT-PCR – Reverse Transcriptase Polymerase Chain Reaction

SDS – Sodium Dodecyl Sulfate

SEM – Standard Error Means

SKM – Skeletal muscle

STE – Sucrose, Tris, EGTA (mitochondrial isolation buffer)

TAE – Tris-Acetate EDTA buffer

UCP – Uncoupling Protein

$\gamma\delta$ – T-Cells expressing Gamma Delta T-cell receptor chains

General Introduction

Chapter 1

1 Introduction

1.1 General Introduction

Obesity and resulting subsequent diseases are one of the biggest plagues of the industrialised world and an ever increasing threat to the health and quality of life of millions of people. Unlimited food availability and a more resident life style are probably two of the main reasons for this significant increase in overweight or obese people in the western world. A better understanding of the underlying metabolic mechanisms and their regulation and, more importantly, the identification of potential targets for treatments are crucial. One very promising direction of research is naturally occurring thermogenesis and the regulation thereof used by endotherms to maintain a relatively constant core body temperature between 35°C and 40°C. During the last centuries, heating became more available and affordable and therefore less energy needs to be used for thermogenesis nowadays. Nonetheless a significant part of the resting metabolic rate in humans is used to maintain a core body temperature of 37°C which is metabolically very costly (Arciero *et al.* 1993; McCrady-Spitzer *et al.* 2012). About two thirds of the resting metabolic rate is used to maintain a constant temperature, while one third accounts for maintenance of cellular integrity, ionic gradients and protein turnover among others (Landsberg *et al.* 2009). The resting metabolic rate of an average man amounts to roughly 1700 kcal/day (Arciero *et al.* 1993), which represents 60-75% of the total daily energy expenditure, but the resting metabolic rate can vary between individuals by 600kcal/day. Mild cold exposure can increase the daily energy expenditure. While human metabolism slows down slightly during sleep, many endothermic animals even enter a controlled state of hypothermia, called hibernation. The concept of hibernation impressively demonstrates that it is more economical to reduce body temperature for a certain amount of time before heating it up to 37°C again, sometimes several times in one winter. The amount of energy that goes into the heating process after a hibernation bout is substantial, but obviously still more efficient for these animals than to constantly keep the body temperature up. If it was possible to identify and specifically control these mechanisms in the human body, obesity and its related problems could be treated much more effectively than presently possible.

Mitochondria are at the centre of aerobic metabolism and thus promising targets for the development of new treatments. But not only are mitochondria at the centre of interest in mammalian metabolism, they are also implicated in various diseases, including autoimmune diseases, as will be discussed in this chapter. In the following sections, some of the many functions of mitochondria will be illustrated.

1.2 The Mitochondrion

In eukaryotic cells mitochondria (singular mitochondrion) carry out many different tasks and are vital for survival in an aerobic environment. Mitochondria appear as small organelles (0.5-1.0 μm in diameter) with a double membrane when looked at in two dimensions. Recent three-dimensional analyses (Plecita-Hlavata *et al.* 2008) show that mitochondria are in fact continuous columnar intracellular structures (Figure 1-1B and C). They are the major energy transducing site within the cell where many metabolic activities such as oxidative phosphorylation, citrate-cycle, fatty acid β-oxidation, synthesis and degradation of amino acids (urea cycle) as well as syntheses of iron-sulphur clusters and haemes take place. Furthermore, mitochondria are essential for tight control of the redox system, calcium homeostasis, controlled cell death (apoptosis) and the transformation of food derived compounds into utilizable cellular energy as Adenosine-triphosphate (ATP). However, mitochondria in different tissues perform different jobs, resembling the high importance and flexibility of this organelle. Altogether, mitochondria are indispensable for homeostasis of the cell.

According to the endosymbiotic theory proposed by Mereschkowsky in 1905 (Martin *et al.* 1999) mitochondria were bacteria endocytosed into bigger eukaryotic cells to coexist in symbiosis. This is why mitochondria possess an outer, permeable membrane left over from the endocytosis and a semi-permeable inner membrane enclosing the mitochondrial matrix which holds soluble enzymes, the genetic machinery, nucleotide cofactors, inorganic ions and substrates. Both membranes are divided by the intermembrane space which is one of two mitochondrial compartments with the matrix being the other. To significantly increase the membrane surface area the inner membrane

is folded into cristae and packed with proteins and enzymes for all the different mitochondrial functions (Figure 1-1A).

This specific structuring is the basis for the mitochondria's primary function, the conversion of substrates into utilizable energy by generation of ATP for the cell. Furthermore a phenomenon not entirely understood is the constant shift in morphology through fusion and fission with emerging evidence of importance in almost all mitochondrial functions (Okamoto *et al.* 2005).

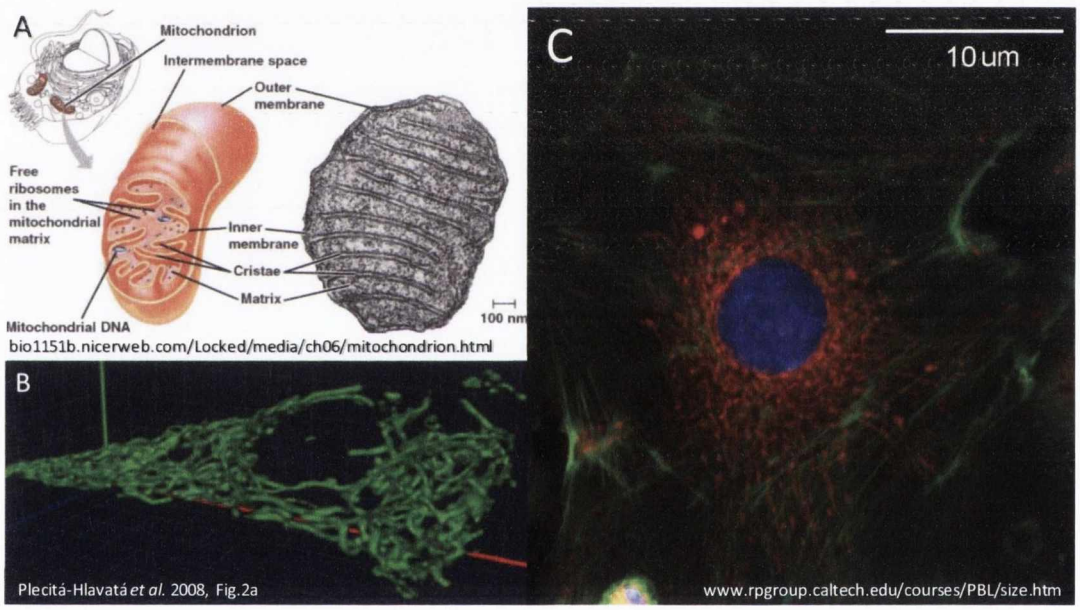


Figure 1-1: Visualization of mitochondrial structure

(A) Schematic of a mitochondrion on the left and a 2D electron microscopic picture of a mitochondrion on the right. (B) 4Pi imaging of a 3D mitochondrial network in mRoGFP-transfected INS-1E cells. (C) 2D bovine pulmonary cells illustrating actin-TRITC (green), mitochondria-FITC (red) and nucleus-DAPI (blue) fluorescence.

1.3 Oxidative Phosphorylation

The unique structure of mitochondrial compartments enables mitochondria to supply the cell with utilizable energy in the form of ATP. The synthesis of ATP from ADP and inorganic phosphate (P_i) predominantly occurs across and within the mitochondrial inner membrane in a process termed oxidative phosphorylation. The energy released by oxidation of nutrients is used to generate an electrochemical gradient across the inner mitochondrial membrane to drive the synthesis of ATP by a complex metabolic pathway. This electrochemical gradient, also known as proton motive force (PMF) consists of a potential difference and a pH-gradient (Brand 1995). In oxidative phosphorylation electrons from reduction equivalents $NADH+H^+$ and $FADH_2$ are transferred to the electron transport chain (ETC) of the respiratory chain and follow a redox potential along the ETC and pass through all complexes of the respiratory chain until they are finally transferred to molecular oxygen which is reduced to water. By following the potential along the respiratory chain protons are pumped from the matrix to the inter membrane space (IMS) by complexes I, III and IV which generates the PMF. The conserved energy in the PMF is then used by F_1F_0-ATP-synthase to add P_i to ADP and form ATP while protons are flowing back into the mitochondrial matrix dissipating the membrane potential (Stock *et al.* 2000). This relation was proposed by Mitchell in 1967 (Mitchell *et al.* 1967) in his chemiosmotic model and summarizes the very complex biochemical reactions. The schematic in Figure 1-2 illustrates this (adapted from Oelkrug *et al.* 2010). Electrons of NADH-linked substrates are donated to NADH-Q oxidoreductase (complex I) while further electron entry sites are the succinate dehydrogenase (complex II) and FAD-linked glycerol-3-phosphate dehydrogenase (mGPDH) as well as the electron transfer flavoprotein (ETF) which is fuelled by β-oxidation respectively. NADH produced in β-oxidation enters through complex I as well. From the entry complexes the electrons are transferred to ubiquinone (Q) which is reduced to QH_2. From here the electrons are usually transferred to Q-cytochrome c oxidoreductase (complex III) before finally reducing oxygen (½ O_2) to water at cytochrome c oxidase (complex IV). This flow of events is generally regarded as forward electron transfer to generate the membrane potential to drive ATP synthesis at the F_1F_0-ATP-synthase (also referred to as complex V). The membrane potential may also be dissipated by UCPs (UCP1 in Figure 1-2). UCP1 is activated by free fatty acids (FFA) and inhibitable by purine nucleotides (Guanosine

diphosphate, GDP). However, some electrons may leak back specifically at the I_F and I_Q sites of complex I to form reactive oxygen species (ROS) like superoxide (O_2^-), indicated with stars in the figure. This phenomenon is known as reverse electron flow. The mGPDH and ETF are regarded to be potent ROS producers as well. When the electron flow through complex I is blocked with Rotenone, ROS production is significantly increased with complex I substrates because the I_F site of complex becomes more reduced and transfer of electrons to molecular oxygen is more likely. However, in the presence of substrates that provide electrons directly to the ubiquinone pool, Rotenone significantly reduces ROS production.

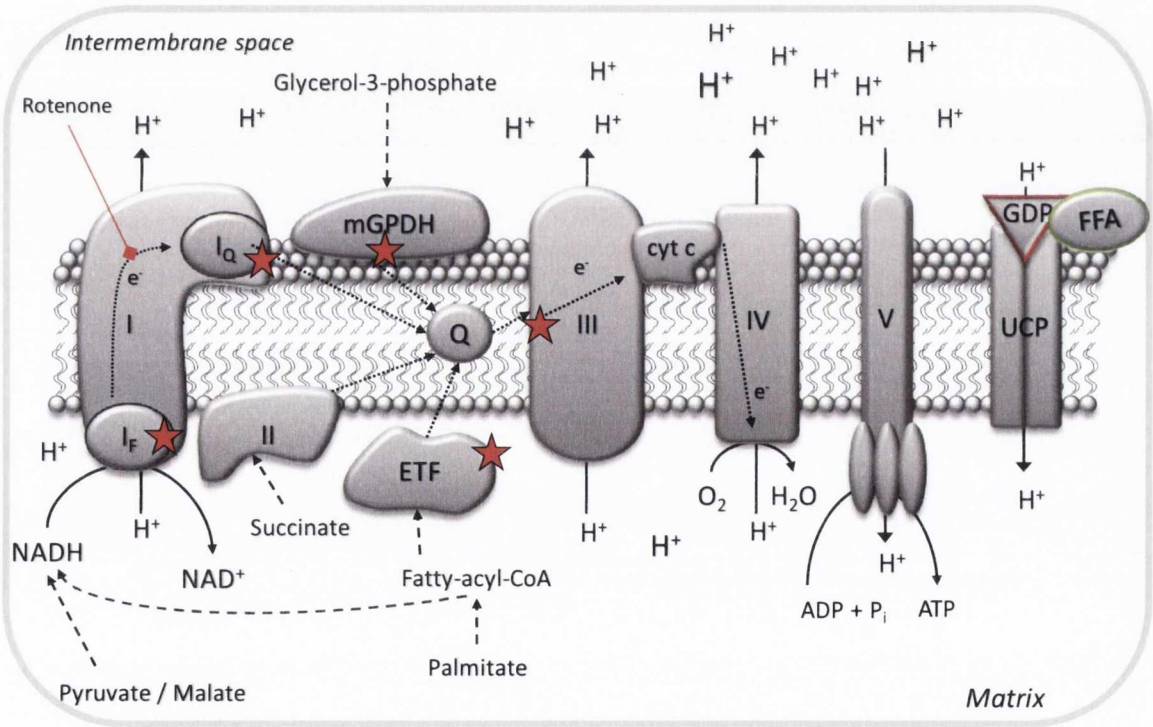


Figure 1-2: Sites of substrate entry and ROS production in the respiratory chain in BAT mitochondria.

Dashed arrows indicate substrate entry to the respiratory chain complexes (roman numerals I, II, III, IV and V), dotted arrows show electron flow and straight solid arrows indicate proton flow. Adapted from (Oelkrug *et al.* 2010).

1.4 Mitochondrial Glycerol-3-Phosphate Dehydrogenase (mGPDH)

The mitochondrial glycerol-3-phosphate dehydrogenase (mGPDH) is located on the outer side of the inner mitochondrial membrane with a molecular weight of about 81kDa. It is part of the glycerol-3-phosphate shuttle (Figure 1-3) together with the NAD-dependent cytosolic glycerol-3-phosphate dehydrogenase (cGPDH) to make cytosolic NADH available for mitochondrial oxidative phosphorylation. NADH generated in glycolysis is oxidised to NAD^+ while dihydroxyacetone phosphate is reduced to glycerol-3-phosphate by cGPDH. Glycerol-3-phosphate (G3P) is then oxidised to dihydroxyacetone phosphate by FAD-linked mGPDH and two electrons from the reduction of $FADH_2$ to FAD^+ are transferred to co-enzyme Q (Klingenberg 1970; Garrib *et al.* 1986). This shuttle therefore catalyses the interconversion of dihydroxyacetone phosphate and glycerol-3-phosphate with the net oxidation of cytosolic NADH and connects glycolysis with the mitochondrial respiratory chain for rapid ATP generation under aerobic conditions (Estabrook *et al.* 1958; Klingenberg *et al.* 1961). The glycerol-3-phosphate shuttle circumvents complex I and electrons enter the respiratory chain via ubiquinone, so only complex III and complex IV can pump protons across the inner mitochondrial membrane. It is important to note that the efficiency of ATP generation is lower in the glycerol-3-phosphate shuttle pathway than when reducing equivalents enter the respiratory chain at complex I, and hence only 2 ATPs are generated per atom of oxygen or per pair of electrons instead of 3 ATPs (Dawson 1979). Because this system provides a means of fast ATP production from glycolytic reduction equivalents it is not surprising that expression of mGPDH is highest in tissues of sudden high ATP demand such as the flight muscle or sperm cells, but also in thermogenic tissues like BAT. Accordingly, mGPDH expression is highest in BAT followed by skeletal muscle, brain, kidney and liver in mice (Koza *et al.* 1996).

The expression of mGPDH is also dramatically increased by 3,3'5'-tri-iodothyronine (T3) in heart, kidney and liver mitochondria (Dummler *et al.* 1996). The upregulation of mGPDH following treatment with T3 was confirmed in liver mitochondria. However, succinate dehydrogenase activity and expression were also significantly increased by T3 while other respiratory chain complex activities and expression levels remained unchanged (Mracek *et al.* 2005). Expression and activity of mGPDH peaked 24h after T3

application, but during the following 24h-72h past T3 treatment the specific activity fell by 30%. It was proposed that the significant increase in mGPDH activity and expression is due to de novo synthesis rather than kinetic activation of mGPDH (Mracek *et al.* 2005).

Furthermore, the glycerol-3-phosphate shuttle has been proposed to be involved in a thermogenic cycle to generate heat and regulate body weight (Lardy *et al.* 1990; DosSantos *et al.* 2003) due to the "waste" of energy by inserting electrons to the respiratory chain at ubiquinone instead of complex I. In support of a thermogenic function UCP1-/- mice showed 50% increased mGPDH activity in interscapular BAT mitochondria compared to WT controls (Hofmann *et al.* 2001) and even more intriguingly mGPDH expression is increased in BAT mitochondria of WT animals in response to cold acclimation (Koza *et al.* 1996). Interestingly, mGPDH ablated mice display normal cold acclimation and show unaffected body temperature elevation after treatment with thyroid hormone (Brown *et al.* 2002). However, mGPDH knock-out mice had a reduced body mass index and showed a reduction in white adipose tissue mass.

Another theory (Alfadda *et al.* 2004) predicted that knock-out of mGPDH would lead to changes in the NADH/NAD^+ ratio and hence affect glucose metabolism, because recycling of cytosolic NAD^+ by the glycerol-3-phosphate shuttle was disrupted. However, NADH/NAD^+ ratios were not affected by to mGPDH knock-out and the authors concluded that this was probably due to a redundancy between the various shuttles (e.g. the malate-aspartate shuttle).

Besides functioning in the glycerol-3-phosphate shuttle, cGPDH has other functions, like formation of glycerol-3-phosphate for triacylglycerol synthesis, and is widely expressed in almost all tissues. The mGPDH on the other hand is expressed in high amounts in BAT, muscle, placenta, testes, pancreatic islets, brain, fibroblasts and amniocytes, and in lower levels in kidney and liver (Houstek *et al.* 1975; MacDonald 1981; Chretien *et al.* 1994; Koza *et al.* 1996; MacDonald *et al.* 1996; Jung *et al.* 1997; Scholz *et al.* 1997; Chowdhury *et al.* 2000; Honzik *et al.* 2006). This selective expression pattern suggests that the glycerol-3-phosphate shuttle is not needed equally between tissues.

A significant percentage of mitochondrial ROS production is due to mGPDH (Grivennikova *et al.* 2010). In brain mitochondria respiring on glycerol-3-phosphate, ROS production by mGPDH increased in the presence of increasing amounts of calcium

(Tretter *et al.* 2007). The mGPDH possesses a calmodulin-like Ca^{2+} binding site which lowers the K_m for glycerol-3-phosphate and therefore increases the activity of the enzyme (Rutter *et al.* 1992; Idahl *et al.* 1995).

Glycolytic prostate cancer cell lines showed increased expression of mGPDH and antioxidant enzymes (Chowdhury *et al.* 2005). This suggests that the mGPDH is up-regulated due to a highly glycolytic environment, which contributes to the overall increase in ROS generation.

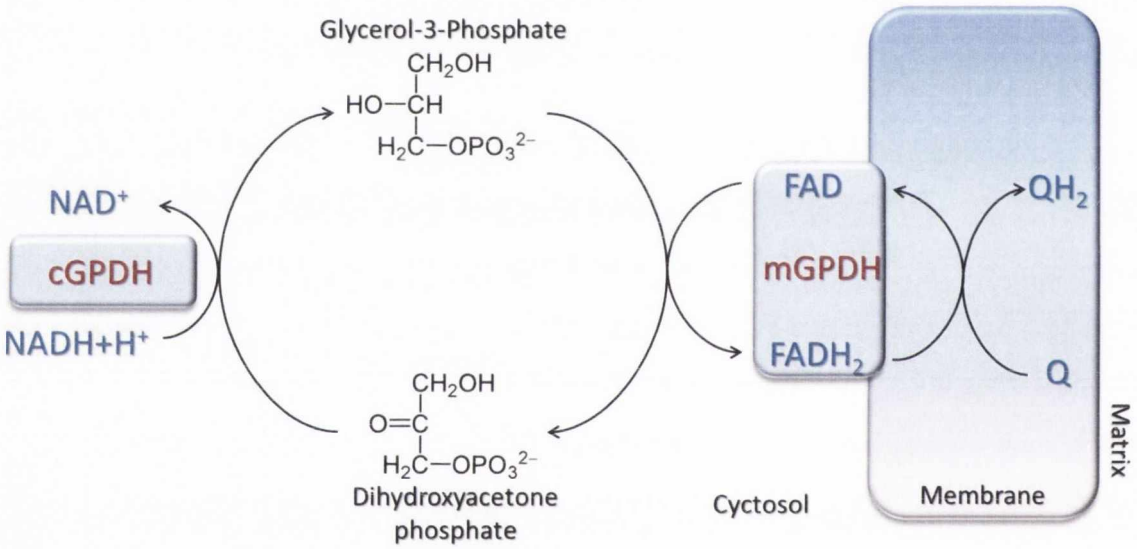


Figure 1-3: Glycerol-3-phosphate shuttle.

Schematic of the glycerol-3-phosphate shuttle. Enzymes are illustrated in red and reduction equivalents and ubiquinone (Q) in blue.

1.5 Mitochondrial proton leak

The re-entry of protons to the mitochondrial matrix through the inner mitochondrial membrane by means other than the ATP synthase is termed proton leak (Nicholls 1974). Oxidative phosphorylation is therefore never fully coupled in either isolated mitochondria or mitochondria *in situ* (Brand *et al.* 1994). In fact the substantial amount of 20 to 25% of the basal metabolic rate in rats are due to proton leak (Rolfe *et al.* 1999) with the ATP synthase not working due to inhibition with Oligomycin or absence of ADP (Brand 1977). When ATP is synthesized (state 3 respiration) the proton leak is lowest, and maximal when ATP synthase is not producing ATP (State 4 respiration) (Brown *et al.* 1986; Nicholls *et al.* 1989; Porter *et al.* 1998).

1.6 Protein mediated proton leak

Uncoupling proteins (UCPs) are about 32kDa in mass and are members of the mitochondrial anion-transporter superfamily located in the mitochondrial inner membrane. They consist of about 300 amino acids organized in six transmembrane α-helices in a tripartite structure with the C- and N-termini reaching into the intermembrane space and thereby into the cytosolic side of the inner mitochondrial membrane. Very recently the crystallographic determination of the three-dimensional structure of UCP2 was successful and confirmed predictions from sequence homology modelling experiments with the Adenine Nucleotide Carrier (ANT1). These show UCPs in the mentioned tripartite structure with two hydrophobic transmembrane helices connected by a hydrophilic loop on the matrix side of the inner mitochondrial membrane (Pebay-Peyroula *et al.* 2003).

The three UCPs 1, 2 and 3 together with plant-UCP represent the core of the uncoupling protein family (Laloi *et al.* 1997). Furthermore, UCP4 and UCP5 (also known as BMCP, brain-mitochondrial-carrier-protein) were considered to be members of the family of uncoupling proteins in earlier days (Sanchis *et al.* 1998; Mao *et al.* 1999). However, more recent studies do not include them anymore but rather suggest they are precursors to uncoupling proteins 1,2 and 3 today (Hanak *et al.* 2001).

The ability to uncouple the respiratory chain from ATP synthesis has been demonstrated in proteoliposomes, but the *in vivo* function remains elusive and is not yet fully understood. Two main hypotheses are presently under discussion. One describes UCP3 as a transporter of free fatty acids or fatty acid anions out of the matrix to reduce the accumulation to toxic levels (Hesselink *et al.* 2005). The second hypothesis suggests the protection from generation of harmful oxygen radicals with a negative correlation between mitochondrial uncoupling and oxidative damage (Skulachev 1998). The term "mild uncoupling" is introduced here, describing the controlled reduction of membrane potential through a UCP mediated proton leak (Papa *et al.* 1997). By reducing the membrane potential the redox state of reduction equivalents is altered and the probability of a transfer of electrons to oxygen reduced.

1.7 Uncoupling protein 1

The first uncoupling protein (UCP1) was discovered in brown adipose tissue (BAT) while researching non-shivering thermogenesis (NST). It was then called thermogenin, because of its ability to generate heat. Since its discovery in the 1970s (Heaton *et al.* 1978) several homologues were identified in 1997 which led to the renaming of thermogenin to UCP1 (Fleury *et al.* 1997). The mechanism of NST allows human neonates, small mammals and rodents to defend their body temperature against acute cold exposure without muscle shivering. In brown adipose tissue cells, the major source of NST, mitochondria are clustered in high density and abundantly express UCP1 as mitochondrial membrane protein with up to 60µg/mg in cold-adapted rodents (Stuart *et al.* 2001). Upon activation, UCP1 reduces the membrane potential by catalysing the back flux of protons from the intermembrane space (IMS) through the inner mitochondrial membrane to the mitochondrial matrix and thereby uncoupling ATP-synthase from the respiratory chain. The energy from substrate oxidation that is conserved in the proton gradient is not fixed chemically as ATP but dissipated as heat. In the western lifestyle where heating is readily available, thermogenesis is less important compared to the situation in earlier days where a significant amount of energy was used to generate heat. The fact that humans in the industrialised world need less energy for thermogenesis may also have contributed to the increasing problem of overweight and obesity.

In 1985 UCP1 was cloned and its uncoupling function could be confirmed in yeast and proteoliposomes (Klingenberg *et al.* 1985; Stuart *et al.* 2001).

1.7.1 Regulation of UCP1

The exact molecular mechanisms of UCP functions are still a matter of discussion even after 30 years of research. Most is known about UCP1 in BAT which is activated by noradrenaline after cold acclimation or acute excess food intake ("overeating") (Ricquier *et al.* 1986). Noradrenaline activates UCP1 in BAT by a signal through the β3-adrenergic receptor, but triggers other pathways through α1- and α2-adrenergic receptors too (Cannon *et al.* 2004).

Two models are currently proposed for the activation of UCP1 by free fatty acids. This phenomenon has been studied extensively, but the molecular mechanism remains unresolved. The first model suggests a role of fatty acids as cofactors for the direct transport of protons by UCP1 along its aqueous channel (Winkler *et al.* 1994). Fatty acids would collocate within this channel and catalyse the transport of protons along their acidic moieties through the membrane and into the mitochondrial matrix. So far, no such binding sites have been identified, but replacement of two histidines (His 145 and His 147) cause a loss of proton transport (Bienengraeber *et al.* 1998). The second model proposes fatty acids to be protonophores in themselves and that UCP1 does not directly catalyse the transport of protons but rather cycles fatty acid anion head groups back out of the matrix. Protonated fatty acids would spontaneously flip-flop across the inner mitochondrial membrane, be deprotonated and actively transported back out by UCP1 (Garlid *et al.* 1996) driven by the high negative membrane potential inside the mitochondria.

Purine nucleotides have been reported to bind and inhibit UCP1 activity (Nicholls 1974). The binding of nucleotides is one of the main characteristics of UCP1 and was crucial for the identification and isolation of this protein (Heaton *et al.* 1978). Purine nucleotide binding sites were identified on the outer leaflet of UCP1 (Ledesma *et al.* 2002). Therefore nucleotides can only bind to the cytosolic side of UCP1 (Klingenberg *et al.* 1999), unlike fatty acid interaction with UCP1 which remains largely unknown. UCP1 is

thought to function as a dimer, and only one nucleotide can bind per dimer (Klingenberg 1984; Klingenberg *et al.* 1999). Only purine ribose di- and trinucleotides (GDP and ADP, GTP and ATP) are bound with strong preference whereas the monophosphate nucleotides AMP and GMP are poor ligands. Moreover, only free nucleotides bind to and inhibit UCP1, but not Mg^{2+} chelates (Klingenberg 1988). The binding of purine and pyrimidine nucleotides is pH dependent with raised affinity at a pH above 7.2 (Klingenberg *et al.* 1999).

BAT mitochondria of normothermic and otherwise untreated animals are usually coupled due to low free fatty acid concentration and inhibition of UCP1 by high concentrations of ATP. Upon activation of UCP1 by fatty acid stimulation, endogenous ATP is depleted and bound ATP released. Together with higher amounts of free fatty acids this leads to UCP1 catalysed proton transport, i.e. uncoupling. Furthermore, UCP1 is serine-phosphorylated following cold acclimation which increases its activity (Carroll *et al.* 2008).

Recently, our laboratory demonstrated that the cytoplasmic proteasome is required for ubiquitinylation and degradation of UCP1 in BAT and thymus mitochondria and that the half-life of UCP1 *in vitro* in an ubiquitin conjugating–proteasome degradation system corresponds to the degradation rate of UCP1 *in vivo* (i.e. 30-72h in brown adipose tissue and 3h in thymus). In addition, we demonstrated that degradation of UCP1 is inhibited by the proteasome inhibitor MG132 and that dissipation of the mitochondrial membrane potential inhibits degradation of UCP1. There also appears to be a greater amount of ubiquitinylated UCP1 associated with BAT mitochondria from cold-acclimated animals (Clarke *et al.* 2012).

1.7.2 Expression of UCP1

UCP1 was long thought to be exclusively expressed in BAT, but various reports of UCP1 expression in other tissues have been made. Several publications demonstrated expression of UCP1 in white adipose tissue (WAT) (Garruti *et al.* 1992; Commins *et al.* 1999; Koza *et al.* 2000), but it has been suggested that BAT depots can sporadically occur in WAT and that UCP1 is therefore not expressed in WAT itself (Cannon *et al.* 2004). More

recent studies by our laboratory could prove the presence of UCP1 mRNA and protein in mitochondria of thymus cells (thymocytes) (Carroll *et al.* 2004a; Adams *et al.* 2008a). UCP1 expression in the murine thymus is age related and declines rapidly three weeks after birth which coincides with the weaning process. Ablation of UCP1 resulted in decreased apoptotic potential in thymocytes and UCP1-/- mice showed increased frequencies of CD4 CD8 double positive T-cells in the periphery (spleen), indicating a major impact of UCP1 absence on thymic T-cell selection (Adams *et al.* 2010). Moreover, UCP1 has recently also been detected in the skin (Mori *et al.* 2008). The relevance of UCP1 for human metabolism and non-shivering thermogenesis has been questioned for years since it was thought that functional BAT with UCP1 expression was only present in neonates, but not mature humans. The presence of interscapular active BAT in adult humans was demonstrated recently which confirmed BAT and UCP1 as a promising target for treatment of metabolic conditions in humans (Cypess *et al.* 2009).

1.8 Uncoupling protein 2

Uncoupling protein 2 (UCP2) mRNA is found ubiquitously in vertebrates and UCP2 protein is detected in a few cell types and tissues including thymus, spleen, lung, stomach, intestine, brain and white adipose tissue, a variety of innate immune cells (macrophages and NK cells) and pancreatic β-cells (Arsenijevic *et al.* 2000; Krauss *et al.* 2002). It shares 59% sequence identity with UCP1 and is found mainly in parts of the immune system (Fleury *et al.* 1997; Gimeno *et al.* 1997; Pecqueur *et al.* 2001). It is thought that UCP2 protein detection in many tissues is due to UCP2 expression not in parenchymal cells, but in resident or invading macrophages or macrophage homologues. One example is UCP2 protein detection in rat liver, where UCP2 is expressed in specialised resident macrophages (Kupffer cells), but not in parenchymal liver cells (Larrouy *et al.* 1997). Because of its location it is assumed that UCP2 does not play a role in thermogenesis, as was confirmed in loss of function studies, where UCP2 ablated mice were able to defend their body temperature and did not show alterations in body weight and composition in the cold. The short half-life of less than 1h (Rousset *et al.* 2007; Azzu *et al.* 2008; Giardina *et al.* 2008), combined with a tight posttranslational control of protein synthesis indicates the relevance of UCP2 in mitochondrial and cellular function

(Pecqueur *et al.* 2001; Hurtaud *et al.* 2006). It is important to keep in mind that expression levels of UCP2 protein can be up to 1000-fold less compared to UCP1 in BAT (Pecqueur *et al.* 2001). As a result, proton conductance or substrate transport, whatever the function of UCP2 may be, is expected to be much lower as well compared to UCP1 in BAT. The three-dimensional structure of UCP2 (see Figure 1-4A and B) as the first of the uncoupling proteins, has very recently been resolved by NMR molecular fragment searching (Berardi *et al.* 2011) after discussing potential structural models generated from sequence homologies with the close relative protein adenine nucleotide translocase (ANT) for decades.

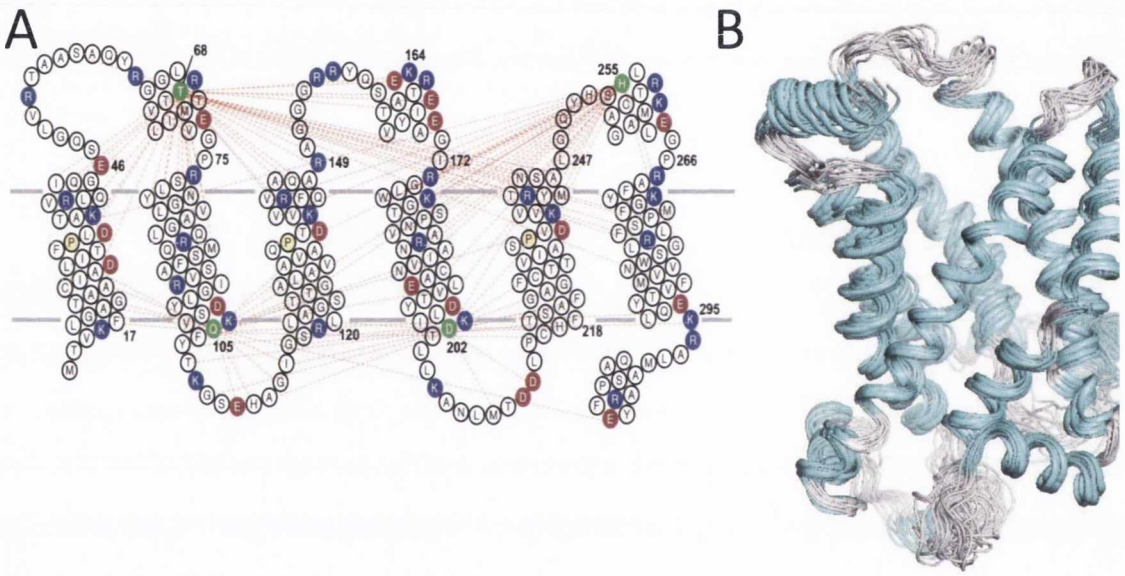


Figure 1-4: Structure of UCP2

(A) UCP2 sequence and membrane topology showing basic (blue) and acidic (red) residues, conserved prolines (green) and proline links (yellow). (B) An ensemble of 15 low-energy structures derived from NMR restraints. Taken from Berardi *et al.* 2011

Currently, one of the best understood functions of UCP2 is control of glucose stimulated insulin secretion (GSIS) in pancreatic β-cells. In contrast to "normal" cells which rigorously regulate substrate uptake, pancreatic β-cells use the substrate supply to regulate ATP production and the cytosolic ADP/ATP ratio. UCP2 has been shown to significantly change the membrane potential and therefore the ADP/ATP ratio. Hence, UCP2 controls depolarization of the cellular membrane leading to recruitment of GLUT1

(human) and GLUT2 (rodents) glucose transporters and subsequent insulin secretion (GSIS).

Another proposed function of UCP2 is the control of mitochondrial ROS production (Negre-Salvayre *et al.* 1997a; Arsenijevic *et al.* 2000). Macrophage function was impressively affected by UCP2 knock-out as it allowed UCP2-/- macrophages to clear infections of *Toxoplasma gondii* and *Salmonella typhimurium* more effectively than their WT counterparts probably due to a higher oxidative burst (Arsenijevic *et al.* 2000). When stimulated with LPS, UCP2 deficiency promoted the expression of inducible NO synthase, nitric oxide and ROS production as well as the release of proinflammatory cytokines from macrophages. (Kizaki *et al.* 2002; Emre *et al.* 2007b). Toll-like-receptor (TLR) 4-induced ROS signalling in primary cultures of macrophages introduced UCP2 as a key player in macrophage activation, as stimulation with LPS leads to rapid downregulation of UCP2 by JNK and p38 pathways. This resulted in increased ROS production and therefore a feedback loop to further activation of p38 and ERK pathways (Emre *et al.* 2007b) which clearly shows the importance of UCP2 regulation in ROS-inducible MAPK signalling during macrophage activation. In addition, higher mitochondrial ROS production enhanced NF-κB activation in spleen of LPS-treated UCP2-/- mice (Bai *et al.* 2005).

The single nucleotide polymorphism 866G/A in the human UCP2 promoter region has been associated with a variety of autoimmune diseases. UCP2 expression is reduced in lymphocytes and macrophages of individuals with the G allele compared to individuals with the A allele. The G allele is also associated with increased susceptibility to multiple sclerosis (Vogler *et al.* 2005). Moreover, the 866G/A polymorphism has been linked to a variety of autoimmune and several other inflammatory diseases (Emre *et al.* 2010). In particular, UCP2-/- mice developed higher disease scores in experimental autoimmune encephalomyelitis (EAE) and showed accelerated development of diabetes mellitus type 1 after multiple low-dose injections with streptozotocin compared to their WT counterparts (Vogler *et al.* 2006; Emre *et al.* 2007a). UCP2 also influences cytokine production. Following *Listerial* infection interleukin (IL)-1b, IL-6 and interferon gamma (INFγ) were increased (Rousset *et al.* 2006) and these cytokines were elevated additionally to tumour necrosis factor alpha (TNFα) in spleens of UCP2-/- mice following LPS stimulation (Bai *et al.* 2005). $CD4^+$ lymphocytes of UCP2-/- mice produced higher levels of TNFα and IL-2 during EAE (Vogler *et al.* 2006). On the other hand overexpression of UCP2 in transgenic

mice displayed lower levels of IL-4 and IL-6 after treatment with LPS compared to WT littermates (Horvath *et al.* 2003).

Taken together, the evidence suggests a role of UCP2 in a normally operating immune system and absence or overexpression influences mitochondrial function and thus cellular homeostasis and function of UCP2 expressing cells.

1.9 Uncoupling protein 3

Uncoupling protein 3 (UCP3) was first discovered by Boss *et al.* in 1997 and is 57% identical to UCP1 and 72% identical to UCP2 (Boss *et al.* 1997) in genomic sequence. Because of the similarity to UCP1, UCP3 was predicted to be involved in thermogenesis (Samec *et al.* 1998). UCP3 is expressed mainly in heart and skeletal muscle mitochondria (Boss *et al.* 1998; Cunningham *et al.* 2003; Carroll *et al.* 2004b; Krauss *et al.* 2005) and was initially of great interest as an anti-obesity and anti-type 2 diabetes target (Campfield *et al.* 1998; Comuzzie *et al.* 1998). Although UCP3 content in skeletal muscle mitochondria is about 1000-fold lower than that of UCP1 in BAT mitochondria, UCP3 is still of great physiological relevance in resting metabolic rate as there is a much bigger muscle mass in comparison to BAT tissue, especially in adult humans. However, none of the expected phenotypes of cold sensitivity or obesity were observed in UCP3-/- compared to WT mice (Gong *et al.* 2000; Vidal-Puig *et al.* 2000). Research into the effects of UCP3 ablation yielded ambiguous results. Some reports found no effects on state 4 oxygen consumption or proton leak (Vidal-Puig *et al.* 2000; Cadenas *et al.* 2002), while others were able to show those effects (Gong *et al.* 2000). *In vitro* experiments and UCP3 reconstitution into vesicle membranes suggest that UCP3 facilitates a fatty-acid dependent, nucleotide inhibitable UCP1-like proton leak (Jaburek *et al.* 1999; Echtay *et al.* 2001). These effects could be confirmed in isolated mitochondria where a purine-nucleotide sensitive proton leak was observed upon addition of superoxide (Echtay *et al.* 2002) or polyunsaturated fatty acid oxidation products (4-hydroxy-2-nonenals) (Echtay *et al.* 2003), but the specificity of the activation by fatty acid oxidation products was questioned by Shabalina *et al.* (Shabalina *et al.* 2006). Overexpression of human UCP3 in skeletal muscle in mice resulted in a significant loss of body weight and hyperphagia (Clapham *et al.* 2000), but the resulting increased proton leak may well have been an artefact due to increased protein abundance and not of a regulated protein-mediated proton leak in isolated

skeletal muscle mitochondria (Cadenas *et al.* 2002). In vitro work of UCP2/3 overexpressed in cells found that calcium was transported over the mitochondrial membrane (Trenker *et al.* 2007; Graier *et al.* 2008), although these reports were contested by Brookes *et al.* (Brookes *et al.* 2008). Sequence analysis and symmetry modelling with known mitochondrial transporters predicted UCPs to be keto-acid transporters (Robinson *et al.* 2008). Recently, evidence was provided that UCP3 translocates in vitro generated lipid hydroperoxides from the matrix of isolated mitochondria with net manifestation of uncoupling (Lombardi *et al.* 2010). Hence, it is still a matter of investigation as to what UCP3 actually catalyses.

Starvation as a means of physiological alteration increases the abundance of UCP3 2-3-fold per mg mitochondrial protein, but this is not reflected by an increase in proton leak in skeletal muscle mitochondria of fasted compared to fed animals (Cadenas *et al.* 1999; Zhou *et al.* 2000). This indicates a more complex mechanism of control like covalent modification rather than simple protein abundance. This of course makes sense in that, although UCP3 has a short half-life of about 0.5-4 hours (Azzu *et al.* 2010) its function needs to be under much tighter control as even small alterations in proton leak and therefore basal metabolic rate manifest itself in significantly increased energy expenditure over time. There is evidence that 20-25% of resting metabolic rate in rodents (Rolfe *et al.* 1999) and about 52% of basal muscle oxygen consumption in intact skeletal muscle in the rat are due to proton leak (Rolfe *et al.* 1994). In an elegant study on Pima Indians it has been shown that inter-individual variations in resting metabolic rate can influence the development of obesity where the baseline difference between weight gainers and subjects not gaining weight was only 290kJ/d (Ravussin *et al.* 1988). Therefore even small increases in proton leak would have a large impact on energy metabolism specifically over time in long term conditions.

MDMA (3,4-methylenedioxymethamphetamine) is a synthetic, psychoactive drug that promotes a feeling of well-being, increased energy, euphoria, emotional warmth and diminished anxiety, but also distortions in time, perception, and tactile experiences. Physiological effects include interference with the body's ability to regulate temperature. In high doses this can lead to hyperthermia, which can result in liver, kidney and cardiovascular system failure and eventually death (Henry *et al.* 1992). MDMA triggers sympathetic noradrenaline release in BAT and skeletal muscle tissue and there is

evidence of MDMA inducing hyperthermia *in vivo* by UCP3 activation in mice (Mills *et al.* 2003). Additionally to the known psychotropic effect, MDMA triggers the sympathetic nervous system which may manifest itself in activation of endogenous UCP3 in skeletal muscle mitochondria in a similar way as noradrenaline activates UCP1 in BAT by triggering the release of free fatty acids following cold acclimation (Nicholls *et al.* 1984; Cannon *et al.* 2004; Shabalina *et al.* 2004; Nicholls 2006). A study recently published by our laboratory reported increased non-phosphorylating oxygen consumption in skeletal muscle mitochondria dependent on phosphorylation state of UCP3 after whole animal treatment with MDMA but not PBS (Kelly *et al.* 2011a). Facultative thermogenesis in skeletal muscle is thought to be mediated by noradrenaline induced activation of thyroid hormone regulated UCP3 (Gong *et al.* 1997; Lombardi *et al.* 2002). UCP3 expression and activation is thus directly dependent on noradrenaline and subsequent fatty acid mobilisation (Sprague *et al.* 2007).

Recently another control mechanism for UCP2 and UCP3 was suggested where glutathionylation acts as a switch to control uncoupling proteins (Mailloux *et al.* 2011).

The fact that UCP1, UCP2 and UCP3 are expressed in a variety of tissues, including the expression of all three UCPs in the thymus, may suggest that UCPs have different functions. But not only the inter-UCP functions may vary, but also the function of one UCP in a certain tissue compared to the function of the same UCP in another tissue. One example for this might be UCP1 which catalyses a proton leak in brown adipose tissue mitochondria to generate heat in non-shivering thermogenesis, but is most probably not involved in thermogenesis in the thymus. There are a few well known examples of proteins that have an alternative function besides the primary function. This phenomenon is called "protein moonlighting" (Jeffery 2003). An example for a moonlighting protein is the glyceraldehyde-3-phosphate dehydrogenase (GAPDH) which, apart from catalysing the conversion of glyceraldehyde-3-phosphate to 1,3-diphosphoglycerate, has also multiple alternative (moonlighting) functions (Sriram *et al.* 2005). GAPDH is the same protein as uracil DNA glycosylase and catalyses DNA repair by exising uracil (Meyer-Siegler *et al.* 1991). Moreover the GAPDH protein plays also roles in endocytosis (Robbins *et al.* 1995), microtubule bundling (Kumagai *et al.* 1983), phosphate group transfer (Kawamoto *et al.* 1986), nuclear tRNA export (Singh *et al.* 1993), and vesicular transport (Tisdale 2001) among others.

1.10 UCPs and Obesity

Small changes in the proton leak across the inner mitochondrial membrane can significantly affect the overall energy homeostasis in cells and consequently the whole organism. Uncoupling proteins are thought to uncouple the respiratory chain from ATP syntheses by catalysing a proton leak across the inner mitochondrial membrane and, as a result, the mitochondrial electrochemical gradient is dissipated. Mitochondrial uncoupling as a means to reduce body fat has been demonstrated in studies where the synthetic uncoupling agent dinitrophenol (DNP) was used to increase proton leak and energy flux (Cutting *et al.* 1933; Tainter *et al.* 1933). However, even today body builders use DNP as dieting aid to increase their metabolic rate and trim away fat. The proton leak created by DNP however is under no control and an overdose can easily be fatal (Grundlingh *et al.* 2011). UCP1 has been demonstrated to generate heat by uncoupling in brown adipose tissue mitochondria. Moreover, MDMA has been demonstrated to increase the proton leak in muscle mitochondria by phosphorylation and activation of UCP3 triggered by MDMA. This identifies MDMA as a promising compound to target obesity and obesity related diseases. A controlled proton leak and consequently elevated energy usage due to increased UCP3 activity would enable an increased energy flux and help to treat obesity. Of course a tight control of the uncoupling by UCP3 would have to be in place. Therefore in humans UCP3 in muscle mitochondria is a very promising target. However, as UCP3 has been associated with hyperthermia following MDMA treatment (Mills *et al.* 2003), the heat generated by uncoupling through UCP3 would have to be minimised and tightly controlled.

1.11 ROS and UCPs

Reactive oxygen species (ROS) is a collective term for highly reactive oxygen containing radical and non-radical compounds. The paternal ROS in the cell is considered to be superoxide (O_2^-) from which hydrogen peroxide (H_2O_2), hydroxyl-radical ($OH^·$) and fatty acid peroxidation products like 4-hydroxy-2-nonenal (HNE) are formed. ROS are generated at a variety of different places in the cell either deliberately or as a by-product of metabolism.

The main source of intracellular ROS generation is the mitochondrial respiratory chain in most cells excluding macrophages. Conditions resulting in complete reduction of complex I and III (NADH dehydrogenase and cytochrome c oxidase) favour direct diversion of electrons to molecular oxygen to produce superoxide (Lambert *et al.* 2009). Electrons that flow back as a result of reduction of flavinprotein-linked substrates to complex I are also transferred to oxygen to generate ROS (Lambert *et al.* 2004). More mitochondrial proteins contribute to ROS production including complex II (succinate:ubiquinone oxidoreductase) (McLennan *et al.* 2000), the 2-oxoglutarate dehydrogenase complex (Starkov *et al.* 2004), mGPDH (Mracek *et al.* 2009), xanthine oxidase and NAD(P)H oxidases, but it can also be formed enzymatically by semiubiquinone in the mitochondrial electron transport chain.

ROS production is increased in state 4 (non-phosphorylating state) with a high proton electrochemical gradient in isolated mitochondria (Korshunov *et al.* 1998). An artificial uncoupler or the addition of ADP reduces the membrane potential, increases oxygen consumption and drastically decreases superoxide production (Skulachev 1996).

According to the theory of ROS and aging, reduced ROS production results in less oxidative damage and prolonged life. There are several ROS defence mechanisms in place to reduce oxidative damage. Superoxide is enzymatically converted to hydrogen peroxide by SODs (superoxide dismutase) and hydrogen peroxide can then be further reduced to water by catalase or glutathione peroxidase. However these systems target existing ROS whereas uncoupling of the mitochondrial respiratory chain from ATP synthesis would reduce ROS production (mild uncoupling), thus mitochondrial ROS production can be controlled by mild uncoupling. A moderate uncoupling activity of UCPs would lower the membrane potential and result in a reduction of the redox state of the respiratory chain complexes and thus minimize the transfer of electrons to molecular oxygen and the formation of superoxide by shortening the lifetime of semiubiquinone (Miwa *et al.* 2003). Ablation of UCPs would therefore take away the control of the redox state of respiratory chain complexes and control of ROS generation by the respiratory chain.

For years it was thought that ROS are only damaging biological systems whereas nowadays it is clear that ROS are essential components in many cellular functions (Finkel 2003; Buetler *et al.* 2004). ROS are important regulatory mediators of many physiological

responses including redox-dependent transcriptional regulation (Arrigo 1999; Liu *et al.* 2005), ion transport (Kourie 1998) as well as protein phosphorylation (Finkel 1998; Rhee *et al.* 2005).

High levels of ROS induce apoptosis as exposure of T lymphocytes to moderate levels of hydrogen peroxide induces mitochondrial ROS and NF-κB dependent apoptosis (Slater *et al.* 1995; Dumont *et al.* 1999). Superoxide and hydrogen peroxide also enhance IL-2 production in activated T lymphocytes and stimulate the expression of IL-2 receptor (IL-2R) (Roth *et al.* 1987; Los *et al.* 1995). IL-2 and IL-2R are produced in T lymphocytes after antigen presentation to the TCR and activation. The IL-2 IL-2R interaction stimulates growth, development and survival of antigen-specific cytotoxic T-cells and is also crucial for the maturation of regulatory T-cells (Tregs) in the thymus which control and prevent the immune system from reacting with self-antigens and also protect from autoimmunity (Gregori *et al.* 2012).

In another example, the mitochondrial production of ROS in macrophages is important for signalling in activation and vital for effective killing of phagocytised microorganisms. UCP2 expressed in macrophages and other immune effector cells controls mitochondrial ROS production and therefore also activation and function of these cells (Arsenijevic *et al.* 2000).

1.12 Cold Acclimation

Cold acclimated animals have to defend their body temperature by raising the energy expenditure for thermogenesis which is primarily achieved by higher thermogenic activity in BAT, termed non-shivering thermogenesis, and shivering promoted thermogenesis in skeletal muscle (Nicholls *et al.* 1984). In non-shivering thermogenesis the expression of UCP1, the mitochondrial content in brown adipocytes (Nicholls *et al.* 1984) and the number of mature brown adipocytes is increased along with an increase in mitochondrial proteins that contribute to the enhanced metabolic capacity of this tissue (Bukowiecki *et al.* 1982). Both shivering and non-shivering thermogenesis take place as soon as cold acclimation is initiated. Shivering occurs through a constant nervous stimulation of skeletal muscle leading to perpetual contraction and relaxation of muscle

fibres (Behrens *et al.* 1977; Suzuki *et al.* 1997). Gradually, with increasing duration of cold exposure, non-shivering thermogenesis takes over and replaces shivering thermogenesis completely as the major source of heat production in rodents (Cannon *et al.* 2004).

1.13 Noradrenaline signalling in brown adipose tissue cells and muscle fibres

Noradrenaline (Norepinephrine) triggers various different signal cascades and pathways in the body. The stimulatory effect of noradrenaline in brown adipose tissue and skeletal muscle on cellular and mitochondrial metabolism and consequently also oxygen consumption are discussed here. Noradrenaline binds to G-protein coupled β3-adrenergic receptors in the membrane of mature brown adipose tissue cells and muscle fibres and activates protein kinase A (PKA) through a cAMP signal. PKA in turn phosphorylates and thus activates a number of target proteins in the cell.

1.14 Resveratrol

Diminished mitochondrial oxidative phosphorylation and aerobic capacity are associated with reduced longevity. Resveratrol is thought to mimic the beneficial adaptations of exercise and caloric restriction on cellular metabolism and therefore increase overall health and lifespan. These beneficial effects include anticancer and anti-inflammatory properties and reduction of blood sugar levels among other cardiovascular improvements. Resveratrol has therefore been the focus of many animal and human studies reviewed by Catalgol *et al.* (2012) and Fernandez-Marcos *et al.* (2011).

Resveratrol (trans-3,5,4'-trihydroxystilbene) is a natural polyphenolic compound that is produced by various plants as a phytoalexin when under attack by pathogens such as bacteria or fungi (Leiro *et al.* 2004). Resveratrol is found in significant amounts (up to 50-100μg/g) in the skin of red grapes (Shakibaei *et al.* 2009) and is also well known for its antioxidant properties (Baur *et al.* 2006). It also occurs in peanuts, mulberries, some legumes and the root extract of the weed *Polygonum cuspidatum* (Baolin et al. 2004). Because of the presence in red grapes resveratrol has been associated with the phenomenon of the "French Paradox" (Catalgol *et al.* 2012). The French Paradox was introduced in 1992 when a study based on epidemiological data from French people showed a low incidence of coronary heart diseases despite the consumption of a diet high in saturated fat. Moderate wine consumption (almost 57% of the overall alcoholic drink consumption in France) was proposed as the possible reason and resveratrol was introduced as a potentially beneficial food supplement (Renaud *et al.* 1992). However, red wine contains very little resveratrol (0.1-14.3mg/l) and beneficial effects of resveratrol in studies on mainly mice and rats use concentrations of 20mg/kg - 400mg/kg over periods from 2 weeks to 15 months. In human trials only an extremely high dose of a proprietary formulation of resveratrol (3-5g) with improved bioavailability lowered blood sugar levels (Elliott *et al.* 2008).

Among the many beneficial effects of resveratrol is the prolonging of lifespan, which has been reported for some model systems for aging. For instance, it was demonstrated that resveratrol extended the life of the yeast *Saccharomyces cerevisiae* (Howitz *et al.* 2003), the fruit fly *Drosophila melanogaster* (Wood *et al.* 2004), the nematode worm *C. Elegans* (Wood *et al.* 2004) and the fish *Nothobranchius furzeri*

(Valenzano *et al.* 2006). Resveratrol also prolonged the lifespan of mice with a high calorie intake by increasing the insulin sensitivity and decreasing the expression of Insulin-like growth factor 1 (IGF-1). In addition, the AMP-activated protein kinase (AMPK) and peroxisome proliferator-activated receptor-coactivator 1α (PGC-1α) activities were also increased. The mechanism behind these effects was suggested to be resveratrol mediated activation of FOXO (a forkhead transcription factor with gene targets that contribute to longevity and stress resistance initially identified in *Caenorhabditis elegans*) and of insulin-like growth factor-binding protein 1 (IGFBP-1). Another proposed mechanism of resveratrol mediated longevity is the specific activation of an evolutionary conserved family of NAD^+ dependent class III histone deacetylases known as sirtuins (SIRT) (Barger *et al.* 2008). More specifically, resveratrol significantly increases SIRT1 activity in mice which is consistent with the finding, that resveratrol mimics Sir2-dependent lifespan extension during caloric restriction in various species (Lin *et al.* 2000; Howitz *et al.* 2003; Rogina *et al.* 2004). Taken together, resveratrol is an interesting candidate as an anti-aging molecule.

It is important to note that caloric restriction itself has been associated with prolonged lifespan and healthy aging (Speakman *et al.* 2011). Two main mediators of these effects are SIRT1 and one of the many SIRT1 targets, PGC-1α. In liver, adaptations to caloric restriction are promoted by the concerted function of SIRT1 and PGC-1α by adjusting the genetic program for gluconeogenesis and glycolysis (Rodgers *et al.* 2005). Although SIRT1 was originally described as a factor regulating lifespan, DNA repair and apoptosis (Blander *et al.* 2004; Sinclair 2005), it also facilitates the modulation of cellular metabolism by sensing NAD^+ levels following changes in nutritional status (Lin *et al.* 2002; Brunet *et al.* 2004; Picard *et al.* 2004; Rodgers *et al.* 2005). Most of these SIRT1 dependent adaptations are due to activated PGC-1α. PGC-1α physically interacts with SIRT1 and is activated by deacetylation of multiple lysine sites to induce transcription of its respective gene targets (Rodgers *et al.* 2005).

PGC-1α is a transcriptional coactivator that is regarded to be one of the key metabolic controllers in the cell. It is activated by signals that are related to energy and nutrient homeostasis. Upon activation, PGC-1α induces and coordinates gene expression that controls various pathways depending on the tissue and other coactivators. Mitochondrial biogenesis, fibre-type switching in skeletal muscle, the thermogenic

response in BAT and metabolic pathways involved in the response to fasting in liver are under the control of PGC-1α. Expression of metabolic genes is activated by the specific interaction of PGC-1α with ubiquitous transcription factors that bind to the promoter region of those target genes and activate gene expression (Puigserver 2005). Because PGC-1α is involved in the regulation of so many crucial pathways, its activity is under specific and very tight control (Fernandez-Marcos *et al.* 2011).

Reactive oxygen species (ROS) are mainly produced during normal mitochondrial function and are among many other functions also important in promoting aging. Effects of caloric restriction on cellular metabolism will therefore most likely also be observed in tissues with high levels of mitochondrial activity, like BAT or skeletal muscle tissue. These two tissues both express uncoupling proteins which can regulate mitochondrial ROS production as illustrated in detail in section 1.10 (ROS and UCPs). Resveratrol specifically activates SIRT1 (Howitz *et al.* 2003; Borra *et al.* 2005) and consequently PGC-1α, which is why a role for resveratrol in the control of mitochondrial biogenesis and metabolism seems logical.

Lagouge *et. al.* (2006) investigated this possibility and described increased aerobic capacity in mice treated with 400mg/kg/day resveratrol for 15 months, evidenced by increased running time and oxygen consumption in muscle fibres compared to untreated controls. These effects were associated with induction of genes of oxidative phosphorylation and mitochondrial biogenesis and were largely explained by a resveratrol-mediated increase in PGC-1α activity due to decreased in PGC-1α acetylation. Additionally to an increased aerobic capacity and mitochondrial biogenesis, resveratrol treated mice that were also fed a high-fat (HF-) diet were protected from diet-induced obesity and insulin resistance, while food intake and overall activity did not differ between resveratrol treated and untreated mice. Animals that were fed the HF-diet showed significantly increased body weight compared to mice that had also been treated with resveratrol. Indeed, resveratrol treated HF-diet fed mice showed similar body weights as chow fed controls and the difference to the untreated HF-diet fed controls was explained by significantly increased basal energy expenditure, measured by indirect calorimetry. The body weight difference was accounted for decreased white fat depots in resveratrol treated mice on a HF-diet compared to controls. Interestingly, resveratrol treated HF-diet fed mice were able to defend their core body temperature more

efficiently than HF-diet fed mice without resveratrol treatment during acute cold exposure, indicating effects of resveratrol on the thermogenic capacity in mice (Lagouge *et al.* 2006). In another study aimed at the effects of resveratrol in the context of a high-fat diet, Baur *et al.* (2006) showed that resveratrol protected mice from some of the negative effects of a obesity, but resveratrol treatment did not protect the mice from a significant weight gain that was attributable to white fat mass (Baur *et al.* 2006). The reason for the discrepancies between the results of the two studies is not clear, but dosage and duration differed significantly which may explain the non-consistent observations. While Lagouge *et al.* (2006) treated animals with 400mg/kg/day resveratrol for 15 weeks (Lagouge *et al.* 2006), Baur *et al.* (2006) used only 22.4mg/kg/day, but for a prolonged duration of 15 months (Baur *et al.* 2006). Lagouge *et al.* (2006) attributed the phenotype of protection against the increase in white adipose tissue mass to activation of PGC-1α and subsequent increase of UCP3 protein in resveratrol treated mice. In that respect UCP3 has been associated with regulation of flux of lipid substrates and the protection against obesity (Dulloo *et al.* 2001; Fisler *et al.* 2006) and it was proposed that resveratrol dependent upregulation of UCP3 results in a switch toward fatty acid oxidation in skeletal muscle of resveratrol treated mice (Dirks Naylor 2009). Contrary to these reports, Barger *et al.* (2008) did not observe an increase in PGC-1α and UCP3 in murine skeletal muscle (Barger *et al.* 2008). However, it is possible that resveratrol only activates PGC-1α in context with high-fat feeding and does not affect PGC-1α or UCP3 under conditions of standard feeding. In fact, resveratrol decreased UCP3 expression in C2C12 myotubes (Amat *et al.* 2007), indicating that PGC-1α and UCP3 may be induced by resveratrol only under specific conditions. However, Barger *et al.* (2008) treated the animals in their study with 80-times less resveratrol (4.9mg/kg/day) than the amount of resveratrol used by Lagouge *et al.* (400mg/kg/day), albeit for a longer duration, which may be an explanation for the inconsistent observations.

Nonetheless, resveratrol remains an interesting, naturally occurring substance that appears to have very beneficial effects and protects from metabolic disease and improves health and survival in animals on a high-fat diet.

1.15 Changes in nutrition of mammals pre and post weaning

All mammals undergo a transition from the suckling state to a weaned state. The main source of energy for a mammal changes with the weaning as well. For example, in mice the transition from mother milk feeding which is high in fat and protein to a dry diet (rodent standard chow) usually happens three weeks after birth. The standard rodent chow for experimental animals contains a much higher amount of carbohydrates compared to the amount of carbohydrates in mother milk and the animals therefore undergo a shift from a diet with protein and fat as main energy sources to a diet with carbohydrates as the main source of energy.

1.16 The Immune System

The central quality of the immune system is to differentiate between self and non-self. Identifying and clearing foreign pathogens like bacteria, viruses or parasites from the system is the immune systems main purpose. It consists of several different T-cell types produced and matured in a number of different organs including the bone marrow, thymus, spleen and the lymphatic system. All cells of the immune system are derived from pluripotent, haemopoietic stem cells in the bone marrow including white blood cells (leukocytes) and tissue cells (Figure 1-5). Leukocytes basically differentiate in two different pathways to cells of the lymphoid or the myeloid linage. The lymphoid pathway gives rise to B- and T-lymphocytes and natural killer (NK) cells whereas the myeloid line produces mononuclear and polymorphonuclear (PMN) leukocytes, as well as platelets and mast cells. The immune system is comprised of the innate and the adaptive system. The innate immune system is the body's first line of defence against bacterial, viral, fungal or parasitic challenges and mounts an immediate and generalized, but short lived response whereas the adaptive immune system is highly specific and is characterized by a vast variety of T-and B-cell receptors which recognize a specific epitope of a pathogen/antigen. It also preserves memory cells which allow for a much faster and more vigorous response to reinfection with a known antigen. These mature lymphoid cells may live for several years and build up an antigen library over time providing the body with an excellent defensive system.

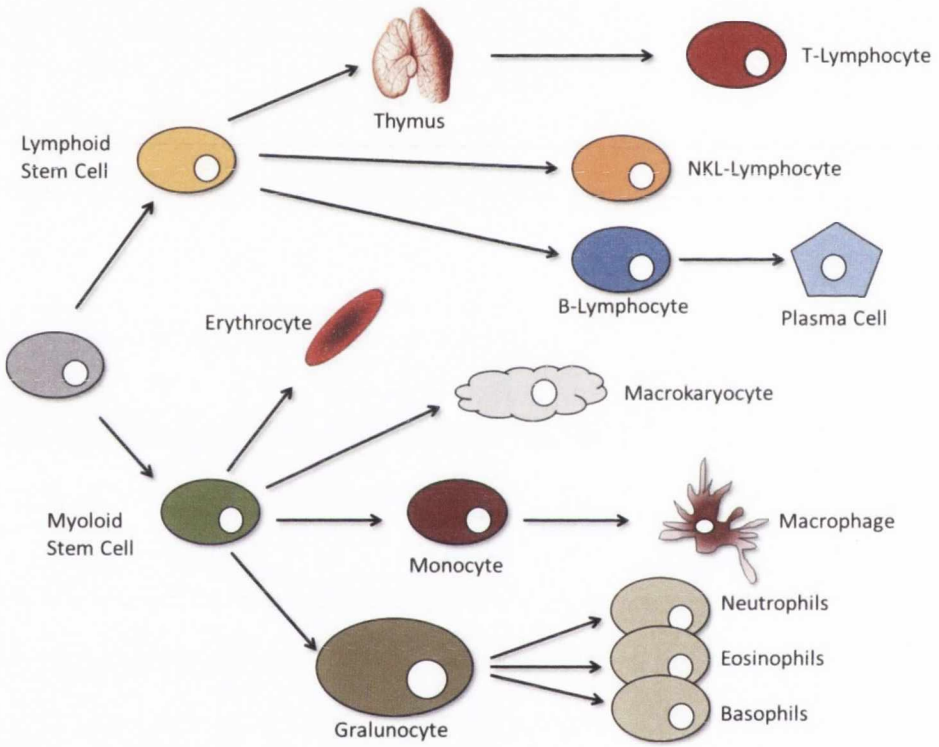


Figure 1-5: Overview of maturation of pluripotent bone marrow derived haemopoietic stem cells.

1.16.1 The innate immune system

In a healthy individual the innate immune system is functional from birth and protects efficiently against harmful microorganisms without the need of exposure to any pathogen beforehand. This response is unspecific and does therefore protect against a broad variety of infectious agents, but it is not long lasting. The innate immune system consists of the constitutive and the inducible immunity.

The constitutive immunity consists of natural barriers and antimicrobial secretions in all different kinds of defence. The skin represents a very significant fence with the secretion of sweat and acids containing antimicrobial substances. All cavity surfaces of the body such as the nose or the lung are covered with mucus and or filamentous layers to capture and excrete possibly harmful organisms. Together with this highly efficient excretion system antimicrobial substances provide a further layer of protection. Furthermore commensal organisms in the gut and bacteria on the skin secrete bacteriocines and acids and compete with intruders for vital nutrients at the same time. This normal bacterial flora generates a protective environment.

The inducible innate immune system consists of innate immune cells and soluble effector substances. Pathogen recognition receptors (PRR) recognize pathogen recognition patterns and trigger the inducible response. The general features of these heterogeneous proteins include opsonisation, activation of complement, phagocytosis, activation of proinflammatory signalling pathways and induction of apoptosis (Janeway *et al.* 2002). Among the best characterized PRRs are the Toll-like receptors (TLR) and intracellular nucleotide-binding oligomerization domain (NOD)-like receptor proteins (NLR). TLRs are prominent on the cell surface or membranes of lysozomes and endosomes where they detect pathogens whereas NLR are expressed in the cytosol and detect intracellular intruders such as viruses (Akira *et al.* 2006). If a PRR recognizes a conserved microbial component called pathogen associated molecular pattern (PAMP; Janeway et al. 2002) and is activated a conserved host defense signal pathway which triggers the expression of a particlar set of immune response genes. PAMPs are ususally shared by more than one organism and therefore a broad variety of potentially harmful pathogens can be identified (Medzhitov 2001).

Phagocytic cells of the myeloid linage such as macrophages, PMN and dendritic cells (DC) primarily mediate the inflammatory innate immune response by either killing pathogens directly or by secreting cytokines, chemical signals to recruit more immune cells to the site of infection. Furthermore natural killer (NK)-cells identify infected cells and efficiently kill them, hence the name. Infection with viruses which can only replicate within a host cell causes alterations on the host cell membrane which are detected by NK cells and activates an extracellular killing mechanism leading to the destruction of the damaged cell. A similar mechanism is also thought to play a role in host defence against transformed tumour cells (Lanier 2005). The innate immune system functions without prior exposure to a pathogen and is therefore very fast acting. The most prominent proinflammatory cytokine is Interferon-γ (IFNγ) which triggers a full blown inflammatory response by directing more cells to the site of infection and activating them to destroy and secrete even more cytokines, usually until the threat is exterminated. A small population of T-cells ($CD8^+$) of the lymphoid linage also express NK markers (NKT-cells), present cytotoxic properties and are therefore capable of killing cells similar to the NK-cells (Biron *et al.* 2001).

Macrophages and DCs are tissue-resident and replenished from a pool of circulating monocytes. Monocytes are derived from the bone marrow and may circulate for several days before entering tissues. They specialize in phagocytosis and destruction of microorganisms in intracellular vesicles by bactericidal reagents such as reactive oxygen species (ROS). This so called respiratory burst gives rise to a significant amount of ROS like superoxide and hydrogen peroxide (Babior *et al.* 1973) produced primarily by NADPH oxidases of the NOX/DUOX family of proteins in mitochondria (Lambeth 2002). Currently it is discussed that ROS is not only used to destroy engulfed bacteria, but is also essential for cell signalling. Therefore modulation of the ROS signal in activated macrophages is of vital importance for a functioning macrophage and immune system.

DCs are considered the principal link between the innate and adaptive immune systems as these cells are professional antigen presenting cells (APC). Despite their watchman function with PRRs they can also sense pathogens indirectly via inflammatory mediators produced by various cells including macrophages, NK cells and endothelial cells (Pulendran *et al.* 2006). Immature DCs patrol the system and upon engulfment of a pathogen the antigen is processed to be presented with the major histocompatibility

complex (MHC) class 2 receptor to prime T-cells and mount the adaptive immune response. Activated DCs migrate to the lymph nodes and undergo maturation shutting off their pathogen collection properties and present now MHC class 2 molecules along with a range of other surface molecules to prime and activate naïve T-cells.

1.16.2 The Adaptive immune system

There are other immune responses stimulated by exposure to infectious agents with increasing magnitude and defensive capabilities with each successive exposure to a particular microbe, other than the innate immune system. Because this second line of defence develops and adapts as a result of exposure to infections it is called adaptive or acquired immunity. Microorganisms that circumvent or overcome the innate immune system are met by this second defence system which is initiated by presentation of an antigen epitope by APCs to lymphoid B- and T-cells. Once initiated a humoral and a cell mediated response take place usually in parallel. The humoral response is carried out by B-lymphocytes which, after presentation of antigen by APCs, differentiate into antibody-producing plasma cells while T-lymphocytes orchestrate the cell mediated response. The antibodies produced are specific to the presented antigen and coat the targeted microbe to prime it for phagocytosis (process called opsonisation) or bind to secretions including toxins to disable and mark them for destruction. Some antibodies bind to and trigger the release of inflammatory mediators from cells or activate the complement system.

Cell mediated immunity is mediated by T-lymphocytes. Protected from the humoral immunity inside of phagocytes or other host cells, intracellular microbes such as viruses or some specialised bacteria can survive, proliferate and pose reservoirs of infection. Cell mediated immunity promotes the destruction of such infected cells and the microbes residing in them.

About 20% of all leukocytes are mononuclear lymphocytes and are heterogeneous in size and morphology with small, agranular T- and B-cells and larger plasma cells bearing cytoplasmic granules. T- and B-cells are distinguished by their site of differentiation in the thymus and bone marrow respectively.

T-cells are derived from lymphoid precursors and are generated in the bone marrow, migrate to the thymus where they differentiate and undergo positive and negative selection steps to become mature T-cells, able to distinguish self from non-self. In the course of this selection 99% of all T-cells die by apoptosis.

The selection of developing T-cells in the thymus is dependent on recognition of antigen (peptide-MHC complexes) and is responsible for eliminating potentially harmful cells and preserving useful ones (Abbas *et al.* 2007). In the thymus immature T-cells go through a positive and a negative selection process to ensure that only T-cells with the ability to recognise foreign antigens presented by self-MHC complexes survive and enter the circulation. In the positive selection thymocytes whose T-cell receptors (TCRs) bind with low avidity to self-peptide and self-MHC complexes are stimulated to survive and those that do not recognise the self MHC complexes follow a default pathway into apoptosis. This ensures that mature T-cells are self MHC restricted. During positive selection MHC complexes class 1 or class 2 are fixed to ensure that T-cells expressing $CD4^+$ or $CD8^+$ are specific for peptides displayed by their respective MHC complex class (class 1 for $CD8^+$ and class 2 for $CD4^+$ T-cells). In negative selection T-cells bearing TCRs that bind strongly to self MHC molecules which would be autoreactive against self-antigens and cause autoimmune diseases are eliminated. After this rigorous selection, mature T-cells leaving the thymus are self MHC restricted and tolerant to a broad range of self antigens.

The thymus is the site of T-cell maturation where after positive and negative selection only about 1% of T-cells enter the circulation. Roughly 99% of all T-cells entering the thymus die by apoptosis. The thymus is a greyish bi-lobed organ situated just above the heart behind the sternum and its main purpose is to provide a milieu for T-lymphocytes to develop, proliferate, mature and generate their TCR (Ritter 1992). It is primarily active in younger pre-pubescent individuals between gestation and adolescence and diminishes in size and activity the older the individual grows. It is anatomically comprised of an outer cortex where differentiation occurs and an inner medulla where the final maturation happens before the T-cells leave the thymus. Apoptosis is of high importance for the successful selection of T-cells with their reactive TCRs.

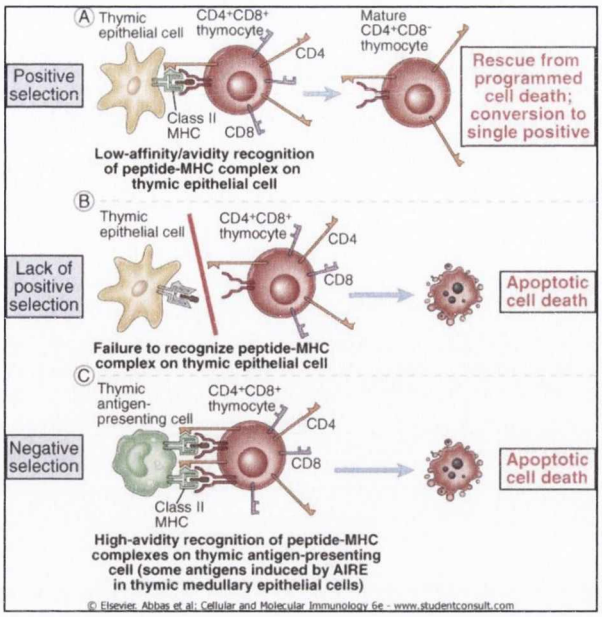


Figure 1-6: Selection processes in the thymus.

A. Positive selection. If the thymocyte TCR engages in a low-affinity interaction with a self MHC molecule on a thymic epithelial cell, it is rescued from programmed cell death and continues to mature. B. Lack of positive selection. If the thymocyte TCR does not engage in any interactions with peptide-MHC molecule complexes on thymic epithelial cells, it will die by a default pathway of programmed cell death. C. Negative selection. If the thymocyte TCR binds peptide-MHC complexes on a thymic antigen-presenting cell with high affinity or avidity, it is induced to undergo apoptotic cell death.

Taken from Abbas *et al.* Figure 8-24 (2007)

1.16.3 Apoptosis in Thymus

Differentiated T-cells are effector cells of the adaptive immune system bearing a clonically generated TCR heterodimer for antigen recognition. The TCR of 95% of T-cells consists of α- and β-chains whereas 5% express γ– and δ-chains at the variable antibody arm to form the TCR complex. The majority of T-cells with α- and β-chain TCRs recognise antigens only when presented by MHC class 2 mostly by professional antigen presenting cells (APC) such as macrophages, B-cells or dendritic cells. $\gamma\delta$ T-cells are an unconventional form of T-cells which do not require the presentation of antigens by APC in the context of MHC class 2 molecules, but are able to recognise antigens directly. Lymph nodes and some areas of the spleen are usually the places for antigen presentation by APCs to cognate lymphocytes, resulting in their differentiation and clonal

expansion. γδ T-cells are present only in low numbers in these tissues indicating that these cells do not usually rely on antigen presentation (Hayday 2000). In that regard it was suggested that γδ-T-cells respond to markers of cell infection or transformation (unique "stress antigens") in a first line of defence hypothesis (Janeway *et al.* 1988; Hayday 2009). Instead of reacting to microbial antigens γδ T-cells are thought to respond to nonpeptide antigens, phosphoantigens, alkylamines, heat-shock proteins and nonclassical MHC class 1 molecules. Furthermore they have been shown to proliferate in response to pathogenic infection by *Mycobacterium tuberculosis*, *Plasmodium spec*, *Toxoplasma gondii*, *Yersinia enterocolitica*, Epstein-Barr virus and early HIV infection (Guerrero *et al.* 2003).

Only 2-4% of circulating lymphocytes are γδ T-cells. But γδ T-cells are found much more frequently in epithelial tissues, supposedly to protect the mucosal surfaces of the body. They present innate-like defence recognizing ligands induced by stress, inflammation or infection and have been reported to process and present peptide antigens to αβ T-cells in an APC manner (Brandes *et al.* 2005), but behave otherwise mostly like their αβ counterparts. These characteristics of both the innate and adaptive immune systems suggest, γδ T-cells represent a conserved, primitive form of immunity (Modlin *et al.* 2005).

Recently, γδ T-cells have been acknowledged as a major source of IL-17. Like their αβ counterparts, IL-17 producing γδs require the transcription factor RORγt for their development (Ivanov *et al.* 2006a). The importance of γδ T-cells in IL-17 production has been further established by reports, indicating that in bacterial infections, they can rapidly produce IL-17 (Lockhart *et al.* 2006; Shibata *et al.* 2007) or even be the main source of IL-17 in some models (Umemura *et al.* 2007).

Classically, αβ T-cells have been divided into two distinct, non-overlapping populations. T-cells expressing the cluster of differentiation co-receptor 4 (CD4) on their cell membrane are defined as "helper" T (Th)-cells and have a central function in the generation, maintenance and regulation of both the humoral and the cellular immune response. These $CD4^+$ effector T-cells are subdivided into two linages based on function and cytokine profile (Mosmann *et al.* 1986). While Th_1 T-cells specialise in cell-mediated defence against intracellular pathogens, particularly viruses but also some bacteria, Th_2 T-

cells mediate humoral immune responses against large extracellular pathogens such as parasites. On the other hand CD8 receptor expressing T-cells are cytotoxic, armed with a variety of cytolytic proteins to kill pathogen-infected cells by inducing apoptosis. Furthermore, $CD4^+$ T-cells need antigen presentation in association with MHC class 2 molecules, whereas $CD8^+$ T-cells require MHC class 1 molecules. The presence of either CD4 or CD8 surface marker therefore limits the type of cell with which it can interact.

1.16.4 Apoptosis in general

Excessive or insufficient apoptosis contributes to various diseases related to ischemia, neurodegeneration, autoimmunity and viral infections and is involved in the growth and regression of tumours (Saikumar *et al.* 1999). When the cells intrinsic suicide mechanism (apoptosis) is activated, it degrades and forms small apoptotic bodies which present an "eat me" signal (phosphatidylserine) on the outer leaflet of the plasma membrane and are then phagocytosed by neighbouring or phagocytic cells without release of potentially harmful contents. The apoptotic machinery exists in all cells except erythrocytes and can be triggered by a range of signals. It can be initiated by intrinsic or extrinsic pathways. Both lead to the subsequent activation of caspases (cysteine-aspartyl-specific protease) that cleave proteins at aspartate residues (caspase-dependent apoptosis) and execute the apoptosis. A well understood example of an extracellular death signal is the binding of FasL on Fas-receptor which triggers caspase-dependent apoptosis by recruitment of FADD and procaspase-8 which is cleaved to the active initiator caspase-8 that cleaves and activates executioner caspases-3 and -7 downstream to induce apoptosis. Apoptosis triggering insults include interference with energy metabolism (partial inhibition of mitochondrial electron transport chain), oxidative stress, DNA-damaging effects of some drugs used in cancer therapy and radiation and removal of growth factors. Table 1 shows a list of intrinsic and extrinsic pathways.

Table 1: Intrinsic and extrinsic members of apoptotic pathways

	Intrinsic	Extrinsic
Apoptosis promoter	Bax	Fas/FasL
	BH3-only proteins	TNFR1/TNF-a
		DR4,5/TRAIL
Inhibitor	Bcl-2	Bcl-xL
		FLIP
Adaptor	Apaf-1	FADD
		TRADD
Initiator caspase	Caspase-9	Caspase-8
Caspase inhibitor	IAP	IAP
Inhibitor of IAP	Smac/Diablo	Smac/Diablo
		Omi/HtrA2
Effector caspase	Caspase-3, caspase-7	Caspase-3, caspase-7

1.16.5 Multiple sclerosis and experimental autoimmune encephalomyelitis (EAE)

Multiple sclerosis (MS) is an autoimmune disease with myelin destruction and neurodegeneration occurring after a long period of chronic inflammation. The main pathological characteristic of MS is the appearance of focal demyelination plaques in the central nervous system (CNS) characterised by infiltration of macrophages and T- and B-cells. MS is the most common neurologic disease of young adults with the onset between 20 and 40 years of age and affects about 2.5 million people worldwide and the number is increasing (McKeown *et al.* 2003). About 2-3 females per one male suffer from the disease indicating the involvement of hormones in disease emergence and progression. It is heterogeneous both clinically and pathologically as different genetic traits might translate into different immune abnormalities, increased vulnerability of CNS tissue to inflammatory insult and or reduced ability to repair damage (Sospedra *et al.* 2005). On pathologic examination inflammation of the CNS and demyelination occurs. Clinical characterisation of the disease sees weakness, paralysis, ocular symptoms with exacerbations and remissions. Imaging of patients with an active form of the disease shows the frequent formation of new lesions in the white matter. MS leads to extensive deficits in motor, neurocognitive, sensation and autonomic functions and results in disabilities through the devastating process in the CNS. There are three different progression types of MS: relapsing-remitting-MS affecting 85-90% of patients and therefore the most frequent form and characterised by changing periods of inactivity and even recovery to a certain extend and clinical exacerbations (Keegan *et al.* 2002). The second form is secondary-progressive-MS which usually follows after initial relapsing-remitting and where patients do not experience amelioration anymore. The third form is primary-progressive-MS which progresses steadily after an insidious disease onset (Keegan *et al.* 2002). Susceptibility to MS is dependent on multiple genetic factors. The primary genetic factors linked to MS susceptibility are thought to be the MHC class 2 region histocompatibility leukocyte antigen (HLA) genes and T-cell receptor (TCR) genes (Keegan *et al.* 2002) although multiple other suggestions are under discussion. A higher rate of disease concordance in monozygotic (25.9%) compared to dizygotic (2.3%) twins or non-twin siblings (1.9%) and higher incidence in offspring of MS patients was reported (Ebers *et al.* 1995).

Among the potentially susceptible genes the common polymorphic and in EAE differentially expressed gene for UCP2 came to attention as it is located on mouse chromosome 7 at 50cM within the EAE susceptible locus *eae4* (Butterfield *et al.* 1998). Additionally to being expressed in a wide variety of tissues including macrophages, T-cells and other immune cells it is also present in spinal cords and lymph nodes of EAE mice and in human MS brain lesions (Ibrahim *et al.* 2001) identifying it as a promising target for MS research.

A murine model of MS is experimental autoimmune encephalomyelitis (EAE) which progresses differently. In C57/BL6 mice the disease pattern and clinical symptoms may follow the primary-progressive form, but can also show relapsing-remitting patterns (Berard *et al.* 2010). In mice EAE is triggered by injection of an antigen (a protein of the myelin sheath) together with adjuvant to trigger a pronounced immune response. The sequence of events in the development of EAE, and by analogy MS, is thought to be initiated by potentially autoreactive T-cells specific for myelin proteins present even in normal individuals. Presentation of myelin antigen together with an adjuvant leads to T-cell activation against epitopes of autologous myelin proteins. These activated T-cells travel to the CNS more readily than naïve T-cells and once the CNS is infiltrated, the T-cells encounter myelin protein epitopes and release cytokines to recruit macrophages and more T-cells which leads to myelin destruction. By myelin break down, epitope spreading leading to disease propagation occurs. APCs in the CNS express high levels of MHC class 2 and co-stimulatory molecules and activate T-cells against all kinds of myelin proteins in the immunologically activated (inflammated) brain tissue thus identifying more potential targets for destruction.

The key feature of MS is primary demyelination of nerve axons leading to signal conduction block or conduction slowing at the site of demyelination. If this occurs in a significant amount of fibres in a given pathway, clinical symptoms and signs will show (McDonald *et al.* 1970). It is thought that during clinical recovery a part of the myelin sheath and conduction is restored, but axonal loss is irreversible and is most likely an important cause of neurological dysfunction in chronic MS.

MS and EAE were considered to be $CD4^+$ Th_1 mediated autoimmune diseases due to the discovery that myelin-reactive T-cells from patients with MS produced cytokines

consistent with a Th_1 mediated response whereas T-cells from healthy individuals produced cytokines of a Th_2-type profile (Crawford *et al.* 2004). However it was found that forms of EAE could be mediated by other T-cell populations including $CD4^+$ Th_2 cells and $CD8^+$ myelin-specific T-cells depending on the model system (Lafaille *et al.* 1997; Huseby *et al.* 2001). Initially, IL-12 was thought be the driving cytokine and key mediator of EAE by inducing differentiation of Th_1 type T-cells and its production of IFNγ, but conclusive evidence of IL-23 and not IL-12 being essential for the development of CNS autoimmune inflammation was produced (Cua *et al.* 2003). Additionally to a possible direct proinflammatory role, IL-23 promotes a third population of memory $CD4^+$ T-cells producing IL-17 distinct from the Th_1 and Th_2 linages, termed Th_{17} cells, was found to be critical for the pathogenesis of EAE (Aggarwal *et al.* 2003; Langrish *et al.* 2005). These Th_{17} cells are now defined as an inflammation promoting $CD4^+$ subset, pathogenic in many autoimmune diseases. For the development of Th_{17} cells the transcription factor orphan nuclear receptor RORγt is critical (Ivanov *et al.* 2006b) and despite their name giving production of IL-17 a range of other cytokines is produced including IL-17A, IL-17F, IL-6, IL-21, IL-22 and TNFα.

Adoptive transfer of highly purified Th_1 cells could induce EAE, but Th_{17} cells deprived of IFNγ producing cells could not induce EAE (O'Connor *et al.* 2008). Although pathological features in EAE induced by Th_1 or Th_{17} cells appear to be different, clinical disease symptoms are similar. Th_1 cells promote expression of monocyte attracting chemokines and macrophage rich infiltrates into the spinal cord while Th_{17} cells activate neutrophil-attracting chemokines and promote neutrophil recruitment and activation mainly in the brain (Kroenke *et al.* 2008; Stromnes *et al.* 2008). Therefore both cell types may play complementary roles in the pathogenesis of EAE.

The role and function of IFNγ has been discussed differentially. Up until recently IFNγ was commonly regarded to be a pro inflammatory cytokine and Th_1 dependent IFNγ production to be vital in triggering and maintaining autoimmune tissue inflammation of MS and EAE (Zamvil *et al.* 1990; Liblau *et al.* 1995). In addition it has been demonstrated that pushing T-cells from a Th_1 to a Th_2 producing response by skewing the cytokine milieu clearly ameliorates EAE (Soos *et al.* 2002; Youssef *et al.* 2002). However recent studies present IFNγ also as a moderator of autoimmune diseases, in particular EAE. EAE

in mice lacking IFNγ or the IFNγ–receptor as well as administration of anti-IFNγ antibodies resulted in more severe disease development, indicating a protective function of IFNγ in EAE (Willenborg *et al.* 1996; Willenborg *et al.* 1999; Furlan *et al.* 2001). However, IFNγ administration to MS patients resulted in aggravated clinical disease and more frequent relapses (Panitch *et al.* 1987). These contradictory findings led to the hypothesis that IFNγ may be important in development and sustainment, but also limitation and moderation of EAE and MS. Elevation of IFNγ in the CNS significantly protected mice from demyelination and lowered disease severity (Lin *et al.* 2007) and it was demonstrated that not only levels of IFNγ are important in the demyelination process , but also the timing of IFNγ expression was of significance in disease progression. IFNγ therefore remains a promising target for development of new treatments for multiple sclerosis.

Additionally, $CD8^+$ T-cell frequencies in inflamed plaques were greater than that of $CD4^+$ T-cells and $CD8^+$ T-cells showed oligoclonal expansion in plaques, CSF and blood, all suggestive of a pathogenic role in MS (Friese *et al.* 2009). Moreover, cell transfer studies suggested a pathogenic function of $CD8^+$ T-cells in EAE (Huseby *et al.* 2001) and both human and murine $CD8^+$ T-cells have been demonstrated to produce IL-17 (Shin *et al.* 1999; Happel *et al.* 2003). However, increased disease severity in mice depleted of $CD8^+$ T-cells suggest a regulatory role in EAE (Weiss *et al.* 2007).

γδ T-cells are another major source of IL-17 as well as other unconventional T-cells like NKT-cells that also secrete innate IL-17. IL-17 producing γδ T-cells, like their αβ Th_{17} counterparts, also require RORγt for development (Ivanov *et al.* 2006b) and can rapidly produce IL-17 in response to bacterial infections or even be the main source of IL-17 in other models (Lockhart *et al.* 2006; Umemura *et al.* 2007). IL-23 induces IL-17 production independent of IL-6 in naïve γδ T-cells, which is essential for driving Th_{17} development (Lockhart *et al.* 2006; Lochner *et al.* 2008).

After γδ T-cells were found in acute brain lesions and cerebrospinal fluid of MS patients with recent disease onset, they have been suggested to contribute to neuroinflammation (Wucherpfennig *et al.* 1992). Deletion of these cells in the EAE model directly prior to disease onset or in the acute phase reduced clinical and pathological EAE disease scores (Rajan *et al.* 1996).

Mice depleted of γδ T-cells showed serious decreases of IFNγ expression in all stages of the disease and reduced IL-1, IL-6 and TNFα levels at disease onset which returned to control levels in the chronic phase of the disease. This shows the importance of γδ T-cells in the regulation of proinflammatory cytokine and chemokine levels in the CNS, which may not require large numbers of cells but could be facilitated by numbers routinely found in the spinal cord and brain of mice with EAE (Rajan *et al.* 1998).

Current therapies include treatment with administration of glatiramer acetate (formerly copolymer-1; Copaxone) which acts as a decoy for the immune system aimed at reducing the number of relapses and slowing the progression of the disease (Weber *et al.* 2007). It is thought to promote the development of Th_2-polarized $CD4^+$ T cells, which may dampen inflammation within the CNS and in addition, it restores numbers of $CD4^+CD25^+Foxp3^+$ regulatory T (Treg) cells generally deficient in multiple sclerosis patients (Hong *et al.* 2005). There are several other therapies available, but in general MS can still not be cured or stopped.

Materials and Methods

Chapter 2

2 Materials and Methods

2.1 Materials

All materials were sourced from Sigma unless stated otherwise.

Protogel	National Diagnostics
Protein G	Calbiochem
PVDF	Millipore
Anti-UCP1	Sigma
Anti-UCP2	Santa Cruz San Diego
Anti-UCP3	Eurogenetec
Anti-PDH	Mitosciences
Anti-GPD2	Santa Cruz San Diego

Addresses of suppliers

Sigma-Aldrich: Vale road, Arklow, Co. Wicklow

Millipore: Tullagreen, Carrigtwohill, Co. Cork

Santa Cruz: Bergheimer Str. 89-2, 69115 Heidelberg, Germany

National Diagnostics: Unit 4 Fleet Business Park, Itlings lane Hessle Hull, HU13 9LX, England

Mitosciences: 1850 Millrace Drive, Suite 3A, Eugene, Oregon 97403

Eurogenetec: LIEGE Science Park, Rue du Bois Saint Jean 5, 4102 Seraing, Belgium

2.2 Animals

All animals were maintained according to the guidelines and regulations of the Irish Department of Health and Children. Experiments were performed under license from the Department of Health and Children and with the approval of the University of Dublin BioResources Ethics Committee and in strict accordance with regulations laid out by LAST Ireland and were compliant with the European Union directives on animal experimentation (86/609/EEC). Animals were housed at 25 ± 1°C in open top cages and had free access to water and standard food and a 12-hour light/dark cycle was in place.

2.3 Wild Type (WT) and UCP1-/- (KO) mice

UCP1 knock-out mice on a C57BL/6 background were originally provided by Dr. Leslie Kozak (Pennington Biomedical Research Center, Baton Rouge, Louisiana, US). Animals were housed in groups of 6 in a specific pathogen free (SPF) environment at 25 ± 1°C in open top cages. All animals were bred in-house and allowed free access to food and water and a 12-hour light/dark cycle was in place. UCP1-/- mice were confirmed to be homozygous by PCR genotyping. All mice were sacrificed by cervical dislocation.

2.4 Wild Type (WT) and UCP2-/- (KO) mice

Wild Type (C57BL/6J) and UCP2 knock-out (B6. 129S4-Ucp2^{tm1Lowl}/J) mice were housed in groups of 6 in a specific pathogen free (SPF) environment at 25 ± 1°C in open top cages. All animals were bred in-house and allowed free access to food and water and a 12-hour light/dark cycle was in place. UCP2-/- mice were confirmed to be homozygous by PCR genotyping. All mice were sacrificed by cervical dislocation.

2.5 Wild Type (WT) and UCP3-/- (KO) mice

Wild Type (B6; 129S4) and UCP3 knock-out (B6; 129S4-Ucp3^{tm1Lowl}/J) mice were housed in groups of 6 in a specific pathogen free (SPF) environment at 25 ± 1°C in open top cages. All animals were bred in-house and allowed free access to food and water and a 12-hour light/dark cycle was in place. UCP3-/- mice were confirmed to be homozygous by PCR genotyping. All mice were sacrificed by cervical dislocation.

2.6 Isolation of genomic DNA for genotyping

Earpunches were taken from mice under sterile conditions and placed in 500µl of fresh digestion buffer and incubated for 4 hours or overnight at 55°C on a slowly spinning rotor until digestion of the tissue sample was complete. Samples were vortexed and spun at 14000g for 10min. 475µl of the supernatant were transferred to 950µl pure, ice-cold Ethanol without disturbing the pellet of undigested hair and debris at the bottom of the tube. The samples in Ethanol were briefly vortexed and the DNA pelleted by centrifugation at 14000g for 10min. Supernatants were removed and the pelleted DNA re-suspended in 30µl DNAse free, sterile water. Any remaining Ethanol was evaporated by incubation of the samples at 65°C for 15min with open lids. DNA was stored at -20°C until further use.

DNA Extraction Solution

100mM Tris, pH 8.5

5mM EDTA

0.2% SDS

200mM NaCl

500ug/ml Proteinase K.

2.7 PCR for genotyping of WT and UCP2-/- mice

The protocol from JAX mice database for strain B6.129S4-Ucp2tm1Lowl/J for UCP2-/- genotyping was used with small alterations. After isolation of genomic DNA from

earpunches (see above) the PCR-reaction was prepared on ice. The GoTaq Hot Start Green Master Mix (Promega) containing GoTaq Hot Start Polymerase, dNTPs, $MgCl_2$ and reaction buffers was used (see Table 2).

Table 2: PCR reaction components for UCP2-/- genotyping

Component	Stock	final	Vol (µl)
2x GoTaq	2x	1x	12.5
Primer forward	20µM	0.8µM	1
Primer reverse	20µM	0.8µM	1
DNA template	pure	1:10	1
MilliQ H_2O			9.5
Final Volume			25

Primers

WT forward	5'-GCGTTCTGGGTACCATCCTA-3'
WT reverse	5'-GCTCTGAGCCCTTGGTGTAG-3'
UCP2-/- Forward	5'-CTTGGGTGGAGAGGCTATTC-3'
UCP2-/- Reverse	5'-AGGTGAGATGACAGGAGATC-3'

Table 3: PCR program for UCP2-/- genotyping

Step	Temperature (°C)	time	
1	95	2 min	
2	95	30 sec	repeat for 35 cycles
3	62	1 min	
4	72	1 min	
5	72	5 min	
6	4	hold	

Following PCR reaction, samples were either analysed directly or stored at -20°C until further use. WT DNA yielded a PCR product of 156bp and UCP2-/- DNA a PCR product of 280bp. For an example of a successful genotyping PCR agarose gel please see Appendix Figure A-1.

2.8 PCR for genotyping of WT and UCP3-/- mice

The protocol from JAX mice database for strain B6;129S4-Ucp3tm1Lowl/J genotyping was used with small alterations. After isolation of genomic DNA from earpunches (see above) the PCR-reaction was prepared on ice. The GoTaq Hot Start Green Master Mix (Promega) containing GoTaq Hot Start Polymerase, dNTPs, $MgCl_2$ and reaction buffers was used (see Table 4 **Table 2**).

Table 4: PCR reaction components for UCP3-/- genotyping

Component	Stock	final	Vol (µl)
2x GoTaq	2x	1x	12.5
Primer WT or UCP3-/-	20µM	0.8µM	1
Primer Common	20µM	0.8µM	1
DNA template	pure	1:10	1
MilliQ H_2O			9.5
Final Volume			25

Primers

WT	5'- GCACTGCGGCCTGTTTTG -3'
Common	5'- ACCCTCTGTCGCCACCATAGT -3'
UCP3-/-	5'- CCTCCACTCATGATCTATAGATC -3'

Table 5: PCR program for UCP3-/- genotyping

Step	Temperature (°C)	time	
1	95	2 min	
2	95	30 sec	┐
3	62	1 min	┘ repeat for 35 cycles
4	72	1 min	
5	72	5 min	
6	4	hold	

Following PCR reaction, samples were either analysed directly or stored at -20°C until further use. WT DNA yielded a PCR product of 600bp and UCP3-/- DNA a PCR product of 300bp. For an example of a successful genotyping PCR agarose gel please see Appendix FigureA-2.

2.9 Agarose gel DNA electrophoresis

A 1.5% agarose gel containing Ethidium Bromide (EtBr, Sigma), Sybr Safe (Invitrogen) or Nancy 520 (Sigma) was prepared and a marker (100bp DNA ladder, Promega) and the PCR products loaded onto the gel. Once loading was complete electrophoresis was run at 150V-200V depending on gel size for 30 minutes with 1x TAE as running buffer.

1x Tris-acetate-EDTA (TAE)
40mM Tris-acetate
1mM EDTA.

EtBr, Sybr Safe or Nancy 520 stained DNA bands were made visible with ultraviolet light at 360nm and gels photographed for analysis.

2.10 Spectrophotometric quantification of nucleic acids

Samples were diluted 1:500 in autoclaved MilliQ dH_2O and read in a spectrophometer at 260nm (absorption maximum for nucleic acids) and 280nm (absorption maximum for aromatic groups in proteins; contamination) and the quotient calculated as a quality control. The concentration was calculated using the following equation

Abs_{260nm} * dilution factor * $extinction\ coefficient_{RNA/DNA}$ = concentration (µg/ml)

Using the Beer-Lambert law it is possible to relate the amount of light absorbed to the concentration of the absorbing molecule. At a wavelength of 260nm, the extinction coefficient for double-stranded DNA is 50 $(\mu g/ml)^{-1}\ cm^{-1}$ and 38 $(\mu g/ml)^{-1}\ cm^{-1}$ for single-stranded DNA and RNA.

2.11 Nanodrop quantification of isolated DNA

Isolated genomic DNA was also quantified using a Nanodrop ND-1000-Spectro-photometer (NanoDrop Technologies, Wilmington, DE, USA) according to the manufacturer's guidelines. 3µl of undiluted DNA in nuclease-free water were used to determine nucleic acid concentration at 260nm and protein contamination at 280nm.

2.12 Isolation of Brown Adipose Tissue mitochondria (BAT)

BAT mitochondria were prepared by a method described previously (Scarpace *et al.* 1991). BAT was removed from the interscapular region of the mouse between the head and the shoulder blades. BAT was washed several times in ice cold (0-4°C) STE buffer and placed into a 50ml beaker containing 30ml of ice cold STE buffer. BAT was chopped carefully in the beaker and poured into a potter homogenizer tube. The tissue was then homogenized by hand with four passes using a pestle of 0.26 inch (loose) clearance, followed by homogenization by hand with 6 passes using a pestle of 0.12 inch (tight) clearance. The homogenate was then filtered through four layers of muslin cloth and the filtrate was centrifuged at 10000g for 11 minutes at 4°C. The supernatant was discarded and the sides of the centrifuge tube were wiped with tissue to remove any fat deposits. The pellet was re-suspended in approximately 20ml STE buffer containing 2% (w/v) de-fatted BSA and centrifuged at 750g for 5 minutes at 4°C. The pellet was discarded and the supernatant was centrifuged at 10000g for 11 minutes at 4°C. The pellet was then re-suspended in STE buffer and centrifuged as above. The resulting mitochondrial pellet was re-suspended gently and thoroughly in a very small volume of STE buffer and used within 6-8 hours of isolation and subsequently stored at -20°C.

Isolation medium (STE)

250mM Sucrose

5mM Trizma-base

1mM EGTA

pH 7.4

2.13 Isolation of Liver mitochondria

Mitochondria were prepared by a method described previously (Chappell 1972). The liver was removed, trimmed of connective tissue and fat and placed into a beaker containing 50ml of ice-cold (0-4°C) STE buffer. It was then chopped finely using scissors, washed several times with ice-cold STE buffer and poured into a potter homogenizer tube. The liver was then homogenized by hand with 10 passes using a pestle of 0.26 inch (loose) clearance followed by homogenization by hand with 10 passes using a pestle of 0.12 inch (tight) clearance. The homogenates were then filtered through four layers of muslin cloth and the filtrate was centrifuged at 750g for 5 minutes at 4°C, pelleting blood and debris. The pellets were discarded and the supernatants were centrifuged at 12000g for 10 minutes at 4°C. The supernatants were discarded and the pellets were re-suspended in approximately 20ml STE buffer containing 2% (w/v) de-fatted BSA and centrifuged at 12000g for 10 minutes at 4°C. The supernatants were discarded and the pellets re-suspended in approximately 25ml of ice cold STE buffer and re-centrifuged at 12000g for 10 minutes at 4°C. The resulting pellets were re-suspended in a very small volume of STE buffer and used within 6-8 hours of isolation and subsequently stored at -20°C.

Isolation medium (STE)

250mM Sucrose

5mM Trizma-base

1mM EGTA

pH 7.4

2.14 Isolation of Kidney mitochondria

Kidney mitochondria were prepared by a method described previously (Chappell 1972). The Kidneys were removed from the abdominal cavity, trimmed of connective tissue and fat and placed into a beaker containing ice cold (0- 4°C) STE buffer. The Kidneys were chopped finely using scissors and washed several times with ice-cold STE buffer. The tissue was poured into a potter homogenizer tube to a final volume of approximately 25ml. The tissue was then homogenized by hand with 10 passes using a pestle of 0.26 inch (loose) clearance followed by homogenization by hand with 10 passes using a pestle of 0.12 inch (tight) clearance. The homogenate was filtered through 4 layers of muslin cloth and the filtrate was centrifuged at 750g for 5 minutes at 4°C. The pellet was discarded and the supernatant was centrifuged at 10000g for 11 minutes at 4°C. The supernatant was discarded and the pellet was re-suspended in approximately 20ml STE buffer containing 2% (w/v) de-fatted BSA and centrifuged at 10000g for 11 minutes at 4°C. This pellet was subsequently re-suspended in STE buffer and centrifuged as above. The resulting mitochondrial pellet was re-suspended in a very small volume STE buffer and used within 6-8 hours of isolation and subsequently stored at -20°C.

Isolation medium (STE)

250mM Sucrose

5mM Trizma-base

1mM EGTA

pH 7.4

2.15 Isolation of skeletal muscle mitochondria

Skeletal muscle of the hind legs of mice were isolated by a method described previously (Bhattacharya *et al.* 1991). Hindquarter muscles (leg muscle) were removed and placed into a beaker containing ice cold (0-4°C) SKMIM buffer. The skeletal muscle was chopped finely using scissors and washed several times using ice-cold SKMIM buffer to remove fat and connective tissue and transferred to isolation medium 2 and incubated on ice for 5 minutes with stirring. The tissue was further disrupted using an Ultra Turrax T25 (Janke & Kunkel IKA-Labortechnik) 3 times for 10 second at half-maximum speed. The homogenate was subjected to centrifugation at 750g for 5 minutes at 4°C. The whitish lipid layer on top of the supernatant was removed and the supernatant centrifuged at 12000g for 11 minutes at 4°C. The resulting mitochondrial pellet was re-suspended in ice-cold SKMIM containing 2% de-fatted BSA (w/v) and centrifuged at 12000g for 11 minutes at 4°C. The pellet was re-suspended in ice-cold SKMIM and centrifuged again at 12000g for 11 minutes at 4°C. The resulting mitochondrial pellet was re-suspended in a very small volume of SKMIM buffer and used within 6-8 hours of isolation and subsequently stored at -20°C.

Isolation medium (SKMIM)	Isolation medium 2
100mM Sucrose	Isolation medium
46mM KCl	0.5% (w/v) BSA
100mM Tris-HCl	0.02% (w/v) nagarse
1mM EGTA	
pH 7.4	

2.16 Protection of phosphorylation state in isolated mitochondria

Mitochondria were isolated as described in sections 2.12, 2.13, 2.14 and 2.15. Where indicated, the ice-cold mitochondrial isolation buffer (STE or SKMIM) was supplemented with phosphatase inhibitors. A inhibitor of protein tyrosine and alkaline phosphatases, sodium ortho-vanadate (O), was activated as previously described (Gordon 1991) and used at a final concentration of 1mM. The mitochondrial isolation buffer was also supplemented with potassium fluoride (KF), an inhibitor of serine and threonine phosphatases, at a final concentration of 10mM. The pH of the ice-cold isolation buffers was adjusted prior to use.

2.17 Mitochondrial protein determination using the Bicinchoninic Acid Assay

Quantification of protein concentrations in tissue samples was carried out using the Bicinchoninic Acid Assay described previously (Smith *et al.* 1985). All of the following solutions (standards or samples) were directly prepared in a 96-well plate. A standard protein solution of BSA was suitably diluted in deionised water from 0 to 0.25 mg/ml. The amount of mitochondrial protein present in the samples was determined by reference to a standard curve derived from the above known concentrations of BSA. Isolated mitochondria were generally diluted in H_2O before analysis so the final concentration of the samples would fall within the range of the standard curve. Once the samples and the standards were prepared, 200µl of a working solution of BCA (1:49 (v/v) BCA: Cu_2SO_4) was added to each well. The plate was then incubated for 30 minutes in an incubator at 37°C. The absorbance of each sample was measured spectrophotometrically at 562nm.

2.18 Sodium Dodecyl Sulphate Polyacrylamide Gel Electrophoresis (SDS-PAGE)

Sodium dodecyl sulphate-polyacrylamide gel electrophoresis (SDS-PAGE) was performed by the method of Laemmli (Laemmli 1970), using a mini-PROTEAN® 3 CELL (Bio-Rad) with a 5% stacking and a 12% resolving gel. The stacking and resolving gels consisted of the following:

Table 6: Ingredients and pipetting of SDS-PAGE gels

RESOLVING GEL	per gel	STACKING GEL	per gel
H_2O	3.35ml	H_2O	6.1ml
1.5M Tris pH 8.8	2.5ml	0.5M Tris pH 6.8	2.5ml
10% SDS	100µl	10% SDS	100µl
PROTOGEL	4.0ml	PROTOGEL	1.33ml
10% APS	50µl	10% APS	50µl
TEMED	5µl	TEMED	10µl

Pre-stained molecular weight marker standards (Bio-Rad) were used. They consisted of myosin (201kDa), β-galactosidase (126.5kDa), bovine serum albumin (90.9kDa), carbonic anhydrase (38.6kDa), soybean trypsin inhibitor (32.2kDa), lysozyme (17.7kDa) and aprotinin (7.4kDa).

The sample buffer was made up as a 4 X strength buffer and was added to the mitochondrial protein so that the final concentration of the sample buffer was 1 X. 5% β-mercaptoethanol (v/v) was added to the sample buffer immediately prior to use. Once the sample buffer and mitochondrial protein were added together, the samples were vortexed briefly and boiled for 10 minutes at 95°C on a heating block. The samples were then loaded into separate wells and electrophoresed first at a constant current of 70V for

30 minutes and followed by 120V for another 45 minutes. A glycine based running buffer was used for electrophoresis.

4 X sample buffer	Running buffer
50 mM Tris-HCl, pH6.8	380mM glycine
10% Glycerol	50mM Tris
2% SDS	0.1% (w/v) SDS
0.02% Bromophenol blue	

2.19 Western Blotting

Following SDS-PAGE, resolved proteins were transferred onto polyvinylidene difluoride (PVDF) membranes (Immobilon-P; Millipore). Transfer was achieved using a Hoeffer semi-dry transfer apparatus at 55mA/membrane for 1.5 hours. First, the stacking gel was removed and the gel was briefly rinsed in semi-dry transfer buffer. One sheet of PVDF membrane was pre-soaked in methanol for 30 seconds and then in distilled water for 1 minute. Six sheets of filter paper cut to the appropriate size of the gel were pre-soaked along with the sheet of PVDF for 15 minutes in transfer buffer. A layered sandwich was then prepared in which the PVDF was placed on top of three layers of filter paper at the anode. The gel was then placed on top, followed by three more layers of pre-soaked filter paper. Air bubbles were removed and the lid with the cathode was placed on top.

Semi-dry Transfer buffer

192mM Glycine

25mM Tris-HCl pH 8.3

13mM SDS

15% (v/v) Methanol

2.20 Immunodetection of proteins

Blocking of the membrane was performed by incubating the membrane in TBS-Tween (0.1%, v/v) containing either 5% (w/v) Marvel milk powder (anti-UCP1, Sigma; anti-

UCP2, Santa Cruz; anti-UCP3, Eurogenetec; anti-PDHE1-α, Mitosciences; anti-GPD2, Santa Cruz) for 1 hour at room temperature. Blots were then incubated in primary antibody (in TBS-Tween containing 5% Marvel milk powder) on a roller overnight at 4°C. Following this primary antibody incubation, the blots were washed 3 x 10 minutes in TBS-Tween. The blots were then incubated with the appropriate horseradish peroxidase (HRP) conjugated secondary antibody in TBS-Tween containing 5% Marvel milk powder for 1 hour at room temperature. Following this blots were washed 3 x 10 minutes in TBS-Tween. Blots were developed using an enhanced chemiluminescence (ECL) detection system (Pierce) for detection of horseradish peroxidase labelled antibodies, by means of the HRP catalysed oxidation of luminol under alkaline conditions and the results were visualized by exposure to Kodak X-Omat LS film.

1x TBS-Tween

20mM Tris

150mM NaCl

0.1% Tween-20

pH 7.6

2.21 Calculation of free calcium concentration in assay buffer

The free Ca^{2+} concentration was calculated using a Ca-EGTA calculator (www.stanford.edu/~cpatton/CaEGTA) using the appropriate buffer concentrations and EGTA and BSA concentrations

2.22 Measurement of mitochondrial Oxygen consumption

All measurements of respiration were made at least in duplicate using an Oxygraph-2k respirometer (Oroboros Instruments). The Oxygraph-2k is a two chamber titration-injection respirometer with a limit of oxygen flux detection of 1pmol*s $^{-1}$*ml^{-1}. The instrumentation allows for O_2-flux measurements with only 0.04mg of mitochondrial protein. Standardised instrumental and chemical calibrations were performed to correct for back diffusion of O_2 into the chamber from the various components; leak from the exterior, O_2-consumption by the chemical medium and sensor O_2-consumption. O_2-flux was resolved by software capable of converting nonlinear changes in the negative time derivative of the oxygen concentration signal. The biological sample (mitochondria or isolated cells) was stirred using a PVDF magnetic stirrer and thermostatically maintained at 37°C. Mitochondria were incubated in KHE buffer containing 5µM atractyloside, 2µg/ml oligomycin, 1µM Rotenone and 0.1% (w/v) de-fatted bovine serum albumin. Before each experiment the medium was equilibrated for 30-40 minutes with air in the Oxygraph chambers until a stable signal was achieved to calibrate for oxygen saturation. At that point the mitochondria were added and a stable background rate was measured. Steady state oxygen consumption rates were then measured in the presence of 10mM succinate or 10mM glycerol-3-phosphate (in the presence of 0.5mM $CaCl_2$; 50nM free Ca^{2+}). Subsequently, 1mM GDP and 40nM free palmitic acid were added and FCCP titrated until no further increase in oxygen consumption could be detected.

KHE buffer

120mM KCl

5mM HEPES

1mM EGTA

pH 7.4

2.23 Measurement of mitochondrial ROS generation

H_2O_2 generation, detected by the Amplex Red assay, was measured essentially as described previously (Dlaskova *et al.* 2006). The assay medium (KHE buffer) contained mitochondria (62.5µg/ml), 5µM Amplex Red, 5U/ml of horseradish peroxidase, 30U/ml superoxide dismutase (SOD), 5µM atractyloside, 2µg/ml oligomycin, 1µM rotenone and 0.1% defatted bovine serum albumin. Fluorescence was detected by a Perkin Elmer LS 55 Fluorometer with excitation set at 570 ± 8nm and emission at 585 ± 4nm. The temperature throughout the experiment was maintained at 37°C. Substrates used were 10mM succinate or 10mM glycerol-3-phosphate (in the presence of 0.5mM $CaCl_2$; 50nM free Ca^{2+}). Where indicated 1mM GDP or 0.25µM of the protonophore carbonyl cyanide p-(trifluoro-methoxy) phenyl-hydrazone (FCCP) was added. Fluorescence was calibrated using known amounts of H_2O_2 on each experimental day.

2.24 Complex II activity assay

The activity of complex II (ubiquinone oxidoreductase) was determined by monitoring the reduction of 2,6-dichloroindophenolate at 600nm on a Shimadzu UVmini-1240 uv-vis spectrophotometer at 30°C. Mitochondria (100µg) were incubated at 30°C for 20 minutes in assay buffer. The reaction was initiated by the addition of 2µg/ml antimycin A, 2µg/ml rotenone, 2mM KCN, 50µM 2,6-dichloroindophenolate and 65µM decylubiquinone. The rate of reduction of 2,6-dichloroindophenolate was monitored for 5 minutes. The enzymatic activity was then inhibited by adding 10mM malonate and the rate of change in absorbance was measured for an additional 5 minutes or until stable. Complex II activity was determined by subtracting the malonate insensitive activity from the total activity.

Assay buffer

25mM potassium phosphate

5mM $MgCl_2$

2.5mg/ml BSA

20mM succinate

0.2mM ATP

pH 7.2

2.25 Glycerol-3-phosphate dehydrogenase activity assay

The activity of glycerol-3-phosphate dehydrogenase was determined by monitoring the reduction of 2,6-dichloroindophenolate at 600nm on a Shimadzu UVmini-1240 uv-vis spectrophotometer at 30°C. Mitochondria (100µg) were incubated in assay buffer containing 2µg/ml antimycin A, 2µg/ml rotenone, 2mM KCN, 50µM 2,6-dichloroindophenolate and 65µM decylubiquinone. Baseline activity was monitored for 5 minutes. The reaction was initiated by the addition of 20mM glycerol-3-phosphate. The rate of reduction of 2,6-dichloroindophenolate was monitored for another 5 minutes.

Assay buffer

25mM potassium phosphate

5mM $MgCl_2$

2.5mg/ml BSA

0.2mM ATP

pH 7.2

2.26 Resveratrol treatment and exercise regime on rats

2.26.1 Animals

Male Wistar rats (430-545g; n=12) were obtained from the BioResources Unit, Trinity College Dublin. They were housed in threes (standard hard-bottomed, polypropylene cages; 44×28×18cm) in a temperature-controlled vivarium (20-22°C), with a 12:12-hour light-dark cycle. Animals were provided with food and water *ad libitum*. Experiments were carried out in strict accordance with regulations laid out by LAST Ireland and were compliant with the European Union directives on animal experimentation (86/609/EEC).

2.26.2 Drug and dosing regime

All rats were handled for one week pre-drug treatment and fed 0.5ml of maple syrup (Maple Joe, Bernard Michaud) to familiarise them with feeding by syringe. *trans*-Resveratrol (>99% purity, Sigma) was administered orally mixed in a solution of maple syrup. Treated animals were given an oral dose of maple syrup and resveratrol suspension (20mg/kg; p.o.), with controls given maple syrup only. Rats were dosed on the same mornings of the exercise protocol, prior to exercise.

2.26.3 Exercise programme

Rats (n=12) were familiarized to motorised treadmills (Exer 3/6 treadmill, Columbus Instruments) by running on the treadmill for 15min (belt speed, 6.7m/min) on 3 consecutive days. They were then assigned to 3 groups: sedentary controls, resveratrol-treated, and exercised (n=4 in each). The exercise protocol consisted of running one hour per day for 12 consecutive days (belt speed, 10-17m/min). The treadmill is equipped with wire loops at one end of the belt through which a mild electric shock can be delivered; these act to motivate the rats to run continuously and were activated at low levels (on average an intensity of three on a scale of 0–10; this represents a current of 1mA with an inter-pulse interval of 2s) throughout all exercise sessions. Rats were observed while exercising to ensure they ran continuously and also to monitor for signs of stress. Untrained rats were placed on stationary treadmills with shock loops activated at low levels for the same duration.

2.26.4 Harvest of tissue samples

The rats were food deprived 24h prior to sacrificing by decapitation 1h following the final treadmill exposure. The interscapular BAT pad, the skeletal muscle tissue of one whole hind leg and the *flexor digitorum brevis* muscle were removed and stored in the respective STE supplemented with phosphatase inhibitors (for mitochondrial isolations) or complete Ringer solutions (for cell isolations) at room temperature until processed as described in sections 2.12, 2.15, 2.27 and 2.28.

2.27 Isolation of mature brown adipose tissue cells

Interscapular brown adipose tissue (BAT) was removed from 6-8 week old Wistar rats after decapitation and all white adipose tissue, muscle and connective tissue removed. The whole tissue was carefully minced with fine scissors and incubated in complete BAT Ringer solution supplemented with 1mg/ml Collagenase from *Clostridium histolyticum* Type II (Sigma, # C6885) on a roller at 37°C for 1h. Following digestion the suspension was filtered through a 70µm filter (Falcon), topped up with complete BAT Ringer solution to stop the reaction and contaminating cells pelleted by centrifugation at 400g for 2min. Floating cells were carefully aspirated off and transferred to a fresh tube and washed in complete BAT Ringer solution. Finally, floating cells were transferred to 1.5ml Eppendorf tubes and stored at room temperature until further use.

Ringer solution	Complete BAT Ringer solution
120 mM NaCl	Ringer solution
3.5 mM KCl	10mM Fructose
1.3 mM $CaCl_2$	10mM Pyruvate
0.4 mM KH_2PO_4	4% fatty-acid free BSA
1 mM $MgCl_2$	
5 mM HEPES	
15 mM D-Glucose	
pH 7.4	

2.28 Isolation and seeding of intact muscle fibres

Single muscle fibres were enzymatically extracted from the *flexor digitorum brevis* (FDB) muscle of male Wistar rats (430-545g) following a protocol optimized for isolation of murine intact muscle fibres and measurement of oxygen consumption in a Seahorse XF24-3 analyser (Schuh *et al.* 2012). Briefly, FDB muscles were removed from the hind feet of Wistar rats, fat and connective tissue trimmed away and the muscle bundle placed in dissociation medium for 1h and 45min at 37°C in a 5% CO_2 incubator. Following dissociation, muscle bundles were moved to pre-warmed complete DMEM and single fibres carefully triturated with a 1ml pipette where the first 2-3mm were cut off. Left over muscle pieces and other debris were removed with forceps and 80-120µl of muscle fibre suspension transferred to a Polyethylenimine (PEI) coated XF24 Cell Culture Microplate to achieve 60-80% confluence and incubated for 1h until the fibres were completely attached. Each well was filled up to 1ml with complete DMEM and the plate incubated overnight at 37°C with 5% CO_2.

Complete DMEM	Dissociation medium
DMEM (Invitrogen, #21063-029)	complete DMEM
50µg/ml Gentamycin	4mg/ml Collagenase Type II
2% fetal bovine serum	

2.29 Measurement of cellular oxygen consumption in brown adipose tissue cells

Brown adipose tissue (BAT) cells were isolated as describe above and kept at room temperature in complete BAT Ringer solution until used. All oxygen consumption measurements were made at least in duplicate using an Oxygraph-2k respirometer (Oroboros Instruments). The Oxygraph-2k is a two chamber titration-injection respirometer with a limit of oxygen flux detection of 1pmol s^{-1} ml^{-1}. The instrumentation allows for O_2-flux measurements with only 0.04mg of mitochondrial protein. Standardised instrumental and chemical calibrations were performed to correct for back diffusion of O_2 into the chamber from the various components; leak from the exterior, O_2-consumption by the chemical medium and sensor O_2-consumption. O_2-flux was resolved by software capable of converting nonlinear changes in the negative time derivative of the oxygen concentration signal. The cellular suspension was stirred using a PVDF magnetic stirrer and thermostatically maintained at 37°C. Oxygen consumption by BAT cells was measured in complete BAT Ringer solution (see section 2.27). Before each experiment the medium was equilibrated for 30-40 minutes with air in the Oxygraph chambers until a stable signal was achieved to calibrate for oxygen saturation. After addition of the BAT cells, an initial high rate was measured which constantly declined over the next 30 minutes until a stable basal rate was measured. After establishing a steady basal rate, 2µM noradrenaline (in 2mM ascorbate solution), 2µg/ml oligomycin, 12.5µM FCCP and 1µM antimycin A were added and the respective stable rates measured. Whenever the relative oxygen concentration in the chamber fell below 50nmol O_2/ml, the PVDF stoppers were lifted and the Ringer solution re-oxygenated until the measurements could be continued.

2.30 Measurement of oxygen consumption rate and extracellular acidification rate in intact muscle fibres

Bioenergetic analyses of cultured intact single muscle fibres were performed in the XF24-3 Extracellular Flux Analyser (Seahorse Bioscience) 24 hours after isolation following the protocol by Schuh *et. al.* 2012. Briefly, intact muscle fibres that were seeded the

previous day (see section 2.28) in a XF24 Cell Culture Microplate were carefully washed twice with Ringer solution (see section 2.27) making sure, that at least 50µl buffer remained in each well between washes and incubated for 1h at 37°C in a CO_2-free incubator. During that time, the drug injections ports A-D of the XF Assay Cartridge were loaded with 10x solutions of the drugs to yield final concentrations of 0.8µg/ml oligomycin, 400nM FCCP, 10mM pyruvate and 1µM Antimycin A respectively. The injections ports of the four recommended Background correction wells and two control wells per group were loaded with Ringer solution only. After a 10-15min incubation of the sensor cartridge 37°C, the sensor cartridge was loaded into the Seahorse XF24-3 Extracellular Flux Analyzer and the program started (see appendix Table A-1 for details).

2.31 Isolation of Thymocytes

Thymocytes were isolated from the thymus as previously described (Buttgereit *et al.* 1994). The thymus was removed from the mouse, trimmed clean of connective tissue and brown fat and transferred to complete RPMI-1640 medium (cRPMI). The thymus and medium were poured onto a nylon mesh (70µm) in a 50ml Falcon tube and using a plunger of a 5ml syringe, the thymus was disaggregated into a suspension of thymus cells. This thymus suspension was centrifuged at 300g for 5 minutes. Any fat droplets present on the surface of the supernatant were removed. The supernatant was discarded and the thymocyte pellet re-suspended in cRPMI and centrifuged again at 300g for 5 minutes. Cells were counted and analysed immediately or stored at -20°C.

Complete RPMI-1640 medium

RPMI-1640

10% fetal bovine serum

Penicillin/Streptomycin mix

2.32 Isolation of Splenocytes

Splenocytes were isolated from the spleen as previously described (Buttgereit *et al.* 1994). The spleen was removed from the mouse, trimmed clean of connective tissue and

transferred to complete RPMI-1640 medium (cRPMI). The spleen and medium were poured onto a nylon mesh (70μm) in a 50ml Falcon tube and using a plunger of a 5ml syringe, the spleen was disaggregated into a suspension of spleen cells. This spleen suspension was centrifuged at 300g for 5 minutes. Any fat droplets present on the surface of the supernatant were removed. The supernatant was discarded and the splenocyte pellet re-suspended in cRPMI and centrifuged again at 300g for 5 minutes. Cells were counted and analysed immediately or stored at -20°C.

Complete RPMI-1640 medium

RPMI-1640

10% fetal bovine serum

Penicillin/Streptomycin mix

2.33 Myelin oligodendrocyte glycoprotein induced Experimental Autoimmune Encephalomyelitis

EAE was induced in C57BL/6 and UCP2-/- mice by s.c. injection of 100μg of myelin oligodendrocyte glycoprotein $(MOG)_{35-55}$ (GenScript) emulsified 1:1 in 100μl complete Freund's adjuvant (CFA; Chondrex Inc.), containing 4mg/ml H37 Ra *Mycobacterium tuberculosis* in the centre of the lower back. Additionally, the mice were injected i.p. with 500ng pertussis toxin (PT; Kaketsuken, Japan) on days 0 and 2. Animals were weighed and monitored for signs of clinical disease on a daily basis. Disease severity was graded as follows: grade 0 – normal; grade 1 – flaccid tail; grade 2 – wobbly gait and hind limb weakness; grade 3 – hind limb weakness or partial paralysis; grade 4 – hind limb paralysis; grade 5 – tetraparalysis/death.

2.34 Cell Counting

Haemocytometer Trypan Blue exclusion Cell counting was performed by diluting 10μl cells (1/10 dilution for CNS tissue and lymph nodes, and 1/20 dilution for spleens) in Trypan blue. 10μl of the cell suspension were then loaded onto a disposable haemocytometer (Hycor Biomedical, UK). The number of viable cells (uncoloured) and

dead cells (dark blue) were then counted using a microscope. The number of cells per ml was calculated according to the manufacturer's protocol by multiplying the cell number in 9 small squares within 1 large square, by 10^4 and by the dilution factor:

Number of cells (ml^{-1}) = cell number in 9 small squares x 10^4 x dilution factor

2.35 Mononuclear Cell Isolation from CNS Tissue

Mice were anaesthetized with 50µl pentobarbital sodium (Euthethal), perfused intracardially with 20ml ice-cold PBS and brain, inguinal lymph node and spleen tissue isolated and transferred to Hanks Balanced Salt Solution containing 3% FCS (HBSS/FCS). Brain tissue was dissociated through a 70µm cell strainer (Nunc), washed through with HBSS/FCS, centrifuged at 170g for 10 minutes at 4°C, and enzymatically digested in Collagenase D (1 mg/ml) and DNase I (10 µg/ml) for 1h at 37°C, with gentle agitation. Cells were washed in HBSS/FCS and re-suspended in 9ml 1.088 g/ml Percoll (see Appendix A). This was underlayed with 5ml 1.122 g/ml Percoll and overlayed with 9ml 1.072 g/ml Percoll, 9ml 1.030 g/ml Percoll and 9ml of 1X PBS. Percoll gradients were centrifuged at 1250g for 45 minutes at 4°C. MNCs were removed from the 1.088 : 1.072 and 1.072 : 1.030 g/ml interfaces and washed twice in HBSS/FCS.

2.36 In vivo Restimulation and FACS Analysis

Isolated cells were restimulated overnight at 37°C / 5% CO_2 with PMA (10ng/ml) and ionomycin (1µg/ml), and cytokine secretion blocked with brefeldin A (5µg/ml). Cells were then washed in FACS buffer (PBS supplemented with 2% FCS), stained for surface markers with anti-CD3, anti-CD4, anti-CD8 and anti-γδ TCR. Cells were fixed and permeabilized with Caltag Fix & Perm Kit, and stained for intracellular cytokines with anti-IFNγ and anti-IL-17. Flow cytometric analysis was performed using a CyAn ADP flow cytometer (DakoCytomation). The flow cytometer was calibrated using the compensation function in the Summit software in conjunction with BD Comp Beads (BD Biosciences). Results were analysed using Summit (DakoCytomation) or FlowJo (Stanford University)

software, with gating determined using the fluorescence-minus-one (FMO) technique, in which a tube of cells contains antibodies conjugated to fluorochromes for all molecules being examined except the one of interest.

2.37 Stimulation of Spleen and Lymph Node Cells *Ex Vivo*

Single cell suspensions were prepared by homogenizing spleen and lymph node tissue through a 40μm cell strainer (Nunc). Cells were centrifuged at 300g for 5 minutes and counted using Trypan Blue exclusion technique. Cells were re-suspended at 2 x 10^6/ml and 100μl of the cell suspension was added to wells of a 96-well 'U-bottomed' tissue culture plate. 100μl of 2μg/ml, 10μg/ml or 50μg/ml MOG, 10ng/ml PMA (Sigma) and 1μg/ml αCD3 (Pharmingen), or medium alone as positive and negative controls, respectively, were added to wells in triplicates. Cells were cultured for 72h after which supernatants were removed for analysis of cytokine production by ELISA.

2.38 Statistical analysis

All results are expressed as mean ± SEM unless otherwise indicated. Mean values were compared using an unpaired student's t-test unless stated otherwise. A P-value of $\leq$ 0.05 was considered significant (* $P \leq 0.05$; ** $P \leq 0.01$; *** $P \leq 0.001$).

Parts of the Materials and Methods section were adapted from Clarke (2011) and Lalor (2010).

T-cell profiles in UCP knock-out mice

Chapter 3

3 Effects of the absence of UCP1, 2 and 3 on the T-cell profile in murine thymus and spleen

3.1 Introduction

UCP1, UCP2 and UCP3 are expressed in the murine thymus and in a variety of other tissues and cell types. UCP1 is primarily found in BAT mitochondria, but is also present in thymus as was shown by our laboratory (Carroll *et al.* 2004a; Carroll *et al.* 2004b; Adams *et al.* 2008a; Adams *et al.* 2008b). While UCP2 is predominantly expressed in spleen, kidney, pancreatic β-cells and immune cells including T-cells, NK-cells and macrophages (Krauss *et al.* 2005), others also showed expression of UCP2 in the thymus of mice and rats (Krauss *et al.* 2002). However, Krauss *et al.* (2002) observed that the absence of UCP2 had no effect on abundance and proportion of CD4 and CD8 single and double positive or double negative T-cell subsets in spleen (Krauss *et al.* 2002). UCP3 is primarily present in skeletal muscle with small amounts also found in BAT. Our laboratory has also demonstrated UCP3 expression in thymus and spleen of mice using immuno-blots and confocal microscopy (Carroll *et al.* 2004b; Kelly *et al.* 2011b). In contrast to UCP2, the absence of UCP1 and UCP3 have been reported to influence $CD4^+$ and $CD8^+$ T-cell frequencies in the thymus and the periphery by affecting the apoptotic potential of thymocytes (Adams *et al.* 2010; Kelly *et al.* 2011b).

The experiments to investigate the effects of UCP1, UCP2 and UCP3 ablation on the CD4 and CD8 lymphocyte profile in thymus and the periphery (spleen and inguinal lymph nodes, ILN, where indicated) in this chapter were performed in 2009 prior to the aforementioned publications by Adams *et al.* in 2010 and Kelly *et al.* in 2011. In addition to clarifying the role of UCPs on the murine T-cell profile, this study also served as a prelude to investigating an experimental autoimmune encephalomyelitis (EAE) model of multiple sclerosis in mice and the effect of the lack of UCP2 on the progression of the disease. Any differences in CD4 or CD8 subsets due to the lack of UCP2, independent of the disease state, were to be identified. Therefore, CD4 and CD8 T-cell frequencies of lymphocytes in untreated WT C57 and WT 129 were compared to UCP1-/-, UCP2-/- (C57 background) and UCP3-/- (129 background) mice in thymus, spleen and, where indicated, inguinal lymph nodes by FACS analyses.

3.2 Results

3.2.1 Effects of UCP1 ablation on T-cell subset composition in thymus and spleen

UCP1 protein is expressed in the thymus of mice and rats and does not seem to be involved in thermogenesis in this organ. In this chapter, a potential role of UCP1 in T-cell selection and apoptosis was investigated by analyses of CD4 and CD8 T-cell populations in thymus and spleen of WT and UCP1 knock-out mice.

Prior to my analyses, 6-8 week old, untreated WT and UCP1-/- mice were sacrificed by cervical dislocation, the relevant tissues harvested, single cell suspensions prepared and analysed by FACS. In FACS analysis, lymphocytes were identified according to size and granularity on forward and side scatter. Within this population, frequencies of CD4 and CD8 single and double positive as well as double negative cells were explored.

Figure 3-1 shows CD4 and CD8 subsets of lymphocytes in spleen and thymus of untreated 6-8 week old WT and UCP1-/- mice. The subsets investigated were CD4 single positive ($CD4^+$), CD8 single positive ($CD8^+$), CD4 CD8 double positive (DP, $CD4^+$ $CD8^+$) and CD4 CD8 double negative cells (DN, $CD4^-$ $CD8^-$).

Figure 3-1A shows frequencies of lymphocytes in spleen of WT compared to UCP1-/- mice in per cent (%) of total lymphocytes. 21.1 ± 0.7 and 23.2 ± 0.6% of total cells were CD4 single positive in WT and UCP1-/- mice respectively. Only very few cells were CD8 single positive (WT 1.5 ± 0.1 and UCP1-/- 1.8 ± 0.1%) and showed no differences between genotypes. CD4 CD8 double positive cells were significantly more abundant in UCP1-/- mice compared to WT mice (WT 9.2 ± 0.0 and UCP1-/- 13.1 ± 0.5%; P=0.0047). The majority of cells were CD4 CD8 double negative, as would be expected in spleen. However, WT mice showed significantly more double negative splenocytes than UCP1-/- mice (WT 61.1 ± 0.6 and UCP1-/- 54.8 ± 0.9%; P=0.0073). In summary, less double positive and more double negative CD4 CD8 cells were detected in spleens of WT compared to UCP1-/- mice. Naturally, double positive cells should not be found in spleen or in circulation because these cells would normally undergo apoptosis in the thymus following T-cell maturation.

Figure 3-1B illustrates frequencies of CD4 and CD8 single and double positive or double negative subsets of thymocytes in WT compared to UCP1-/- mice. UCP1-/- mice showed twice as many CD4 single positive thymocytes compared to WT mice (WT 14.1 ± 0.4 and UCP1-/- 29.8 ± 9.3%; P=0.03). Additionally, WT mice showed a reduction in CD4 CD8 double negative cell populations compared to UCP1-/- mice (WT 1.9 ± 0.4 and UCP1-/- 5.8 ± 1.5%). Almost no CD8 single positive cells were detected in thymus of WT or UCP1-/- mice (WT 1.13 ± 0.1 and UCP1-/- 1.3 ± 0.1%). The majority of T-cells are represented by the CD4 CD8 double positive subset with 81.1 ± 1.1% in WT and significantly less CD4 CD8 double positive T-cells in UCP1-/- thymus (60.6 ± 5.3%; P=0.02).

It is obvious that ablation of UCP1 leads to differences in the murine T-cell population profile. Thymi of UCP1 knock-out mice showed increased CD4 single positive and decreased CD4 CD8 double positive T-cell frequencies confirming a role of UCP1 in the thymus. Surprisingly, this alteration in the thymus manifests itself in the presence of more double positive CD4 CD8 cells and less naïve CD4 CD8 negative cells in spleens of UCP1 knock-out mice.

Table A-2 (Appendix) gives an overview of CD4 and CD8 lymphocyte subsets in spleen and thymus of WT and UCP1-/- mice.

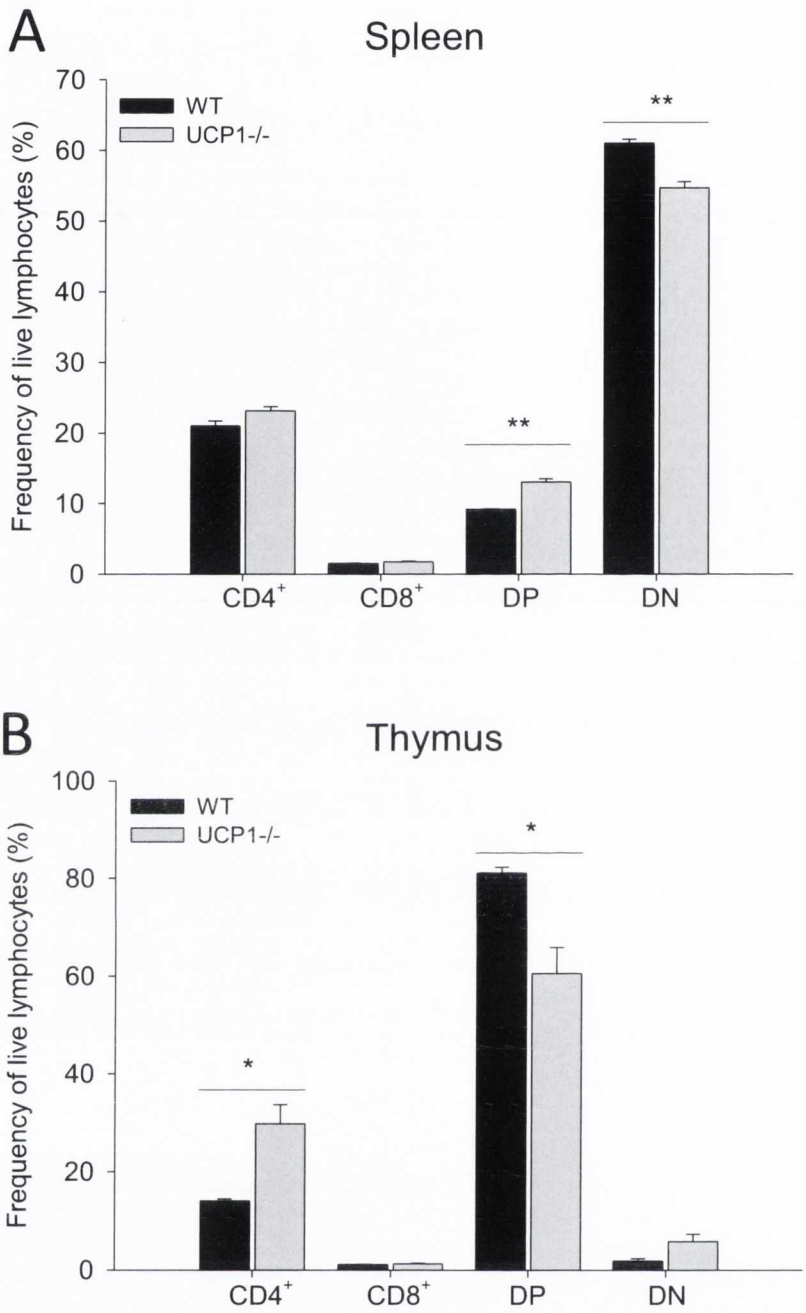


Figure 3-1: Ablation of UCP1 affects T-cell profile in thymus and spleen

(A) Splenocytes and (B) thymocytes of 6-8 week old WT (black) and UCP1-/- (grey) mice were isolated and stained with PE-conjugated anti-CD8 and FITC-conjugated anti-CD4 antibodies (BD biosciences) and analysed on a FACS Cyan machine. Data presented as means ± SEM of three different experiments performed at least in triplicate. P values ≤ 0.05 on unpaired student's t-test were deemed significant (* $P \leq 0.05$; ** $P \leq 0.01$; *** $P \leq 0.001$).

3.2.2 No Effect of UCP2 ablation on T-cell subsets in thymus, spleen and inguinal lymph nodes

After reporting alterations in composition of T-cell subsets and their apoptotic potential in thymi and spleens of UCP1-/- compared to WT mice, the role of UCP2 on the T-cell profile was investigated. UCP2 is a promising candidate, because it is expressed in a variety of immune cells including T-cells. In addition, in preparation of experimental autoimmune encephalomyelitis experiments with UCP2 ablated mice and WT controls any effect on the T-cell profile due to lack of UCP2 was to be ruled out.

Figure 3-2 shows frequencies of $CD4^+$ and $CD8^+$ T-cell subsets in spleen (A) and thymus (B) and Figure 3-3 in inguinal lymph nodes (A) of 6-8 week old untreated male WT and UCP2-/- mice using FACS analysis.

In Figure 3-2A, splenocytes of WT and UCP2-/- mice showed identical frequencies (in %) of CD4 (WT 13.6 ± 3.1 and UCP2-/-14.2 ± 4.8%) and CD8 (WT 11.5 ± 2.5 and UCP2-/-11.4 ± 2.0%) single positive T-cells. The largest population in spleen were CD4 CD8 double negatives (74.8 ± 5.6 in WT and 74.0 ± 6.8% in UCP2-/-) and almost no CD4 CD8 double positive T-cells were detected (less than 1% of total lymphocytes). Altogether, UCP2-/- mice show no differences in CD4 and CD8 T-cell subsets in spleen compared to WT mice. The observed frequencies are within the standard range for lymphocyte populations reported by others (Krauss *et al.* 2002; Lalor 2010).

The spleen is comparable to a large lymph node storing almost half of the body's monocytes which upon activation migrate to target tissues and develop into dendritic cells and macrophages. It furthermore filters the blood and removes and recycles antibody coated erythrocytes and bacteria by blood and lymph node circulation. Therefore, detection of a large CD4 CD8 double negative lymphocyte population in spleens is expected. However, macrophages and natural killer cells also express CD4 on their surface, so these cell types are included in the CD4 single positive population in spleen.

In thymus (Figure 3-2B) the vast majority of lymphocytes were CD4 CD8 double positive (WT 86.9 ± 1.6 and UCP2-/-86.3 ± 1.5%). Only 7.9 ± 1.0 and 9.3 ± 1.1% of lymphocytes were CD4 single positive and 3.4 ± 0.6 and 3.2 ± 0.6% were CD8 single

positive in WT and UCP2-/- respectively. Very little CD4 CD8 double negative lymphocytes were detected in thymus. Because the thymus is the main site of T-cell maturation, almost all of the lymphocytes found in the thymus are CD4/CD8 single or double positive in their different stages of maturation and selection, and very little cells express neither CD4 nor CD8 surface markers.

In inguinal lymph nodes (Figure 3-3) 36.3 ± 1.4% in WT and 42.8 ± 1.6% in UCP2-/- of total lymphocytes were CD4 single positive and 40.2 ± 1.3 and 35.3 ± 2.0% (WT and UCP2-/- respectively) were detected to be CD8 single positive. As in spleen, very little lymphocytes (WT 0.47 ± 0.1 and UCP2-/- 1.66 ± 1.2%) were CD4 CD8 double positive. In an intact system, only CD4 or CD8 single positive cells are allowed to enter the circulation after rigorous selection in the thymus and double positives are usually found in negligible amounts or not at all in the periphery.

Overall, this study found no significant differences in the investigated lymphocyte subsets in thymus or peripheral analysed tissues, which indicates that UCP2 does not affect the frequencies of CD4 and CD8 subsets and therefore the composition of the immune system in this respect.

Table A-2 (appendix) gives an overview of CD4 and CD8 lymphocyte subsets in spleen, thymus and ILN of WT and UCP2-/- mice.

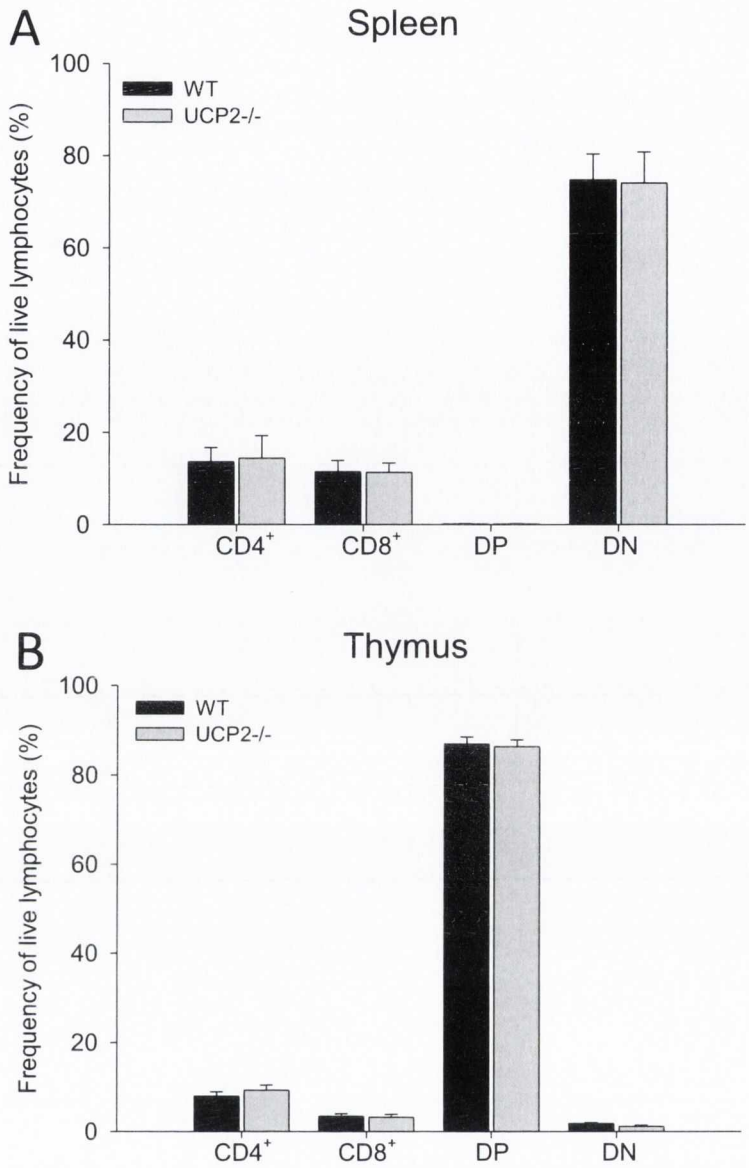


Figure 3-2: Ablation of UCP2 does not affect T-cell profile in spleen and thymus

Single cell suspensions of spleen (A) and thymus (B) of 6-8 week old WT (black) and UCP2-/- (grey) mice were isolated and stained with PE-conjugated anti-CD8 and FITC-conjugated anti-CD4 antibodies (BD biosciences) and analysed on a FACS Cyan machine. Data are means ± SEM of three different experiments performed at least in triplicate. P values ≤ 0.05 on unpaired student's t-test were deemed significant (* $P \leq 0.05$; ** $P \leq 0.01$; *** $P \leq 0.001$).

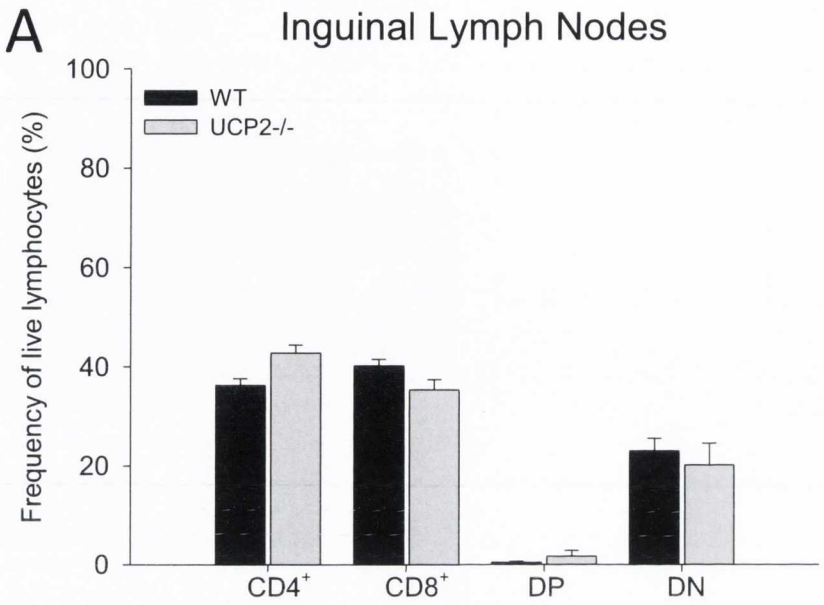


Figure 3-3: Ablation of UCP2 does not affect T-cell profile in inguinal lymph nodes

Single cell suspensions of inguinal lymph nodes (A) of 6-8 week old WT (black) and UCP2-/- (grey) mice were isolated and stained with PE-conjugated anti-CD8 and FITC-conjugated anti-CD4 antibodies (BD biosciences) and analysed on a FACS Cyan machine. Data are means ± SEM of three different experiments performed at least in triplicate. P values ≤ 0.05 on unpaired student's t-test were deemed significant (* $P \leq 0.05$; ** $P \leq 0.01$; *** $P \leq 0.001$).

3.2.3 No effect of UCP2 ablation on the apoptotic potential of thymocytes and splenocytes

In this section the apoptotic potentials of WT and UCP2-/- thymocytes and splenocytes were compared. The cells were either treated with staurosporin (induced) or incubated with a vehicle (spontaneous) for 2h.

Figure 3-4A shows frequencies (in % of total lymphocytes) of murine WT and UCP2-/- splenocytes in spontaneous early and late apoptotic, necrotic and viable states. Cells in early (WT 8.21 ± 1.09 and UCP2-/- 7.76 ± 0.54%) and late apoptosis (WT 22.59 ± 3.47 and UCP2-/-14.91 ± 1.32%) were not significantly changed in UCP2 ablated mice. However, a trend towards decreased late apoptosis in UCP2-/- mice is observable. Almost no cells were necrotic (WT 0.33 ± 0.13 and UCP2-/- 0.55 ± 0.19%), indicating also a good preparation and maintenance of the cells following isolation. The majority of cells did not stain for AnnexinV-APC or Propidium Iodide and are therefore considered viable. Viable cells were more abundant in UCP2-/- compared to WT mice (WT 68.87 ± 4.03 and UCP2-/- 76.87 ± 1.55%), reflecting more late apoptotic cells in WT compared to UCP2-/- splenocytes.

Figure 3-4B illustrates the frequencies (in % of total lymphocytes) of early and late apoptotic, necrotic and viable thymocytes in WT and UCP2-/- mice. No significant differences were observed in any of the investigated conditions. In WT mice 12.66 ± 0.96% of thymocytes were early apoptotic compared to 12.15 ± 0.74% in UCP2-/- mice. About the same amount of cells were in a late apoptotic state in both genotypes (WT 12.43 ± 1.84 and UCP2-/- 11.62 ± 1.39%). Almost no cells were necrotic in thymus (WT 1.40 ± 0.32 and UCP2-/- 1.51 ± 0.22%), while the majority of cells remained viable (WT 73.50 ± 2.99 and UCP2-/- 74.97 ± 2.23%). These findings are surprising as the trends seen in spleen should also be observable in the thymus of these animals.

Figure 3-5A shows the frequencies (in % of total lymphocytes) of early and late apoptotic, necrotic and viable splenocytes in WT and UCP2-/- mice after inducing apoptosis with staurosporin. Significantly more cells were early apoptotic in spleen of UCP2-/- compared to WT (WT 8.04 ± 0.79 and UCP2-/- 13.04 ± 0.85%; $P<0.0001$). As in Figure 3-5A slightly elevated levels of late apoptotic cells were detected in UCP2-/-

compared to WT (WT 37.52 ± 6.34 and UCP2-/- 24.51 ± 3.35%). The frequency of necrotic cells was not altered by incubation with staurosporin and showed no differences between genotypes (WT 0.79 ± 0.20 and UCP2-/- 0.26 ± 0.10%) as was seen in untreated cells. There were again slightly more viable cells in spleens of UCP2-/- compared to WT mice (WT 53.50 ± 6.37 and UCP2-/- 62.08 ± 3.75%).

The comparison of spontaneous and staurosporin induced apoptotic potential resulted in no significant differences in spleens of WT mice. On the other hand, staurosporin treatment significantly increased early (P= 0.000026) and late (P= 0.0099) apoptotic cell frequencies in spleens of UCP2-/- mice, while frequencies of viable cells were significantly reduced (P= 0.00093). The numbers of cells in a necrotic state were not significantly changed by staurosporin treatment in spleens of WT and UCP2 knock-out mice.

In Figure 3-5B thymocytes of WT and UCP2-/- mice were treated with staurosporin over night at 37°C to compare induced and spontaneous apoptosis. Early and late apoptotic cell frequencies were both slightly increased in WT mice compared to UCP2-/- (early apoptotic WT 26.52 ± 3.30 and UCP2-/- 22.41 ± 4.54%; late apoptotic WT 34.39 ± 7.58 and UCP2-/- 25.45 ± 5.77%), whereas necrotic cells were more abundant in UCP2-/- after treatment with staurosporin compared to cells expressing UCP2 (WT 3.93 ± 1.50 and UCP2-/- 13.79 ± 4.15%). On the other hand, frequencies of viable cells were reduced to 35.16 ± 11.35% in WT and 40.59 ± 8.60% in thymi of UCP2 knock-out mice following treatment with staurosporin.

In thymus of WT mice staurosporin treatment significantly induced apoptosis and elevated early (P= 0.00019) and late apoptotic (P= 0.0046) frequencies. Viable cells were significantly reduced compared to frequencies of untreated WT thymocytes (P=0.0014), while changes in cell numbers in a necrotic state were not significant in WT. UCP2-/- thymocytes showed significantly increased frequencies of cells in early apoptosis (P=0.036), late apoptosis (P= 0.024) and necrosis (P=0.0073) as well as significantly reduced viable cell abundance (P=0.00083).

Triggering apoptosis with staurosporin is directly reflected by a significant increase in frequencies of dead or dying cells and reduced viable cells in thymi of WT and UCP2

knock-out animals. Interestingly, staurosporin affected apoptosis only in spleens of UCP2 knock-out mice whereas no effect was seen in spleens of WT animals.

An overview of spontaneous and induced apoptosis in spleen and thymus of WT and UCP2-/- mice is shown in Table A-3 (Appendix).

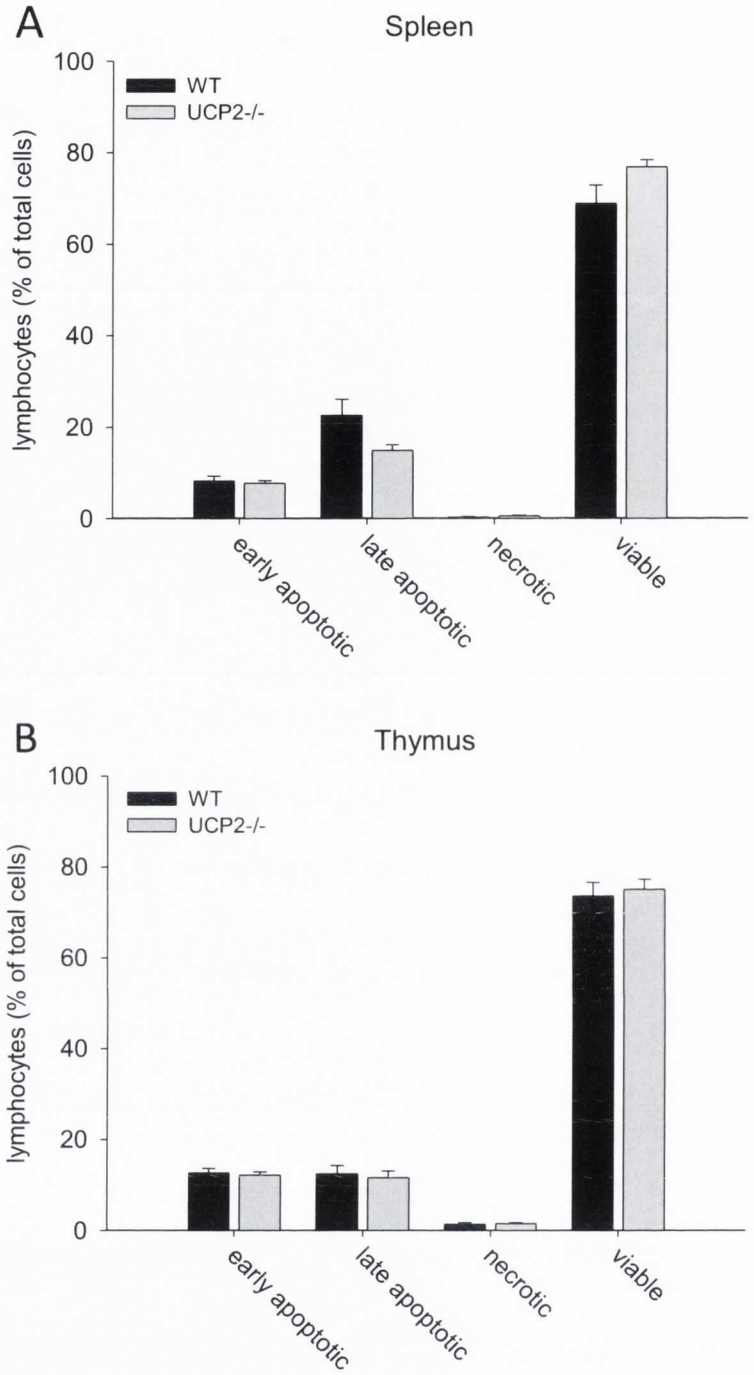


Figure 3-4: Ablation of UCP2 does not affect spontaneous apoptotic potential in splenocytes or thymocytes

Single cell suspensions of spleen (A) and thymus (B) of 6-8 week old WT (black) and UCP2-/- (grey) mice were isolated and incubated with a vehicle (spontaneous) over night at 37°C. Following the incubation cells were stained with the AnnexinV Apoptosis Kit (Annexin V-APC and Propidium Iodide; Millipore) and analysed on a FACS Cyan machine. Data are means ± SEM of three different experiments performed at least in triplicate. P values ≤ 0.05 on unpaired student's t-test were deemed significant (* $P \leq 0.05$; ** $P \leq 0.01$; *** $P \leq 0.001$).

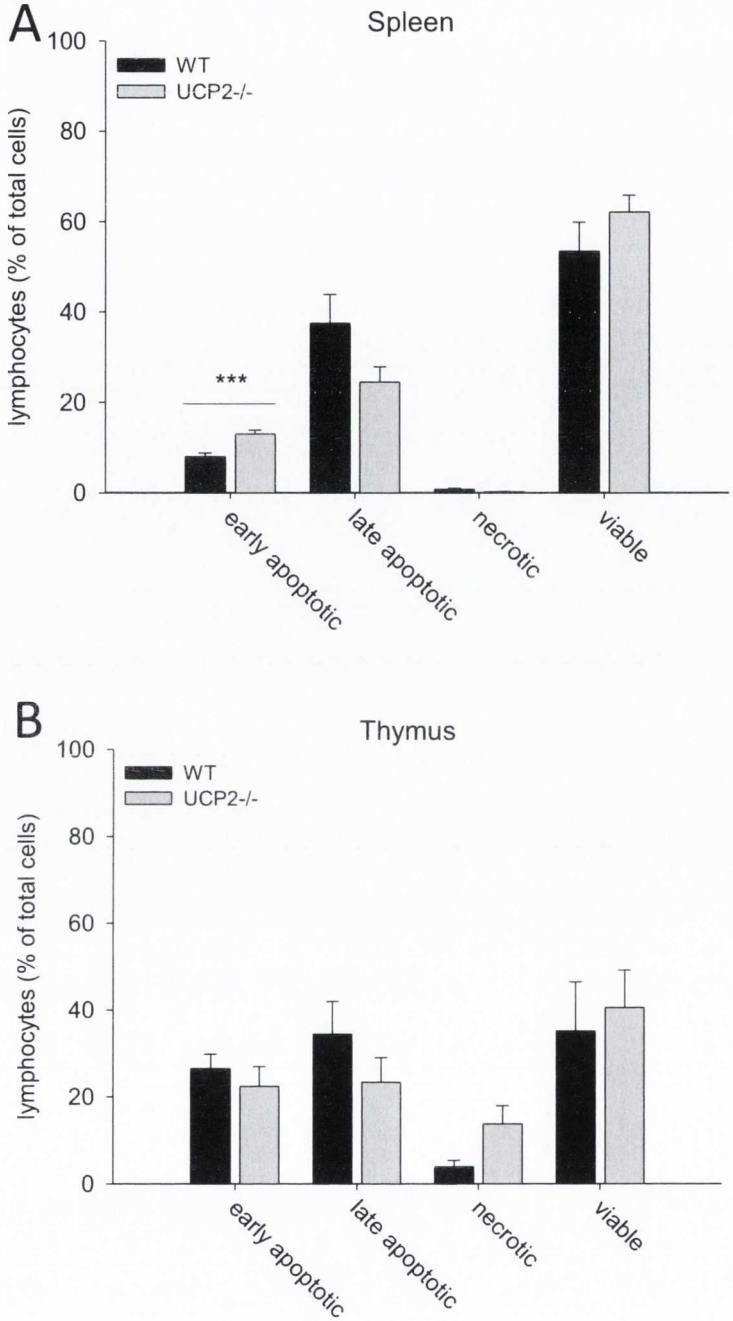


Figure 3-5: Ablation of UCP2 affects Staurosporin induced apoptotic potential in splenocytes, but not in thymocytes

Single cell suspensions of spleen and thymus of 6-8 week old WT (black) and UCP2-/- (grey) mice were isolated and incubated with Staurosporin (induced) over night at 37°C. Following the incubation cells were stained with the AnnexinV Apoptosis Kit (Annexin V-APC and Propidium Iodide; Millipore) and analysed on a FACS Cyan machine. Data are means ± SEM of three different experiments performed at least in triplicate. P values ≤ 0.05 on unpaired student's t-test were deemed significant (* $P \leq 0.05$; ** $P \leq 0.01$; *** $P \leq 0.001$).

3.2.4 UCP3 ablation affects T-cell subsets in thymus and spleen

UCP3 is expressed in the murine thymus together with UCP1 and UCP2 and may also play a role in T-cell maturation and selection and consequently affect the lymphocyte profile.

Figure 3-6 shows CD4 and CD8 lymphocyte subsets in spleen (A) and thymus (B) of 6-8 week old untreated male WT and UCP3-/- mice.

In spleens (Figure 3-6A) 20.6 ± 1.6 and 24.2 ± 0.7% in WT and UCP3-/- mice were CD4 single positive. CD8 single positive cells were significantly elevated in UCP3-/- mice compared to WT and comprised 7.7 ± 0.4 and 10.9 ± 0.3% of total lymphocytes respectively (P=0.001). Almost no CD4 CD8 double positive cells were detected in spleens of both genotypes (WT 0.1 ± 0.0 and UCP3-/- 0.1 ± 0.0%) and no differences were observed. The largest population as before in spleens of UCP1-/-, UCP2-/- and their respective WT controls were CD4 CD8 double negative cells. Double negative cells were significantly reduced in UCP3-/- compared to WT mice (WT 71.6 ± 1.2 and UCP3-/- 64.7 ± 0.4%; P=0.00073).

Figure 3-6B illustrates populations of CD4 and CD8 single and double positive and negative T-cells (in %) in thymus of WT and UCP3-/- mice. In thymus CD4 single positive cells were significantly elevated in UCP3-/- compared to WT with 7.7 ± 0.1 and 9.4 ± 0.3% of total lymphocytes. Single positive CD8 cells represented 3.0 ± 0.3 and 3.9 ± 0.2% of total lymphocytes in WT and UCP3-/- mice respectively and showed no significant differences between genotypes. The largest population of cells were CD4 CD8 double positive in both genotypes and WT mice showed significantly more double positive cells compared to UCP3-/- (WT 88.0 ± 0.3 and UCP3-/- 86.0 ± 0.4%; P=0.014). CD4 CD8 double negative cells were the smallest populations, but WT mice showed significantly more double negative cells than UCP3-/- mice (WT 1.2 ± 0.0 and UCP3-/- 0.7 ± 0.1%; P=0.0013).

UCP3-/- mice showed significantly elevated CD8 single positive and CD4 CD8 double negative populations in the spleen, while CD4 single positive and CD4 CD8 double positive and double negative cells were significantly increased in thymi of KO compared to WT animals.

Table A-2 (Appendix) gives an overview of CD4 and CD8 lymphocyte subsets in spleen and thymus of WT and UCP3-/- mice.

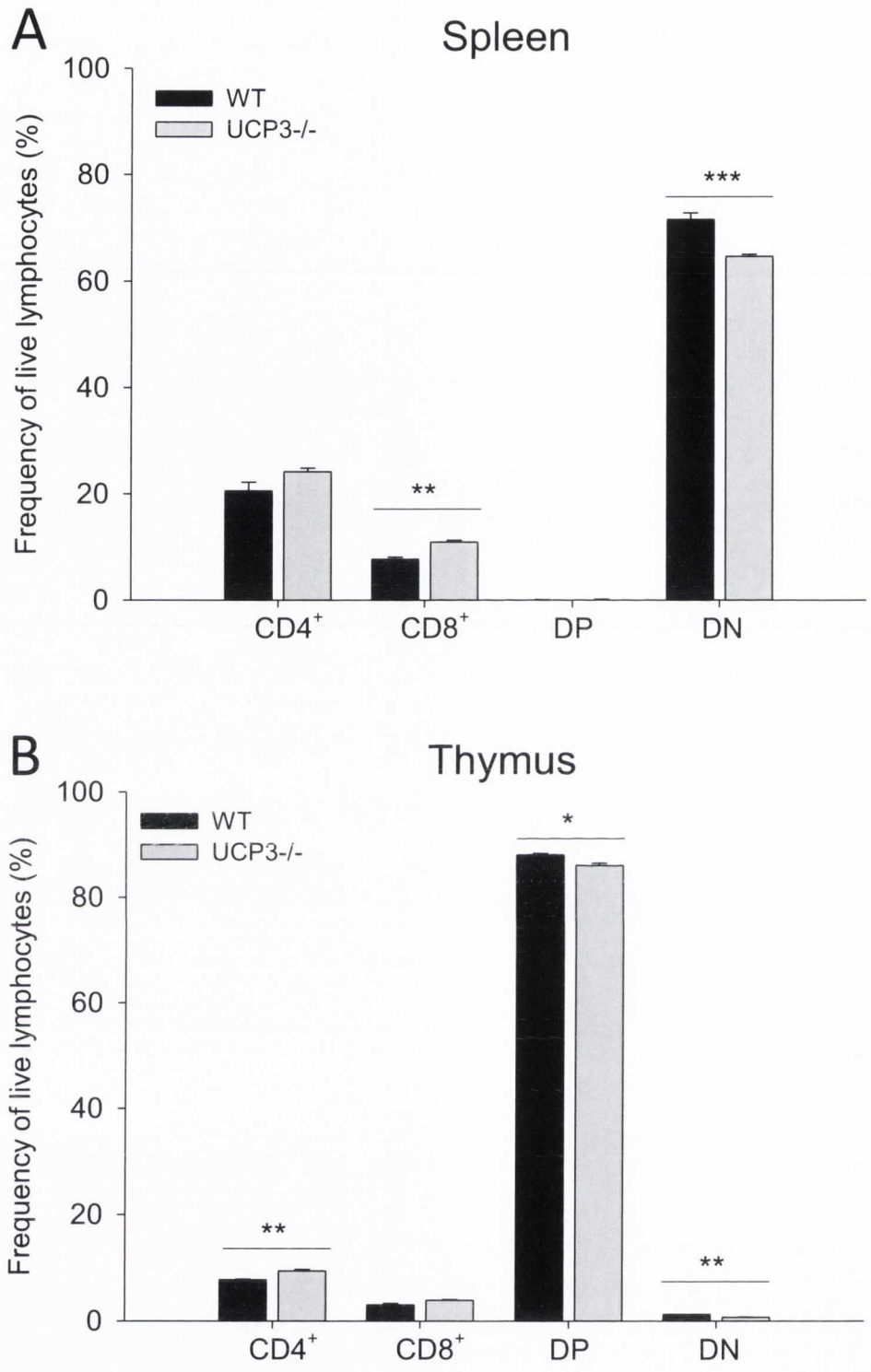


Figure 3-6: Ablation of UCP3 affects the T-cell profile in spleen and thymus

Single cell suspensions of spleen (A) and thymus (B) of 6-8 week old WT (black) and UCP3-/- (grey) mice were isolated and stained with PE-conjugated anti-CD8 and FITC-conjugated anti-CD4 antibodies (BD biosciences) and analysed on a FACS Cyan machine. Data are mean ± SEM of three different experiments performed at least in triplicate. P values ≤ 0.05 on unpaired student's t-test were deemed significant (* $P \leq 0.05$; ** $P \leq 0.01$; *** $P \leq 0.001$).

3.3 Discussion

Adams *et al.* (2010) showed reduced apoptotic potential in lymphocytes from UCP1-/- mice compared to WT mice which resulted in a halving of CD8 single positive and increased double positive CD4 CD8 T-cells both in thymus and in circulation (spleen). In the present study I found increased double positive CD4 CD8 T-cells only in spleen, and not thymus of UCP1-/- mice compared to wild-type mice. CD8 single positive T-cell numbers were not altered in thymus or spleen between genotypes (Figure 3-1). UCP1 ablated mice showed significantly more CD4 single positive and significantly less CD4 CD8 double positive T-cells in the murine thymus. So what could account for the discrepancy between the data presented in this chapter and that of Adams *et al.* (2010)? One explanation for this discrepancy may be the fact, that the animals used in the experiments presented in this chapter were 6-8 weeks old whereas those used by Adams *et al.* (2010) were 3 week old (just weaned) mice. The expression of UCP1 protein in the thymus is relatively high and stable in mice during the first three weeks i.e. the suckling period and drops significantly with the progression of age (Adams *et al.* 2010). Specifically UCP1 protein declines rapidly from the 4^{th} week after birth which coincides with the weaning of mice. So most probably the fact that I used older animals in this study may explain any discrepancies between this study and that of Adams *et al.* (2010). Further investigations on the role of UCPs on thymus function showed that the lack of UCP2 has no effect on CD4 or CD8 positive T-cell frequencies in thymus, spleen or ILN due to absence of UCP2 (Figure 3-2 and Figure 3-3). This present study therefore confirms the results from Krauss *et al.* (2002). Furthermore, apoptotic potential in thymus, spleen or ILN T-cells was unaffected by the absence of UCP2 (Figure 3-4 and Figure 3-5; Table A2, Appendix).

When it comes to UCP3, Kelly *et al.* (2011) showed that a lack of UCP3 affected the T-cell profile of mice. Kelly *et al.* demonstrated that CD4 single positive and CD4 CD8 double negative cells were significantly reduced in thymi of *ad libitum* fed UCP3-/- mice compared to their WT counterparts. My results shown in this chapter demonstrate, that CD4 single positive cells were significantly more abundant in thymi of UCP3-/- mice which contradicts the aforementioned findings by Kelly *et al.* A significant reduction in CD4 CD8 double negative cells in UCP3-/- could be confirmed and additionally a significant

reduction in CD4 CD8 double positive cells was registered which was not described by Kelly *et al.* In spleen of UCP3-/- mice Kelly *et al.* showed significantly elevated CD4 and CD8 single positive and CD4 CD8 double positive T-cells while CD4 CD8 double negative cells were significantly reduced. This study was able to confirm significant reductions of CD8 single positive and CD4 CD8 double negative T-cells due to lack of UCP3 in spleens of mice, but saw no significant difference in CD4 single positive T-cells.

In conclusion UCP1 and UCP3, but not UCP2 affect T-cell profiles in spleen and thymus of mice. The ablation of UCP2 did not alter any of the cell profile subsets in thymus, spleen or inguinal lymph nodes. However, the absence of UCP2 may reduce apoptotic potential both in splenocytes and thymocytes, but the data presented here was not significant and more work is needed to completely rule out involvement of UCP2 in apoptosis. Although not all previously published alterations due to lack of UCP1 or 3 could be confirmed, a role of uncoupling proteins in T-cell composition is evident and needs further investigation.

UCP2 in Experimental Autoimmune Encephalomyelitis (EAE)

Chapter 4

4 UCP2 in Experimental Autoimmune Encephalomyelitis (EAE) – a murine model of Multiple Sclerosis (MS)

4.1 Introduction

Multiple sclerosis (MS) affects over 2.5 million people worldwide and the number of incidents is increasing. Therefore the development of new treatments becomes ever more important. Experimental autoimmune encephalomyelitis (EAE) is a murine model of MS and has been used to characterise and study the underlying mechanisms involved in MS disease onset, progression and more importantly to develop and test treatments. MS and EAE are thought to be autoimmune diseases with the immune system targeting neuronal myelin sheaths leading to primary demyelination of nerve axons. Clinical symptoms in mice include weakness and subsequent paralysis of the tail followed by hind legs and finally front legs to full paralysis.

After initial activation of T-cells by myelin derived protein together with inflammation promoting factors, effector cells are activated and recruited to the CNS where the damage occurs. There are a number of genes and genetic disorders that have been associated with MS. The single nucleotide polymorphism 866G/A, located in the promoter region of UCP2, has been associated with MS among a variety of other autoimmune and inflammatory diseases. More specifically, the G allele leads to impaired UCP2 expression both in lymphocytes and macrophages (Vogler *et al.* 2005) and can result in the development of these diseases. The role of UCP2 in immunology has been investigated in different disease models and settings and was summarized in a recent review by Emre *et al.* (Emre *et al.* 2010). A previous study on the role of UCP2 in EAE by Vogler *et al.* (Vogler *et al.* 2006) found that mice lacking UCP2 (UCP2-/-) suffered (a) a more severe diagnostic rating of EAE at 30 days after disease induction and (b) that the rate of onset of the disease was faster in UCP2 knock-out mice compared to wild-type controls. Also, levels of CD4/TNFα and CD4/IL-2 cells were significantly elevated in UCP2-/- mice compared to controls. In addition, ROS production in CD4 and CD8 cells, but not in macrophages, was significantly increased in cells from UCP2 knock-out mice compared to cells isolated from WT mice. The aforementioned proinflammatory cytokine pattern together with increased ROS production, points towards a regulatory role of UCP2 in this

autoimmune disease model for MS. Based on these facts, I set out to confirm the pathological observations of Vogler *et al.* (2006) and further investigate the function of UCP2 in the onset and severity of the disease. To that end I focused on profiling subsets of T-cells and proinflammatory cytokines thought to be involved in MS and EAE.

4.2 Experimental

A progressive form of EAE was induced in 6-10 week old female C57 WT and UCP2-/- mice by s.c. injection of 100µg myelin oligodendrocyte glycoprotein (MOG_{35-55}) emulsified with 4mg/ml H37 Ra *Mycobacterium tuberculosis* and complete Freud's adjuvant (CFA). MOG serves as the antigen to prime T-cells to target myelin sheaths in the central nervous system (CNS). At days 0 and 2 *Pertussis* toxin (PT; 500ng) was injected i.p. to stimulate an immune response. All animals were monitored daily for symptoms of clinical disease which started to show from day 7. The incidence of disease was 100% in WT and 86% in UCP2-/- mice respectively. Animals presented symptoms beginning with a flaccid tail (score 1), progressing from hind limb weakness to hind limb paralysis and front limb weakness (score 4). None of the mice reached the final stage of complete paralysis (score 5), at which point these individuals would have been sacrificed according to the guidelines and regulations of the Irish Department of Health and Children. Mice were sacrificed 21 days post-immunization with MOG/CFA and spleens, inguinal lymph nodes (ILN) and brains were harvested for analysis. A further 30 day experiment was performed for a full disease progression, but no tissues were harvested or analysed this time. Prior to tissue harvest, mice were perfused with ice- cold phosphate buffered saline (PBS) to wash out all blood and any floating T-cells. Therefore, only tissue infiltrating and residual T-cells were analysed in this study. In the final stage of EAE, conditions in the CNS are represented by data from brain while spleen and ILN represent the situation in the periphery.

4.3 Results

4.3.1 Time course of clinical symptoms and body weight in EAE

First, a time course of disease progression and body weight was generated to investigate any differences due to lack of UCP2 and to pick a timepoint for tissue harvest.

Figure 4-1 shows the average body weight (A) and mean clinical scores (B) of mice in a time course of EAE over 30 days post immunization in 6 independent experiments. In Figure 4-1A the two groups of WT and UCP2-/- mice showed no differences in body mass until day 5, but from day 6 to day 14 the weight loss in WT mice was significant. The lowest average body weight in the whole time course was reached on day 14, before WT mice put on weight again and reached the initial mass 25 days post immunization. On the other hand, UCP2-/- mice gained weight until day 10 and only dropped body mass from day 11 to day 18 before a plateau was reached, followed by weight gain from day 23 onwards. The UCP2-/- mice were, on average, significantly heavier than WT mice between days 7 to 15 and no significant differences remained after that.

The differences in weight loss and gain between WT and UCP2 knock-out mice was reflected by the mean clinical scores of each group (Figure 4-1B). WT mice showed an earlier onset of disease from day 7 compared to UCP2-/- mice, which showed first symptoms 12 days past immunization. The mean clinical scores continued to climb to a maximal value of 2.61 ± 0.22 in WT at day 16 and 2.31 ± 0.23 in UCP2-/- at day 19 post immunisation and stayed roughly the same until day 25. In WT mice the mean score then declined, but in UCP2-/- the score only began to decline at day 29.

After establishing a rough timeline of disease progression and endurance, a time point for tissue analyses was chosen. At 21 days post immunisation both average body weight and average clinical scores were about the same in WT and UCP2-/- mice and reflected the situation in a chronically ill subject with severe clinical disease before remission events. At this point a lot of damage to the CNS would have been done already.

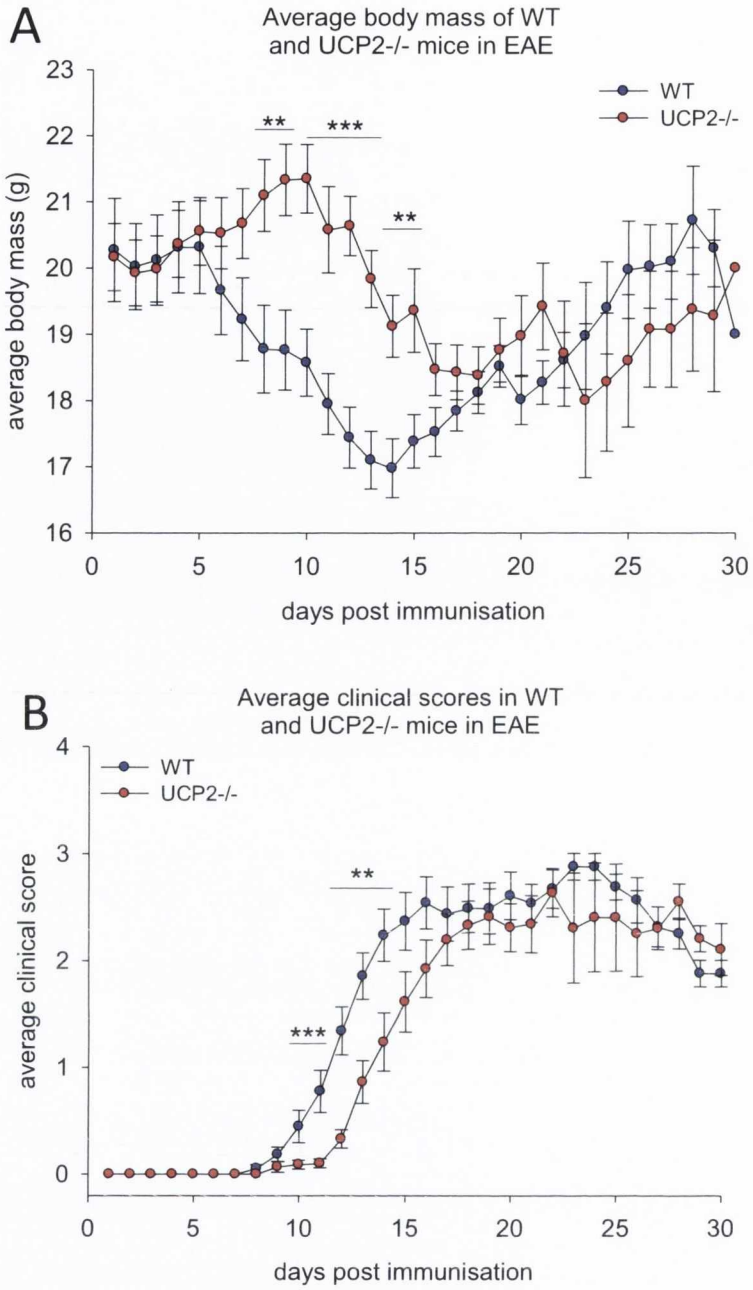


Figure 4-1: UCP2 knock-out delays the onset of EAE in mice

EAE in WT (blue) and UCP2-/- (red) mice was induced by s.c. injection of 100 µg of MOG_{35-55} emulsified in CFA, supplemented with 4 mg/ml H37 Ra *M. tuberculosis*. Mice were injected i.p. with 500 ng pertussis toxin (PT) on day 0 and 2. Animals were weighed and monitored for signs of clinical disease on a daily basis for 30 days. Time course of (A) average body weight (in g) and (B) average clinical score in WT and UCP2-/- mice. Disease severity was graded as follows: grade 0 – normal; grade 1 – flaccid tail; grade 2 – wobbly gait; grade 3 – hind limb weakness; grade 4 – hind limb paralysis; grade 5 – tetraparalysis/death. Results are mean body weight (g) and mean clinical score ± SEM (n = 6; 5 mice per group per experiment in 6 independent experiments). P values ≤ 0.05 on unpaired student's t-test were deemed significant (* $P \leq 0.05$; ** $P \leq 0.01$; *** $P \leq 0.001$).

4.3.2 FACS analysis of T-cell subsets in EAE mice 21 days post immunization

On day 21 post immunization all animals in the WT and UCP2 knock-out groups were sacrificed. Brains, spleens and inguinal lymph nodes (ILN) were harvested, single cell suspensions generated, stimulated overnight and analysed by FACS the following day. Only animals with a clinical score of at least 1 (flaccid tail) at 21 days post immunization were included in the study, regardless of showing more severe or no symptoms earlier in the study.

Figure 4-2 illustrates the percentages of live lymphocytes and $CD3^+$ T-cells in spleen, ILN and brain of WT and UCP2-/- mice in EAE at 21 days. The gate for live lymphocytes was set according to size and granularity in forward and side scatter. $CD3^+$ cells within this group were considered live T-cells for all graphs hereafter.

Clearly, the frequencies of live lymphocytes and $CD3^+$ T-cells did not differ between genotypes in any of the analysed tissues. Therefore, total numbers of live lymphocytes and $CD3^+$ T-cells were not affected by the presence or absence of UCP2 in these tissues. This observation also indicates a consistent isolation and staining procedure. Any differences in T-cell composition due to the lack of UCP2 were ruled out by FACS analyses of untreated WT and UCP2-/- mice (see UCP2 knock-out T-cell profile in Figure 3-2 and Figure 3-3, chapter 3).

In the next step, the T-cell population was further characterised and frequencies of CD4, CD8 and $\gamma\delta$ positive T-cells were measured. Furthermore, intracellular staining against IL-17 and IFNγ was applied within these particular T-cell subsets to further characterise any differences in the involved T-cells subsets and their respective cytokine production between WT and UCP2-/- mice in the response to EAE.

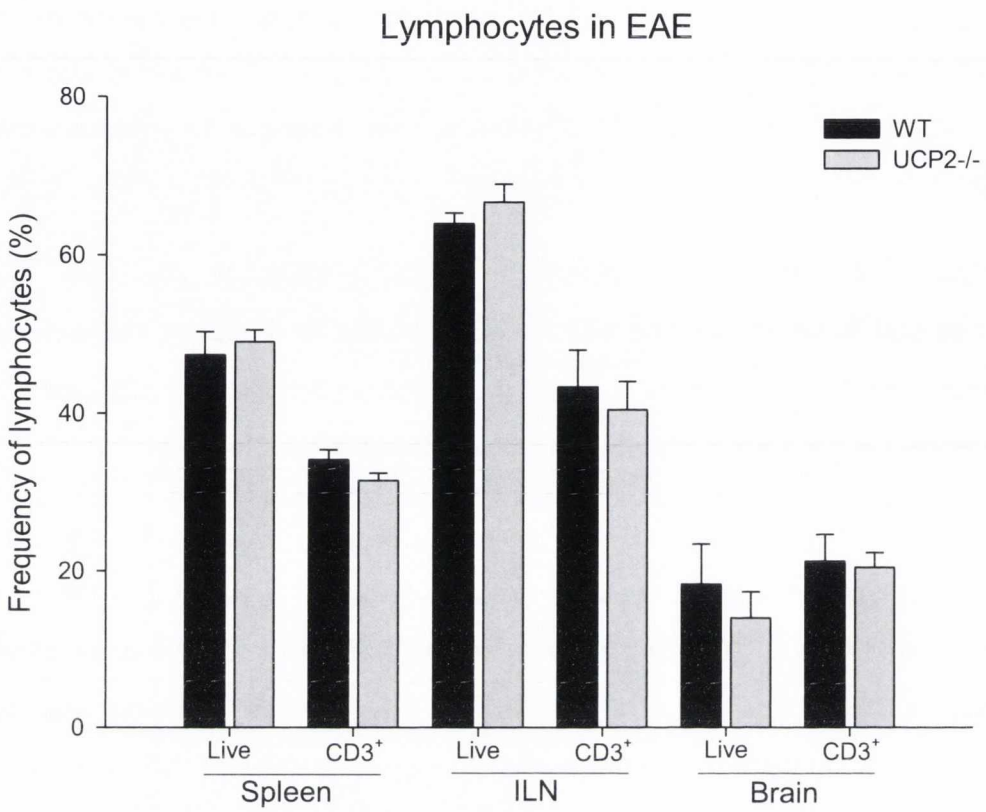


Figure 4-2: Absence of UCP2 does not influence lymphocyte or T-cell content in spleen, ILN and brain of EAE mice

Lymphocytes were isolated from spleen, ILN and brain of EAE mice after perfusion with ice-cold PBS 21 days post immunization with MOG/CFA. Live lymphocytes were identified by gating on forward and side scatter and within this gate the $CD3^+$ population (T-cells) was gated on and used for further analysis. Values are means ± SEM of 6 independent experiments with 5 animals per group per experiment. P values ≤ 0.05 on unpaired student's t-test were deemed significant (* $P \leq 0.05$; ** $P \leq 0.01$; *** $P \leq 0.001$).

4.3.3 T-cell subsets of WT and UCP2-/- mice in Experimental Autoimmune Encephalomyelitis

Figure 4-3 and Figure 4-4 show frequencies (in % of $CD3^+$ cells) of CD4 (Figure 4-3A) and CD8 (Figure 4-3B) and γδ (Figure 4-4) single positive T-cells in brains, spleens and ILN of WT and UCP2-/- mice in EAE. Some trends were observed, although no significant differences between genotypes were detectable.

In Figure 4-3A $CD3^+$ $CD4^+$ T-cell frequencies were slightly elevated in UCP2-/- compared to WT mice in all three tissues. The largest difference was found in the brain, where 20.2 ± 3.6% of $CD3^+$ cells were $CD4^+$ in WT compared to 29.5 ± 6.0% in UCP2-/- mice. In spleen this difference was not observed with 40.9 ± 1.5% of T-cells being $CD4^+$ in WT and 44.4 ± 1.4% in UCP2-/- mice. $CD4^+$ frequencies in ILN only showed negligible differences (WT 51.4 ± 1.2 and UCP2-/- 53.0 ± 2.4%).

Figure 4-3B shows frequencies of $CD3^+$ $CD8^+$ T-cells in spleen, ILN and brain of WT and UCP2-/- mice in EAE 21 days post immunisation. No difference in $CD8^+$ T-cells was detectable in spleen of WT (21.1 ± 2.3%) compared to UCP2-/- (21.7 ± 3.0%), but UCP2-/- mice displayed less $CD8^+$ T-cells in ILN compared to WT mice (WT 34.8 ± 2.9 and UCP2-/- 26.7 ± 3.3%). Again, the biggest difference was observed in the brain were 20.3 ± 6.3% of $CD3^+$ cells were $CD8^+$ compared to only 8.8 ± 3.0% in UCP2-/-. WT mice therefore showed double as many CD8 single positive T-cells as UCP2-/- mice in brains.

Figure 4-4 shows the frequencies of $CD3^+$ $\gamma\delta^+$ T-cells in spleen, ILN and brain of WT and UCP2-/- mice in EAE 21 days post immunisation. $\gamma\delta^+$ T-cells were more abundant in all analysed tissues in UCP2-/- compared to WT mice. In spleen, 3.4 ± 0.6 and 4.2 ± 0.6% of $CD3^+$ T-cells were also γδ positive in WT and UCP2-/- mice respectively. The biggest difference was found in ILN were $\gamma\delta^+$ T-cells were increased almost 2-fold in UCP2-/- (5.6 ± 2.7%) compared to WT mice (2.6 ± 0.3%). This trend continues to show in brains of EAE mice, where 4.1 ± 1.0 (WT) and 6.1 ± 1.4% (UCP2-/-) of $CD3^+$ T-cells were also positive for γδ.

Although these trends were not significant, $\gamma\delta^+$ T-cells were increased in UCP2-/- compared to WT mice in all investigated tissues. Table A-4 (Appendix) summarizes all CD3 positive CD4, CD8 and γδ positive T-cell subsets in EAE mice.

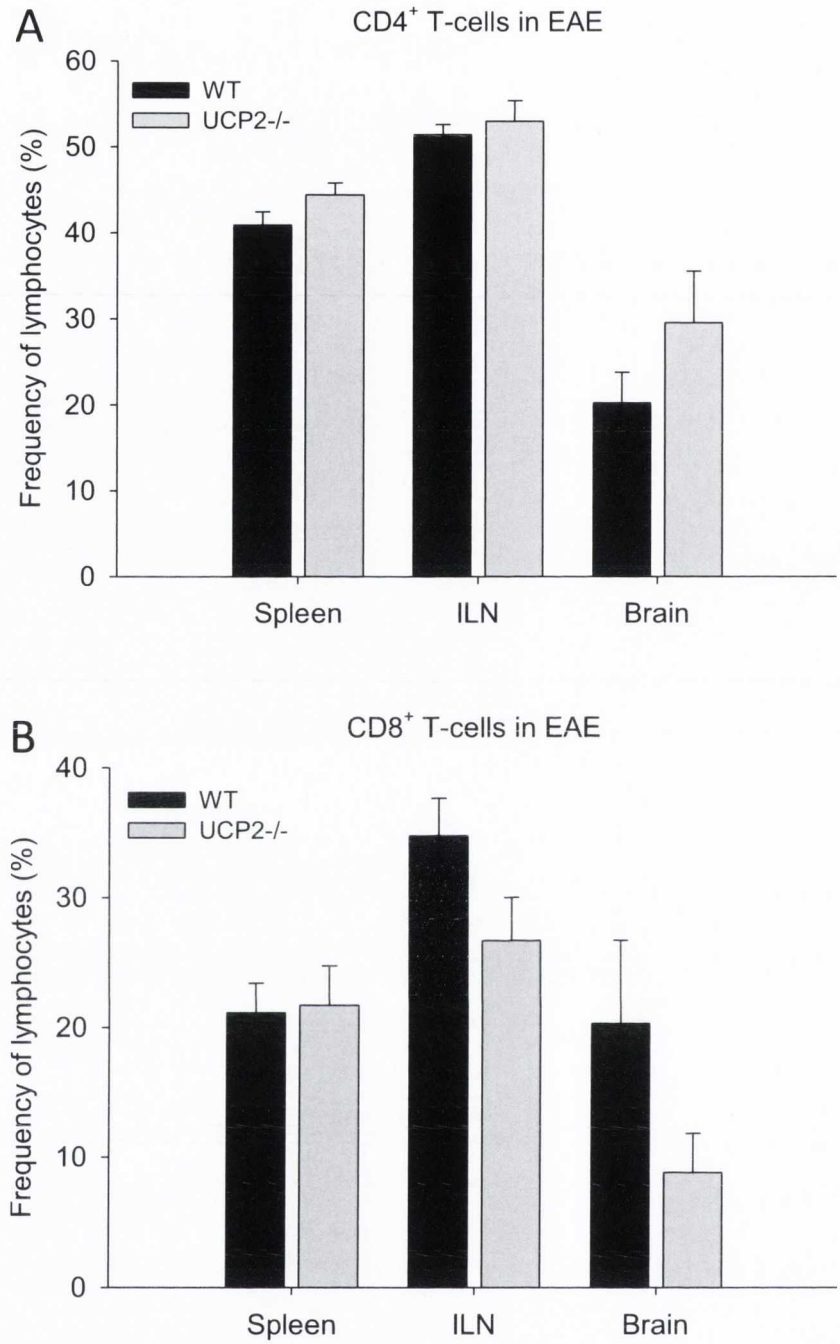


Figure 4-3: Ablation of UCP2 does not change the frequency of CD4 or CD8 T-cells in spleen, ILN and brains of EAE mice

Mononuclear cells were isolated from spleen, ILN and brain of perfused WT (black) and UCP2-/- (grey) animals 21 days after induction of EAE with MOG/CFA. Cells were stained for surface CD4 and CD8 and analysed by FACS. Results are frequencies (in % of live lymphocytes) of CD4 (A) and CD8 (B) positive T-cell frequencies in spleen, ILN and brain of WT and UCP2-/- mice. Values are means ± SEM of 6 independent experiments with 5 animals per group per experiment. P values ≤ 0.05 on unpaired student's t-test were deemed significant (* $P \leq 0.05$; ** $P \leq 0.01$; *** $P \leq 0.001$).

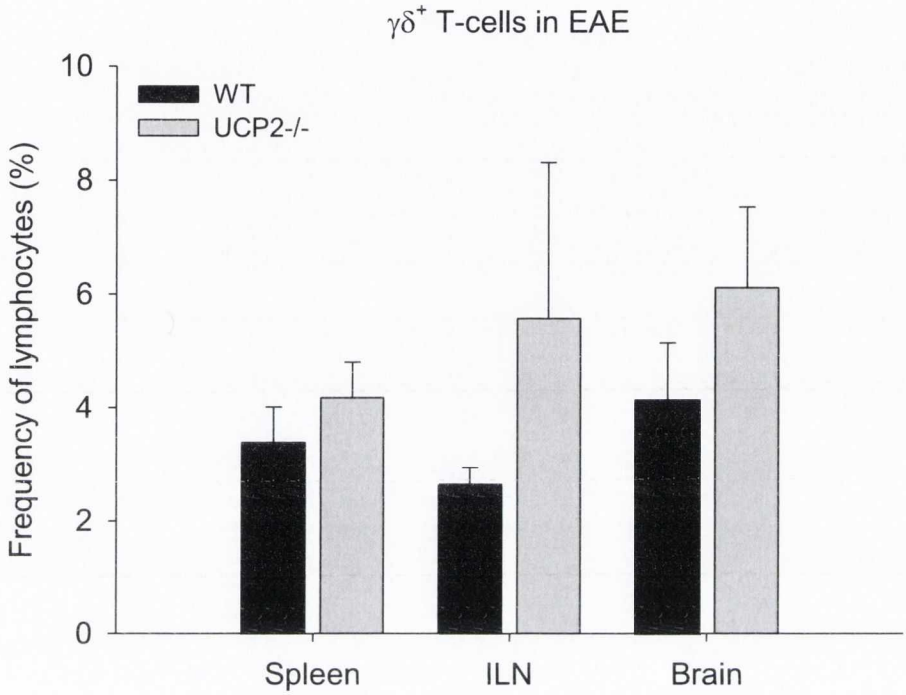


Figure 4-4: Ablation of UCP2 does not change the frequency of γδ T-cells in spleen, ILN and brains of EAE mice

Mononuclear cells were isolated from spleen, ILN and brain of perfused WT (black) and UCP2-/- (grey) animals 21 days after induction of EAE with MOG/CFA. Cells were stained for surface γδ markers and analysed by FACS. Results are frequencies (in % of live lymphocytes) of γδ positive T-cell frequencies in spleen, ILN and brain of WT and UCP2-/- mice. Values are means ± SEM of 6 independent experiments with 5 animals per group per experiment. P values ≤ 0.05 on unpaired student's t-test were deemed significant (* $P \leq 0.05$; ** $P \leq 0.01$; *** $P \leq 0.001$).

4.3.4 IL-17 positive T-cells in brain, spleen and ILN of WT and UCP2-/- EAE mice

After surface staining with colour-conjugated antibodies and permeabilization and fixation of the cells, specific pro-inflammatory cytokines were stained with intracellular antibodies for FACS analysis. The intracellular staining of T-cells against IL-17 and IFNγ gave new insights to the actual composition of the immune response to EAE challenge and possible involvement of UCP2.

The following section illustrates the frequencies of IL-17 positive CD4 (Figure 4-5A), CD8 (Figure 4-5B) and γδ (Figure 4-6) positive T-cells within the $CD3^+$ population of mononuclear cells isolated from spleen, ILN and brain of EAE challenged WT and UCP2-/- mice 21 days post immunization with MOG/CFA.

Figure 4-5A shows frequencies of IL-17^+ $CD4^+$ T-cells in spleen, ILN and brain of WT and UCP2-/- mice. In spleen and ILN very small proportions of the total $CD4^+$ T-cell population were also IL-17 positive. In comparison, a much larger amount of CD4 positive T-cells were positive for IL-17 in brains of WT (13.1 ± 3.1%) and UCP2-/- (11.1 ± 2.6%) mice. The frequencies of IL-17 producing $CD4^+$ T cells showed no variance neither in spleens of mice of both genotypes (WT 3.1 ± 0.4 and UCP2-/- 2.9 ± 0.5%) nor in ILN of WT (2.0 ± 0.2%) and UCP2-/- (2.8 ± 0.8%) mice. The almost 4-fold increased frequency of IL-17 positive $CD4^+$ T-cells in brains compared to peripheral tissues of both genotypes clearly illustrates, that the brain as part of the CNS is the target tissue of the autoimmune reaction in EAE.

Figure 4-5B displays frequencies of IL-17 positive $CD8^+$ T-cells in spleens, ILN and brains of WT and UCP2-/- mice in EAE 21 days post immunisation. Alterations in frequencies of IL-17 positive $CD8^+$ T-cells between genotypes were detected neither in brains nor in ILN or spleens. As seen before in IL-17 positive $CD4^+$ T-cells (Figure 4-5A), spleens and ILN as peripheral tissues showed only small amounts of IL-17 positive $CD8^+$ T-cells, whereas numbers in brains of both genotypes were 4-fold higher compared to peripheral tissues. In spleen only 1.8 ± 0.2 and 2.2 ± 0.3% of $CD8^+$ cells were also IL-17 positive in WT and UCP2-/-. ILN only showed 1.2 ± 0.2 (WT) and 1.0 ± 0.3% (UCP2-/-) of

$CD8^+$ T-cells were IL-17 positive while in brains of WT and UCP2-/- mice 10.0 ± 2.8 and 9.9 ± 3.3% were IL-17 positive.

Figure 4-6 shows frequencies of IL-17 positive $\gamma\delta^+$ T-cells in spleen, ILN and brain of WT compared to UCP2-/- mice in EAE 21 days post immunisation. In spleens 29.4 ± 5.8 and 30.9 ± 5.2% of $\gamma\delta^+$ T-cells were also IL-17 positive in WT and UCP2-/- mice. ILN contained the highest amount of IL-17 positive $\gamma\delta^+$ T-cells with 36.3 ± 7.05 in WT and 33.4 ± 5.9% in UCP2-/- animals compared to 18.8 ± 4.7 and 13.2 ± 2.6% in brains of WT and UCP2-/- mice respectively.

Altogether, no significant differences in any IL-17 positive T-cell population were detectable, nonetheless a trend towards reduced IL-17 positive $CD4^+$ and IL-17 positive $\gamma\delta^+$ T-cell frequencies in brains of UCP2-/- compared to WT mice (Figure 4-5A and Figure 4-6) was observed, whereas no such trend was found in peripheral tissues (spleen or ILN) of these animals. $\gamma\delta^+$ T-cells are known as a source of IL-17 in inflammation and are also thought to play a major role in disease progression and severity of MS and EAE. It is therefore not surprising to see that larger contingents of $\gamma\delta^+$ T-cells were producing IL-17 in the target tissues compared to the other analysed T-cell populations. However, it is important to keep in mind that only very little T-cells are $\gamma\delta$ positive compared to the amount of CD4 and CD8 T-cells present, as seen in Figure 4-5 and Figure 4-6. Table A-5 (Appendix) summarizes all frequencies of IL-17 positive $CD4^+$, $CD8^+$ and $\gamma\delta^+$ T-cells in EAE mice.

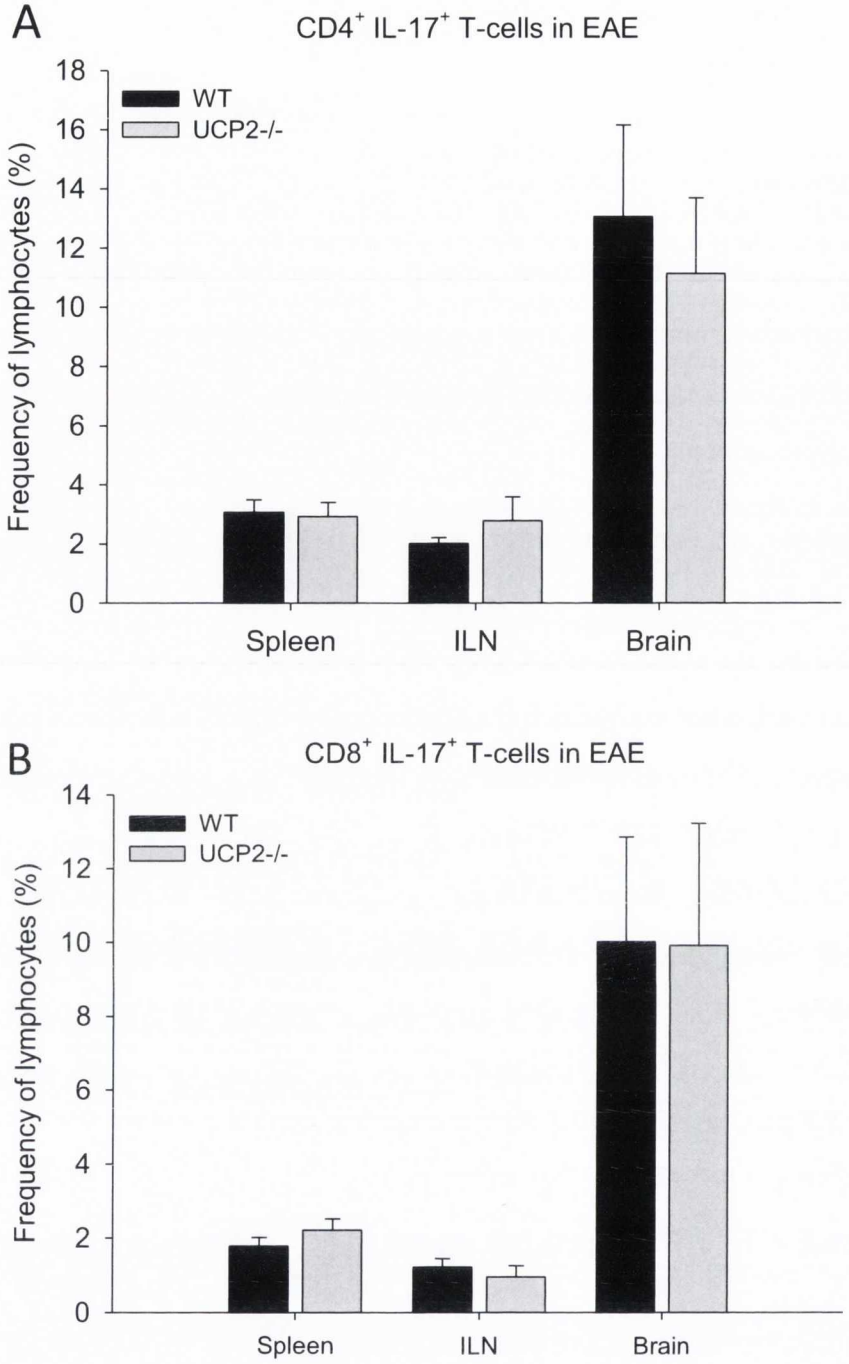


Figure 4-5: Ablation of UCP2 does not change the frequencies of IL-17 positive CD4 or CD8 positive T-cells in spleen, ILN and brains of EAE mice

Mononuclear cells were isolated from spleen, ILN and brain of perfused WT (black) and UCP2-/- (grey) animals 21 days after induction of EAE with MOG/CFA. Cells were stained for surface CD4 (A) and CD8 (B) and intracellular IL-17 and analysed by FACS. Results are frequencies (in % of $CD3^+$ cells) of IL-17 positive CD4 or CD8 positive T-cell frequencies in spleen, ILN and brain of WT and UCP2-/- mice. Values are means ± SEM of 6 independent experiments with 5 animals per group per experiment. P values ≤ 0.05 on unpaired student's t-test were deemed significant (* $P \leq 0.05$; ** $P \leq 0.01$; *** $P \leq 0.001$).

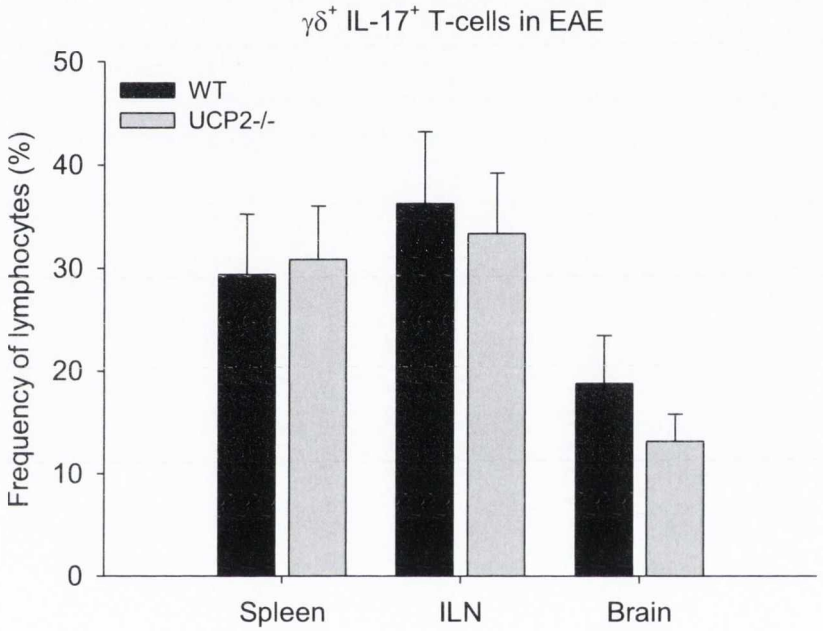


Figure 4-6: Ablation of UCP2 does not change the frequencies of IL-17 positive γδ positive T-cells in spleen, ILN and brains of EAE mice

Mononuclear cells were isolated from spleen, ILN and brain of perfused WT (black) and UCP2-/- (grey) animals 21 days after induction of EAE with MOG/CFA. Cells were stained for surface γδ and intracellular IL-17 and analysed by FACS. Results are frequencies (in % of $CD3^+$ cells) of IL-17 positive γδ positive T-cell frequencies in spleen, ILN and brain of WT and UCP2-/- mice. Values are means ± SEM of 6 independent experiments with 5 animals per group per experiment. P values ≤ 0.05 on unpaired student's t-test were deemed significant (* $P \leq 0.05$; ** $P \leq 0.01$; *** $P \leq 0.001$).

4.3.5 IFNγ positive T-cells in brain, spleen and ILN of WT and UCP2-/- mice in EAE

After investigation of the role of IL-17 positive T-cell populations in EAE in different tissues of WT and UCP2 knock-out mice, the same method was applied to investigate IFNγ positive T-cell frequencies in tissues of EAE mice.

The following section illustrates the frequencies of IFNγ positive CD4 (Figure 4-7A), CD8 (Figure 4-7B) and γδ (Figure 4-8) positive T-cells within the $CD3^+$ population of mononuclear cells isolated from spleen, ILN and brain of EAE challenged WT and UCP2-/- mice 21 days post immunization with MOG/CFA.

Figure 4-7A illustrates IFNγ positive $CD4^+$ T-cells in spleen, ILN and brain of WT and UCP2-/- mice. In spleens of WT mice 14.2 ± 6.3% of CD4 T-cells were also IFNγ positive compared to only 6.2 ± 1.6% in UCP2-/-. No differences were detectable between genotypes in ILN and brains with 1.3 ± 0.1 and 2.2 ± 0.9% in ILN and 18.2 ± 3.7 and 18.0 ± 3.3% in brains of WT compared to UCP2 mice respectively.

Figure 4-7B shows the frequencies of $IFN\gamma^+$ cells within $CD8^+$ T-cell populations in spleen, ILN and brain of EAE challenged WT and UCP2 mice. As was demonstrated for IFNγ positive $CD4^+$ T-cells in spleen seen in Figure 4-7A, only half the amount of $CD8^+$ T-cells were IFNγ positive in spleens of UCP2-/- mice compared to WT (WT 20.5 ± 5.8 and UCP2-/- 9.8 ± 2.4%). ILN of WT (8.8 ± 0.9%) compared to UCP2-/- (7.6 ± 1.5%) mice did not show any differences in IFNγ positive $CD8^+$ T-cells. Almost half of all brain invading $CD8^+$ T-cells were also IFNγ positive, but these frequencies were no different in WT (45.5 ± 9.4%) compared to UCP2-/- (38.9 ± 9.0%) mice. The highest percentage of IFNγ positive T-cells were $CD8^+$ T-cells in all three analysed tissues compared to $CD4^+$ and $\gamma\delta^+$ T-cells, which potentially makes $CD8^+$ T-cells the most potent producers and major source of IFNγ particularly in brains of infected mice.

The percentage of IFNγ positive $\gamma\delta^+$ T-cell population was consistently elevated in WT compared to UCP2-/- mice in all three investigated tissues, as seen in Figure 4-8. WT mice showed double the percentage of IFNγ positive $\gamma\delta^+$ T-cells in spleen compared to UCP2-/- mice (WT 10.0 ± 3.3 and UCP2-/- 5.0 ± 1.7%). This elevation was not as distinct in

ILN and brain as in spleen, but an overall trend towards elevated IFNγ^+ T-cell populations in WT compared to UCP2-/- was present. In ILN WT showed 4.2 ± 1.0% compared to 3.0 ± 0.7% in UCP2-/- mice. The portion of IFNγ positive CD8$^+$ cells in brains of WT was also slightly higher compared to UCP2-/- (WT 5.6 ± 1.5 and UCP2-/- 4.7 ± 1.5%).

Although all these differences were not significant, they still reflect and confirm a trend towards reduced pro-inflammatory cytokine positive T-cell populations in UCP2-/- mice compared to WT at 21 days post immunisation with MOG/CFA. This trend was already seen with IL-17 positive T-cell populations in Figure 4-5 and Figure 4-6.

Table A-6 (Appendix) summarizes all frequencies of IFNγ positive CD4$^+$, CD8$^+$ and $\gamma\delta^+$ T-cells in EAE mice.

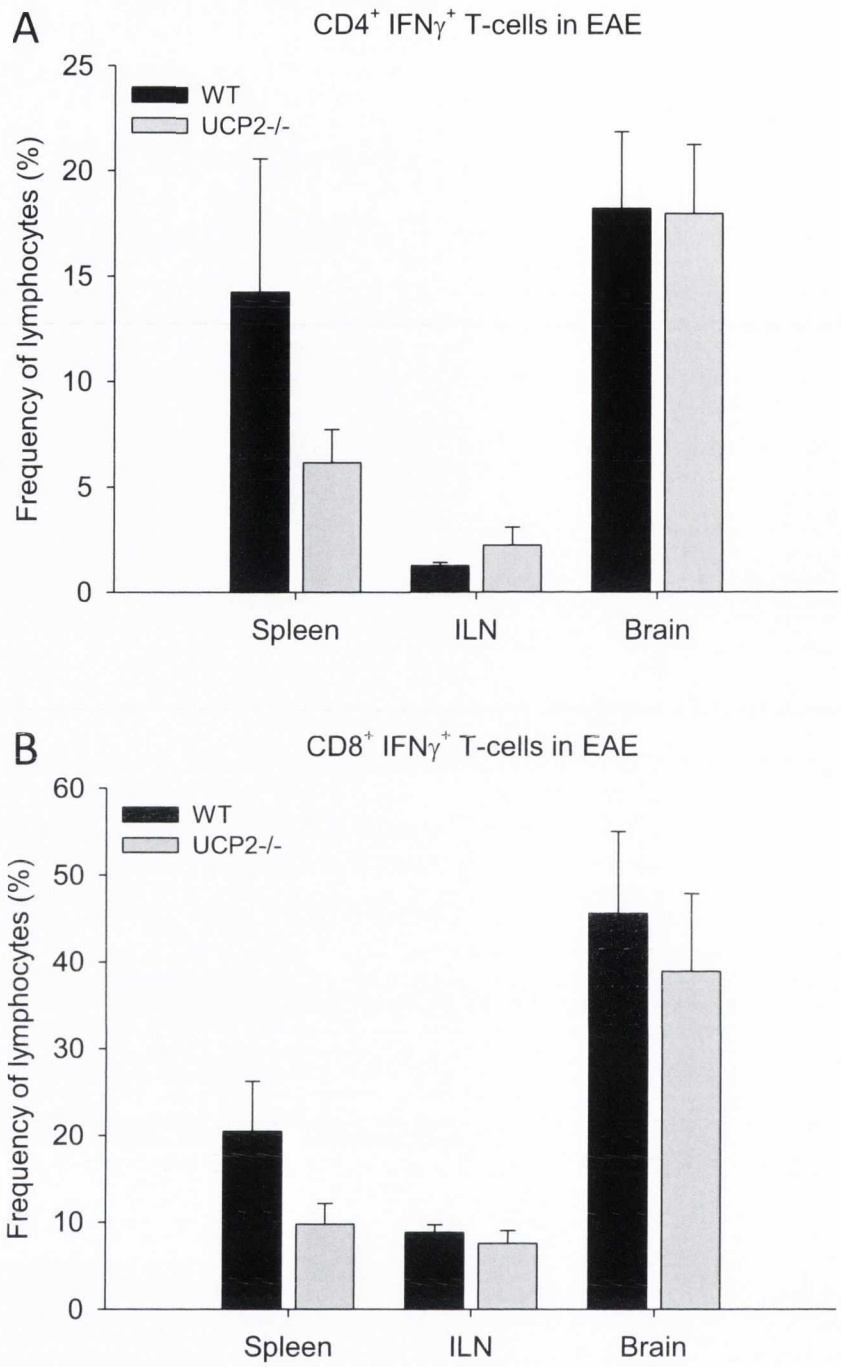


Figure 4-7: Ablation of UCP2 does not change the frequencies of IFNγ positive CD4 or CD8 positive T-cells in spleen, ILN and brains of EAE mice

Mononuclear cells were isolated from spleen, ILN and brain of perfused WT (black) and UCP2-/- (grey) animals 21 days after induction of EAE with MOG/CFA. Cells were stained for surface CD4 (A) and CD8 (B) and intracellular IFNγ and analysed by FACS. Results are frequencies (in % of $CD3^+$ cells) of IFNγ positive CD4 or CD8 positive T-cell frequencies in spleen, ILN and brain of WT and UCP2-/- mice. Values are means ± SEM of 6 independent experiments with 5 animals per group per experiment. P values ≤ 0.05 on unpaired student's t-test were deemed significant (* $P \leq 0.05$; ** $P \leq 0.01$; *** $P \leq 0.001$).

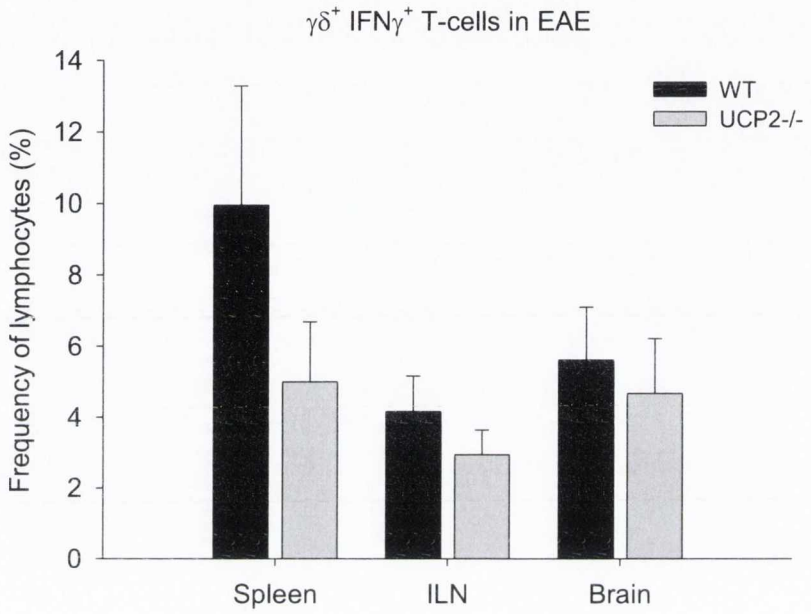


Figure 4-8: Ablation of UCP2 does not change the frequencies of IFNγ positive γδ positive T-cells in spleen, ILN and brains of EAE mice

Mononuclear cells were isolated from spleen, ILN and brain of perfused WT (black) and UCP2-/- (grey) animals 21 days after induction of EAE with MOG/CFA. Cells were stained for surface γδ and intracellular IFNγ and analysed by FACS. Results are frequencies (in % of $CD3^+$ cells) of IFNγ positive γδ positive T-cell frequencies in spleen, ILN and brain of WT and UCP2-/- mice. Values are means ± SEM of 6 independent experiments with 5 animals per group per experiment. P values ≤ 0.05 on unpaired student's t-test were deemed significant (* $P \leq 0.05$; ** $P \leq 0.01$; *** $P \leq 0.001$).

4.3.6 IL-17 and IFNγ cytokine profile in EAE

Antigen recall experiments were performed to determine the absolute MOG-specific cytokine production of infiltrating and residual T-cells in spleen and ILN. T-cells isolated from tissues of WT and UCP2-/- mice 21 days post immunization were stimulated with varying amounts of MOG and IL-17 and IFNγ production was measured with ELISA. No cytokine production data could be generated for mononuclear cells isolated from brains of EAE mice because all cells isolated from brain tissue were used for FACS analyses. This is unfortunate as the brain is the representative tissue for the whole CNS and thus the target site of myelin destruction and the triggering of clinical symptoms in EAE. However, it can be assumed, that the state and activity of tissue infiltrating MOG-specific T-cells in the brain is reflected by the cytokine production of MOG specific infiltrating and residual cells in spleen and ILN.

Before ELISA, cells (2×10^5) of spleen and ILN single cell suspensions of EAE mice were stimulated with increasing amounts of MOG, medium alone as negative and background control or PMA and anti-CD3 as a positive control for three days. Following the incubation cells were pelleted by centrifugation and supernatants taken to be analysed by sandwich ELISA with IL-17 and IFNγ primary antibodies.

Figure 4-9 and Figure 4-10 show the MOG-specific cytokine production of spleen and ILN from WT and UCP2-/- mice after re-stimulation with increasing concentrations of MOG at 21 days post induction of EAE by immunization with MOG. IL-17 and IFNγ production in spleen (Figure 4-9) and ILN (Figure 4-10) of EAE mice were analysed.

The production of IL-17 protein by splenocytes of WT and UCP2-/- mice showed no significant differences (Figure 4-9A). There was a small trend to a slightly higher IL-17 production in UCP2-/- compared to WT cells in all three doses of MOG. The production of IL-17 protein following re-stimulation was overall dose-dependent with increasing amounts of MOG stimulating increased IL-17 production of cells to the same extent in WT and UCP2-/- splenocytes. PMA/aCD3 treated cells showed the highest IL-17 production rates of all tested conditions and no difference was detectable between genotypes in this positive control. However, WT cells treated with medium alone (negative control) showed reduced IL-17 background production rates compared to UCP2-/- lymphocytes. In general

IL-17 production rates were slightly elevated in splenocytes of UCP2-/- mice compared to WT cells.

MOG specific production of IFNγ protein by antigen recall in splenocytes is shown in Figure 4-9B. As before with IL-17 (Figure 4-9A), re-stimulation with increasing amounts of MOG resulted in a non-linear, but dose-dependent increase of IFNγ protein production by splenocytes. WT showed slightly lower concentrations of IFNγ compared to UCP2-/- in all MOG stimulations. However, the signal was increased in UCP2-/- compared to WT in negative (medium alone) controls, indicating a higher unspecific background production of IFNγ protein in KO cells. On the other hand the maximal IFNγ production potential represented by the positive control with phorbol mysteric acid (PMA) and an anti-CD3 antibody (aCD3) was reduced in UCP2-/- mice compared to WT.

Figure 4-10A illustrates IL-17 production in re-stimulated lymphocytes isolated from ILN of WT and UCP2-/- mice 21 days post immunisation with MOG/CFA. WT cells showed slightly elevated IL-17 production compared to UCP2-/- cells in all three MOG treated conditions in a dose dependent manner. However, reactivation of ILN cells with MOG resulted in only small increases in IL-17 production compared to the rates seen for the negative control (medium only). The background production rate of ILN cells was very similar in both genotypes. Stimulation with PMA/aCD3 as positive control resulted in the highest signal as expected, but UCP2-/- showed slightly reduced production of IL-17 potentially indicating a reduced total productive capacity in cells lacking UCP2.

IFNγ protein produced by ILN lymphocytes (Figure 4-10B) showed the same pattern as seen in Figure 4-9B with only slightly elevated production of IFNγ in WT compared to UCP2-/- cells after stimulation with MOG. This response was dose dependent as well, but showed only little increase in IFNγ production due to MOG compared to the treatment with medium only (negative control). The background production rate of IFNγ was also not altered in ILN cells comparing WT and UCP2-/-. However, positive control cells of UCP2-/- mice treated with PMA/aCD3 produced slightly more IFNγ compared to WT cells.

Taken together, cells isolated from spleen or ILN showed different patterns when comparing WT and UCP2-/- cells. While WT splenocytes showed lower production of cytokines after stimulation with MOG, WT cells isolated from ILN produced slightly more

cytokines than UCP2-/- cells. However, none of these differences were significant and were only trends. As expected, PMA/aCD3 completely activated $CD3^+$ cells and resulted in the highest measured cytokine production and was slightly reduced in cells from UCP2 knock-out mice. This indicates a potential, minor effect of UCP2 on overall cytokine production capacity in the analysed cells.

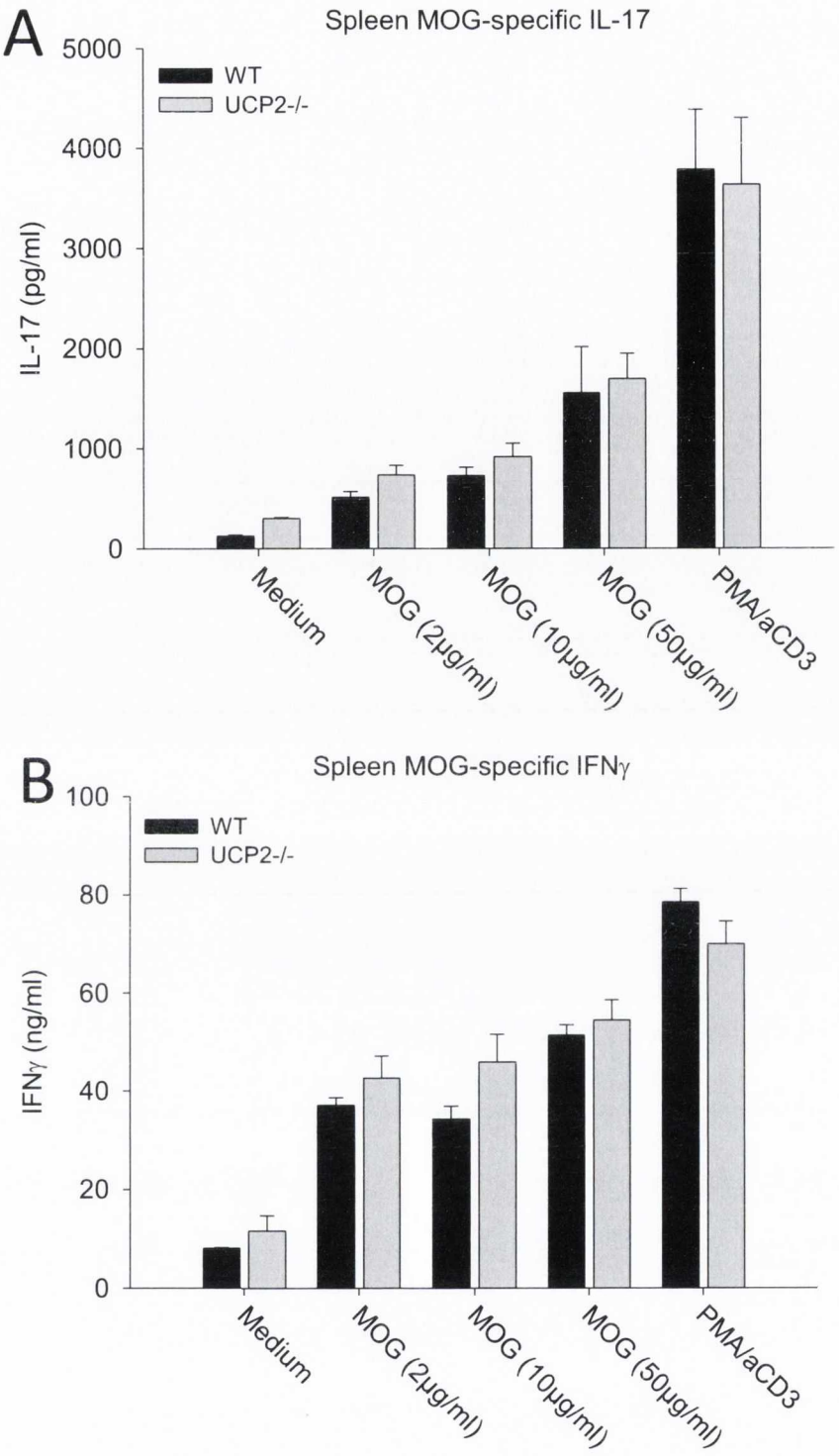


Figure 4-9: Ablation of UCP2 does not affect IL-17 or IFNγ production of spleen of EAE mice

Mononuclear cells were isolated from spleens of perfused WT (black) and UCP2-/- (grey) animals 21 days after induction of EAE with MOG/CFA. After incubation of cells with medium alone (negative control), increasing concentrations of MOG or PMA/aCD3 (positive control) for 3 days, the MOG-specific IL-17 (A) and IFNγ (B) production of WT and UCP2-/- cells was measured by ELISA in an antigen recall experiment. P values ≤ 0.05 on unpaired student's t-test were deemed significant (* $P \leq 0.05$; ** $P \leq 0.01$; *** $P \leq 0.001$).

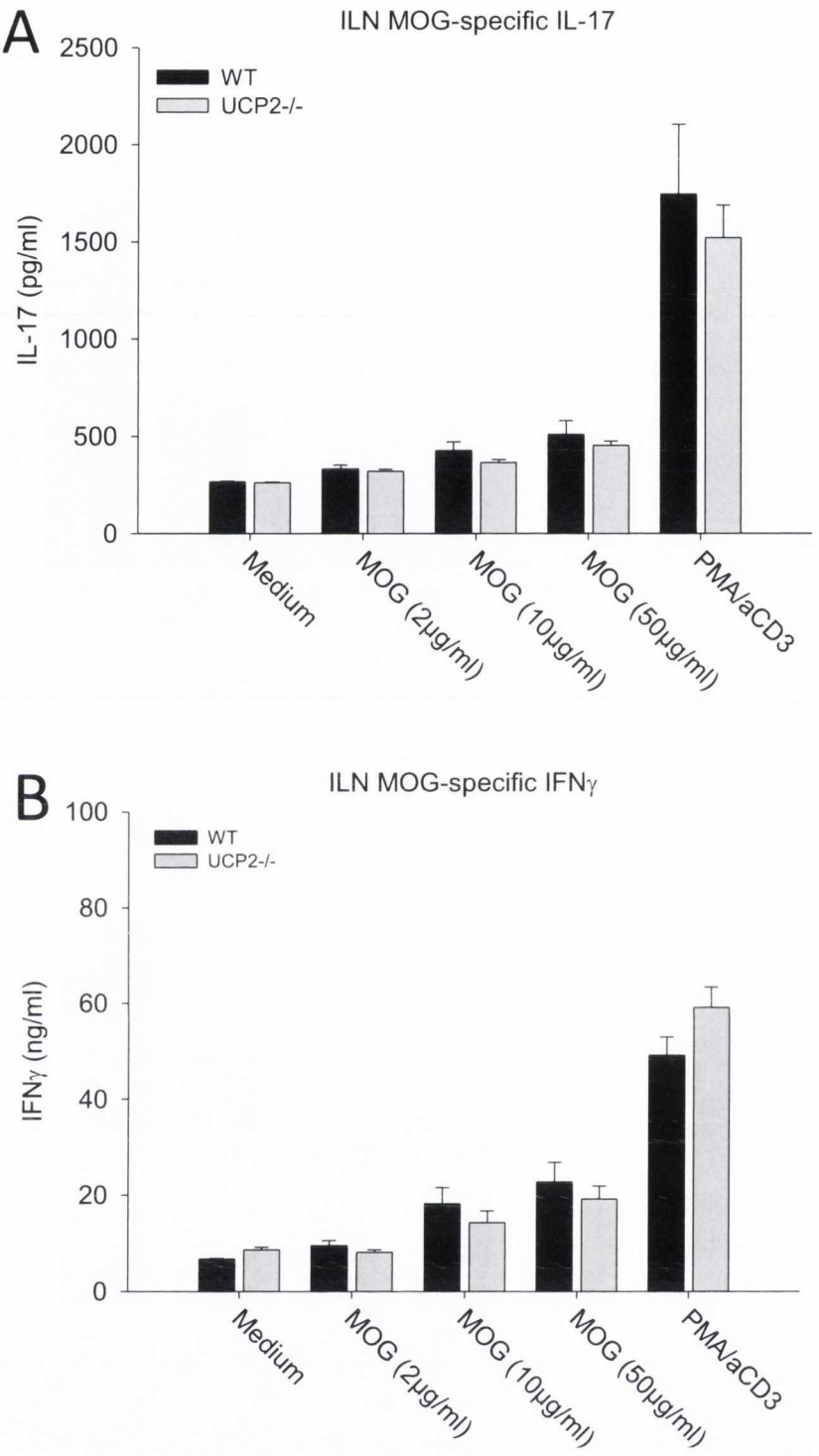


Figure 4-10: Ablation of UCP2 does not affect IL-17 or IFNγ production in ILN of EAE mice

Mononuclear cells were isolated from ILN of perfused WT (black) and UCP2-/- (grey) animals 21 days after induction of EAE with MOG/CFA. After incubation of cells with medium alone (negative control), increasing concentrations of MOG or PMA/aCD3 (positive control) for 3 days, the MOG-specific IL-17 (A) and IFNγ (B) production of WT and UCP2-/- cells was measured by ELISA in an antigen recall experiment. P values ≤ 0.05 on unpaired student's t-test were deemed significant (* $P \leq 0.05$; ** $P \leq 0.01$; *** $P \leq 0.001$).

4.4 Discussion

The aim of the study described in this chapter was to investigate the role of UCP2 in EAE, a murine model of MS. The study was based primarily on a publication by Vogler *et al.* (2006) who reported, that ablation of UCP2 caused a more serious development of EAE. Among the differences between UCP2 knock-out mice and WT controls observed by Vogler *et al.* (2006) was a significantly higher clinical score from 16 days post immunisation and a delayed onset of the disease in mice not expressing UCP2 (Vogler *et al.* 2006). I set out to reconfirm the results of Vogler et al. (2006) and determine whether other pro-EAE T-cells, not considered by Vogler *et al.* (2006) were involved. In addition to CD4 and CD8 positive T-cells, Th_{17} and $\gamma\delta$ T-cells as well as the production of IL-17 and IFNγ by these individual populations was investigated. IL-17 produced by Th_{17} T-cells, a distinct T-cell line of $CD4^+$ T-cells, and by $\gamma\delta$ T-cells has been reported to be of fundamental importance in EAE and MS. Within the CD4 positive T-cell populations, IL-17 produced by Th_{17} cells and IFNγ primarily produced by Th_1 cells seems to be vital in triggering and maintaining autoimmune tissue inflammation in MS and EAE (Zamvil *et al.* 1990; Liblau *et al.* 1995). However, IFNγ is not simply a pro-inflammatory cytokine, but appears to be important in moderation of disease progression and severity. Thus a controlling function cannot be disqualified, which adds to the complexity of the underlying mechanisms of disease onset and progression.

The time courses of body mass and clinical score in Figure 4-1A and B both show an earlier onset of disease in WT compared to UCP2-/- mice, but not a more serious development of the disease. Vogler and colleagues reported a delayed onset of the disease in UCP2 knock-out animals (Vogler *et al.* 2006) and this observation was confirmed by my experiments. However, Vogler *et al.* (2006) also reported the development of a more severe disease, as evidenced by a higher clinical score in UCP2-/- mice compared to WT controls from 17 days after EAE induction. In my experiments, the clinical score and hence disease severity did not differ between WT and UCP2 knock-out mice, suggesting that UCP2 does not protect from EAE.

The induction of EAE was similar in my experiments and the study by Vogler *et al.* (2006), but a few discrepancies emerge. Vogler *et al.* (2006) used 150µg of MOG dissolved in water and emulsified with 50µl of CFA with 4mg/ml *Mycobacterium tuberculosis* to

induce EAE followed by two injections of 400ng of pertussis toxin at days 0 and 2. I used only 100µg MOG, but emulsified with 100 µl CFA (also with 4mg/ml *Mycobacterium tuberculosis*). Following EAE induction two injections of 500ng of pertussis toxin were given at days 0 and 2. In summary, Vogler *et al.* (2006) used more MOG, less CFA and less pertussis toxin in their induction of EAE compared to my protocol.

It is noteworthy that in the time course presented by Vogler *et al.* (2006) the increase in disease severity in UCP2 knock-out mice from day 17 onward was quite sudden, while disease progression of UCP2 knock-out mice was very similar to that of WT mice before day 17. Moreover, WT control mice only reached an average clinical score of around 1.5 and UCP2 knock-out mice a clinical score around 2.5, but only late in the time course of the disease (from day 17). These facts are surprising, as according to Hooke laboratories a professional company, which provides MOG/CFA kits for induction of EAE and uses a very similar guide to that described by Vogler *et al.* (2006) to score clinical disease severity in EAE mice, MOG immunized C57/Bl6 mice usually develop a progressive form of EAE with the first clinical symptoms showing between 8 and 10 days after induction of EAE and a steady worsening of the symptoms up to 14 days. In addition, 14 days after EAE induction the clinical symptoms normally remain unchanged and mice show an average clinical score of 3.2 to 3.5 (Hooke Laboratories). However, in the study by Vogler *et al.* (2006) WT controls only develop a very low clinical disease score, while UCP2 knock-out mice developed a clinical score matching that described by Hooke Laboratories for WT control mice. WT and UCP2 knock-out mice in my experiments, however, showed clinical symptoms with an average clinical score comparable to that shown by Hooke Laboratories. It would therefore appear that Vogler *et al.* (2006) did not fully induce EAE in all mice used in the experiment.

Another interesting observation was that in my experiments the animals started to gain weight from 15 days after induction of EAE, which is indicative of remission. Clinical scores remained the same even after WT animals restored their body weight at 25 days after EAE induction to the weight they had at the beginning of the experiments. Unfortunately Vogler *et al.* (2006) did not show body weight data for their EAE mice, but they did not see any kind of remission, rather a progressive form of the disease. Moreover, in my study not only the disease onset occurred earlier in WT mice, but also disease remission and subsequent recovery of bodyweight appeared to start earlier in WT

compared to UCP2-/- mice. Taken together, my experiments showed that ablation of UCP2 resulted in a delayed onset of the disease, but did not affect overall disease severity or progression.

While there were discrepancies on the level of disease onset and progression between the results shown by Vogler *et al.* (2006) and the results obtained in my study, similarities between the two studies were found on a cellular level. No significant differences in frequencies of $CD4^+$, $CD8^+$ or $\gamma\delta^+$ T-cell and IL-17 or IFNγ positive subsets were detected in brain, spleen or ILN between genotypes 21 days after immunisation with MOG/CFA, thereby confirming the observations of Vogler *et al.* (2006) who also saw no differences in $CD4^+$ or $CD8^+$ T-cell numbers. In my study, the role of a third T-cell population ($\gamma\delta$ T-cells) in EAE was investigated, but no alterations in frequencies of infiltrating $\gamma\delta$ T-cells due to ablation of UCP2 were observed. Additionally, frequencies of IL-17 and IFNγ positive CD4, CD8 and $\gamma\delta$ positive T-cells remained unaffected by UCP2 knock-out. This observation was confirmed by analyses of IL-17 and IFNγ protein production by splenocytes and lymphocytes of WT and UCP2 knock-out mice in antigen recall experiments (ELISA), which showed no significant differences between genotypes.

It appears that the earlier onset of the clinical symptoms in WT mice observed in the present study was not caused by any of the parameters measured here, but may well be due to increased TNFα and IL-2 positive $CD4^+$ and $CD8^+$ T-cells described by Vogler *et al.* (2006). In my study, measurement of IL-17 and IFNγ were favoured over measurement of TNFα and IL-2 as IL-17 and IFNγ have been reported to be of central role in the development and progression of EAE (Zamvil *et al.* 1990; Liblau *et al.* 1995; Aggarwal *et al.* 2003; Langrish *et al.* 2005). Interestingly, $CD8^+$ T-cells showed the highest portion of IFNγ^+ T-cells in EAE in spleen, ILN and brain of WT and UCP2-/- mice (Figure 4-7B), potentially identifying them as the major source of interferon. As described in the introduction, IFNγ is vital for disease initiation and progression particularly from Th_1 cells, but also for differentiation of Th_{17} cells (O'Connor *et al.* 2008). However, IFNγ is also involved in disease control and moderation thus no clear pro- or anti-inflammatory function can be attributed to IFNγ. Reduced numbers of IFNγ positive $CD4^+$, $CD8^+$ and $\gamma\delta^+$ T-cells in spleens, but not ILN or brains from UCP2-/- animals may imply, that the circulating IFNγ was reduced, but this was not reflected by cytokine titres measured by

ELISA (Figure 4-9 and Figure 4-10). Thus, alterations in frequencies of cytokine positive T-cells do not necessarily have to mirror actual cytokine levels and confirmation of cytokine production by ELISA is important for meaningful results.

Although frequencies of $CD4^+$, $CD8^+$ and $\gamma\delta^+$ T-cells were similar or lower in brains compared to spleen and ILN of WT and UCP2-/- mice, IL-17 and IFNγ positive proportions of CD4 and CD8 positive cells were highest in brains of animals in EAE (Figure 4-5 and Figure 4-7). This reflects the high inflammatory state of the CNS compared to peripheral tissues. Unfortunately, all brain cells were used up for FACS analyses and no additional antigen recall experiments were performed to determine the absolute cytokine production by brain cells of animals subjected to EAE.

One possible explanation for the delayed clinical phenotype in UCP2-/- compared to WT mice could be the fact, that UCP2-/- mice are in a primed inflammatory state (Bai *et al.* 2005) and that IFNγ expression in the CNS prior to immunisation with MOG protects against demyelination (Lin *et al.* 2007). In this respect, an increased inflammatory state due to UCP2 knock-out would be beneficial and reduce the effects of EAE.

In summary, no significant differences in the cellular or cytokine profiles were found in WT compared to UCP2-/- 21 days after EAE induction despite significant shifts in mass and clinical disease score between genotypes. However, WT mice lost weight and developed clinical symptoms earlier than UCP2-/- animals, but also gained weight again at the time of tissue harvest. This indicates that amelioration of UCP2 significant altered the course of EAE, but these alterations could not be identified in this work. The samples were taken quite late in the progression of EAE and experiments around the time of the first clinical symptoms may have resulted in a different outcome and potentially clarified the involvement of UCP2 in disease onset and progression. Moreover, it would be very interesting to compare the acquired data to control animals not immunised with MOG to get a better understanding of the involvement of T-cells and cytokines in EAE and redefine targets for future studies.

UCP2 Bioenergetics

Chapter 5

5 UCP2 bioenergetics

5.1 Introduction

UCP2 protein is known to be expressed primarily in cells of the immune system including macrophages (Arsenijevic *et al.* 2000), thymocytes and splenocytes (Fleury *et al.* 1997; Gimeno *et al.* 1997; Pecqueur *et al.* 2001), but is also prominently expressed in pancreatic β-cells (Krauss *et al.* 2002). In addition, UCP2 protein is expressed in kidney mitochondria at relatively high levels, whereas in liver UCP2 is only present in specialised macrophages (Kupffer cells) and the overall presence of UCP2 protein in whole liver homogenates or isolated mitochondria is negligible (Larrouy *et al.* 1997). Liver mitochondria are therefore used regularly as a negative control in studies involving function of uncoupling proteins. The function of UCP2 remains under investigation, but a substantial amount of research showed that UCP2 is not catalysing a net proton leak (Jaburek *et al.* 1999; Echtay *et al.* 2001; Considine *et al.* 2003; Brand *et al.* 2004a; Brand *et al.* 2004b) and is most certainly not involved in heat generation like UCP1 in BAT. Apart from the presence of UCP2 in immune cells with a probable role in macrophage mediated defence against *Toxoplasma gondii* infection (Arsenijevic *et al.* 2000), UCP2 is also known to have a role in control of glucose sensitive secretion of insulin in pancreatic β-cell islets (for review see Brand *et al.* 2010). The involvement of UCP2 in pancreatic insulin secretion stimulated by glucose is quite well understood (Brand *et al.* 2010), but the role of UCP2 in other cells and tissues is not clear. Several studies have suggested the UCP2 may have a role in "mild-uncoupling" and hence regulation of reactive oxygen species (ROS) production by mitochondria (Negre-Salvayre *et al.* 1997b; Arsenijevic *et al.* 2000; Echtay *et al.* 2002; Krauss *et al.* 2003; Bai *et al.* 2005; Vogler *et al.* 2006; Emre *et al.* 2007b). I chose kidney (high levels of UCP2) and liver (low levels of UCP2) mitochondria from UCP2 knock-out and wild-type mice to test whether UCP2 has a role in "mild-uncoupling" and hence in the regulation of ROS production. More specifically, the experiments were designed to examine the effects of the presence (WT) or absence of UCP2 (UCP2-/-) on oxygen consumption and reactive oxygen species production (ROS) in liver and kidney mitochondria. Succinate and glycerol-3-phosphate were used as substrates, because they both feed electrons to the respiratory chain at the ubiquinone cycle, i.e. succinate via the succinate dehydrogenase (complex II) and glycerol-3-

phosphate via the mitochondrial glycerol-3-phosphate dehydrogenase (mGPDH), but at different sides of the mitochondrial inner membrane (succinate on the inner side and glycerol-3-phosphate on the outer side). In all experiments rotenone was present to prevent electron back flow through complex I and thus generation of ROS at that site. Furthermore, in the case of succinate, the presence of rotenone prevents the accumulation of oxaloacetate and consequently inhibition of the tricarboxylic acid cycle and succinate dehydrogenase activity. The design of these experiments is comparable with the design used by a former member of our laboratory, Kieran Clarke (Clarke 2011). He was able to establish, that BAT mitochondria showed significantly increased respiration rates with glycerol-3-phosphate as substrate and increased mGPDH activity in UCP1-/- mice when compared to WT controls (Clarke 2011). Due to time limitations on his part, Kieran was unable to answer the question as to whether the observed increase in oxygen consumption rate and mGPDH activity were due to elevated mGPDH abundance in UCP1 knock-out mice compared to controls. This latter question pertaining to UCP1 knock-out mice is also addressed in this chapter.

5.2 Results

5.2.1 Increased abundance of mitochondrial glycerol-3-phosphate dehydrogenase in brown adipose tissue mitochondria of UCP1-/- mice

During an earlier investigation of the effects of UCP1 ablation on mitochondrial function (specifically mitochondrial ROS production), increased oxygen consumption rates in BAT mitochondria of UCP1 knock-out compared to WT mice with pyruvate/malate and glycerol-3-phosphate (G3P) as substrates were observed. Subsequent investigation demonstrated that specific activities of complex I and mitochondrial glycerol-3-phosphate dehydrogenase (mGPDH) were increased in BAT mitochondria of UCP1 ablated mice compared to BAT mitochondria of WT mice, but no other respiratory chain complex activities were altered in BAT mitochondria of UCP1-/- mice. Immunodetection of complex I (as measured by subunit NDUFA5) showed significantly more abundant complex I (NADH-dehydrogenase) protein in BAT mitochondria of UCP1-/- mice (compared to wild-type controls) while complex II abundance (succinate dehydrogenase, SDH) remained unchanged. All experiments of the aforementioned observations were performed by Kieran Clarke in the course of his PhD (Clarke, 2011) and a publication of these findings is currently in preparation. However, the question whether mGPDH protein was also more abundant in BAT mitochondria of UCP1-/- compared to WT mice has not been answered yet. I present evidence that mGPDH protein abundance is also significantly elevated in BAT mitochondria of UCP1-/- mice compared to WT animals.

Figure 5-1A shows an immunoblot of mGPDH (at 81kDa) from three independent preparations of BAT mitochondria from WT and UCP1-/- mice and the respective detection of pyruvate dehydrogenase (PDH) as loading control at 44kDa (subunit E1-alpha). The bands for mGPDH in all three preparations of BAT mitochondria from UCP1-/- mice are clearly stronger compared to those from WT mice while the PDH signal remains unchanged. Figure 5-1B shows the ratio of signal density of the respective mGPDH and PDH bands for WT and UCP1-/- BAT mitochondria following densitometric analysis (area under the curve). mGPDH protein abundance was 3-fold greater in BAT mitochondria of UCP1-/- mice compared to mGPDH abundance in BAT mitochondria of WT controls ($P=0.003$). This observation is in line with the functional data, which showed increased

oxygen consumption with G3P as substrate and increased specific mGPDH enzyme activity. It is noteworthy that succinate supported oxygen consumption and SDH specific enzyme activity were not affected by UCP1 ablation in BAT mitochondria.

It is now evident, that increased mitochondrial oxygen consumption with G3P as substrate and increased mGPDH activity per mg mitochondrial protein was due to elevated levels of mGPDH in BAT mitochondria of UCP1-/- mice. In the next section of this chapter I determine whether similar observations also hold true for mitochondria from UCP2-/- mice.

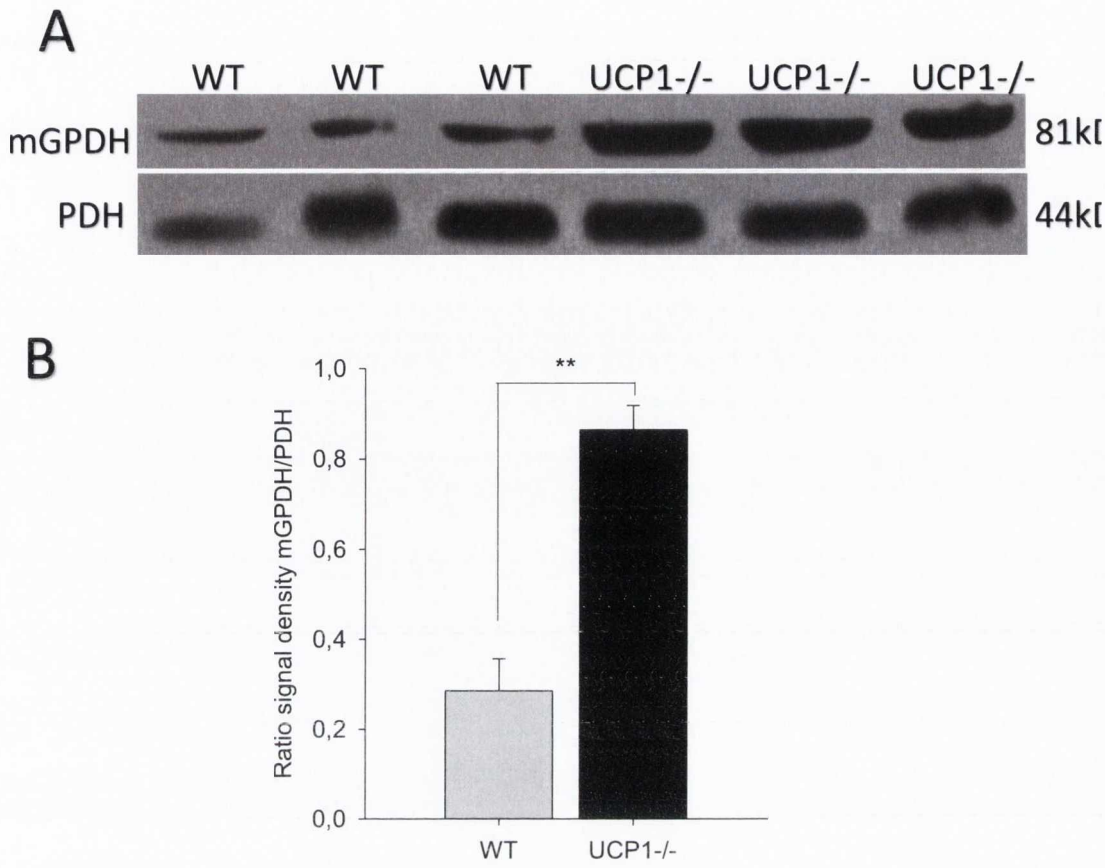


Figure 5-1: UCP1 ablation results in increased mGPDH protein abundance in BAT mitochondria of UCP1-/- mice

(A) Immunoblots of mGPDH expression and PDH loading controls in BAT mitochondria of WT and UCP1-/- mice. Mitochondria were isolated as described in section 2.12 and submitted to western blotting as described in section 2.18, 2.19 and 2.20. Following SDS-PAGE immunoblotting with anti-GPD2 (1:100, Santa Cruz S-16) and anti-PDH-E1-alpha (1:2000, Mitosciences, cat#MSPO3) was performed and expression levels of mGPDH and PDH estimated by densitometry. (B) Densitometry quantification of mGPDH expression in BAT mitochondria of WT and UCP1-/- mice. Data are presented as mean +/- SEM of signal strength of three independent WT and UCP1-/- BAT mitochondria isolations. Densitometry measurements (area under the curve, ImageJ) were done following immunoblotting and expression levels of mGPDH normalized against PDH signals. (One way ANOVA, ** P=0.003)

5.2.2 Increased Glycerol-3-phosphate supported oxygen consumption in liver and kidney mitochondria of UCP2-/- mice

UCP1 ablation results in a decreased steady state oxygen consumption and in increased ROS production in isolated BAT mitochondria with succinate as substrate. Interestingly, G3P supported oxygen consumption and also mGPDH activity and abundance are upregulated by the deletion of UCP1 in BAT mitochondria. In this experiment, the question was addressed if ablation of UCP2, a UCP1 homologue, results in a similar phenotype in UCP2 expressing tissues. To this purpose oxygen consumption and ROS production rates in UCP2 expressing wild-type kidney mitochondria were compared to kidney mitochondria isolated from UCP2 ablated animals and specifically mGPDH activity and abundance were investigated. Liver mitochondria are usually used as negative controls for UCP knock-out effects as no UCPs are expressed in significant levels in the murine liver (except UCP2 in specialized, hepatic resident macrophages, called Kupffer cells; Larrouy *et al.* 1997).

Figure 5-2 shows oxygen consumption rates (in $nmolO_2*min^{-1}*mg$ mitochondrial $protein^{-1}$) of liver mitochondria isolated from WT and UCP2-/- mice. The mitochondria were either respiring on succinate (Figure 5-2A) or glycerol-3-phosphate (G3P, Figure 5-2B) in the presence of rotenone, oligomycin, atractyloside and 0.1% BSA. After establishing a constant non-phosphorylating rate (state 4), mitochondria were treated with GDP, palmitate and FCCP to measure complete uncoupled rates.

Figure 5-2A compares oxygen consumption rates of WT and UCP2-/- liver mitochondria respiring on succinate as substrate. The rates in state 4 and after the addition of GDP and palmitate were very similar in WT and UCP2-/- liver mitochondria. The uncoupled rate (FCCP) was lower in UCP2-/- compared to WT, but this difference was not significant (see Table A-7 Appendix for rates). This observation is not surprising as liver mitochondria express UCP2 protein in negligible amounts and were therefore not expected to show any differences other than possible compensatory effects for the deletion of UCP2. With G3P as substrate (Figure 5-2B), liver WT mitochondria were respiring at 4.99 ± 1.19 and UCP2-/- mitochondria at 12.76 ± 3.52 (in nmol O_2/min/mg; P=0.02) in state 4. Treatment with GDP and palmitate did not change the oxygen consumption rates compared to the state 4 rates in both genotypes. After treatment with

GDP and palmitate WT liver mitochondria showed significantly lower respiration compared to UCP2-/- mitochondria (GDP WT 4.82 ± 1.31 and UCP2-/- 12.86 ± 3.44, P=0.02; palmitate WT 5.14 ± 0.98 and UCP2-/- 14.83 ± 4.24, P=0.01). Following titration with FCCP rates in liver WT mitochondria were significantly higher than in liver mitochondria isolated from UCP2-/- mice (WT 5.13 ± 0.99 and UCP2-/- 15.73 ± 4.44, P=0.01). Taken together, UCP2-/- liver mitochondria showed roughly 2.5-fold higher oxygen consumption rates compared to rates of WT liver mitochondria in state 4, after addition of GDP, palmitate and FCCP with G3P as substrate (Figure 5-2B). This increase in G3P supported oxygen consumption was unexpected as, firstly, liver mitochondria are not known to express UCP2 in large amounts and, secondly, mGPDH expression is usually very low in liver mitochondria. Now the question arises, what alterations, if any, mitochondria isolated from a UCP2 expressing tissue like kidney will show?

However, no difference between oxygen consumption rates in UCP2 expressing WT kidney mitochondria and kidney mitochondria from UCP2-/- mice respiring on succinate were detectable under the described conditions (Figure 5-3A). The rates in state 4 and after addition of GDP and palmitate were higher in kidney compared to liver mitochondria in both genotypes, whereas the uncoupled FCCP rate was about the same in liver and kidney mitochondria of WT animals respiring on succinate.

Oxygen consumption rates in kidney mitochondria of WT and UCP2 ablated mice with succinate as substrate differed neither in state 4, after addition of GDP and palmitate, nor in the maximal uncoupled state following FCCP titration (Figure 5-3A). When G3P was used as substrate (in the presence of $CaCl_2$), kidney mitochondria isolated from UCP2-/- mice also showed the phenomenon of significantly increased oxygen consumption compared to mitochondria isolated from kidneys of WT mice (Figure 5-3B). In state 4, the oxygen consumption rates in WT and UCP2-/- mitochondria were 6.91 ± 2.14 and 17.16 ± 4.19 nmolO_2/min/mg (P=0.03). Following treatment with GDP, oxygen consumption rates did not change in WT (6.70 ± 2.24) or UCP2-/- mitochondria (17.27 ± 4.19; P=0.03). The addition of palmitate and FCCP did not affect the rates in WT or UCP2-/- mitochondria and oxygen consumption remained significantly higher in mitochondria from UCP2-/- compared to WT animals (see Table A-7 Appendix for absolute values; palmitate WT vs. UCP2-/- P=0.009; FCCP WT vs. UCP2-/- P=0.003).

With glycerol-3-phosphate as substrate, UCP2-/- liver and kidney mitochondria showed roughly 2.5-fold higher oxygen consumption rates compared to WT liver and kidney mitochondria in state 4, after addition of GDP, palmitate and in the uncoupled state after FCCP titration (Figure 5-2A and B, Figure 5-3A and B). The fact, that liver mitochondria of UCP2-/- mice displayed the same increase in G3P supported oxygen consumption rates as kidney mitochondria was unexpected. This leads to the question as to whether UCP2 ablation caused this increase in G3P supported oxygen consumption by increases in mGPDH enzyme activity or an upregulation of mGPDH abundance. This will be addressed in the following section.

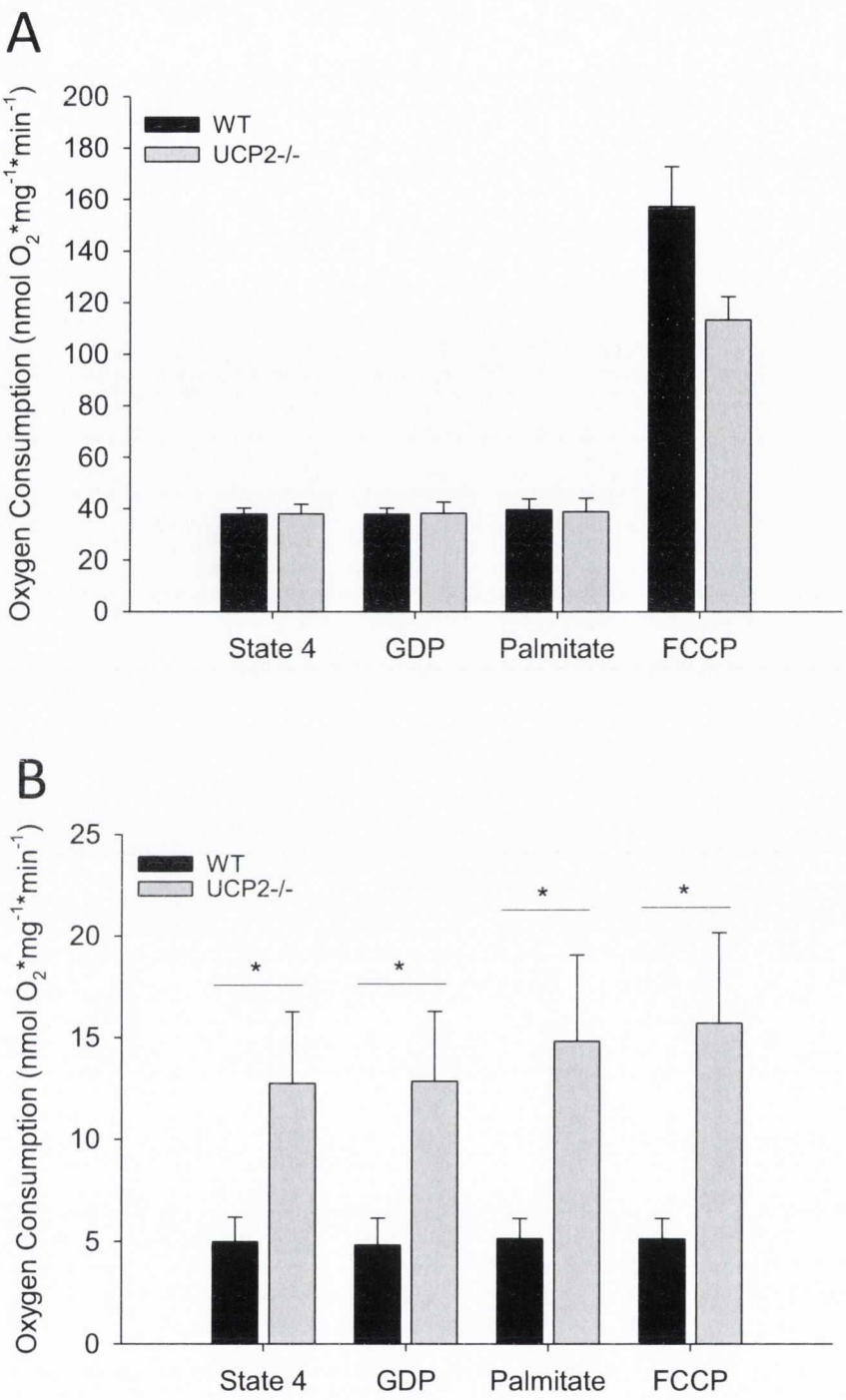


Figure 5-2: Ablation of UCP2 results in increased oxygen consumption in liver mitochondria with glycerol-3-phosphate as substrate.

Oxygen consumption of liver mitochondria isolated from 6-10 week old C57 WT and UCP2-/- mice respiring on (A) Succinate or (B) Glycerol-3-Phosphate (with 0.5nM free $CaCl_2$ present) in KHE buffer supplemented with Oligomycin, Atractyloside, Rotenone and 0.1% BSA. Mitochondria were treated with GDP and palmitate and finally FCCP was titrated until complete uncoupling occurred. P values ≤ 0.05 on unpaired student's t-test were deemed significant (* $P \leq 0.05$; ** $P \leq 0.01$; *** $P \leq 0.001$)

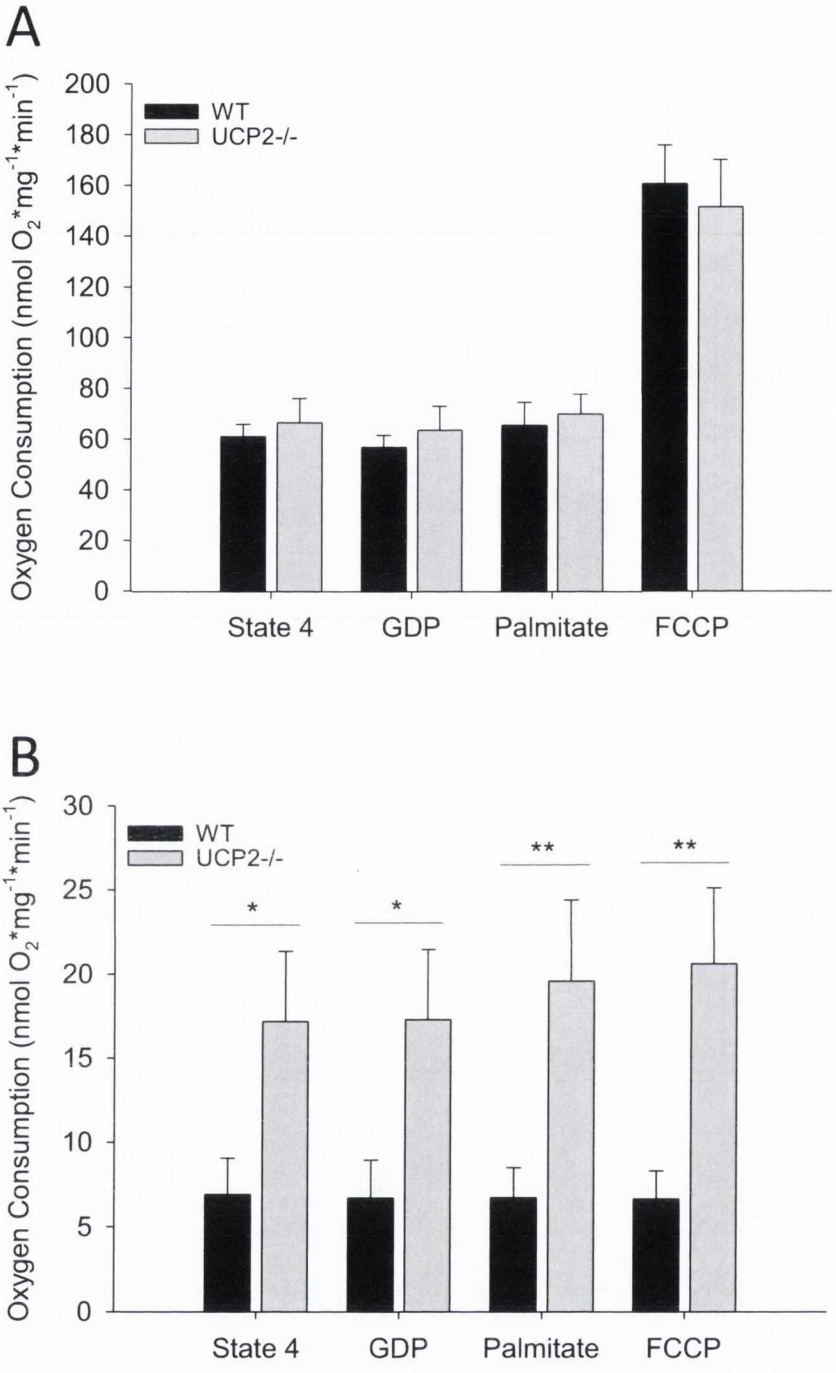


Figure 5-3: Ablation of UCP2 results in increased oxygen consumption in kidney mitochondria with glycerol-3-phosphate as substrate.

Oxygen consumption of kidney mitochondria isolated from 6-10 week old C57 WT and UCP2-/- mice respiring on (A) Succinate or (B) Glycerol-3-Phosphate (with 0.5nM free $CaCl_2$ present) in KHE buffer supplemented with Oligomycin, Atractyloside, Rotenone and 0.1% BSA. Mitochondria were treated with GDP and palmitate and finally FCCP was titrated until complete uncoupling occurred. P values ≤ 0.05 on unpaired student's t-test were deemed significant (* $P \leq 0.05$; ** $P \leq 0.01$; *** $P \leq 0.001$)

5.2.3 Increased mitochondrial glycerol-3-phosphate dehydrogenase specific activity in liver and kidney mitochondria of UCP2-/- mice

Oxygen consumption rates with glycerol-3-phosphate (G3P) as substrate were significantly increased in liver and kidney mitochondria of UCP2 ablated mice. To investigate whether this increase was due to increased activity of the mGPDH or other adaptations, specific enzyme activities of mGPDH were measured spectrophotometrically in liver and kidney mitochondria of WT and UCP2 knock-out mice. Succinate dehydrogenase activities in WT and UCP2-/- mitochondria were also measured to ensure any changes in activity were specific to mGPDH.

Figure 5-4 illustrates specific enzyme complex activity in liver (Figure 5-4A) and kidney (Figure 5-4B) mitochondria isolated from WT and UCP2 ablated mice. Enzyme activities are displayed as the change of Dichlorophenolindophenol (DCPIP) per min and mg of mitochondrial protein (nmolDCPIP/min/mg). Succinate dehydrogenase (SDH) activity was the same in liver (WT 17.6 ± 0.9, UCP2-/- 16.7 ± 0.2; p=0.51; Figure 5-4A) and kidney mitochondria (WT 21.2 ± 0.50, UCP2-/- 22.0 ± 1.25; p=0.67; Figure 5-4B) of WT and UCP2 knock-out mice, reflecting directly the oxygen consumption measurements presented in Figure 5-2A and Figure 5-3A, where mitochondrial oxygen consumption rates with succinate as substrate were unaffected by UCP2 ablation. Specific activity of mGPDH however was significantly increased in UCP2-/- animals compared to WT. In liver mitochondria, mGPDH activity was 5.4 ± 0.4 in WT and 8.7 ± 0.13 in UCP2-/- (Figure 5-4A; P=0.012). Kidney mitochondria showed slightly higher mGPDH activity compared to liver mitochondria with 8.24 ± 1.16 in WT and 13.56 ± 0.43 (P=0.05) in UCP2-/- kidney mitochondria (Figure 5-4B).

The specific enzyme activities of SDH and mGPDH therefore directly reflect the results seen in the oxygen consumption measurements illustrated in Figure 5-2 and Figure 5-3 where succinate supported oxygen consumption rates did not differ between genotypes both in liver and kidney mitochondria, but with G3P as substrate (in the presence of $CaCl_2$), liver and kidney mitochondria of UCP2-/- animals respired at significantly increased rates compared to WT mitochondria. I can therefore confirm that the observed elevated oxygen consumption with G3P as substrate in UCP2-/- mitochondria is due to increased enzyme activity. Subsequently, the question was

addressed whether this observed increase in activity was due to direct regulation of the specific mGPDH activity or whether this higher activity correlated with higher protein abundance.

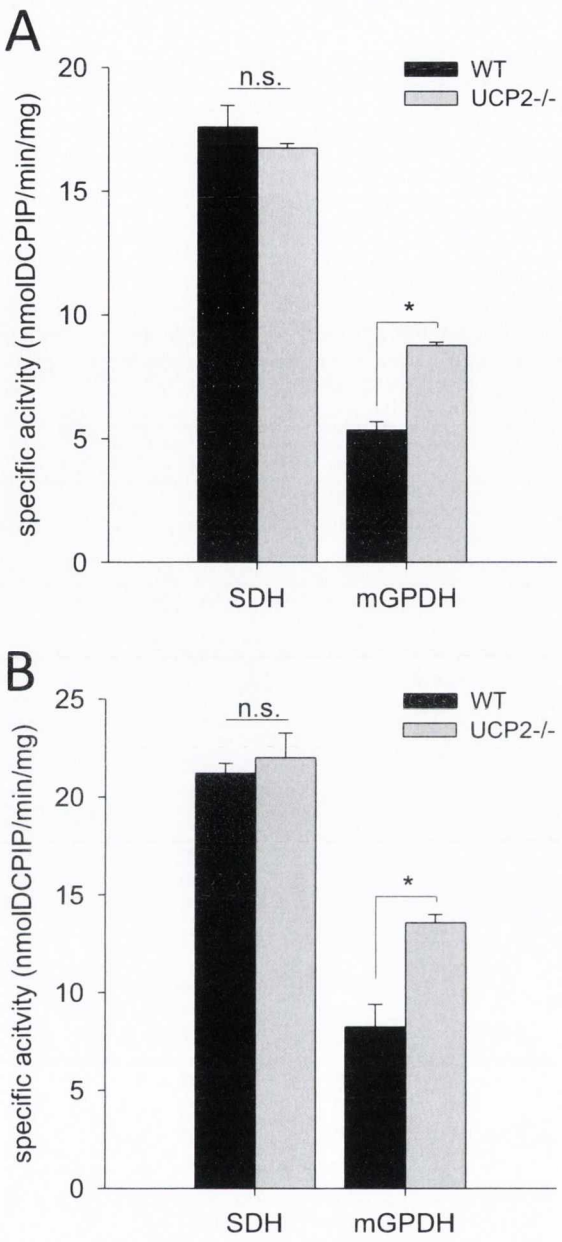


Figure 5-4: Ablation of UCP2 results in increased mitochondrial glycerol-3-phosphate dehydrogenase activity in liver and kidney mitochondria.

Liver and kidney mitochondria were isolated and SDH and mGPDH specific activities measured spectrophotometrically by reduction of DCPIP at 600nm in (A) liver and (B) kidney mitochondria of WT and UCP2-/- mice as described in sections 2.13, 2.14, 2.24 and 2.25 and. P values ≤ 0.05 on unpaired student's t-test were deemed significant (* P ≤ 0.05; ** P ≤ 0.01; *** P ≤ 0.001)

5.2.4 Increased mGPDH expression in liver and kidney mitochondria of UCP2 ablated mice

UCP2 ablation resulted in increased G3P supported oxygen consumption rates and increased specific enzyme activity of mGPDH in kidney mitochondria and, surprisingly, also in liver mitochondria. To answer the question whether mGPDH specific activity was altered or mGPDH abundance increased in UCP2 knock-out mice, expression levels of mGPDH were assessed by immunoblotting.

Figure 5-5A shows an immunoblot of mitochondrial protein isolated from livers of WT and UCP2-/- mice. Protein detection of mGPDH was performed with an antibody specific for mGPDH (top lane of bands, see section 2.18, 2.19 and 2.20) at a molecular weight of 81kDa and an antibody specific for pyruvate dehydrogenase at a molecular weight of 44kDa (PDH, lower lane of bands) as a loading control. The first three lanes contained mitochondria isolated from livers of WT animals and the following three lanes liver mitochondria isolated from UCP2 ablated mice. As a positive control for mGPDH detection, murine wild-type brown adipose tissue mitochondria were included in the western blot (not shown). The bands both in WT and UCP2-/- lanes appear quite faint, reflecting the low expression levels of mGPDH in liver mitochondria. However, signal intensity is not the same for all three samples in the WT and UCP2-/- group. Specifically, the first two WT bands from the left appear slightly fainter then the third one. In the UCP2-/- group the intensity of the first and third band from the left (signal number 4 and 6 counting from left) appear to be less compared to the signal in lane 5 although all three contain mitochondria isolated from UCP2-/- liver. To quantify the intensity of mGPDH signal and to be able to quantitatively compare expression levels of mGPDH in WT and UCP2 knock-out animals, densitometry was performed and signal strength of mGPDH bands normalized against PDH signal intensity to correct for potential differences in the amount of loaded protein sample.

Figure 5-5B illustrates the expression levels of mGPDH in liver mitochondria of WT and UCP2-/- animals relative to the PDH signal. Although the difference between WT and UCP2-/- mGPDH expression was not significant, the pattern is obvious: UCP2 ablated animals express twice as much mGPDH in liver mitochondria compared to WT animals ($P=0.23$).

Figure 5-6A shows the detection of mGPDH in kidney mitochondria of WT and UCP2-/- mice by immunoblotting as described for mGPDH detection in liver mitochondria in Figure 5-5. The first three lanes show signals for mGPDH in WT and the last three bands for UCP2-/- mitochondria isolated from kidney. The top set of bands shows detection of mGDPH at 81kDa and the lower set of bands shows detection of PDH at 44kDa as a loading control. Kidney mitochondria usually do not express large amounts of mGPDH and thus the signal strength for WT mitochondria is quite low. However it is clear, that the signals in the lanes containing UCP2-/- kidney mitochondria are stronger compared to WT bands. Quantification of the mGPDH/PDH expression level ratios by densitometry is shown in Figure 5-6B. Relative signal strength of mGPDH was 2.16-fold higher in kidney mitochondria of UCP2 ablated mice compared to WT animals (P=0.017).

Taken together, it was demonstrated that mGPDH protein was more abundant in liver and kidney mitochondria of UCP2 ablated mice compared to expression levels in WT animals.

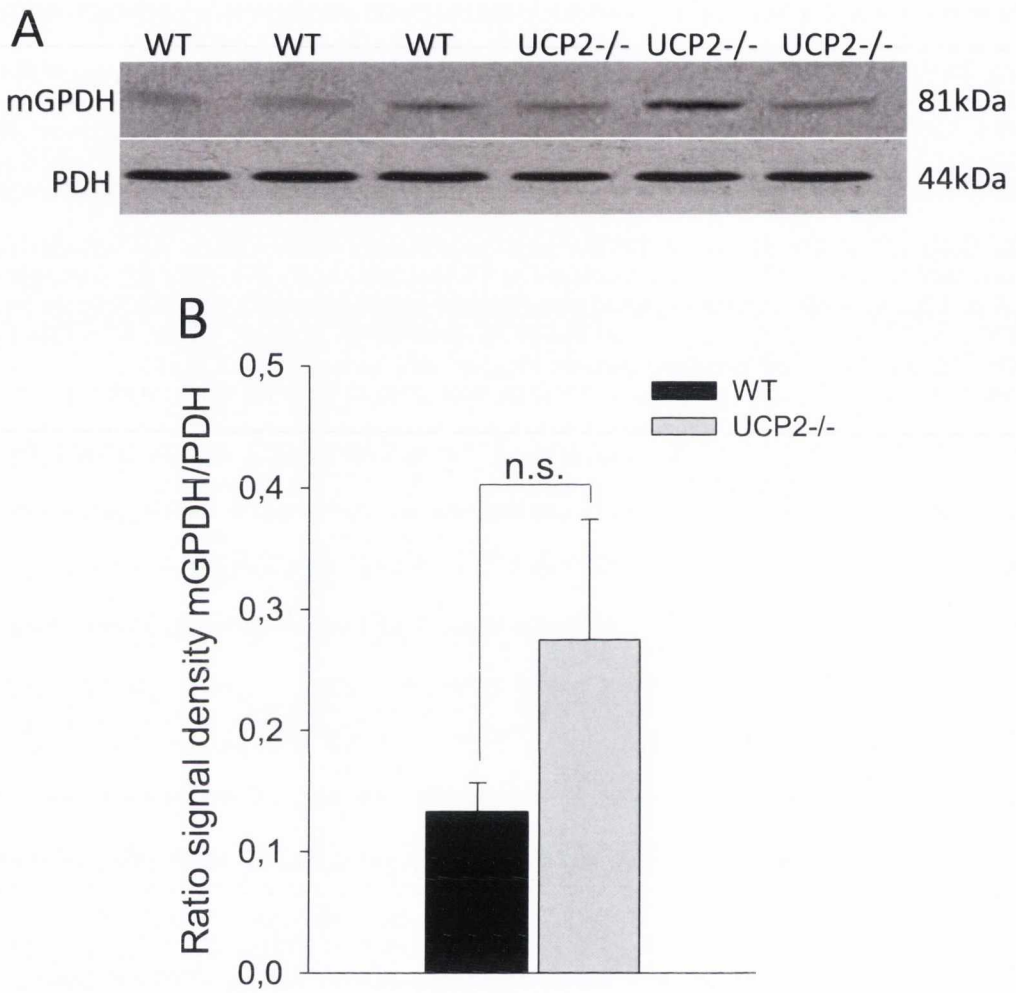


Figure 5-5: Ablation of UCP2 results in increased mitochondrial glycerol-3-phosphate dehydrogenase expression in liver mitochondria.

(A) Liver mitochondria were isolated as described in section 2.13, followed by SDS-PAGE and immunodetection using anti-mGPDH antibody (Santa Cruz GPD2; 1:100) and anti-PDH-E1 alpha (Mitosciences, 1:2000). (B) Bands were quantified by densitometry using ImageJ software and presented as expression level ratios of mGPDH/PDH. P values ≤ 0.05 on unpaired student's t-test were deemed significant (* $P \leq 0.05$; ** $P \leq 0.01$; *** $P \leq 0.001$)

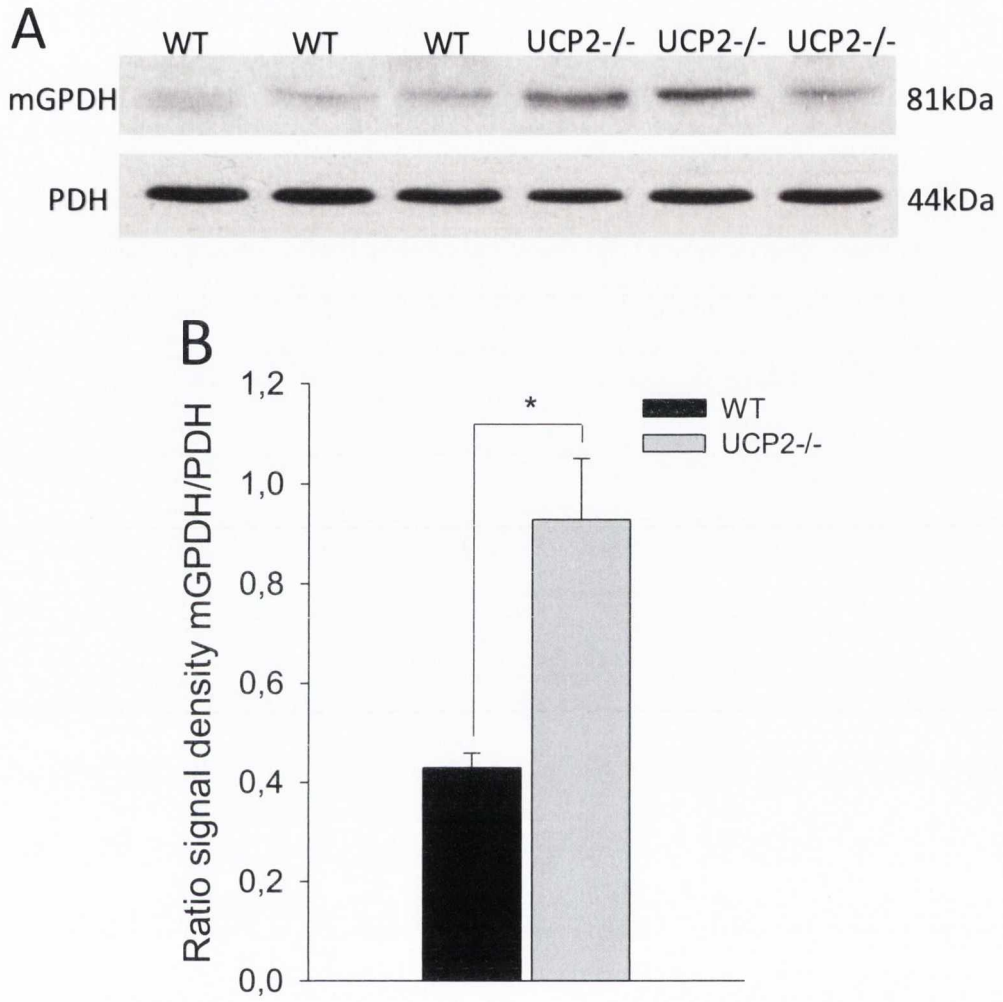


Figure 5-6: Ablation of UCP2 results in increased mitochondrial glycerol-3-phosphate dehydrogenase expression in kidney mitochondria.

(A) Kidney mitochondria were isolated as described in section 2.14, followed by SDS-PAGE and immunodetection using anti-mGPDH antibody (Santa Cruz GPD2; 1:100) and anti-PDH-E1 alpha (Mitosciences, 1:2000). (B) Bands were quantified by densitometry using ImageJ software and presented as expression level ratios of mGPDH/PDH. P values ≤ 0.05 on unpaired student's t-test were deemed significant (* $P \leq 0.05$; ** $P \leq 0.01$; *** $P \leq 0.001$)

5.2.5 No effect of UCP2 ablation on ROS production by liver and kidney mitochondria

UCP1 ablation results in significantly increased ROS production in BAT mitochondria with both succinate and glycerol-3-phosphate as substrates. UCP2 has long been associated with control of ROS production and is therefore a likely candidate to answer the question whether ablation of UCP2 can affect ROS production rates in UCP2 expressing kidney mitochondria. Liver mitochondria of UCP2 ablated mice are not expected to show changes in ROS production as UCP2 is not endogenously expressed in liver. A moderate uncoupling activity of UCPs would result in a reduction of the redox state of the respiratory chain complexes and thus minimize the transfer of electrons to molecular oxygen and the formation of superoxide. Ablation of UCP2 would therefore abolish the control of the redox state of respiratory chain complexes and control of ROS generation by the respiratory chain. Moreover, mGPDH is a potent ROS producer itself (in addition to its influence on respiratory chain complex redox state by reducing ubiquinone) and UCP2 knock-out animals have increased mGPDH abundance and activity, as was demonstrated for the first time in this section. Taken together, UCP2 ablation was expected to increase mitochondrial ROS production, especially with G3P as substrate.

ROS production rates were determined using the Amplex Red probe in the presence of horse radish peroxidise (HRP) and superoxide dismutase (SOD) in liver and kidney mitochondria isolated from WT and UCP2-/- mice. Amplex Red reacts with H_2O_2 with a 1:1 stoichiometry to produce highly fluorescent Resorufin. An excess amount of exogenous SOD ensures conversion of all superoxide to H_2O_2 for detection. Measurement with Amplex Red therefore provides a more complete estimation of ROS production rates in isolated mitochondria compared to other dyes that detect superoxide production only. ROS production should be maximal in a non-phosphorylating state when the proton gradient is not dissipated by ATP synthase and the respiratory chain complexes are maximally reduced. After a stable state 4 rate was obtained, mitochondria were treated with GDP and palmitate and FCCP titrated to measure ROS production in the uncoupled non-phosphorylating state. All ROS production rates are expressed as pmol of H_2O_2 per min and mg mitochondrial protein (pmol H_2O_2*min^{-1}*mg^{-1}).

Figure 5-7A shows ROS production rates in WT liver mitochondria respiring on succinate. The highest rates were found in state 4 (substrate only) with a small inhibition after GDP injection, another small inhibition after palmitate treatment and a significant reduction to half the initial rate in state 4 after FCCP titration. UCP2-/- mitochondria showed the highest rate in state 4 as well, but no alteration due to GDP and palmitate injections was detectable. Titration with FCCP halved the ROS production rate compared to the state 4 rate. Surprisingly, all rates in UCP2-/- were lower than those measured in WT liver mitochondria respiring on succinate.

Liver mitochondria of WT mice respiring on glycerol-3-phosphate (Figure 5-7B) showed the highest rates of ROS production in state 4. The addition of GDP and Palmitate reduced the rates slightly and artificial uncoupling with FCCP yielded the lowest rate measured. In contrast, the treatment of liver mitochondria isolated from UCP2-/- mice and respiring on glycerol-3-phosphate with GDP increased the ROS-production rate, while the addition of palmitate lowered the rate again, even below the initial state 4 rate. Uncoupling with FCCP resulted in a rate about half of the measured state 4 rate and was therefore the lowest. The highest rate measured was in UCP2-/- liver mitochondria in state 4 in the presence of GDP.

Figure 5-8A illustrates ROS production rates in UCP2-/- and WT kidney mitochondria respiring on succinate. As in mitochondria isolated from livers of WT mice in Figure 5-7A, the highest rate was obtained in state 4 and was reduced after addition of GDP and palmitate, and titration with FCCP reduced ROS production further. Kidney mitochondria from UCP2-/- mice showed reduced ROS production in state 4 respiring on succinate and unaltered ROS production following administration of GDP and palmitate. The addition of FCCP reduced ROS production to about half the rate in state 4.

Figure 5-8B shows ROS production rates of kidney mitochondria isolated from WT or UCP2-/- mice respiring on glycerol-3-phosphate. In kidneys of WT mice again the highest rates were measured in state 4. GDP and palmitate reduced the rate slightly and was further reduced by the addition of FCCP. Kidney mitochondria of UCP2-/- showed the highest ROS production rate in the presence of palmitate, while state 4 and GDP rates were identical and lower than the rate in the presence of palmitate. FCCP addition reduced the ROS production rate to half the rate in state 4.

Under the analysed conditions, all ROS production rates were lower in UCP2-/- compared to WT mitochondria regardless of tissue or substrate. WT mitochondria showed a constant reduction in the rates to the same extent with each addition of chemicals indicating a dilution effect of the Amplex Red probe. However, this was not seen in UCP2-/- mitochondria under the same conditions and with the same treatments. None of the mentioned differences between genotypes were significant.

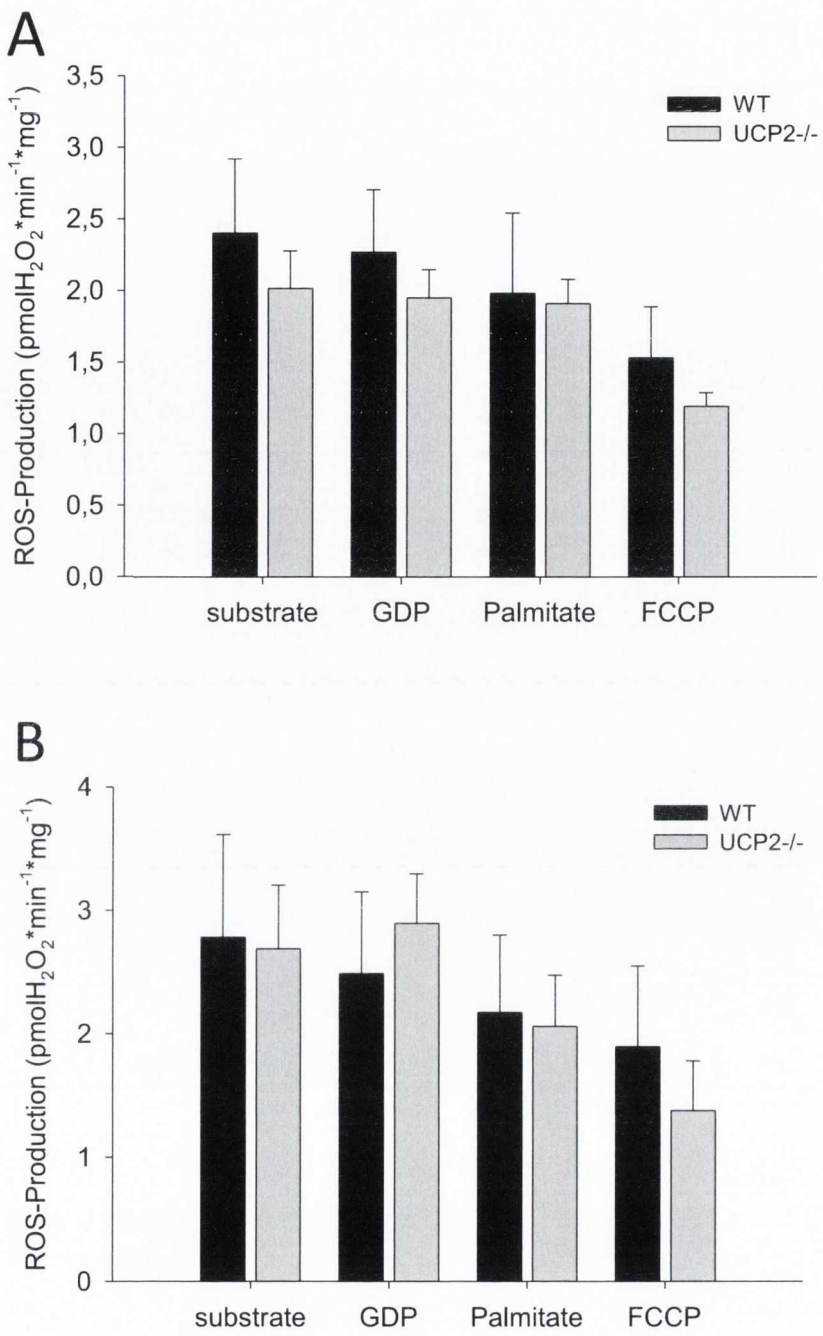


Figure 5-7: Ablation of UCP2 does not change ROS production rates in liver mitochondria with succinate or glycerol-3-phosphate as substrate.

ROS production rates (in pmol H_2O_2*min^{-1}*mg^{-1}) in isolated liver mitochondria from WT (black columns) and UCP2-/- mice (grey columns) respiring on succinate (A) and Glycerol-3-Phosphate (B). ROS production was measured using Amplex Red in the presence of HRP, exogenously added SOD, Rotenone, Oligomycin, Atractyloside and 0.1% BSA. P values ≤ 0.05 on unpaired student's t-test were deemed significant (* P ≤ 0.05; ** P ≤ 0.01; *** P ≤ 0.001).

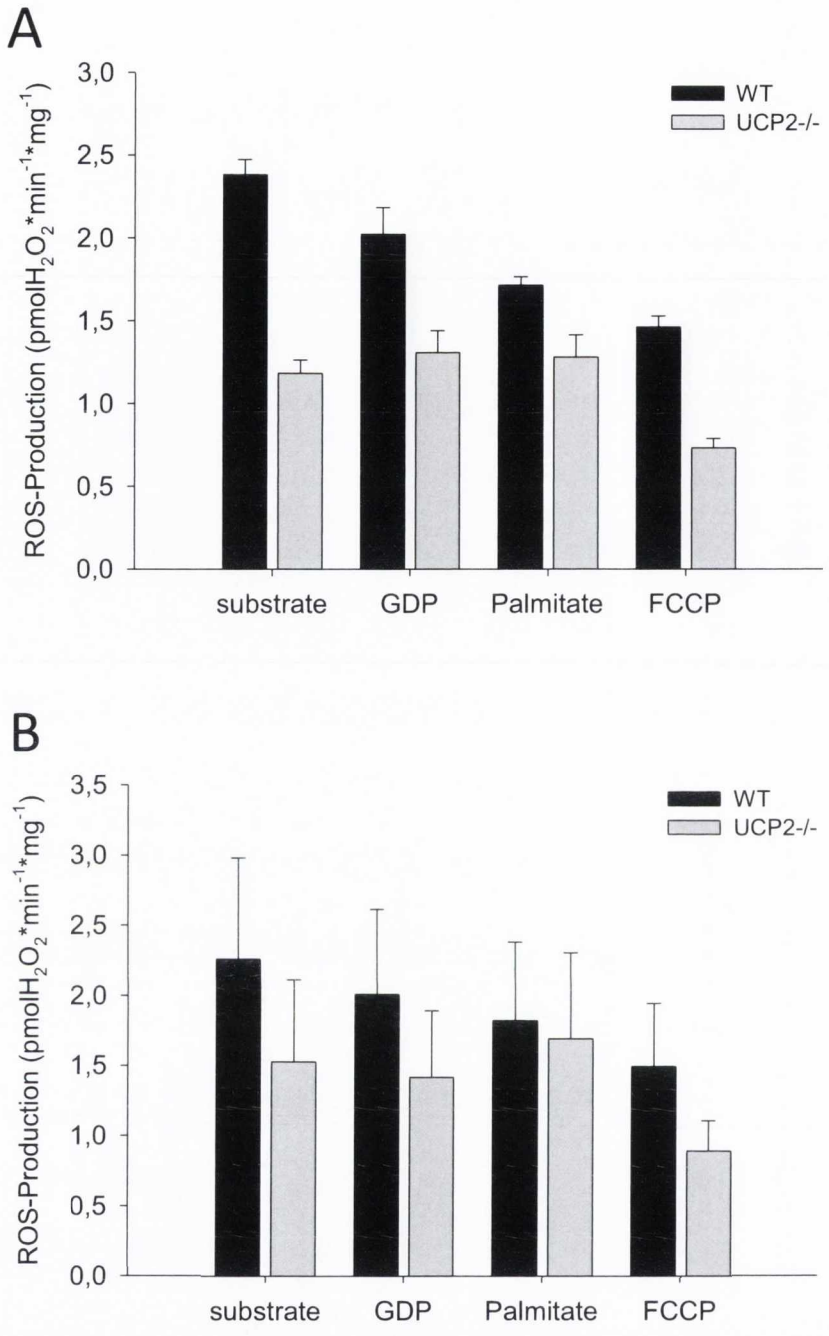


Figure 5-8: Ablation of UCP2 does not change ROS production rates in kidney mitochondria with succinate or glycerol-3-phosphate as substrate.

ROS production rates (in pmol H_2O_2*min^{-1}*mg^{-1}) in isolated kidney mitochondria from WT (black columns) and UCP2-/- mice (grey columns) respiring on succinate (A) and Glycerol-3-Phosphate (B). ROS production was measured using Amplex Red in the presence of HRP, exogenously added SOD, Rotenone, Oligomycin, Atractyloside and 0.1% BSA. P values ≤ 0.05 on unpaired student's t-test were deemed significant (* P ≤ 0.05; ** P ≤ 0.01; *** P ≤ 0.001).

5.3 Discussion

The aim of this chapter was to investigate the effects of the absence of UCP2 on mitochondrial function. Specifically, oxygen consumption and ROS production in isolated liver and kidney mitochondria of WT and UCP2-/- mice were examined. Two different substrates were chosen (succinate and glycerol-3-phosphate) and oxygen consumption and reactive oxygen species rates measured in the presence of rotenone to inhibit complex I. Inhibition of complex I by rotenone eliminates reverse electron flow so that only ROS generated through succinate dehydrogenase and glycerol-3-phosphate dehydrogenase and downstream of their entry into the electron transport chain can be detected (Lambert *et al.* 2004). Interestingly, oxygen consumption was affected by UCP2 ablation only with glycerol-3-phosphate as substrate but not with succinate as substrate. A large portion of this chapter was aimed at explaining this differential observation.

The results showed that there were no significant differences in oxygen consumption and ROS production rates in liver and kidney mitochondria with succinate as substrate in a comparison between WT and UCP2-/- animals. A known inhibitor ligand of UCPs, GDP, did not lower oxygen consumption and palmitate, which is known to overcome GDP inhibition of UCPs, did not increase oxygen consumption in WT mitochondria in the presence or absence of GDP. Therefore UCP2 did not uncouple mitochondria which would have resulted in a higher state 4 oxygen consumption rate in kidney mitochondria isolated from WT compared to UCP2-/- animals. This observation was further endorsed by the fact that the artificial uncoupler FCCP significantly increased oxygen consumption in mitochondria isolated from liver (WT P=0.0000002; UCP2-/- P=0.00002) and kidney (WT P = 0.00001; UCP2-/- P=0.002) in WT and UCP2-/- animals (Figure 5-2A and Figure 5-3A). This also demonstrates that the mitochondrial preparation yielded intact, functional kidney and liver mitochondria. Lack of UCP2 did not change ROS production and neither GDP nor palmitate significantly affected ROS production rates. Uncoupling following titration with FCCP resulted in reduced ROS production compared to state 4 production rates (Figure 5-7A and B, Figure 5-8A and B), which confirms that a reduction in membrane potential reduces mitochondrial ROS production as was proposed previously (Skulachev 1996; Brand 2000).

However, oxygen consumption with glycerol-3-phosphate (G3P) as substrate was significantly higher in liver and kidney mitochondria of UCP2-/- animals compared to mitochondria of WT mice in state 4 (Figure 5-2B and Figure 5-3B). This indicates elevated mGPDH activity (and possibly expression levels) in mitochondria from UCP2-/- mice compared to those from WT reflecting a potential effect due to lack of UCP2.

The fact that this phenomenon was seen in both liver and kidney mitochondria suggests a systemic adaptation to the absence of UCP2 rather than a tissue specific event in UCP2 expressing cells. It was also noted that G3P supported mitochondrial oxygen consumption in liver and kidney remained the same following addition of GDP and palmitate. Interestingly, titration with FCCP did not increase oxygen consumption in mitochondria respiring on G3P as was observed for mitochondria respiring on succinate. One might think that the mitochondria respiring on G3P were uncoupled as no further increase of oxygen consumption on addition of FCCP would be possible if that was the case, but FCCP did increase respiration rates in mitochondria from the same preparation when succinate was used as a substrate. This demonstrated that the mitochondria from these preparations were intact and therefore coupled. It is noteworthy, that Kieran Clarke did not register an increase in oxygen consumption rates with FCCP in BAT mitochondria respiring on glycerol-3-phosphate neither. Therefore the inability of FCCP to increase glycerol-3-phosphate supported oxygen consumption rates is consistent between the three investigated tissues BAT, liver and kidney and the two individual studies by Clarke and by me. The explanation for this differential observation between G3P and succinate respiring mitochondria is not clear, but a few possibilities are discussed.

One explanation for the fact that FCCP titration could not stimulate oxygen consumption may be that liver and kidney mitochondria respiring on G3P were at their respective maximal rate of oxygen consumption in state 4 and this was not further increasable with FCCP.

Another possibility might be that the mitochondria respiring on G3P are damaged due to opening of the mitochondrial permeability transition pore as a result of $CaCl_2$ uptake, as calcium was only present in the medium when G3P was used as substrate, but not with succinate as substrate. However, this is highly unlikely, as the mitochondrial permeability transition pore is reported to be triggered by Ca^{2+} at concentrations in the

micromolar range (Hunter *et al.* 1979; Brustovetsky *et al.* 2002) whereas we only used $CaCl_2$ in the nanomolar range (exterior) in the experiments where G3P was used as substrate. Furthermore, previous experiments in our laboratory (by Kieran Clarke) demonstrated that oxygen consumption rates in BAT mitochondria respiring on succinate were not different in the presence of nanomolar (exterior) $CaCl_2$ compared to rates without $CaCl_2$. In addition, incubation of BAT mitochondria with the specific Ca^{2+}-uniport inhibitor Ruthenium Red did not inhibit oxygen consumption rates in isolated BAT mitochondria respiring on G3P. These observations reassure me, that the nanomolar concentrations of calcium I was using did not cause opening of the permeability transition pore and confirm the specific activation of mGPDH by Ca^{2+} that I observe. In addition, others have used 200nM free Ca^{2+} in mitochondrial respiration measurements with glycerol-3-phosphate as substrate without having triggered permeability transition pore opening (Quinlan *et al.* 2012). The mGPDH is located on the outer side of the inner mitochondrial membrane and thus no Ca^{2+}-transport is needed for mGPDH activation. From the two observations that a) succinate supported oxygen consumption was the same in the presence or absence of $CaCl_2$ and that b) inhibition of Ca^{2+}-transport by Ruthenium Red did not change the oxygen consumption rates with G3P as substrate, an additional conclusion was drawn: The increase in oxygen consumption in BAT mitochondria with G3P as substrate was due to specific activation of mGPDH by Ca^{2+} and not an activation of another dehydrogenase or the respiratory chain complexes. All of the aforementioned observations were made in murine BAT mitochondria by Kieran Clarke (Clarke 2011). The aforementioned controls by Clarke were not repeated in the present study for liver and kidney mitochondria of UCP2-/- mice, because the exact same conditions were used and similar results were observed. In conclusion, a similar adaptation to ablation of UCP1 in BAT mitochondria and ablation of UCP2 in liver and kidney mitochondria must be in place in the respective knock-out animals. It would be very interesting to investigate whether UCP3 ablation results in the same phenotype as was described for UCP1 and UCP2 deletion, because expression levels of mGPDH in skeletal muscle are the second highest in mice following levels of mGPDH expression in BAT (Koza *et al.* 1996).

After having established that the activation of mGPDH by $CaCl_2$ was specific and the increased oxygen consumption rate with G3P in UCP2 knock-outs was due to UCP2

ablation, I focused on investigating the adaptations that led to the described phenotype. To find out whether the oxygen consumption with G3P was higher in mitochondria of UCP2 knock-out due to increased mGPDH activity or also mGPDH abundance, the specific succinate dehydrogenase and mitochondrial glycerol-3-phosphate dehydrogenase activities in liver and kidney of WT and UCP2-/- mice were measured and abundance of mGPDH estimated by immunodetection. Figure 5-4A and B show that the increase in oxygen consumption with G3P as substrate (Figure 5-2B Figure 5-3B) correlates with increased activity of the mGPDH enzyme complex, whereas SDH specific enzyme complex activity remained the same in mitochondria of WT and UCP2 ablated animals. These results mirror the results obtained by Clarke for the effects of UCP1 ablation in BAT mitochondria. Next, the question arose whether this increase in mGPDH activity was due to upregulation of enzyme activity or the result of an increase in enzyme abundance. This question could not be answered by Clarke (2011) in his study due to time limitations, but was addressed in Figure 5-1.

Detection by immunoblotting and densitometric quantification of the mGPDH signal in BAT mitochondria of UCP1 ablated mice showed that indeed mGPDH protein levels were increased in UCP1 knock-out mice. The same methodology was used to investigate the expression levels of mGPDH in UCP2 ablated mice and the same result was found (Figure 5-5 and Figure 5-6). UCP2 ablation therefore also increases mGPDH expression in mice. But what is the function of increasing mGPDH abundance and activity and why does the loss of UCP2 (and UCP1) trigger it? There are a few hypothetical explanations that come to mind.

Recent data suggests that UCP2 may be a metabolic switch to control glucose and fatty acid metabolism and it was demonstrated that UCP2 promotes a switch toward fatty acid metabolism in fasted animals (Andrews *et al.* 2008). This hypothesis is supported by the fact that ablation of UCP2 leads to reduced mitochondrial fatty acid oxidation and increased glucose utilisation (Pecqueur *et al.* 2008). So, if cells in UCP2 knock-out animals were more glycolytic, an increase in mGPDH or rather the entire glycerol-3-phosphate shuttle would enable the cells to rapidly generate ATP in mitochondria by oxidative phosphorylation using reduction equivalents from the cytosol. In addition, it is known that the glycerol-3-phosphate shuttle recycles cytosolic reduction equivalents and an upregulation of the shuttle would be beneficial to maintain a high glycolytic phenotype.

Another explanation for the increased mGPDH expression and function in UCP knock-out mice may be that in times of high energy demand, glycerol from the breakdown of triacylglycerides is phosphorylated to glycerol-3-phosphate and enters the glycolysis pathway after conversion to dihydroxyacetone phosphate by mGPDH with the net introduction of 2 electrons to the respiratory chain. However, most phenotypes associated with UCP2 ablation support the theory of a more glycolytic metabolism in UCP2 knock-outs (Pecqueur *et al.* 2008).

Upregulation of mGPDH may of course also be a compensatory adaptation to loss of facultative thermogenesis by UCPs (especially UCP1 in BAT). So far, no thermogenic function has been described for UCP2, but then UCP2 is expressed in very small amounts compared to UCP1 in BAT and may thus only generate miniscule amounts of heat by uncoupling. Increasing the activity and abundance of the glycerol-3-phosphate shuttle may compensate for loss of thermogenic potential by elimination of UCPs.

The mGPDH is an important ROS production site in mitochondria and increased mGPDH activity is correlated with increased ROS production (Mracek *et al.* 2009). Because ROS are not only cytotoxic agents, but are also involved in important cellular functions like various signalling pathways, inflammation or apoptosis, regulation of mGPDH and its contribution to ROS production may be important in UCP knock-out mice.

UCP1 and especially UCP2 have long been associated with the regulation of mitochondrial ROS production. The influence of UCP2 on ROS production has been investigated abundantly, but conflicting results make conclusions difficult. Hence, control of ROS production by UCP2 remains a controversially discussed subject (Nedergaard *et al.* 2003; Rousset *et al.* 2004; Shabalina *et al.* 2011)

In this chapter, ROS production rates of mitochondria isolated from WT and UCP2-/- mice were investigated. Increased ROS production rates were expected in the absence of control of ROS production by UCP2 together with increased mGPDH activity and abundance, which is a significant source of mitochondrial ROS. Surprisingly, ROS production rates did not differ between WT and UCP2 ablated liver and kidney mitochondria in state 4 with succinate or G3P as substrates (Figure 5-7 and Figure 5-8). No significant changes in ROS production rates were observed following addition of GDP or palmitate suggesting a) that UCP2 uncoupling cannot be regulated by these

compounds, b) that UCP2 may require an unknown activator which was not present in the experimental conditions applied here or c) that UCP2 indeed does not have an uncoupling activity. The addition of FCCP halved the ROS production rate in both liver and kidney mitochondria (not significant), which confirms previous observations that uncoupling, and thus lowering the membrane potential (and/or possibly alteration of Q-redox state), reduces ROS production.

The fact that GDP and palmitate did not affect ROS production rates confirms the results seen in Figure 5-2 and Figure 5-3 where oxygen consumption rates also remained unchanged by GDP and palmitate. UCP2 may therefore not be regulated by GDP and palmitate.

In all studies on primary cells and mitochondria involving UCP2, it is important to note that UCP2 expression levels can be up to a 1000-fold less compared to expression levels of UCP1 in BAT (Pecqueur *et al.* 2001) and thus it is possible that the absence of UCP2 may not manifest in changes in oxygen consumption or ROS production rates in the investigated tissues due to low abundance. Another explanation may be that although ROS production may have been influenced by UCP2 ablation, the mitochondrial antioxidant defences were upregulated in mitochondria of UCP2 knock-out animals or even that any differences in ROS production were mopped up by antioxidants and simply did not register in the chosen methods. In fact, UCP2 ablated animals showed increased levels of Mn-superoxide dismutase (Durmaz *et al.* 1999; de Bilbao *et al.* 2004). In support of the hypothesis that UCP2 ablation increases antioxidant defences, de Bilbao *et al.* also showed decreased lipid peroxidation in brains of UCP2 knock-out mice following ischemia and increased glutathione activity in UCP2 knock-out mice (de Bilbao *et al.* 2004). Overall, UCP2 knock-out mice appeared to be more protected from oxidative damage than WT controls, which may explain the upregulation of oxidative defences in UCP2 ablated animals.

In conclusion, absence of UCP2 does not increase mitochondrial ROS production in liver and kidney of UCP2 knock-out mice. More experiments are needed to investigate the underlying mechanisms of increased mGPDH abundance and activity in UCP ablated animals.

UCP3 Bioenergetics

Chapter 6

6 UCP3 bioenergetics

6.1 Introduction

UCP3 is primarily expressed in skeletal muscle and to a lesser extent in BAT mitochondria. The function of UCP3 is still under investigation. Our laboratory recently published that UCP3 is phosphorylated and activated by systemic treatment with MDMA (Kelly *et al.* 2011a) which resulted in increased state 4 oxygen consumption i.e. increased proton leak in skeletal muscle mitochondria of MDMA treated compared to mitochondria of PBS treated animals. MDMA (3,4-methylenedioxymethamphetamine) is a synthetic, psychoactive drug, that among other physiological effects, interferes with the body's ability to regulate its temperature. High doses can lead to hyperthermia, which can result in liver, kidney and cardiovascular system failure and eventually death. MDMA is thought to trigger sympathetic noradrenaline release and thus activate UCP3 directly or indirectly in skeletal muscle and possibly also BAT tissue by phosphorylation (Kelly *et al.* 2011a).

In this study, I used more physiological animal treatments known to affect UCP3 expression or function to address the question whether phosphorylation of UCP3 can be triggered non-pharmacologically and whether this phosphorylation results in altered mitochondrial function.

In order to test whether UCP3 phosphorylation and activation can be induced adrenergically in skeletal muscle mitochondria, animals were either subjected to cold-acclimation over 3 months or treated with systemic (i.p.) noradrenaline injections. Mitochondria were isolated in the presence or absence of phosphatase inhibitors to protect the phosphorylation state. Treatment of brown adipocytes with noradrenaline has been demonstrated to mobilise fatty acids and activate UCP1 (Matthias *et al.* 2000). Furthermore, exogenous noradrenaline activates thermogenesis in BAT as was dramatically demonstrated by Foster and Frydman (Foster *et al.* 1978). Still the question remained whether all noradrenaline-induced thermogenesis was attributable to brown adipose tissue activity, or whether other tissues could respond in a thermogenic way too.

For the cold-acclimation studies I used WT and UCP1-/- mice. UCP1-/- mice represent the optimal model to investigate the potential capacity of UCP3 to mediate

non-shivering thermogenesis in skeletal muscle (Golozoubova *et al.* 2001). Our hypothesis was that the lack of UCP1 in BAT, and therefore diminished cold tolerance, augments the UCP3 catalysed proton leak and hence mediate heat production in skeletal muscle. It was expected that increases in UCP3 abundance or activity should manifest in increased state 4 oxygen consumption when the phosphorylation state of mitochondria during the isolation was preserved as was demonstrated in animals following MDMA treatment (Kelly *et al.* 2011a).

Apart from cold-acclimation, other physiological situations were investigated to determine, whether UCP3 can be phosphorylated under physiological conditions. UCP3 expression is increased 3-fold following a 24h starvation period. However, others did not see increased proton leak in skeletal muscle mitochondria following starvation (Cadenas *et al.* 1999). Preservation of the phosphorylated state of UCP3 might also preserve its activity in isolated mitochondria and should manifest in increased state 4 oxygen consumption due to mild uncoupling.

6.2 Results

6.2.1 No effect of Noradrenaline treatment on SKM mitochondria

Figure 6-1 shows oxygen consumption rates of murine skeletal muscle (SKM) mitochondria in state 4 and the maximum respiratory capacity following artificial uncoupling (FCCP), isolated in the presence of phosphatase inhibitors. Mice were injected i.p. with noradrenaline (NA) or PBS and tissue samples were taken one hour following administration. Figure 6-1A illustrates mitochondrial oxygen consumption rates with succinate as substrate and no difference between noradrenaline and PBS treated animals was detectable. However, when the same mitochondria were respiring on G3P in the presence of 50nM free Ca^{2+}, an elevated rate was observable in state 4, but not FCCP in muscle mitochondria of NA treated mice compared to PBS treated ones. This indicates an increase in mGPDH activity, probably due to the preservation of phosphorylation, after systemic exposure to a single high dose of NA. No effect was seen with succinate as substrate. So, one hour after treatment phosphorylation of mGPDH was still present and protected with phosphatase inhibitors at the applied concentrations, but any other immediate and short lived effects on the respiratory chain were lost at this point. A shorter incubation period after injection of NA or PBS was therefore tested with no effect on oxygen consumption rates (data not shown). Furthermore, the effects of noradrenaline on UCP3 may be very small and do not result in statistically significant alterations in mitochondrial oxygen consumption, but long term effects may very well have an impact on overall substrate utilization, coupling efficiency and energy expenditure.

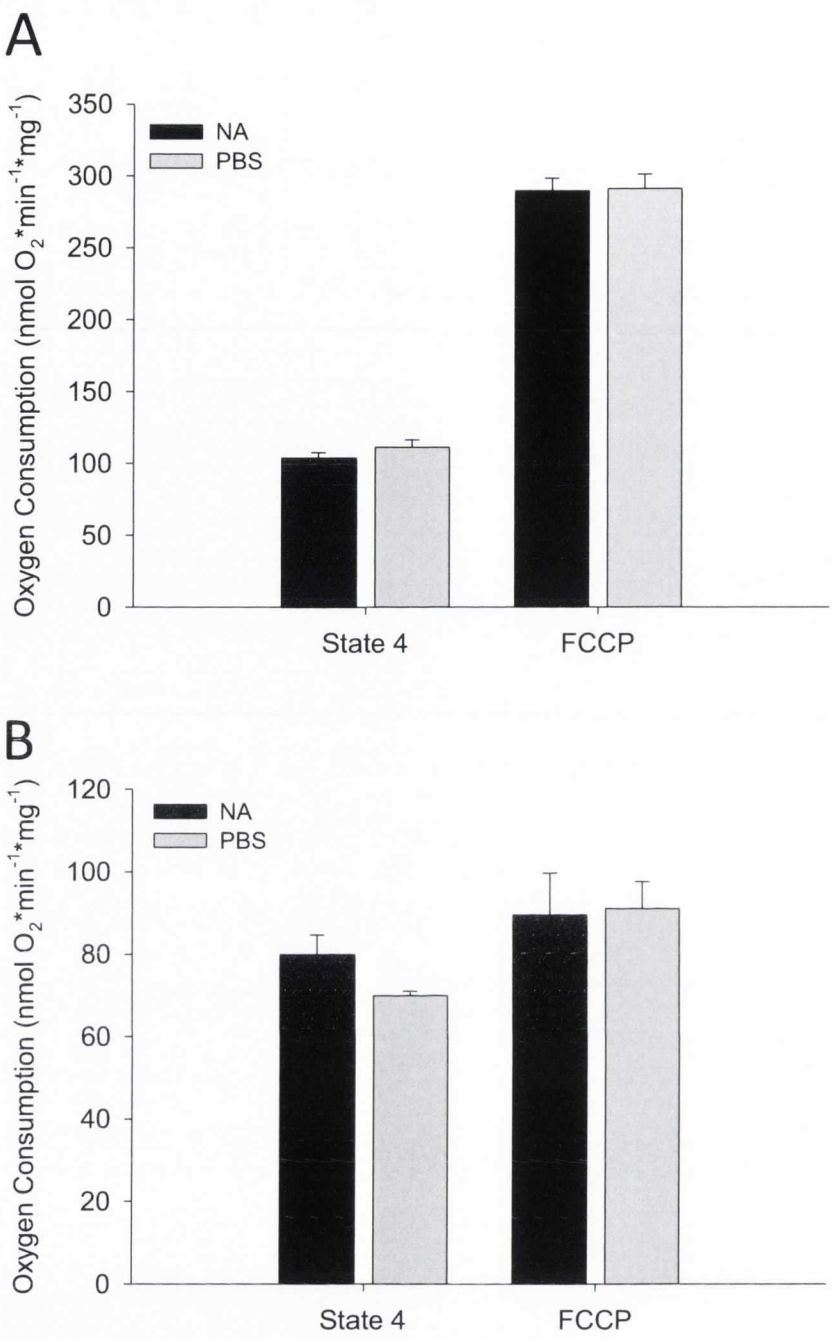


Figure 6-1: Systemic treatment with noradrenaline does not affect oxygen consumption in skeletal muscle mitochondria.

Oxygen consumption rates (nmol O_2*min^{-1}*mg mitochondrial $protein^{-1}$) with succinate (A) or glycerol-3-phosphate (B) as substrate in state 4 and uncoupled state (FCCP) of SKM mitochondria isolated in the presence of phosphatase inhibitors from WT mice injected i.p. with 2mg/kg body weight noradrenaline or PBS alone. Results are expressed as means ± SEM of 3 experiments, each experiment performed in triplicate. P values ≤ 0.05 on unpaired student's t-test were deemed significant (* P ≤ 0.05; ** P ≤ 0.01; *** P ≤ 0.001).

6.2.2 Effects of short term starvation on SKM mitochondria

Acute starvation for 24h has been reported to increase UCP3 protein content in skeletal muscle mitochondria at least 3-fold. However, no increased state 4 oxygen consumption rate due to uncoupling has been reported up to date. In this experiment, the phosphorylation and activation of UCP3 was investigated following this physiological challenge.

Figure 6-2 illustrates an anti-UCP3 immunoblot of 50µg skeletal muscle and liver mitochondria, isolated in the presence or absence of phosphatase inhibitors (+/- PI). Mitochondria of fed (Figure 6-2A) and 24h fasted (Figure 6-2B) animals were used and anti-pyruvate dehydrogenase (PDH) antibody employed to control for equal loading. A signal at 32kDa was indicative of UCP3 and at 44kDa for PDH. All SKM mitochondria preparations of fed and fasted animals were positive for UCP3, regardless of phosphatase inhibitor treatment, but no signal for UCP3 was detected in liver mitochondria. All mitochondria of the fed and fasted animals show identical signal strength for PDH, which shows equal loading of total protein. It is important to notice that the signal strength of UCP3 was less in mitochondria of fed animals (Figure 6-2A), compared to signal strength of UCP3 in fasted animals (Figure 6-2B).This shows that UCP3 protein was present more abundantly in skeletal muscle mitochondria of fasted animals than in fed animals, and that signal strength was not dependent on isolations with or without phosphatase inhibitors.

Figure 6-3 and Figure 6-4 show oxygen consumption rates of skeletal muscle mitochondria from fed or food deprived (24h) WT mice isolated in the presence or absence of phosphatase inhibitors. In Figure 6-3A mitochondria were isolated in the presence of phosphatase inhibitors and were respiring on succinate. State 4 and the FCCP uncoupled oxygen consumption rates were not different in fed or fasted state (State 4: fed 67.6 ± 2.5; starved 70.3 ± 6.5, P=0.71 and FCCP: fed 230.8 ± 10.9; starved 198.3 ± 8.5, P=0.07). Skeletal muscle mitochondria of starved mice isolated without phosphatase inhibitors showed significantly reduced state 4 non-phosphorylating (fed 66.4 ± 1.9; starved 54.4 ± 2.2, P=0.014) and uncoupled oxygen consumption rates (FCCP fed 223.0 ± 8.0; starved 142.6 ± 7.4, P=0.00018) compared to fed animals (Figure 6-3B). Mitochondria respiring on glycerol-3-phosphate and isolated in the presence of phosphatase inhibitors

(Figure 6-4C) were very similar in state 4 non-phosphorylating (fed 53.2 ± 2.9; fasted 56.4 ± 2.9) or FCCP uncoupled oxygen consumption rates (fed 129.4 ± 9.4; fasted 130.5 ± 7.4) in fed compared to fasted mice indicating no effect on mGPDH due to phosphorylation after acute starvation. In Figure 6-4D, skeletal muscle mitochondria of fed mice isolated without phosphatase inhibitors also showed no significant differences to mitochondria of fasted animals, but a small trend towards a lower oxygen consumption rate in mitochondria of fasted mice was seen in state 4 non-phosphorylating (fed 50.9 ± 2.1; fasted 41.6 ± 2.6) and FCCP uncoupled states (fed 121.8 ± 8.1; fasted 96.2 ± 8.0). Table 7 shows the respiratory control ratios (RCR) of mitochondria respiring on succinate and isolated in the presence or absence of PI. RCRs are calculated as the ratio of state 3 phosphorylating oxygen consumption and state 4 non-phosphorylating oxygen consumption. RCRs are regularly used to express coupling efficiency, and therefore integrity, of isolated mitochondria. The higher the RCR, the better was the mitochondrial preparation and the more intact were the mitochondrial membranes. Table 7 highlights that mitochondria isolated from fed animals showed significantly higher RCRs and were therefore more coupled than mitochondria isolated from fasted animals. This significant difference was dependent on the phosphorylation state of the mitochondrial preparation. Mitochondria that were isolated in the presence of PI (RCR fed compared to fasted +PI P=0.02) showed a less significant RCR difference compared to mitochondria isolated without PI (RCR fed compared to fasted -PI P=0.0001).

Taken together, the fact that FCCP uncoupled rates were lower in mitochondria of fasted animals compared to mitochondria of fed animals with succinate as substrate, indicate a reduction in respiratory chain activity following short term fasting. This phenomenon was dependent on the phosphorylation state of the mitochondrial preparation. Lower oxygen consumption rates in fasted compared to fed mice were only detectable in isolations without phosphatase inhibitors, but protection of the phosphorylation state with phosphatase inhibitors in mitochondrial preparations abolished all significant differences in state 4 non-phosphorylating and FCCP uncoupled oxygen consumption rates.

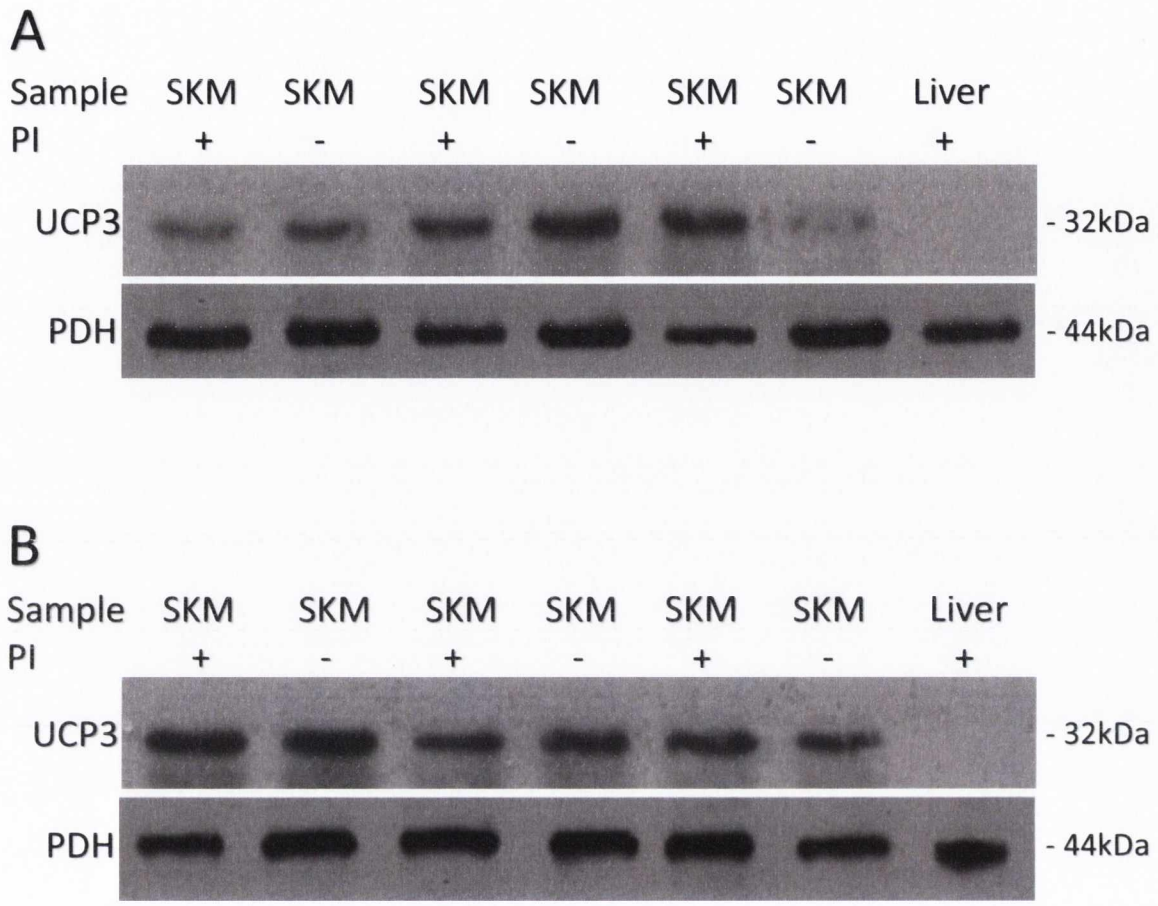


Figure 6-2: Short term starvation significantly increases UCP3 protein abundance in SKM of WT mice

Anti-UCP3 immunoblot of 50µg skeletal muscle mitochondrial protein (SKM) isolated in the presence or absence of phosphatase inhibitors (+-PI) and 50µg liver mitochondria as negative control of A) ad libitum fed animals and B) 24h fasted animals. Mitochondria were isolated as described in section 2.15 and submitted to western blotting as described in section 2.18, 2.19 and 2.20 using anti-UCP3 (1/1000, Eurogenetec) and anti-PDH-E1-alpha (1/1000, Mitosciences, cat#MSPO3) for immunodetection as indicated.

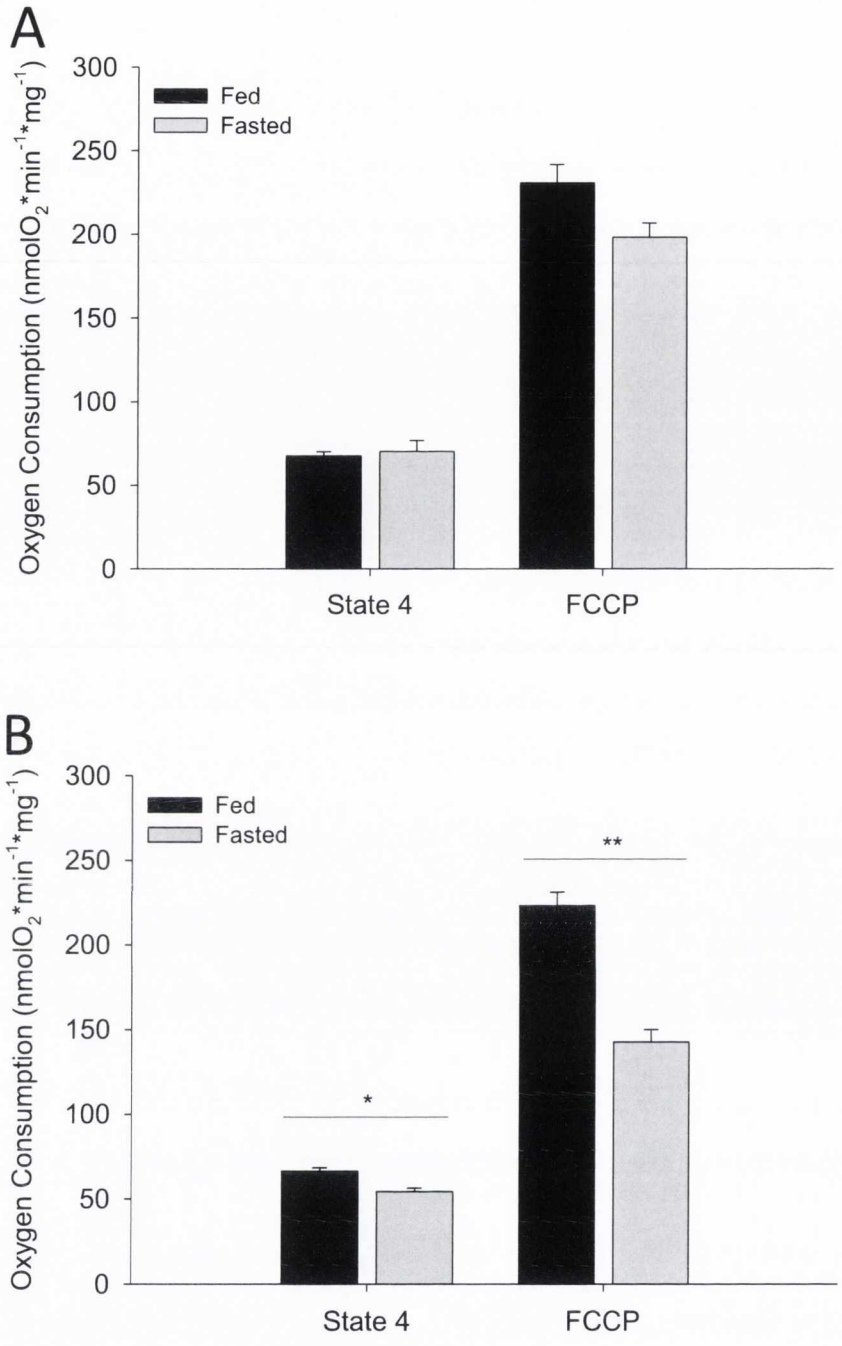


Figure 6-3: Short term starvation does not affect oxygen consumption in skeletal muscle mitochondria respiring on succinate

State 4 non-phosphorylating and FCCP uncoupled oxygen consumption rates (nmol O_2*min^{-1}*mg mitochondrial $protein^{-1}$) in SKM mitochondria of fed compared to 24h starved WT mice isolated with (A) or without (B) phosphatase inhibitors respiring on succinate. Data is expressed as mean ± SEM of at least 3 experiments, each experiment performed in triplicate. P values ≤ 0.05 on unpaired student's t-test were deemed significant (* $P \leq 0.05$; ** $P \leq 0.01$; *** $P \leq 0.001$).

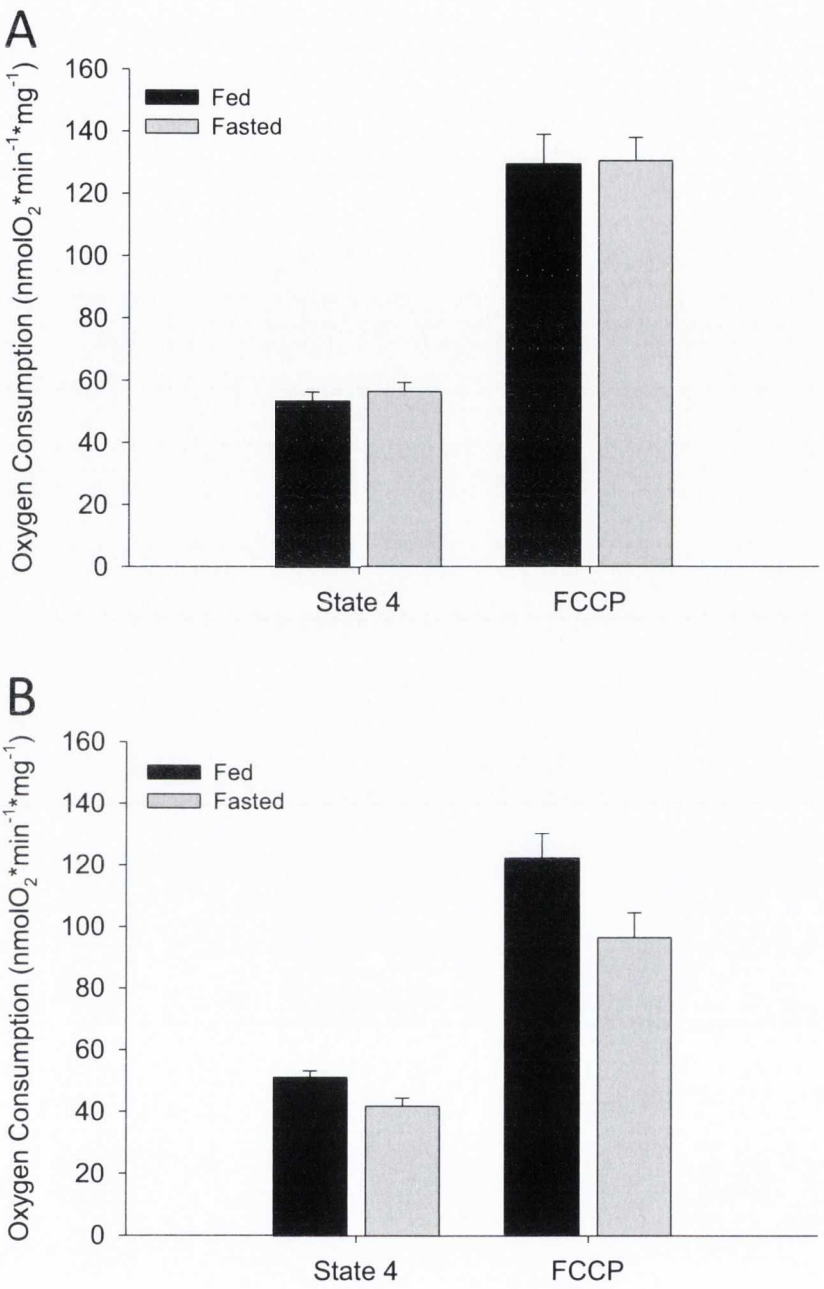


Figure 6-4: Short term starvation does not affect oxygen consumption in skeletal muscle mitochondria respiring on glycerol-3-phosphate

State 4 non-phosphorylating and FCCP uncoupled oxygen consumption rates (nmol O_2*min^{-1}*mg mitochondrial $protein^{-1}$) in SKM mitochondria of fed compared to 24h starved WT mice isolated with (A) or without (B) phosphatase inhibitors respiring on glycerol-3-phosphate. Data is expressed as mean ± SEM of at least 3 experiments, each experiment performed in triplicate. P values ≤ 0.05 on unpaired student's t-test were deemed significant (* $P \leq 0.05$; ** $P \leq 0.01$; *** $P \leq 0.001$).

Table 7: Respiratory control ratios

RCRs of mitochondria respiring on succinate and isolated from fed or fasted animals with or without phosphatase inhibitors (+/- PI). Values are means ± SEM. Student's unpaired t-test was used to determine significant differences between fed and fasted RCRs (* $P \leq 0.05$; ** $P \leq 0.01$; *** $P \leq 0.001$)

	fed	fasted	t-test
+PI	3.41 ± 0.03	2.85 ± 0.15	* P = 0.02
-PI	3.36 ± 0.03	2.62 ± 0.03	***P = 0.0001

6.2.3 Effects of cold acclimation on SKM and BAT mitochondria in WT and UCP1-KO mice

UCP1 is known to be of vital importance in non-shivering thermogenesis, but no thermogenic function has been reported for UCP3 so far. However, the capacity of UCP3 to uncouple oxidative phosphorylation has been demonstrated on several occasions (Boss *et al.* 2000; Harper *et al.* 2002), giving it the potential to at least participate in thermogenesis. WT mice are able to defend their body temperature, first by generating heat through shivering. After an acclimation period of about three days, shivering is gradually replaced by non-shivering thermogenesis through activated BAT with active UCP1. However, UCP1-/- mice cannot defend their core body temperature and have to rely completely on shivering or alternative thermogenic pathways. Our laboratory reported pharmacological activation of UCP3 due to phosphorylation following MDMA treatment in the presence of phosphatase inhibitors (Kelly *et al.* 2011a). MDMA has been reported to raise the body temperature by unknown mechanisms. With cold acclimation, the activation of UCP1 in activated BAT and UCP3 in skeletal muscle was investigated. Specifically UCP3 in skeletal muscle mitochondria of UCP1-/- mice was of great interest, as UCP3 might adept a thermogenic function to compensate for the lack of UCP1 and might be activated by phosphorylation in accordance with MDMA treatment. Acclimation to the cold represents a more physiological treatment compared to MDMA treatment.

Figure 6-5 and Figure 6-6 illustrate the oxygen consumption rates in SKM mitochondria of cold acclimated WT compared to UCP1-/- mice respiring on succinate (Figure 6-5A and B) or glycerol-3-phosphate (Figure 6-6A and B) in state 4 and following FCCP titration to achieve the maximal uncoupled rate in the presence or absence of phosphatase inhibitors. In Figure 6-6A, the state 4 oxygen consumption rate was significantly higher in WT (82.1 ± 3.9) compared to UCP1-/- mitochondria (53.0 ± 1.0, P=0.0005) isolated in the presence of phosphatase inhibitors and respiring on succinate. Also the FCCP maximal uncoupled rate was significantly higher in mitochondria of WT compared to UCP1-/- mice (304.2 ± 12.5 and 161.6 ± 4.8 respectively, P=0.0001). In the absence of phosphatase inhibitors (Figure 6-5B), WT mitochondria respiring on succinate showed only slightly, but not significantly higher oxygen consumption rates compared to mitochondria of UCP1-/- mice in state 4. The maximal uncoupled rate (FCCP) was still

significantly higher in WT compared to UCP1-/- (P=0.006), but not to the same extent as in Figure 6-5A. Mitochondria of WT animals isolated in the presence of phosphatase inhibitors and respiring on glycerol-3-phosphate (Figure 6-6A) showed significantly higher oxygen consumption in state 4 compared to UCP1-/- mitochondria. The uncoupled rate with FCCP was still considerably higher in WT compared to UCP1-/- mitochondria, but that difference was not significant. Mitochondria of WT muscle tissue, that were isolated without phosphatase inhibitors and respiring on glycerol-3-phosphate (Figure 6-6B) showed slightly increased oxygen consumption rates both in state 4 and following artificial uncoupling with FCCP (not significant).

Figure 6-7 compares state 4 and FCCP uncoupled oxygen consumption rates of SKM mitochondria isolated from room temperature (RT) or cold acclimated (CA) WT mice in the presence or absence of PI. With succinate as substrate, cold acclimated mitochondria displayed significantly higher state 4 and FCCP uncoupled oxygen consumption compared to mitochondria from animals acclimated to RT. This observation was independent of the phosphorylation state with increased oxygen consumption in mitochondrial isolations with or without PI.

Figure 6-8 shows the oxygen consumption rates in BAT mitochondria isolated from WT mice with or without phosphatase inhibitors. The state 4 oxygen consumption rate of BAT mitochondria respiring on succinate was not different in BAT mitochondria of cold acclimated WT mice plus and minus phosphatase inhibitors (Figure 6-8A). The state 4 rates were inhibitable by GDP to the same extent, regardless of treatment with phosphatase inhibitors. This indicates that the GDP inhibitable portion of the state 4 rate, attributed to uncoupling by UCP1 in BAT, was not affected by phosphatase inhibitor treatment. The initial state 4 rate was almost completely recoverable by artificial uncoupling with FCCP after inhibition with GDP. The same observations were made with mitochondria respiring on glycerol-3-phosphate in the presence of 50nM free Ca^{2+}, only that all rates were higher confirming the high expression levels of functional mGPDH in BAT and its up-regulation by cold acclimation (Figure 6-8B). The state 4 oxygen consumption rate was also significantly inhibitable with GDP and recovered with FCCP as demonstrated in oxygen consumption measurements of BAT mitochondria with succinate as substrate.

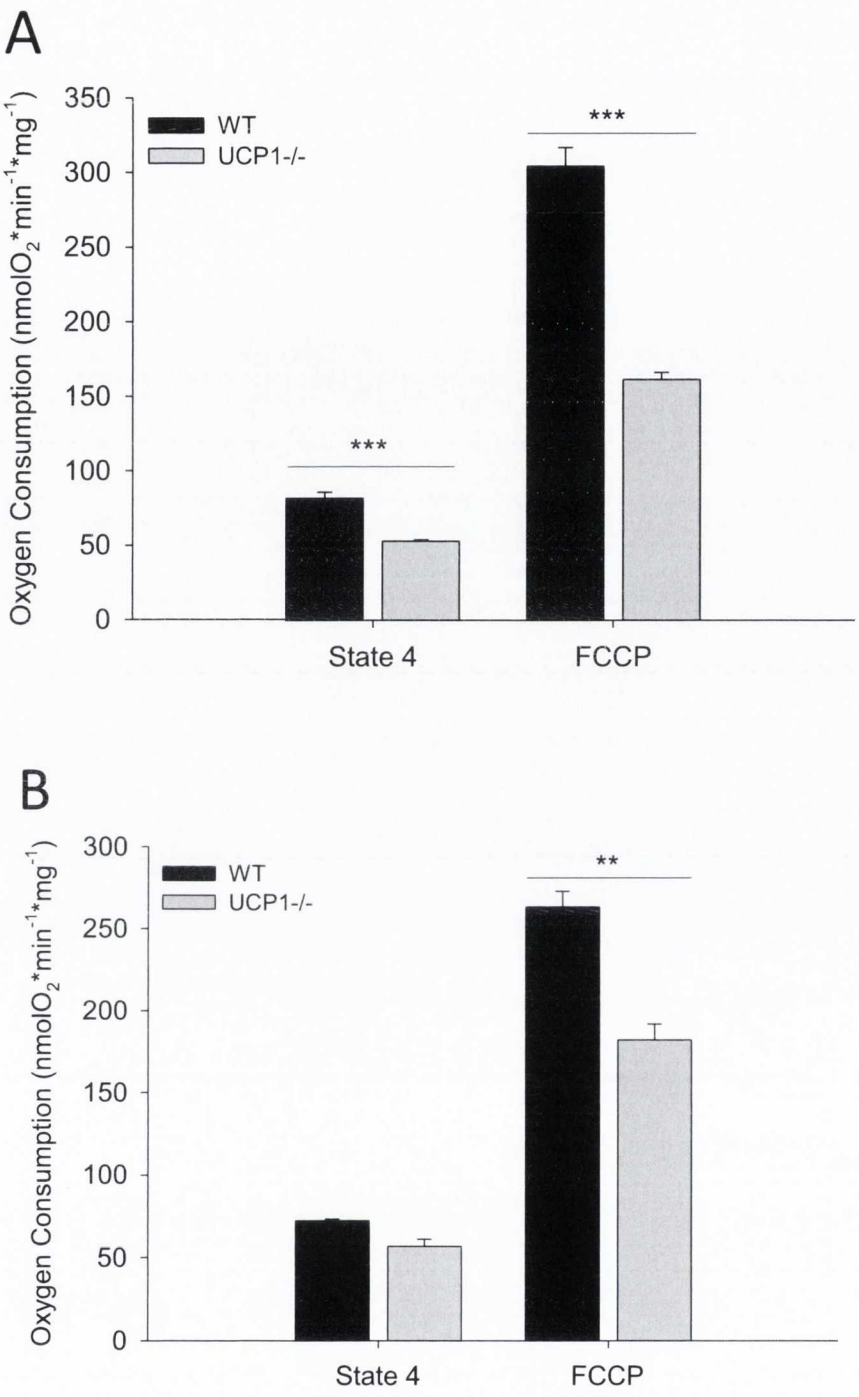


Figure 6-5: Reduced oxygen consumption in skeletal muscle mitochondria of cold acclimated UCP1 knock-out mice respiring on succinate

Oxygen consumption rates (nmol O_2*min^{-1}*mg mitochondrial $protein^{-1}$) in SKM mitochondria of cold acclimated WT and UCP1-/- mice plus (A) and minus (B) phosphatase inhibitors respiring on succinate in state 4 and after titration with FCCP. Data is expressed as mean ± SEM of at least 3 experiments, each experiment performed in triplicate. P values ≤ 0.05 on unpaired student's t-test were deemed significant (* P ≤ 0.05; ** P ≤ 0.01; *** P ≤ 0.001).

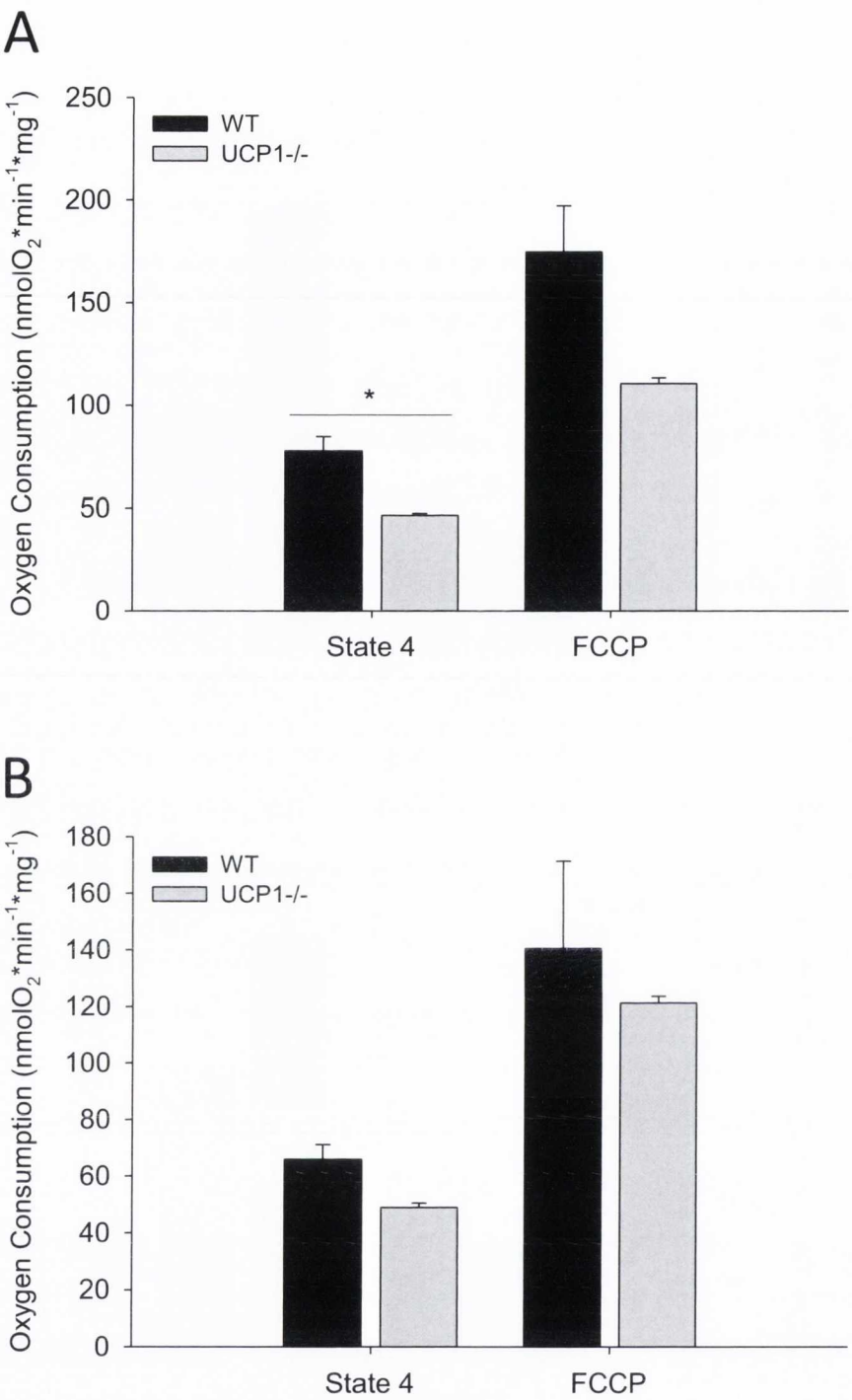


Figure 6-6: Reduced oxygen consumption in skeletal muscle mitochondria of cold acclimated UCP1 knock-out mice respiring on glycerol-3-phosphate

Oxygen consumption rates (nmol O_2*min^{-1}*mg mitochondrial $protein^{-1}$) in SKM mitochondria of cold acclimated WT and UCP1-/- mice plus (A) and minus (B) phosphatase inhibitors respiring on glycerol-3-phosphate in state 4 and after titration with FCCP. Data is expressed as mean ± SEM of at least 3 experiments, each experiment performed in triplicate. P values ≤ 0.05 on unpaired student's t-test were deemed significant (* $P \leq 0.05$; ** $P \leq 0.01$; *** $P \leq 0.001$).

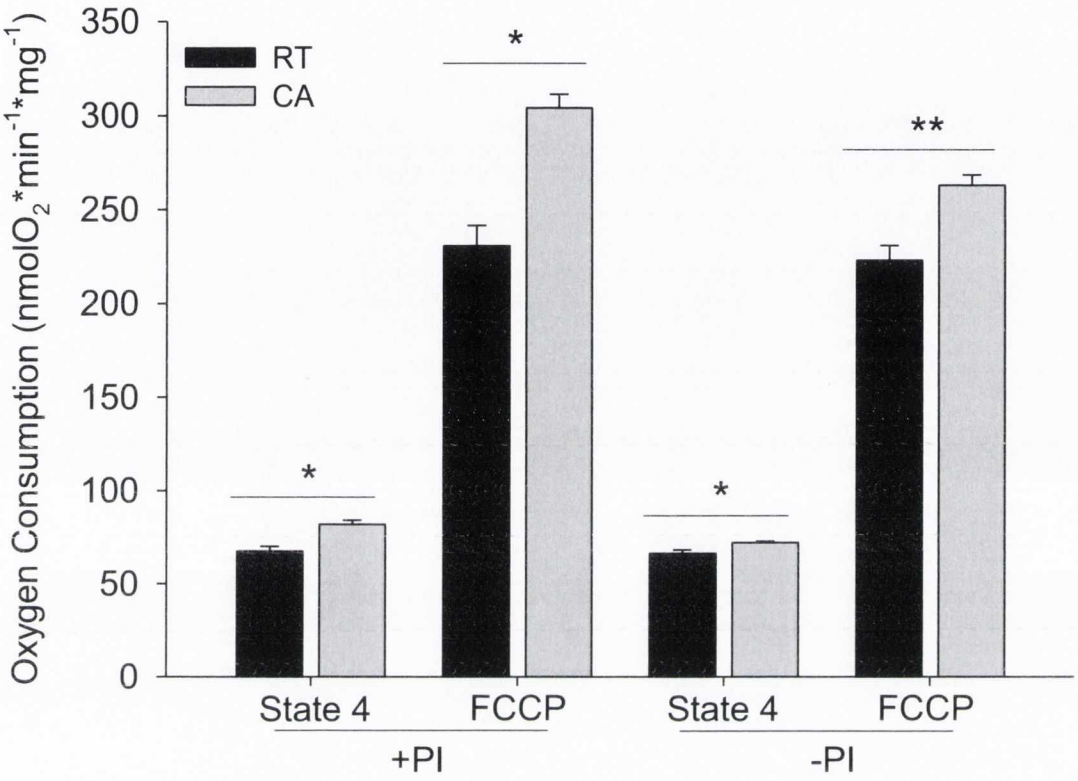


Figure 6-7: Increased oxygen consumption in skeletal muscle mitochondria of cold acclimated WT mice respiring on succinate

Succinate supported state 4 non-phosphorylating and FCCP uncoupled oxygen consumption rates of SKM mitochondria isolated from room temperature or 4°C cold acclimated WT mice. Mitochondria were isolated in the presence (+PI) or absence (-PI) of phosphatase inhibitors. Data is expressed as mean ± SEM of at least 3 experiments, each experiment performed in triplicate. P values ≤ 0.05 on unpaired student's t-test were deemed significant (* $P \leq 0.05$; ** $P \leq 0.01$; *** $P \leq 0.001$).

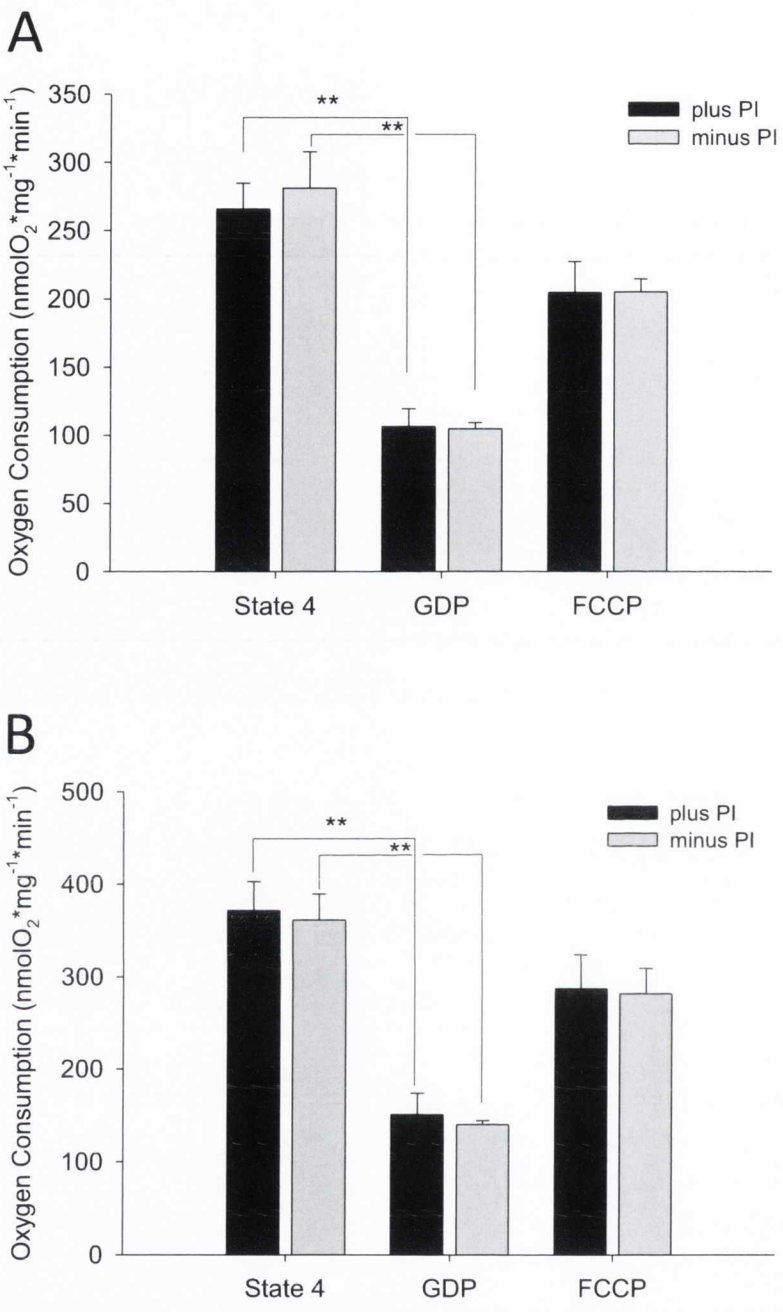


Figure 6-8: No effect of protection of phosphorylation on oxygen consumption in BAT mitochondria of cold acclimated WT mice

Oxygen consumption rates (nmol O_2*min^{-1}*mg mitochondrial $protein^{-1}$) in BAT mitochondria of cold acclimated WT mice plus and minus phosphatase inhibitors (plus/minus PI) respiring on succinate (A) and glycerol-3-phosphate (B) in state 4 in the presence of oligomycin, after addition of 1mM GDP and titration with FCCP. Data is expressed as mean ± SEM of at least 3 experiments, each experiment performed in triplicate. P values ≤ 0.05 on unpaired student's t-test were deemed significant (* $P \leq 0.05$; ** $P \leq 0.01$; *** $P \leq 0.001$).

6.3 Discussion

In this study, I assessed the potential activation of UCP3 by phosphorylation under physiological conditions. Our laboratory previously presented evidence that systemic treatment with MDMA results in phosphorylation and activation of UCP3 to catalyse a proton leak in murine skeletal muscle mitochondria. To successfully measure elevated state 4 oxygen consumption the phosphorylation state had to be preserved during isolation of mitochondria by including phosphatase inhibitors in the isolation buffers (Kelly *et al.* 2011a).

One physiological situation animals encounter in the wild is cold stress. Prolonged cold exposure results in noradrenaline release and β3-adrenergic activation of BAT (Cannon *et al.* 2004) and heat generation by shivering is gradually replaced by UCP1 mediated non-shivering thermogenesis. It is thought that MDMA induced skeletal muscle hyperthermia may be triggered similarly by noradrenaline release and subsequent UCP3 activation in skeletal muscle (Sprague *et al.* 2007). WT mice were therefore injected with noradrenaline to artificially stimulate adrenergic pathways and try to mimic the effects of MDMA and exposure to the cold. Noradrenaline treatment of mice did not increase oxygen consumption in SKM mitochondria isolated in the presence of phosphatase inhibitors compared to mitochondria isolated from WT mice injected with PBS (Figure 6-1). Succinate supported state 4 oxygen consumption was significantly increased following titration with FCCP showing that the mitochondria were intact and coupled. Oxygen consumption in mitochondria respiring on G3P was also increased by FCCP, but to a much lesser extent. A similar phenomenon was already reported in chapter 5 of this work. An earlier study demonstrated a massive increase in whole animal oxygen consumption in cold acclimated WT mice following an injection of noradrenaline at thermoneutrality (Golozoubova *et al.* 2001). In contrast the effect in UCP1 ablated mice was much smaller and the authors concluded that no alternative noradrenaline-sensitive mechanism for non-shivering thermogenesis was in place to compensate for lack of UCP1. The data presented in Figure 6-1 confirmed these findings on a mitochondrial level. Having said that, data presented by Golozoubova *et al.* (2001) also showed that noradrenaline induced a peak in oxygen consumption in WT mice almost instantly and elevated the oxygen consumption only for about 30 minutes. Animals in my study

however were injected with noradrenaline and left for 1 hour before isolation of mitochondria to keep the procedure consistent with that of MDMA treatment for comparability. Thus, any effects of noradrenaline treatment on heat production in skeletal muscle may have been missed due to the later time (1h) of intervention. However, an immediate isolation of SKM mitochondria after NA injection did not show any effects either.

Short term fasting (24h) had been reported to significantly increase UCP3 protein in skeletal muscle mitochondria, but no changes in oxygen consumption or proton conductance were demonstrated (Cadenas *et al.* 1999; Zhou *et al.* 2000). We hypothesize that if UCP3 is upregulated it may also be activated by phosphorylation as was demonstrated for mitochondria isolated with phosphatase inhibitors (PI) from MDMA injected animals (Kelly *et al.* 2011a). To test this hypothesis, animals were deprived of food for 24h and SKM mitochondria isolated in the presence or absence of PI. UCP3 protein was present in higher amounts in fasted SKM mitochondria compared to mitochondria isolated from skeletal muscle of fed animals, while PDH abundance remained unaffected (Figure 6-2). This increase in signal strength was independent of isolations with or without PI. Succinate supported oxygen consumption rates in state 4 and after artificial uncoupling with FCCP were significantly reduced in mitochondria of fasted compared to fed mice in preparations without PI, but not in mitochondria isolated in the presence of PI (Figure 6-3A and B). G3P supported state 4 and uncoupled (FCCP) oxygen consumption rates in mitochondria isolated in the presence or absence of PI were not significantly different in fed compared to fasted animals (Figure 6-4A and B). Taken together, this shows that an increase in UCP3 protein does not translate to decreased coupling of the respiratory chain i.e. increased state 4 oxygen consumption due to phosphorylation and activation of UCP3 following short term starvation. If anything, the presented data would support the hypothesis that preservation of UCP3 phosphorylation following short term starvation maintains coupling efficiency in SKM mitochondria. In mitochondrial isolations without PI state 4 and FCCP uncoupled rates were significantly lower in fasted compared to fed animals which indicates the importance of phosphorylation preservation for the function of UCP3. These observations support our hypothesis of UCP3 activation by phosphorylation following treatment with MDMA (Kelly *et al.* 2011a).

To elucidate whether UCP3 could be activated through phosphorylation I looked at cold-acclimation in further experiments. Prolonged exposure to low temperatures triggers activation of non-shivering thermogenesis, involving noradrenaline signalling, fatty acid mobilisation and upregulation and activation of UCP1 in BAT which results in increased state 4 and GDP inhibitable oxygen consumption. Noradrenaline signalling plays a central role in this process, as pointed out before (Cannon *et al.* 2004). We proposed that there may be an element of non-shivering thermogenesis in skeletal muscle in wild-type mice and hypothesised that UCP3 in SKM (and or BAT) mitochondria might compensate for the lack of UCP1 in BAT of UCP1-/- mice and adapt a role as major heat producer by catalysing a proton leak across the inner mitochondrial membrane. This would enable animals to defend their body temperature by non-shivering thermogenesis and should manifest itself in increased state 4 oxygen consumption in SKM and maybe also in BAT mitochondria. SKM mitochondria of cold adapted animals lacking UCP1 and isolated in the presence of PI showed significantly reduced non-phosphorylating state 4 oxygen consumption compared to WT mice (Figure 6-5A; P=0.0005) with succinate as substrate. FCCP significantly increased oxygen consumption in both UCP1-/- and WT SKM mitochondria, which indicates that the mitochondria were intact following isolation. Surprisingly, FCCP induced respiration rates were also significantly lower in SKM mitochondria of animals lacking UCP1. This has not been described for room temperature adapted animals and indicates that the overall maximum respiratory chain capacity may be reduced in animals not expressing UCP1. Although UCP1 is not found in WT SKM mitochondria, the lack of UCP1 may have currently unknown consequences in tissues other than BAT. Interestingly, the significant reduction in non-phosphorylating respiration in UCP1-/- SKM mitochondria compared to WT following cold acclimation was dependent on the preservation of phosphorylation. In preparations performed without PI oxygen consumption in state 4 was not significantly lower, but the reduced FCCP rate in UCP1-/- mitochondria remained significantly reduced (Figure 6-5B) as seen in preparations with PI. Furthermore, state 4 oxygen consumption of UCP1-/- mitochondria remained roughly the same in mitochondrial isolations with or without PI. On the other hand, oxygen consumption in WT mitochondria isolated in the presence of PI was significantly higher than in isolations without PI (Figure 6-5A; P=0.01). This is contrary to our prediction. In UCP1-/- animals UCP3 was thought to be activated and to adopt the function of UCP1 in BAT or muscle to generate heat by increased uncoupling. Such an adapted thermogenic

function should manifest in an increased state 4 oxygen consumption rate that would possibly be phosphorylation sensitive. However, state 4, and interestingly also FCCP uncoupled oxygen consumption in WT, but not UCP1-/- animals was affected only in the presence of PI. The same observations apply for G3P supported oxygen consumption of SKM mitochondria isolated with or without PI. Again only mitochondria of WT animals and isolated in the presence of PI showed significantly increased state 4 oxygen consumption compared to UCP1-/- mitochondria following cold acclimation (Figure 6-6A and B). State 4 and FCCP uncoupled oxygen consumption rates were significantly lower in SKM mitochondria of WT mice housed at room temperature than in SKM mitochondria isolated from cold acclimated mice (Figure 6-7). This effect was not dependent on the phosphorylation state of the isolated mitochondria.

In BAT mitochondria of cold adapted WT animals isolated in the presence or absence of PI no differences in state 4 oxygen consumption or after addition of GDP and FCCP were detectable (Figure 6-8A and B). Unfortunately, no data for UCP1-/- BAT mitochondria was obtained due to difficulties to isolate sufficient amounts of mitochondria on each experimental day. Interscapular BAT depots in UCP1-/- mice were very small and hard to identify. In general, UCP1-/- mice were very fat and exhibited a vast amount of WAT, both peritoneal and subcutaneously. The original protocol for cold acclimation of UCP1-/- mice had to be prolonged by 4 weeks to allow for optimization of BAT mitochondria isolation and PI treatment. However, no consistent measurements were possible in BAT mitochondria of UCP1-/- mice, because UCP1-/- mice showed only small amounts of BAT tissue and therefore only minimal amounts of mitochondria could be isolated.

If UCP3 were to acquire a thermogenic function to compensate for the lack of non-shivering thermogenesis in BAT mitochondria, an increased state 4 oxygen consumption rate in SKM mitochondria as well as a significant upregulation of UCP3 protein would have been expected. It appears that lack of UCP1 is affecting mitochondrial function in SKM, but in the opposite way than anticipated. In fact, UCP3 upregulation had been reported before in muscle of cold acclimated UCP1-/- mice (Shabalina *et al.* 2010). Shabalina *et al.* (2010) found no effects on proton leak or oxygen consumption in UCP1-/- mice compared to WT. In the study by Shabalina *et al.* pyruvate and free fatty acids were used as substrates, whereas the oxygen consumption data presented in this chapter was

generated with succinate and glycerol-3-phosphate as substrates. Shabalina *et al.* (2010) had shown increased oxygen consumption in UCP1-/- muscle mitochondria with fatty acids as substrate while we demonstrated significantly reduced oxygen consumption in UCP1-/- muscle mitochondria with succinate and G3P substrates. The usage of different substrates may explain the discrepancy between the two studies.

Taken together, the MDMA induced increase in state 4 oxygen consumption in isolated SKM mitochondria could not be mimicked by systemic noradrenaline treatment. Moreover, short term starvation failed to induce the effects seen with MDMA treatment. Cold acclimation increased state 4 and FCCP uncoupled oxygen consumption in skeletal muscle from WT animals compared to rates in mitochondria of mice housed at RT, but the hypothesized increase of oxygen consumption due to elevated uncoupling activity of UCP3 in SKM of mice lacking UCP1 was not observed. UCP3 has been reported to be significantly upregulated in SKM mitochondria following short term starvation (Cadenas *et al.* 1999; Zhou *et al.* 2000) and also in cold acclimated UCP1-/- mice compared to cold acclimated WT animals (Shabalina *et al.* 2010). However, both physiological treatments used in this study resulted in reduced oxygen consumption compared to control animals, which does not support the proposed physiological phosphorylation and activation of UCP3. One possible explanation may be that all oxygen consumption rates were measured with succinate or G3P as substrates, while conditions like starvation or cold acclimation favour metabolism of mobilized fatty acids and therefore effects on UCP3 may become more apparent with fatty acids as substrate. Another logical conclusion is that UCP3 can only be phosphorylated pharmacologically and not in its native state under physiological conditions. These results confirm that upregulation of UCP3 protein in skeletal muscle mitochondria does not result in increased state 4 oxygen consumption and therefore not in increased proton leak as reported previously and that these observations are not dependent on phosphorylation state of isolated mitochondria. Nonetheless is UCP3 a promising target for the development of new treatments against obesity. A compound similar to MDMA, which pharmacologically triggers the phosphorylation and activation of UCP3 without the psychotropic effects, would be needed. However, this drug would have to have a very short half-life to allow for better control and to avoid potentially damaging side effects like hyperthermia.

Resveratrol and Exercise

Chapter 7

7 Resveratrol and Exercise

7.1 Introduction

Exercise increases mitochondrial biogenesis, insulin sensitivity, glucose tolerance and metabolic capacity in skeletal muscle tissue and is generally associated with beneficial effects. These effects are mainly mediated by PGC-1 α, which is deacetylated and activated by SIRT1 in response to conditions of high energy demand. These conditions include calorie restriction or fasting, acute cold exposure and of course exercise. A polyphenolic compound found in various plants and most prominently in the skin of red grapes, called resveratrol, is thought to mimic the effects of calorie restriction and possibly also of exercise. Mechanistically it is a known activator of SIRT1 *in vitro* and *in vivo* and may therefore indirectly activate PGC-1α.

In the present work the effects of a short term resveratrol treatment on metabolism in cells and isolated mitochondria of skeletal muscle and brown adipose tissue compared to a moderate exercise regime and untreated controls were investigated. In addition, the role of UCP1 in BAT and UCP3 in skeletal muscle in resveratrol or exercise mediated metabolic changes are explored.

7.2 Results

7.2.1 Effects of Resveratrol and Exercise on BAT cell oxygen consumption

Resveratrol is thought to mimic some of the effects of exercise. In this section, the adaptations of resveratrol treatment and exercise were investigated in brown adipose tissue and skeletal muscle of rats treated with a (low) amount of resveratrol or moderate exercise in comparison to untreated control animals.

Figure 7-4 shows cellular oxygen consumption rates (in nmol O_2/min/5*10^4 cells) of mature brown adipose tissue (BAT) cells isolated from control animals and rats treated with resveratrol or an exercise regime (for details see Materials and Methods section 2.26) measured with an Oxygraph-2k (Oroboros). After addition of cells to the pre-calibrated incubation buffer (complete BAT Ringer) an initial fast rate was observed which declined constantly until the rate stabilized after about 30min and was taken as the basal cellular respiration rate (Basal). The basal rate was significantly decreased in BAT cells of exercised animals (Basal Exercised 2.63 ± 0.24) compared to controls (Basal Control 4.18 ± 0.61; P=0.03) and resveratrol treated animals (Basal Resveratrol 3.62 ± 0.17; P=0.004), but no significant difference was observed between basal oxygen consumption rates of BAT cells from control and resveratrol treated rats. Addition of noradrenaline triggered a steep and instantaneous increase in oxygen consumption rates in all three groups. The noradrenaline stimulated oxygen consumption rate was increased 6.8-fold in control animals (NA Control 27.20 ± 3.71; P=0.00003), 11.1-fold in resveratrol treated animals (NA Resveratrol 39.63 ± 2.56; P=0.000000001) and 6-fold in exercised animals (NA Exercised 14.98 ± 0.96; P= 0.0000000003). The degree as to which noradrenaline stimulated oxygen consumption in BAT cells was also significantly different between the three groups as cells from resveratrol treated animals showed the highest rate of stimulation compared to cells from controls (P=0.03) or exercised (P=0.02) animals. However, the degree of stimulation of oxygen consumption with noradrenaline was not significantly different between BAT cells of control and exercised animals (P=0.48). The non-phosphorylating oxygen consumption rate after addition of oligomycin was significantly reduced in BAT cells of control (16.01 ± 2.15; P=0.02), resveratrol treated (16.40 ± 1.21; P=0.000001) and exercised rats (7.89 ± 0.35; P=0.000016) compared to noradrenaline stimulated oxygen consumption rates as expected. The oxygen

consumption rates in the presence of oligomycin where not significantly different between BAT cells from resveratrol treated and control rats, but BAT cells isolated from exercised animals showed significantly reduced non-phosphorylating oxygen consumption rates compared to resveratrol treated (P=0.00005) or control rats (P=0.005). Artificial uncoupling with FCCP increased oxygen consumption rates slightly compared to non-phosphorylating rates in the presence of oligomycin in BAT cells isolated from control (21.06 ± 3.02), resveratrol treated (19.90 ± 1.79) and exercised rats (10.12 ± 0.89), but this increase was not significant in all three groups. Complete inhibition of mitochondrial complex III and therefore mitochondrial oxygen consumption by addition of antimycin A resulted in a marked decrease in oxygen consumption in BAT cells from control (1.36 ± 0.21; P=0.00001), resveratrol treated (1.27 ± 0.11;P=0.00000006) and exercised animals (0.77 ± 0.04; P=0.000000002). The differences in the antimycin A inhibited oxygen consumption rates were not significant between the three groups, showing that non-mitochondrial oxygen consumption was not affected by the treatments and equal numbers of cells were used in the experiments.

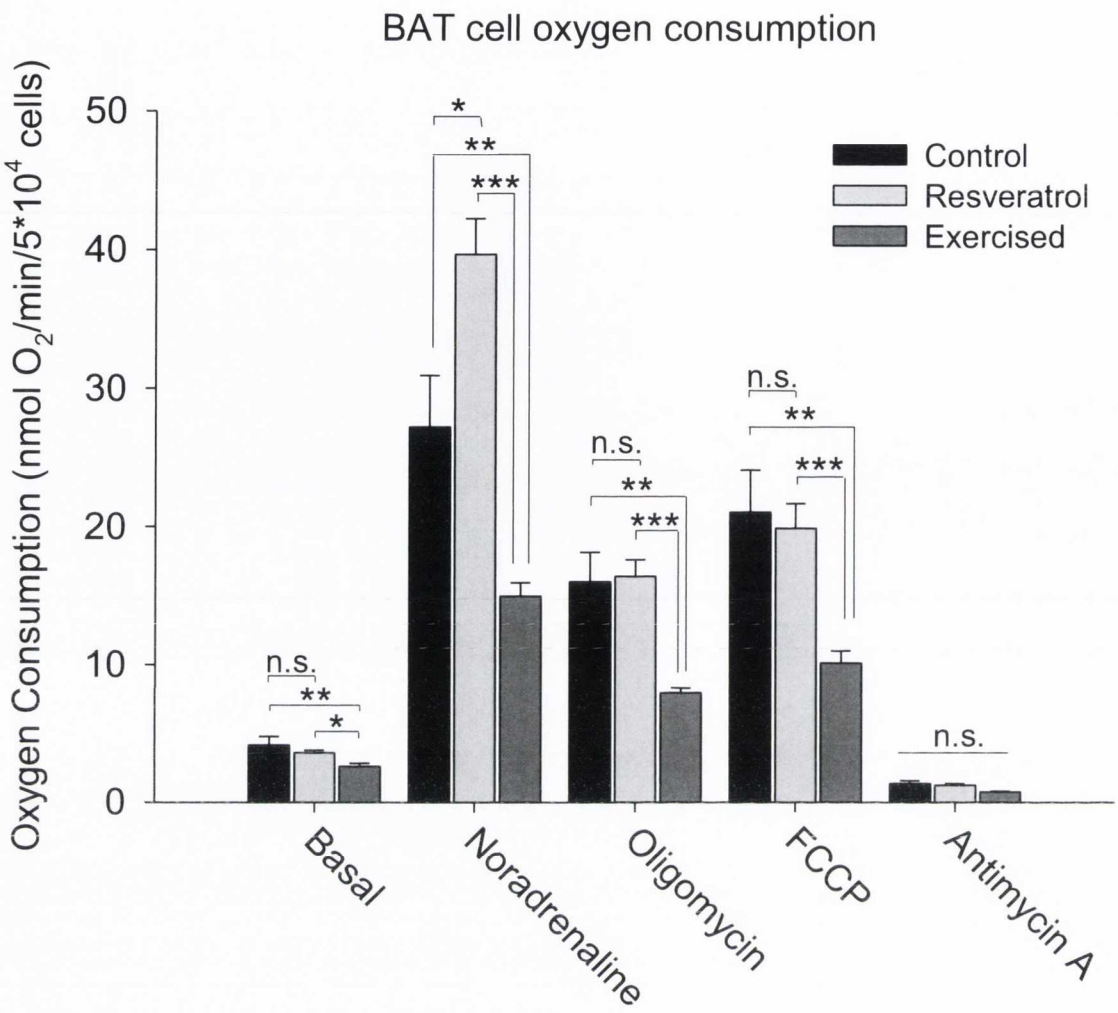


Figure 7-1: Resveratrol increases response to Noradrenaline in BAT cells and Exercise reduces metabolic capacity in BAT cells.

Oxygen consumption of isolated mature BAT cells isolated from Resveratrol treated, exercised or untreated (control) rats measured with an Oroboros Oxygraph-2k in complete Ringers BAT solution (see Materials and Methods section 2.29). Illustrated are the oxygen consumption rates with Pyruvate, Fructose and Glucose as substrates (basal), after maximal physiological stimulation with noradrenaline, the non-phosphorylating rate (oligomycin), maximal non-physiological respiratory capacity (FCCP) and non-mitochondrial oxygen consumption rate (antimycin A). Measurements were performed in duplicate for each condition on four individual days. Data were analyzed by unpaired student's t-test. (* $P<0.05$; ** $P<0.01$; ***$P<0.001$).

7.2.2 Resveratrol and Exercise do not affect skeletal muscle fibre oxygen consumption and extracellular acidification

Figure 7-2 illustrates the cellular oxygen consumption rates (OCR in pmolO_2/min) of intact muscle fibres isolated from control, resveratrol treated and exercised rats. The fibres were isolated from the *flexor digitorum brevis* (FDB) muscles in the hind feet of rats following a slightly modified protocol optimized for isolation of FDB muscle fibres from mice and measurement of cellular oxygen consumption with a Seahorse XF24-3 Analyser (Schuh *et al.* 2012). The basal respiratory rate was measured in the presence of glucose as substrate and was elevated in muscle fibres of exercised animals (290.39 ± 67.81) compared to resveratrol treated (181.50 ± 20.51) or control rats (215.51 ± 44.01), although this difference was not significant. Addition of oligomycin lowered the oxygen consumption rate in muscle fibres of all three groups. In the control (119.83 ± 17.30) and exercised group (169.65 ± 44.91) this reduction was not significant, but muscle fibres of resveratrol treated animals (109.10 ± 8.47) showed significantly reduced oxygen consumption in the presence of oligomycin compared to basal rates (P=0.03). Uncoupling with FCCP and the addition of pyruvate increased the oxygen consumption rates as expected, but these changes were not significant (Control: 141.75 ± 29.69; Resveratrol: 180.83 ± 35.31; Exercised: 261.69 ± 105.48). It is noteworthy that the FCCP stimulated rate was not further increasable by addition of pyruvate in the exercised group (262.94 ± 75.38), whereas fibres of control (183.92 ± 25.66) and resveratrol treated animals (234.27 ± 45.87) respired faster after the addition of pyruvate compared to the FCCP uncoupled rate. Pyruvate was added FCCP in this experiment to provide the muscle fibres with an additional substrate and to replenish tricarboxylic acid cycle components. The last addition (antimycin A) inhibited the mitochondrial complex III in the respiratory chain and significantly reduced the oxygen consumption rate in fibres of control (47.09 ± 13.44; P=0.009), resveratrol treated (65.28 ± 9.49; P= 0.02) and exercised animals (62.83 ± 2.25; P= 0.05).

Overall there were no significant differences found in the oxygen consumption rates of intact muscle fibres following exercise and resveratrol treatment compared to control animals. The relatively low stimulation of respiration by FCCP and the large day to day variability within the groups (large standard error means) indicate, that the muscle

fibres were not in optimal condition and thus drawing conclusions from these results is difficult.

The Seahorse XF24-3 Analyser allows for simultaneous measurement of oxygen consumption rate (OCR) and extracellular acidification rate (ECAR in mpH/min) which is shown in Figure 7-3 for intact muscle fibres of control, resveratrol treated and exercised rats under the same conditions as the OCR measurements. Basal ECAR was highest in fibres of the control group (40.54 ± 11.60), followed by fibres of resveratrol treated animals (30.26 ± 6.74) and was lowest in fibres isolated from exercised animals (15.89 ± 9.20). However, these differences were not significant. Addition and thus inhibition of mitochondrial F_1F_0-ATP synthase with oligomycin surprisingly resulted in a non-significant reduction of ECAR in all three groups (Control: 15.94 ± 5.15; Resveratrol 17.26 ± 8.94; Exercised 10.17 ± 4.82). It was expected that inhibition of mitochondrial oxygen consumption would push the cellular metabolism more towards glycolysis and lactate fermentation, hence increase ECAR. The same applies for the addition of FCCP. Disruption of the mitochondrial membrane potential and therefore increased mitochondrial oxygen consumption without the production of ATP should have increased glycolysis to satisfy the cellular ATP demand. However, the opposite was the case, where ECAR of control fibres was 8.68 ± 1.36, ECAR of fibres from resveratrol treated animals was 14.64 ± 8.01 and that of exercised rats 4.42 ± 3.15. Surprisingly, addition of pyruvate increased the ECAR in fibres of all three groups up to or beyond the ECAR in the presence of oligomycin (Control: 19.57 ± 2.58; Resveratrol: 18.19 ± 8.42; Exercised 9.69 ± 4.10). Antimycin A completely inhibited mitochondrial oxygen consumption and should therefore increase ECAR significantly, but instead the ECAR of fibres from control (9.29 ± 1.93), resveratrol treated (7.66 ± 4.34) and exercised animals (4.79 ± 2.35) was reduced.

The rate changes in ECAR indicate that the basic experimental setup was correct, but it may be that the isolation procedure of the muscle fibres did not yield sufficiently intact fibres in their native state. However, the differences between the groups in ECAR directly reflect the differences between the groups in OCR, where fibres of resveratrol treated and control animals showed similar rates, and fibres of exercised rats showed higher oxygen consumption rates and reduced extracellular acidification rates. In that respect, the presented results are consistent. However, the ECAR did not change as expected in all three groups and together with the high variability in OCR and insignificant

induction of oxygen consumption with FCCP, it appears that the experimental parameters were not optimal and need more optimisation to increase reliability of the method. It may be that the parameters adapted from a protocol optimised for mice muscle fibres were inadequate for measurements in muscle fibres from rats as those are larger, longer and also have other varying properties compared to murine muscle fibres.

To further investigate the effects of resveratrol treatment and exercise on mitochondrial function, the oxygen consumption of isolated BAT and SKM mitochondria was examined.

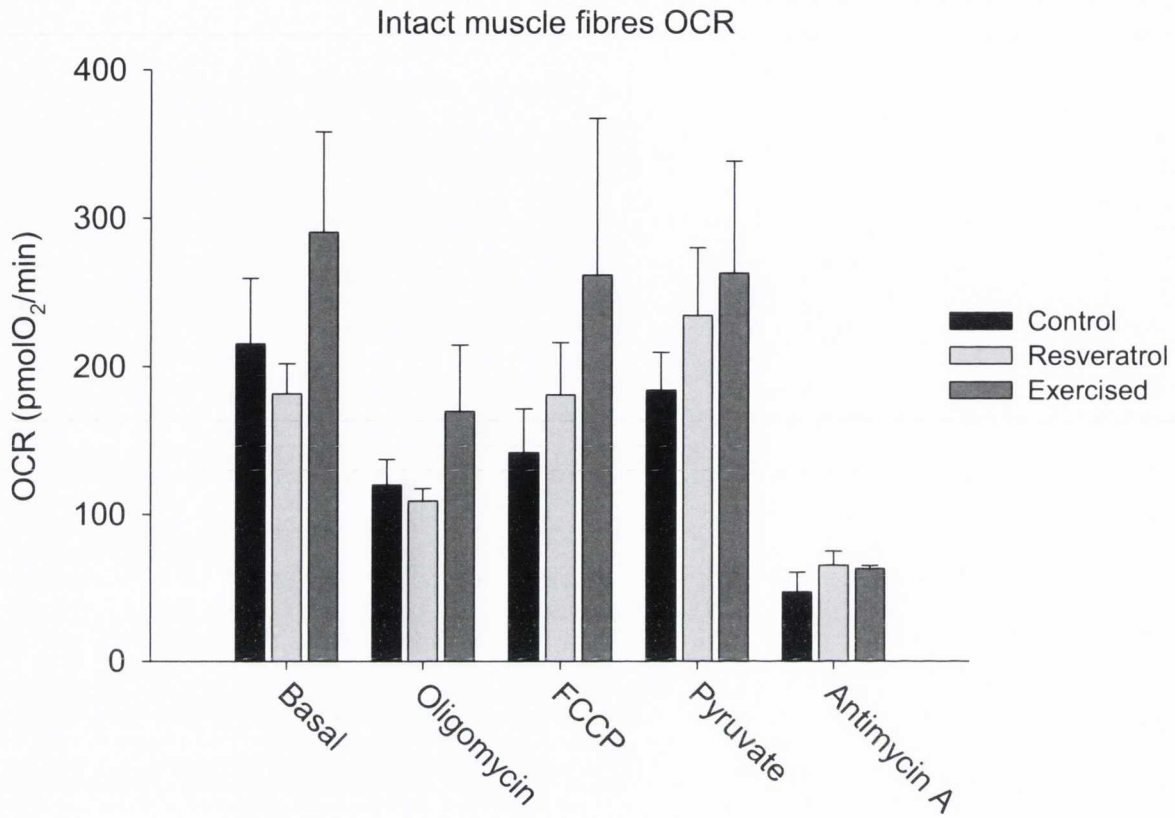


Figure 7-2: Resveratrol treatment and exercise do not affect oxygen consumption in isolated intact muscle fibres.

The oxygen consumption rate (OCR in $pmolO_2/min$) of muscle fibres isolated from resveratrol treated, exercised or untreated (control) rats were measured with Seahorse XF24-3 Analyser (see Materials and Methods section 2.30). Illustrated are the cellular oxygen consumption rates with glucose as substrate (basal), non-phosphorylating rates (oligomycin), maximal non-physiological respiratory capacity (FCCP), after replenishing the cells with an additional substrate (pyruvate) and after inhibition of mitochondrial oxygen consumption (antimycin A). Measurements were performed in quadruplets for each condition on four individual days. Data was analysed by unpaired student's t-test. (* $P<0.05$; ** $P<0.01$; ***$P<0.001$)

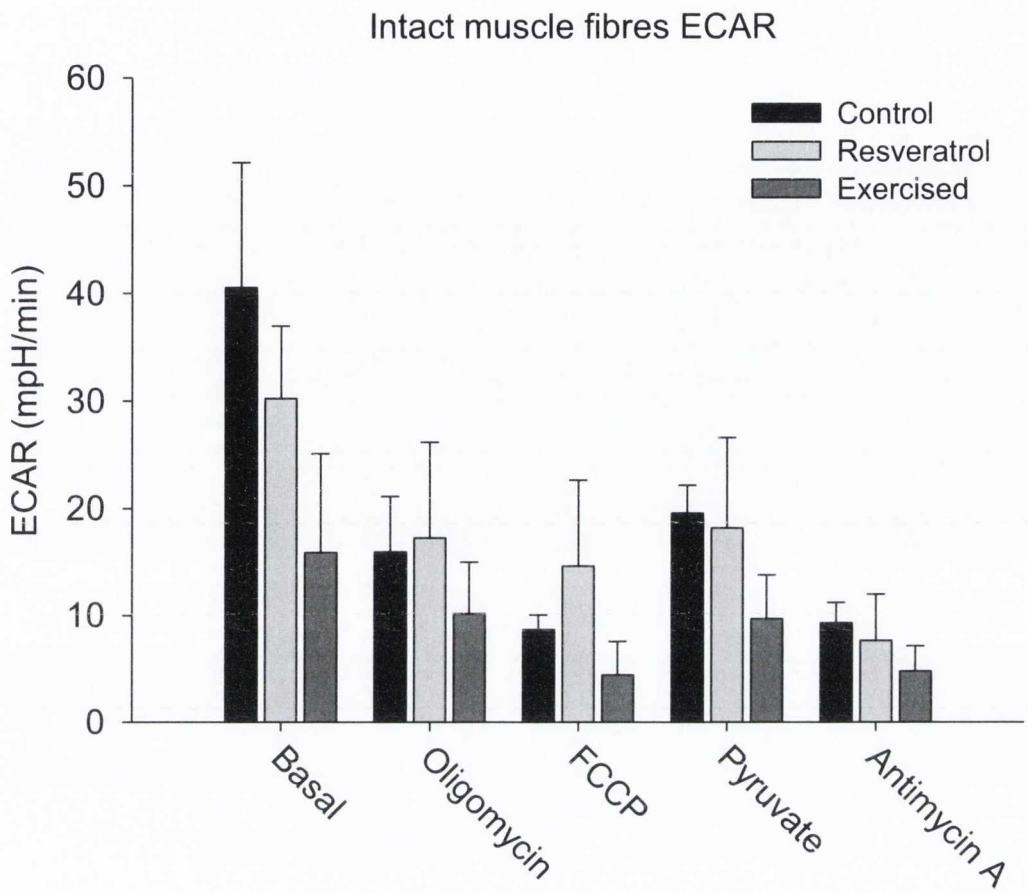


Figure 7-3: Resveratrol treatment and exercise do not affect the extracellular acidification rate (ECAR) in isolated intact muscle fibres.

The extracellular acidification rate (ECAR in mpH/min) of muscle fibres isolated from resveratrol treated, exercised or untreated (control) rats were measured with Seahorse XF24-3 Analyser (see Materials and Methods section 2.30). Illustrated are the extracellular acidification rates with glucose as substrate (basal), non-phosphorylating rates (oligomycin), maximal non-physiological respiratory capacity (FCCP), after replenishing the cells with an additional substrate (pyruvate) and after inhibition of mitochondrial oxygen consumption (antimycin A). Measurements were performed in quadruplets for each condition on four individual days. Data was analysed by unpaired student's t-test. (* $P<0.05$; ** $P<0.01$; ***$P<0.001$)

7.2.3 Effects of Resveratrol and Exercise on oxygen consumption in BAT and SKM mitochondria

Figure 7-4 illustrates oxygen consumption rates of brown adipose tissue (BAT) mitochondria in four different states. The basal oxygen consumption rate with pyruvate/malate and succinate as substrates was not different in BAT mitochondria of resveratrol treated compared to exercised rats. Nonetheless BAT mitochondria of control animals showed significantly increased oxygen consumption rates compared to rates in BAT mitochondria of resveratrol treated (P=0.027) or exercised (P=0.001) animals. Oligomycin significantly reduced oxygen consumption in BAT mitochondria of control animals, but resveratrol treated or exercised BAT mitochondria showed only a small reduction in oxygen consumption upon oligomycin addition. However, the leak rate (oligomycin) was significantly higher in BAT mitochondria of control animals compared to BAT mitochondria of resveratrol treated (P=0.018) or exercised (P=0.009) rats. GDP significantly reduced respiration in BAT mitochondria of the control group (P=0.0019), but oxygen consumption rates were not significantly different in BAT mitochondria of resveratrol treated and exercised compared to control animals. Upon addition of FCCP, respiration increased in BAT mitochondria of all three groups, but this increase was only significant in BAT mitochondria of the control group which also showed significantly greater oxygen consumption compared to rates in BAT mitochondria of resveratrol treated (P=0.016) or exercised (P=0.017) animals.

The basal respiration rate was significantly different from the state 4 oligomycin inhibited rate only in BAT mitochondria of the control group but not in BAT mitochondria of resveratrol treated or exercised animals. The same observation applies to the transition from the oligomycin inhibited to the GDP treated rate and GDP to FCCP rate.

The fact that oxygen consumption in BAT mitochondria was inhibitable with oligomycin and more so with GDP, and that this reduction was overcome by the addition of the artificial uncoupler FCCP to restore the rates to the initial (basal) oxygen consumption rates in all three groups, demonstrates that the isolated BAT mitochondria were intact and coupled.

The observation that GDP reduced oxygen consumption more significantly in BAT mitochondria of control rats compared to BAT mitochondria of resveratrol treated and exercised animals indicates the involvement of the GDP-inhibitable UCP1 which catalyses a tightly controlled proton leak in BAT mitochondria. It may be that UCP1 was a) more active or b) more abundant per mg mitochondrial protein in BAT mitochondria of control rats compared to BAT mitochondria of exercised or resveratrol treated animals.

Figure 7-5 shows oxygen consumption rates of skeletal muscle (SKM) mitochondria in four different states. The basal oxygen consumption rate with pyruvate/malate and succinate as substrates was not different in SKM mitochondria of resveratrol treated rats compared to exercised or control animals. Addition of ADP stimulated a ~2-fold increase in oxygen consumption in SKM mitochondria of resveratrol treated, exercised and control animals and treatment with oligomycin reduced the oxygen consumption to the same extent in all three conditions. Stimulation with FCCP increased oxygen consumption ~4-fold, showing that the maximal respiratory capacity in SKM mitochondria was not affected by treatment with resveratrol or by exercise compared to controls.

I conclude that the SKM mitochondria were intact and coupled and that exercise or treatment with resveratrol does not alter the physiological or non-physiological maximal respiratory capacities or leak rate in SKM mitochondria.

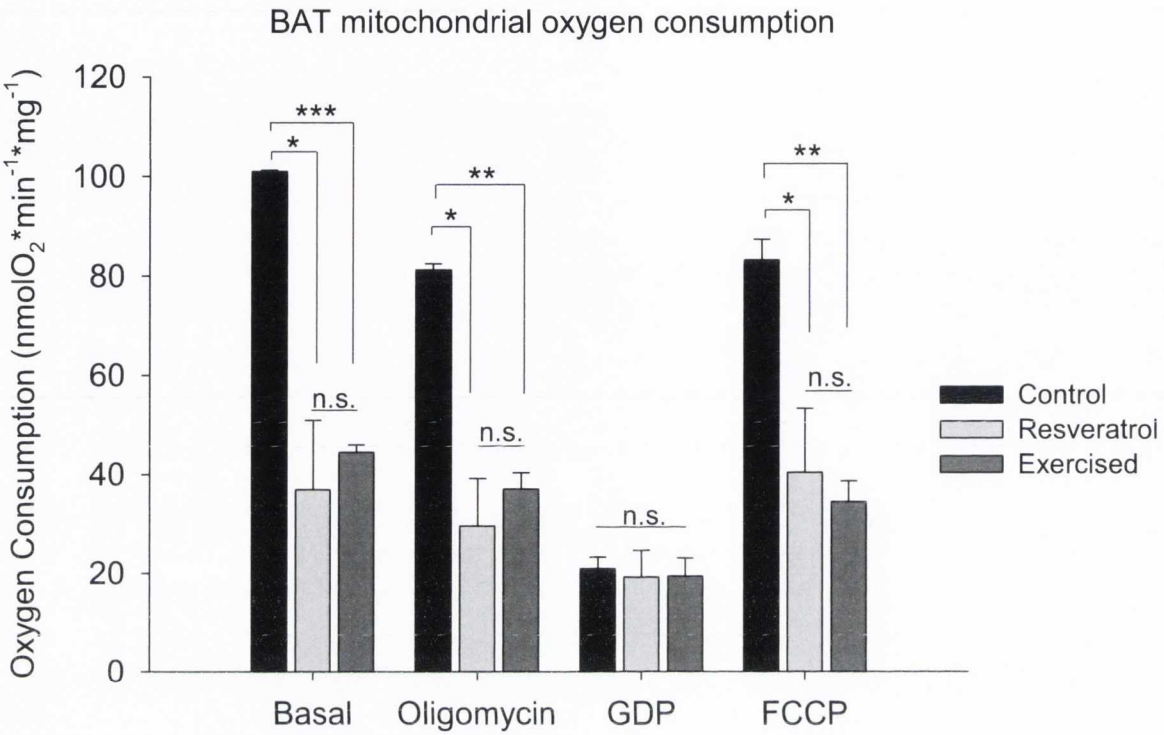


Figure 7-4: Resveratrol treatment and exercise reduce oxygen consumption in brown adipose tissue mitochondria.

Oxygen consumption of brown adipose tissue (BAT) mitochondria isolated from resveratrol treated, exercised or untreated (control) rats measured with an Oroboros Oxygraph-2k (see Materials and Methods section 2.12). Illustrated are the mitochondrial oxygen consumption rates with pyruvate/malate and succinate as substrate (basal), the non-phosphorylating rates (oligomycin), the UCP1 independent leak rates (GDP) and maximal non-physiological respiratory capacity (FCCP). Measurements were performed in duplicate for each condition on three individual days. Data were analyzed by unpaired student's t-test. (* $P<0.05$; ** $P<0.01$; *** $P<0.001$)

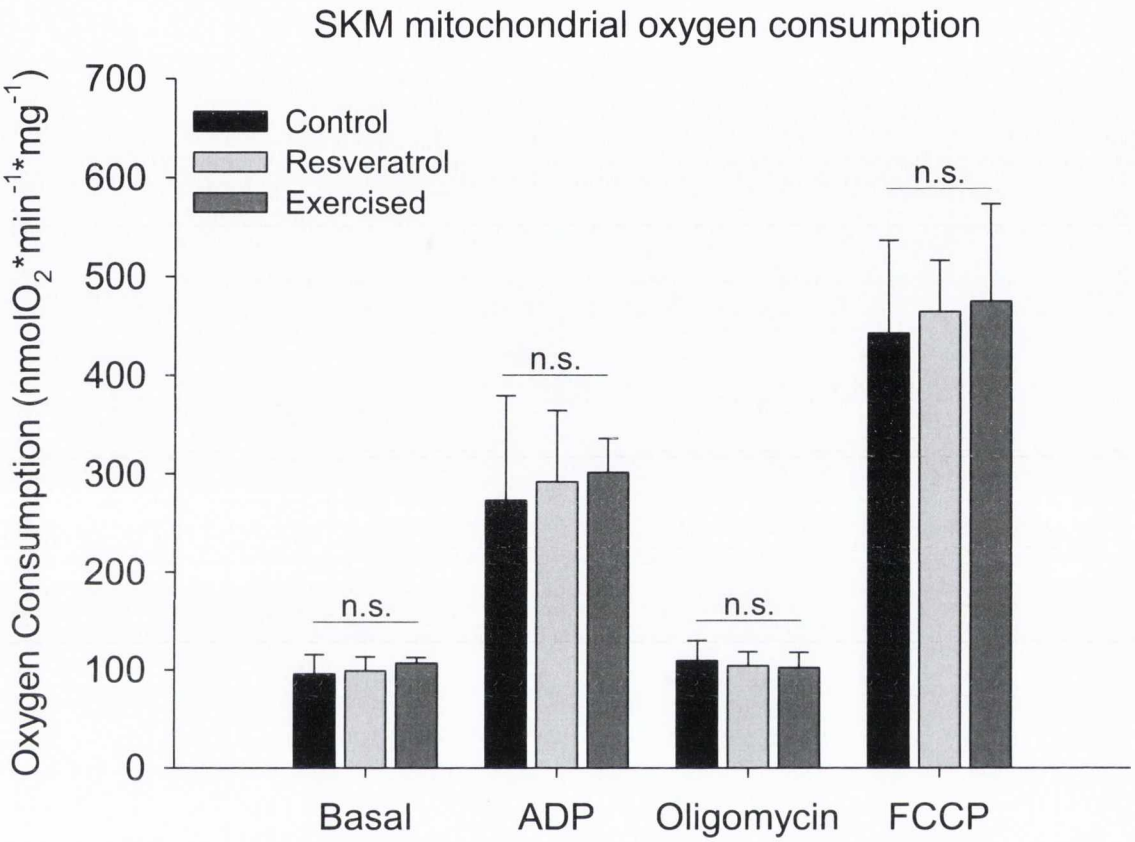


Figure 7-5: Resveratrol treatment and exercise do not affect mitochondrial function in skeletal muscle mitochondria

Oxygen consumption of skeletal muscle mitochondria isolated from Resveratrol treated, exercised or untreated (control) rats measured with an Oroboros Oxygraph-2k (see Materials and Methods section 2.15). Illustrated are the mitochondrial oxygen consumption rates with pyruvate/malate and succinate as substrate (basal), the non-phosphorylating rates (oligomycin), the UCP1 independent leak rates (GDP) and maximal non-physiological respiratory capacity (FCCP). Measurements were performed in duplicate for each condition on three individual days. Data were analyzed by unpaired student's t-test. (* $P<0.05$; ** $P<0.01$; *** $P<0.001$)

7.2.4 Resveratrol treatment or Exercise do not affect UCP1 expression in BAT or UCP3 expression in SKM mitochondria

Resveratrol is thought to mimic some of the effects of moderate exercise. I found no effects of resveratrol treatment or exercise on oxygen consumption rates or extracellular acidification rates in intact muscle fibres and no differences in oxygen consumption rates in isolated skeletal muscle mitochondria. However, oxygen consumption rates in mature BAT cells and isolated BAT mitochondria showed significant differences between the groups. The responsiveness to noradrenaline was increased by resveratrol and decreased by exercise. In general, exercise reduced oxygen consumption rates in BAT cells in all investigated conditions, while oxygen consumption rates of BAT cells from resveratrol treated and control animals were very similar besides the previously mentioned effect on increased noradrenaline responsiveness in BAT cells of resveratrol treated rats. Because the non-phosphorylating oxygen consumption rate was reduced in BAT cells of exercised animals and increased in isolated BAT mitochondria of resveratrol treated animals, it was deemed necessary to estimate relative expression levels of UCP1 in BAT mitochondria (and UCP3 in skeletal muscle mitochondria) by immunodetection.

Figure 7-6A shows a representative Immunoblot of UCP1 (32kDa) and PDH (44kDa) as a loading control BAT mitochondria of control, resveratrol treated and exercised rats. It is obvious, that there was no difference in the expression level of UCP1 between the three groups. To quantify the expression levels of UCP1 in BAT mitochondria, densitometry measurements were performed and the UCP1 signal normalized with the PDH signal for each group. Figure 7-6B illustrates the ratios of UCP1/PDH and confirms, that UCP1 expressions levels were not changed in BAT mitochondria by the treatment with resveratrol or by exercise.

Not surprisingly, UCP3 expression in skeletal muscle mitochondria of control, resveratrol treated and exercised rats was not changed by the treatments either, as was demonstrated by immunodetection of UCP3 in Figure 7-7A. Densitometric quantification of the UCP3 signal was normalised with the signal for PDH and relative expression levels of UCP3 are illustrated as ratios of UCP3/PDH in Figure 7-7B, confirming, that UCP3 expression was not affected by the treatments.

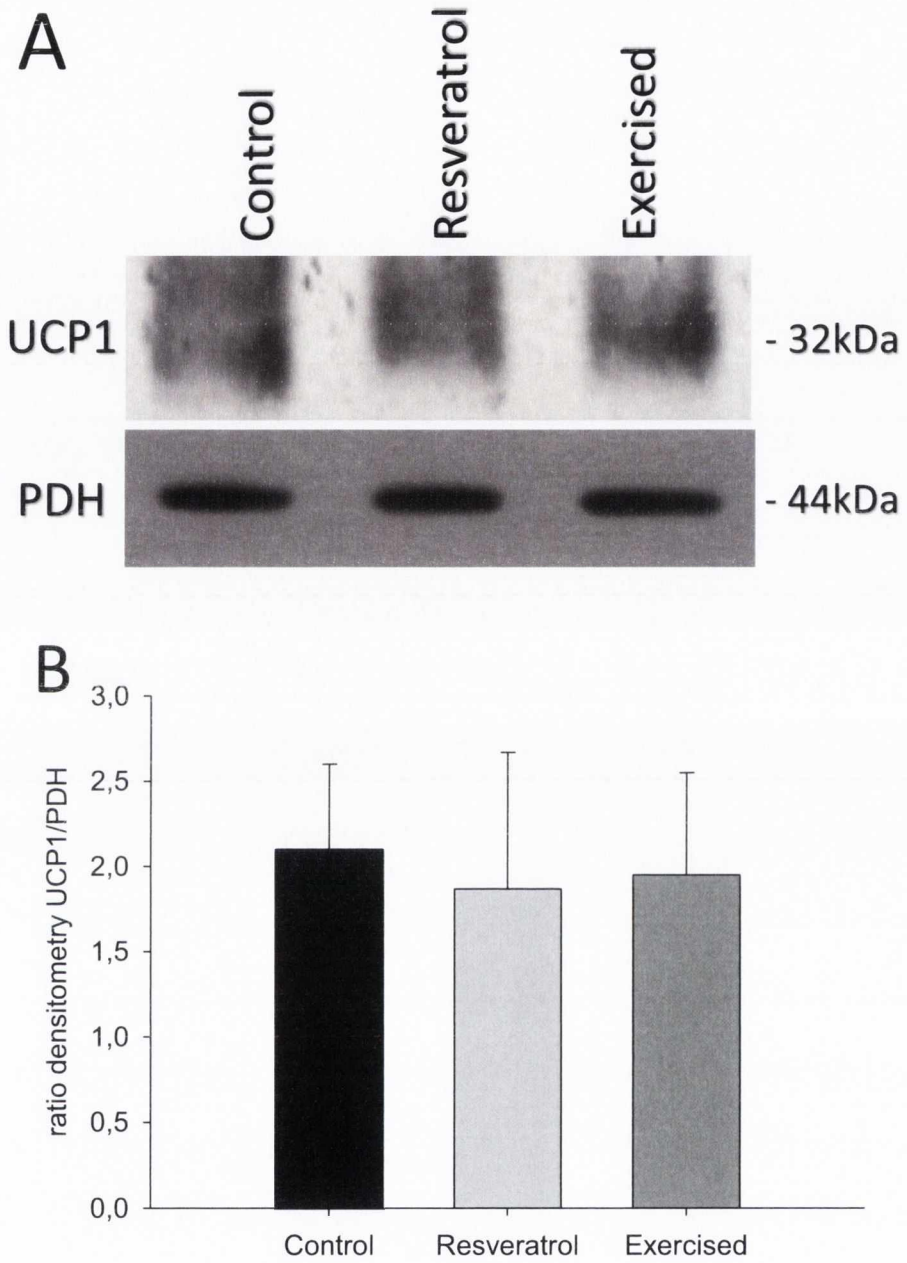


Figure 7-6: Resveratrol treatment and exercise do not affect expression of UCP1 in BAT mitochondria

(A) BAT mitochondria were isolated as described in section 2.12, followed by SDS-PAGE and immunodetection using anti-UCP1 antibody (Sigma; 1:1000) and anti-PDH-E1 alpha (Mitosciences, 1:2000). (B) Bands were quantified by densitometry using ImageJ software and presented as expression level ratios of UCP1/PDH. Immunoblots were performed in triplicate. P values ≤ 0.05 on unpaired student's t-test were deemed significant (* $P \leq 0.05$; ** $P \leq 0.01$; *** $P \leq 0.001$)

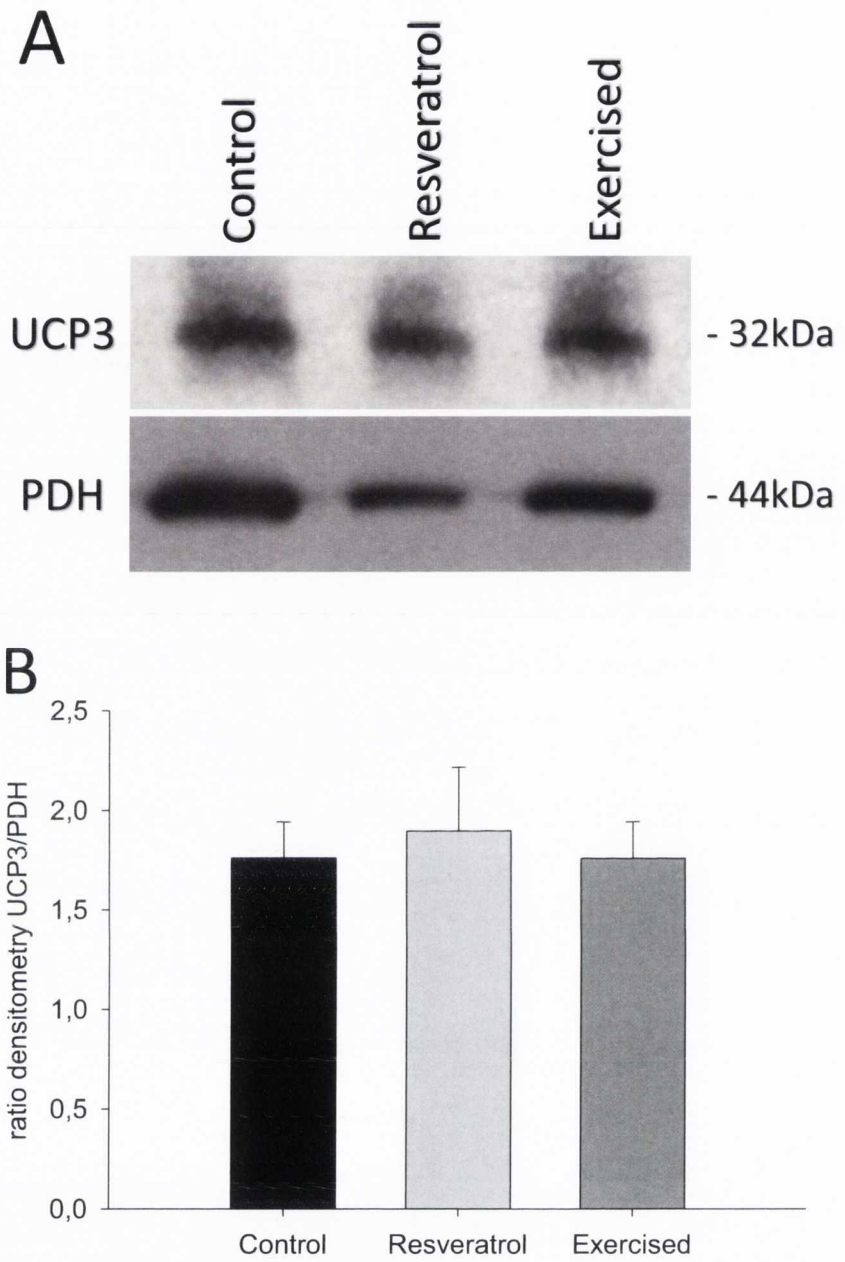


Figure 7-7: Resveratrol treatment and exercise do not affect expression of UCP3 in skeletal muscle mitochondria

(A) Skeletal muscle mitochondria were isolated as described in section 2.15, followed by SDS-PAGE and immunodetection using anti-UCP3 antibody (Eurogenetec; 1:1000) and anti-PDH-E1 alpha (Mitosciences, 1:2000). (B) Bands were quantified by densitometry using ImageJ software and presented as expression level ratios of UCP3/PDH. Immunoblots were performed in triplicate. P values ≤ 0.05 on unpaired student's t-test were deemed significant (* $P \leq 0.05$; ** $P \leq 0.01$; *** $P \leq 0.001$)

7.3 Discussion

Resveratrol is thought to mimic some of the effects of exercise. A few studies reported beneficial effects of resveratrol treatment on muscle physiology and performance (Baur *et al.* 2006; Lagouge *et al.* 2006; Dirks Naylor 2009). The various groups used a range of different dosages of resveratrol and varying durations of treatments, which makes comparisons between the individual studies difficult. Even so, it was demonstrated that resveratrol increases PGC-1α and UCP3 protein expression and upregulation of UCP3 was suggested to be a possible mediator in the protection against diet induced obesity and metabolic disease. Most studies focused on the effects of resveratrol on skeletal muscle metabolism, glucose tolerance and insulin resistance and to my knowledge, the effects of resveratrol on brown adipose tissue were never addressed prior to the experiments presented in this chapter.

In my experiments no changes in oxygen consumption in muscle fibres or isolated skeletal muscle mitochondria were detected in resveratrol treated and exercised rats compared to untreated control animals. These findings contradict those reported by Lagouge *et. al.* (2006), who showed increased biogenesis in skeletal muscle and a fibre-type switch from the glycolytic to the oxidative muscle fibre type in resveratrol treated mice. However, those changes were only demonstrated for muscle tissue of the glycolytic type, while no effect of resveratrol was found in oxidative muscle fibres. This is surprising as resveratrol is thought to increase mitochondrial biogenesis and respiratory capacity in muscle fibres by activating SIRT1 and consequently PGC-1α, a prominent controller of oxidative phosphorylation and mitochondrial biogenesis.

The discrepancy may be explained by the use of different animal models (mice or rats) and significant differences in animal treatment in the experiments. Lagouge *et al.* (2006) used mice treated for 15 weeks with 400mg/kg resveratrol per day while I used rats treated for only 2 weeks with only 20mg/kg resveratrol per day. Furthermore, Lagouge *et al.* (2006) reported that the differences in mice treated with resveratrol compared to controls only showed in animals that were fed a high-fat diet (HF-diet) parallel to the resveratrol treatment. In contrast, the rats in my experiments were all fed a standard chow (*ad libitum*). In addition to the differences in diet and the concentration and duration of the resveratrol treatments, tissues from mice and rats may show diverse

reactions to the same treatment simply due to respective body, tissue and cellular conditions in these two species.

Lagouge *et al.* (2006) also reported an increased resistance to acute cold stress in resveratrol treated mice (on a HF-diet) and attributed this observation to elevated thermogenic capacity in these mice, and demonstrated, that resveratrol treated mice on a HF-diet exhibited larger mitochondrial structures (electron microscopy) and increased mtDNA in BAT, consistent with an increase in mitochondrial capacity. No other functional data besides the cold tolerance test was presented. It would have been interesting to explore whether the increased cold tolerance was related to increased mitochondrial BAT activity, and more specifically, increased UCP1 activity and abundance.

In addition to the investigations of the role of resveratrol and exercise on skeletal muscle fibre respiration, the effects of resveratrol treatment and exercise on function of BAT cells were explored. Surprisingly, oxygen consumption rates of BAT cells were significantly different between the three groups (Figure 7-1). On the one hand, exercise reduced the responsiveness of BAT cells to noradrenaline and resulted in lower oxygen consumption rates in all investigated conditions compared to BAT cells isolated from control and resveratrol treated animals. On the other hand, resveratrol treatment increased the responsiveness of BAT cells to noradrenaline, but basal respiration rates and state 4 (non-phosphorylating state in the presence of oligomycin) and FCCP uncoupled rates remained unchanged by resveratrol compared to BAT cells from control animals. The ratios of basal oxygen consumption rate and noradrenaline induced rates were significantly higher in BAT cells of resveratrol treated animals compared to BAT cells from control or exercised rats (Figure 7-1). This shows, that resveratrol does trigger changes in the composition of BAT cells and sensitises BAT to noradrenaline. The fact, that the rates in the presence of antimycin A were not significantly different between the three groups shows, that the non-mitochondrial oxygen consumption in BAT was not affected by the treatments. However, these observations do not hold true for BAT of exercised rats, where oxygen consumption rates were reduced in all states of the measurement (except in the antimycin A inhibited rate). It can be concluded, that resveratrol therefore induces changes in BAT that are the opposite of changes induced by exercise. Thus, resveratrol does not appear to mimic the effects of exercise as indicated from BAT cells. To further explore the underlying mechanisms of the adaptations to

resveratrol or exercise, mitochondria form BAT and skeletal muscle of all three groups were isolated and the mitochondrial oxygen consumption measured.

As expected, the oxygen consumption rates of skeletal muscle mitochondria isolated from control rats did not differ from rates in SKM mitochondria isolated from resveratrol treated or exercised animals (Figure 7-5), confirming the results of the oxygen consumption measurements in intact muscle fibres (Figure 7-2). Not surprisingly, no differences in UCP3 protein expression in skeletal muscle mitochondria were detected (Figure 7-7). However, mitochondria isolated from BAT of control rats showed significantly higher oxygen consumption rates compared to rates in BAT mitochondria of resveratrol treated or exercised animals. On a cellular level, oxygen consumption rates of BAT cells from exercised animals, but not from resveratrol treated rats showed a significant reduction compared to controls (Figure 7-1). Inhibition of UCP1 with GDP ameliorated all differences in oxygen consumption rates between the three groups, which clearly demonstrates the involvement of UCP1 in the adaptations in BAT triggered by resveratrol or exercise (Figure 7-4), although UCP1 protein expression was not altered in BAT mitochondria regardless of the treatment (Figure 7-6). Titration with FCCP maximised the oxygen consumption rates again and, surprisingly, the FCCP stimulated rate in BAT mitochondria of untreated rats (control) was significantly higher compared to those of BAT mitochondria of resveratrol treated or exercised animals. This observation indicates that resveratrol and exercise not only decreased the GDP inhibitable (UCP1 dependent) portion of mitochondrial respiration, but also decreased the respiratory capacity in those BAT mitochondria. The non-phosphorylating state 4 (oligomycin) and FCCP stimulated oxygen consumption rates were not significantly different, but BAT cells express normally little ATPase and oligomycin will therefore not reduce the oxygen consumption rate very much.

The observation, that the reduction in respiration rates seen in BAT cells of exercised animals (Figure 7-1) was not seen in mitochondrial oxygen consumption (Figure 7-4) was unexpected. It could be that exercise reduced the mitochondrial content in BAT cells and that the difference in BAT cell respiration was not seen in mitochondrial oxygen consumption measurements because the same amount of isolated mitochondrial protein was used for all three groups.

It is also noteworthy that all mitochondrial isolations were performed in the presence of phosphatase inhibitors. Due to time limitations on each experimental day, no mitochondria were isolated in the absence of phosphatase inhibitors. Thus, the described effects of resveratrol treatment and exercise in BAT mitochondria may be regulated by phosphorylation of, yet, unknown targets. To clarify the relevance of phosphorylation on the observed results, the experiments should be repeated without protection of the phosphorylation state.

In summary, a low resveratrol dose or moderate exercise do not affect muscle metabolic parameters, as demonstrated on a cellular and mitochondrial level. Interestingly, resveratrol increased the response of BAT cells to noradrenaline, but appeared to decrease mitochondrial oxygen consumption in BAT compared to controls. Moderate exercise, however, reduced respiration rates in BAT cells compared to resveratrol treated and control cells. Furthermore, resveratrol treatment and exercise lowered mitochondrial oxygen consumption rates compared to rates of BAT mitochondria from controls. Resveratrol therefore does not mimic the effects of exercise in BAT. In muscle tissue, resveratrol treatment at low concentrations and moderate exercise did not change muscle fibre or skeletal muscle mitochondrial properties.

General Discussion

Chapter 8

8 General Discussion

In this work I set out to investigate the role of mitochondrial uncoupling proteins in mitochondrial and cellular function and their efficacy under conditions of stress or pathology.

Mitochondrial uncoupling proteins are differentially expressed in various tissues. UCP1 is found primarily in adipocytes in brown adipose tissue and UCP3 expression is prominent in skeletal muscle. UCP2 is expressed primarily in immune cells (particularly macrophages), but also in pancreatic β-cells. The thymus consists of the central medulla and the peripheral cortex and cells in the thymus include thymic stromal cells and cells of the hematopoietic origin (i.e. T-cells). Stromal cells in the thymus are cortical epithelial cells, medullary epithelial cells, and dendritic cells. Of these cell types only dendritic cells are known to express one of the three UCPs, UCP2 (Rousset *et al.* 2006). However, our laboratory has demonstrated that UCP1, UCP2 and UCP3 are also expressed in the thymus, but no discrimination between different cells types was made. Expression of all three uncoupling proteins in thymus suggests their importance in thymic function. We therefore hypothesized a role in T-cell selection and/or maturation, which is the primary function of the thymus after all. Based on this hypothesis I explored lymphocyte profiles in thymus and the periphery (i.e. spleen) of WT and UCP knock-out animals (6-8 weeks old) to screen for possible effects of the absence of UCPs on immune cell profiles. Alterations in cell profiles were found in UCP1 or UCP3 ablated animals. UCP2-/- mice showed no differences in T-cell profile compared to WT mice which confirms the observations by Krauss *et al.* (2002). Furthermore, UCP1-/- mice in my experiments showed significantly increased double positive CD4 CD8 T-cells in spleen which confirms the observation by Adams *et al.* (2010). However, Adams *et al.* (2010) reported a significant reduction of CD8 T-cell frequencies in spleens and thymi of UCP1 ablated mice, whereas no changes in CD8 T-cell frequencies were observed in the present work in spleens or thymi of both genotypes in my studies. In the thymus, UCP1 knock-out mice showed significantly reduced CD4 single positive and reduced CD4 CD8 double positive T-cells in my study, contrary to the observations made by Adams *et al.* (2010). One of the likely causes of the differential observations between my study and those of Adams *et al.* (2010) is the age of the mice and the link between age and UCP1 (and UCP3) expression

levels, in that Adams *et al.* (2010) used pre-weaned 3 week old mice where UCP1 levels are 2 to 3-fold greater than levels in the 6-8 week old weaned mice used by me. Adams *et al.* (2010) was also able to attribute all of the alterations in T-cell frequencies due to ablation of UCP1 to an increased apoptotic potential in UCP1-/- mice. However, the apoptotic potential of WT and UCP1-/- splenocytes and thymocytes was not investigated in my study because the changes in the T-cell profile in the thymus of UCP1 ablated animals did not relate to those seen in spleens of UCP1 knock-out mice and therefore appeared not to be relevant. Accordingly, this line of investigations was discontinued and only after discovery of the age dependent expression of UCP1 in the thymus was this issue revisited by our laboratory (Adams *et al.* 2010), which yielded the results described above.

Investigations of UCP2 knock-out mice showed no alteration of T-cell profile in the thymus or in peripheral tissues and confirming the previous observation by Krauss *et al.* (2002).

The T-cell profile of thymi in UCP3-/- mice showed significant reduction in CD4 CD8 double negative cells which confirms data presented by Kelly *et al.* (2011). My experiments also showed significantly increased CD4 single positive cells and significantly reduced CD4 CD8 double positive cells thymus of UCP3 knock-out mice. These findings contradict those made by Kelly *et al.* (2011) who did not see changes in CD4 abundance in thymus. Again the discrepancy between my data and those of Kelly *et al.* (2011) probably reflect the difference in the age and UCP3 expression levels of my mice (6-8 weeks) compared to those used by Kelly *et al.* (2011) where UCP3 levels in the thymus are about 3-fold greater in 3 week old mice compared to 6-8 week old mice. Furthermore the data presented in chapter 3 confirmed a significant reduction in CD8 single positive and CD4 CD8 double negative cells in spleens of UCP3-/- animals.

In conclusion UCP1 and UCP3, but not UCP2 affect T-cell profiles in spleen and thymus of mice.

UCP2 is expressed in a variety of immune cells other than T-cells and a substantial amount of research shows the importance of UCP2 in various disease models including diabetes and autoimmune diseases. The investigation of the role of UCP2 in these diseases is therefore important for a better understanding and the development of

potential treatments. Based on a publication by Vogler *et al.* (2006) I set out to confirm the function of UCP2 in EAE and add further insight to the role of UCP2 in this disease. Vogler *et al.* (2006) showed a protective role for UCP2 in EAE, thus UCP2-/- mice developed significantly more severe disease compared to WT animals in their hands. In contradiction to Vogler *et al.* (2006) I found no changes in disease severity in UCP2-/- mice compared to WT controls. However, UCP2 knock-out mice displayed a significantly delayed onset of the disease. Analyses of infiltrating and resident T-cells in brains, spleens and lymph nodes 21 days after induction of EAE showed no significant variances in frequencies, but a general trend of reduced IFNγ and IL-17 positive T-cells as well as a slightly reduced inflammatory cytokine production in UCP2-/- mice. In addition to seeing no difference in the T-cell profile in tissues from EAE treated wild-type and UCP2 knock-out mice, as determined by FACS analysis, there was also no significant difference in the cytokine production profile of whole tissue homogenate single cell suspensions of UCP2 knock-out mice compared to WT controls, as determined by ELISA. The fact that animals showed signs of remission at the end of the 30 day incubation period was also contrary to observations made by Vogler *et al.* (2006). Together with the body weight and clinical severity assessment I observed that ablation of UCP2 dampened typical EAE factors which is in contrast to the conclusion by Vogler *et al.* who suggested a protective role of UCP2 in EAE. The discrepancy between the results presented by Vogler *et al.* (2006) and my study can be explained by the fact, that the EAE may not have been induced equally for each animal in the experiments by Vogler *et al.* (2006). This is evidenced by the observation, that the WT mice in the study by Vogler *et al.* (2006) reached a very low average clinical score. In comparison, clinical symptoms observed in EAE induced with a professional MOG/CFA induction kit (Hooke Laboratories) are much more severe as indicated by an average clinical score that is twice as high as the one shown for WT mice in EAE by Vogler *et al.* (2006). However, in my study the average clinical scores of UCP2 knock-out and WT mice in EAE were consistent with the suggested disease progression demonstrated by Hooke Laboratories. So the results of my study undermine the importance of UCP2 in the EAE model of MS. Therefore, further investigations of the role of UCP2 in the EAE model of MS were not continued.

In functional studies on the role of UCP2 in regulating oxygen consumption and ROS production in mitochondria no significant changes were observed in succinate

supported oxygen consumption or ROS production rates in kidney or liver mitochondria isolated from UCP2 knock-out mice. If UCP2 was catalysing a proton leak one might have expected that the absence of UCP2 was manifested as a reduction in state 4 oxygen consumption rate and an increase in the ROS production rate. Surprisingly, oxygen consumption rates in mitochondria from UCP2-/- mice were significantly higher compared to rates in mitochondria of WT controls when glycerol-3-phosphate was used as substrate. This is the first recorded data of increased oxygen consumption in liver and kidney mitochondria from UCP2 knock-out mice compared to those from wild-type mice with glycerol-3-phosphate (G3P) as substrate. This phenomenon correlated with an increased mGPDH abundance and activity in mitochondria of UCP2 knock-out mice. Interestingly, BAT mitochondria from UCP1-/- mice showed the same phenotype and exhibited an increased mGPDH abundance and activity as observed by our laboratory (publication in preparation). The mGPDH enzyme complex itself is considered to be one of the major producers of mitochondrial ROS in the cell (Drahota *et al.* 2002). However, increased mGPDH activity in liver and kidney mitochondria of UCP2-/- mice did not result in increased ROS production rates. The discrepancy may reflect the fact that mitochondrial ROS scavengers and oxidative stress defence systems like glutathione or Mn-superoxide dismutase might dampen any small differences in ROS production. Furthermore ROS defence mechanisms might also be upregulated to protect against increased ROS production in cells lacking UCP2 (Durmaz *et al.* 1999; de Bilbao *et al.* 2004). Although a good number of previous studies demonstrated increased ROS production due to UCP2 knock-out in cells (Negre-Salvayre *et al.* 1997b; Arsenijevic *et al.* 2000; Echtay *et al.* 2002; Krauss *et al.* 2003; Bai *et al.* 2005; Vogler *et al.* 2006; Emre *et al.* 2007b) others did not see such effects (Pecqueur *et al.* 2008). The results presented here are therefore consistent with those studies that show that ablation of UCP2 does not cause an increase in mitochondrial ROS production in cells. A lot of mitochondrial ROS is produced by complex I of the respiratory chain. In this study, substrates that provide electrons directly to the ubiquinone pool in the respiratory chain were used and thus only ROS production downstream of complex I was analysed. The role of UCP2 in ROS production may therefore have been underestimated because one of the most potent ROS production site in mitochondria, complex I, was inhibited by rotenone. Another important point is that UCP2 activation is currently not fully understood and UCP2 may therefore not have been activated and catalysing a proton leak under the conditions used in our study. Another

obvious conclusion might be that UCP2 may not catalyse a proton leak at all. However, the fact that UCP2 ablation results in increased mGPDH abundance and activity is very interesting and should be investigated further. High expression levels of mGPDH have been associated with a glycolytic phenotype of cellular metabolism and hence, UCP2 ablation may have forced a metabolic switch in those animals (MacDonald *et al.* 1990).

In regard to my studies on UCP3 function and activation by phosphorylation in skeletal muscle, I set out to investigate whether phosphorylation and activation of UCP3 could occur under more physiological conditions after our laboratory demonstrated that systemic MDMA treatment resulted in phosphorylation of UCP3 and increased state 4 oxygen consumption in skeletal muscle mitochondria. MDMA triggers noradrenaline release in the sympathetic nervous system and we hypothesised that this noradrenaline release stimulates UCP3 phosphorylation and activation, analogue to the activation of UCP1 seen in BAT following cold acclimation. I therefore treated animals with noradrenaline to mimic the effects of MDMA, but state 4 or FCCP uncoupled oxygen consumption rates with succinate or with G3P as substrates were not affected in SKM mitochondria isolated in the presence of phosphatase inhibitors (PI). The lack of an effect may be the result of missing the optimal time frame for noradrenaline efficacy as discussed in chapter 6. Noradrenaline should trigger a response almost instantaneously as soon as it reaches the respective adrenergic receptors. The time frame of migration/transport of noradrenaline from the intraperitoneal injection locus to the site of action in SKM is not known and a targeted injection (intra muscular) may be more suitable to trigger adrenergic muscle stimulation and subsequent UCP3 phosphorylation and activation. Of course, it may take some time for the phosphorylation of UCP3 to occur after the injection of noradrenaline. However, after the incubation time of 1 hour in the current experimental setup, any short term effects were probably lost. Direct noradrenaline treatment of intact muscle fibres isolated from wild-type and UCP3 knock-out animals would be a more meaningful experiment, because any differences in activation should be seen instantaneously and can be linked directly to UCP3.

Short-term starvation is another physiological condition that is associated with noradrenaline release. Fasting increases skeletal muscle UCP3 protein up to 2 to 3-fold per mg mitochondrial protein (Cadenas *et al.* 1999; Zhou *et al.* 2000) and I was able to confirm this upregulation. This increase in UCP3 protein abundance may also be

accompanied by phosphorylation and activation of UCP3, but state 4 and FCCP uncoupled oxygen consumption rates did not differ significantly in mitochondria isolated from fed or fasted animals isolated in the presence of PI. Surprisingly isolation of mitochondria without protecting *in vivo* phosphorylation resulted in a significant decrease in state 4 and FCCP uncoupled oxygen consumption rates in fasted muscle mitochondria compared to those of fed muscle mitochondria. The opposite observation was expected according to the original hypothesis that starvation increased protein abundance and activity by phosphorylation of UCP3. Protecting *in vivo* phosphorylation did not alter state 4 or FCCP uncoupled oxygen consumption rates in mitochondria isolated from fed animals which shows that the effects described in chapter 6 were specific to fasting and not treatment of the mitochondria with phosphatase inhibitors. Fasting does not seem to affect the overall respiratory chain capacity, but probably works on more subtle levels, because oxygen consumption rates between mitochondria of fed and starved animals and isolated without protecting the *in vivo* phosphorylation state and with G3P as substrate were not significantly different. However, oxygen consumption rates of the same preparation were significantly different with succinate as substrate. Interestingly, respiratory control ratios (RCR) were significantly reduced in mitochondria of fasted animals isolated compared to RCRs of mitochondria isolated from fed animals with succinate as substrate both with and without protecting the *in vivo* phosphorylation state by PI. However, protection of the phosphorylation state resulted in a less significant difference between RCRs of mitochondria from fed and fasted animals. Short-term starvation therefore seems to reduce coupling efficiency, but only in mitochondria where the phosphorylation state was not protected. Phosphorylation of an unknown target or targets following starvation appears to maintain coupling efficiency in mitochondria respiring on succinate, but no effect of increased UCP3 abundance was evident.

Cold acclimation has been reported to activate UCP1 in BAT mitochondria through noradrenaline release and subsequent fatty acid mobilisation which then serves both as fuel and activator of UCP1. MDMA can cause thermogenesis in skeletal muscle, supposedly by noradrenaline signalling. So we hypothesised that UCP3 in BAT and skeletal muscle might adapt the function of catalysing non-shivering thermogenesis in mice that lack the ability to defend their core body temperature by non-shivering thermogenesis due to the absence of UCP1. To test this hypothesis, UCP1 knock-out mice were cold

acclimated and the mitochondrial oxygen consumption rates analysed. Protection of the *in vivo* phosphorylation state with phosphatase inhibitors during isolation of SKM mitochondria from cold acclimated UCP1-/- animals resulted in significantly reduced succinate supported state 4 and FCCP uncoupled oxygen consumption rates and significantly reduced FCCP uncoupled rates when respiring on G3P. These significant reductions were dependent on the preservation of the *in vivo* phosphorylation, because isolations of SKM mitochondria from UCP1 knock-out mice without protection of the phosphorylation state with PI did not show significant differences in succinate supported state 4 oxygen consumption and less significant reduction of oxygen consumption when completely uncoupled with FCCP. Interestingly, no significant differences in oxygen consumption rates were detectable in mitochondria that were isolated from BAT of cold acclimated WT mice with or without PI, indicating that UCP1 activity is not dependent on phosphorylation under cold stress. Therefore, phosphorylation of UCP1 or UCP3 in BAT seems not to be important in cold acclimation. Another possibility is that the phosphorylation of UCP1 or UCP3 is stable enough to not be dependent on the presence of phosphatase inhibitors during the isolation of mitochondria. However, state 4 oxygen consumption rates were significantly inhibitable with GDP and significantly increased following FCCP titration in mitochondria isolated from cold acclimated WT animals. This shows that the mitochondria were intact and functional. Unfortunately, only a limited amount of cold acclimated UCP1-/- animals was available and because the BAT tissue pads were very small in UCP1-/- mice, isolation of sufficient amounts of BAT mitochondria for oxygen consumption measurements was not possible.

Cold acclimation significantly increased mitochondrial oxygen consumption rates in SKM mitochondria of WT mice compared to oxygen consumption rates in SKM mitochondria of room temperature acclimated WT mice in isolations both with or without phosphatase inhibitors. In conclusion, cold acclimation seems to significantly increase metabolic capacity in skeletal muscle mitochondria of WT animals independent of the phosphorylation state.

In conclusion, noradrenaline treatment did not affect oxygen consumption rates. Short term fasting and cold acclimation appeared to trigger opposing effects at least in terms of oxygen consumption rates. While fasting significantly reduced oxygen consumption rates in SKM mitochondria compared to oxygen consumption rates in SKM

mitochondria of fed controls, cold acclimation increased oxygen consumption rates in SKM mitochondria of WT animals compared to RT housed controls as expected. On the other hand SKM mitochondria of cold acclimated UCP1-/- animals showed reduced oxygen consumption rates compared to oxygen consumption of cold acclimated WT mice which is contrary to the original hypothesis. The observations that oxygen consumption rates in cold acclimated UCP1-/- and fasted WT muscle mitochondria were reduced, however, were consistent with each other, albeit not expected. In both cases an increase in non-phosphorylating oxygen consumption due to activation of UCP3 was predicted.

Golozoubova *et al.* (2001) demonstrated that prolonged shivering enabled UCP1 ablated mice to defend their body temperature for weeks in an acute cold stress environment. Furthermore injection of noradrenaline to cold acclimated WT mice at thermoneutrality increased oxygen consumption 4-fold, but UCP1-/- animals showed only a minimal response to noradrenaline. This indicates that cold adaptation in UCP1-/- mice was mediated non-adrenergically (Golozoubova *et al.* 2001) and the actual mechanism is still unknown. The data presented in this work confirm that UCP3 is upregulated in SKM mitochondria under physiological conditions like fasting, but does not mediate increased mitochondrial oxygen consumption and is therefore most likely not involved in cold adaption and physiological facultative thermogenesis.

In summary, this report demonstrates that physiological conditions like starvation or cold acclimation can increase UCP3 abundance, but do not lead to phosphorylation and activation of UCP3 as was previously demonstrated for UCP3 following treatment of mice with MDMA (Kelly *et al.* 2011a).

The polyphenolic compound resveratrol is found in the skin of red grapes and is thought to mimic the metabolic adaptations of exercise by activating SIRT1 and PGC-1α. Lagouge *et al.* (2006) reported an increased mitogenesis in mice fed a high-fat diet and treated with 400mg/mg/day resveratrol for 15 weeks, which resulted in increased oxidative capacity, increased endurance, improved glucose tolerance, improved cold resistance and protection from metabolic disease and weight gain compared to high-fat diet fed control mice, that received no treatment with resveratrol. These beneficial effects were accompanied by PCG-1α and UCP3 upregulation. However, others have not seen protection from diet induced obesity and PGC-1α or UCP3 upregulation, but were

able to confirm that resveratrol treated mice were protected from insulin resistance and improved glucose tolerance (Baur *et al.* 2006). These differences can be explained by the dosage and duration of the resveratrol treatment. While Lagouge *et al.* (2006) treated mice with 400mg/kg/day for 15 weeks in parallel with a high-fat diet, Baur *et al.* (2006) treated mice with only 22.4mg/kg/day resveratrol, but continued the treatment for 15 months. An even lower dose of resveratrol (4.9mg/kg/day) did not affect expression of PGC-1α and UCP3 expression (Barger *et al.* 2008). The results of the experiments shown in chapter 7 were generated from rats that were either treated with 20mg/kg/day resveratrol for 2 weeks or moderately exercised for 1 hour per day for 2 weeks. The mitochondrial and cellular oxygen consumption rates of BAT and skeletal muscle cells and isolated mitochondria were also investigated and here I present functional data for the role of resveratrol and exercise on BAT metabolism for the first time. Contrary to our expectations, resveratrol treatment or exercise did not induce any changes in oxygen consumption rates of skeletal muscle fibers or isolated skeletal muscle mitochondria compared to rates of untreated control rats. The metabolic parameters of BAT cells and isolated BAT mitochondria were also compared between the three groups where significant differences were observed. Resveratrol treatment increased the noradrenaline responsiveness in BAT cells compared to the reaction to noradrenaline in BAT cells from control or exercised rats. In addition, BAT cells of exercised animals showed significantly reduced oxygen consumption rates compared to rates seen in resveratrol treated or control cells. To further dissect this observation, mitochondria were isolated from BAT of resveratrol treated, exercised and control rats and the mitochondrial oxygen consumption measured. In isolated BAT mitochondria, the observations were not in line with those made in BAT cells. BAT mitochondria of control animals showed significantly higher oxygen consumption rates and a significantly greater GDP inhibitable portion of oxygen consumption compared to rates seen in mitochondria from resveratrol treated and exercised animals. Interestingly, the rates in BAT mitochondria of resveratrol treated and exercised rats were not different. This confirms that a low dose of resveratrol can mimic the effects of moderate exercise on the bioenergetics properties of BAT mitochondria, as demonstrated by oxygen consumption measurements. The fact, that the GDP inhibitable portion of oxygen consumption was significantly smaller in BAT mitochondria of resveratrol treated and exercised animals indicates the involvement of UCP1 down regulation in BAT due to the treatments. However, no difference in UCP1

abundance could be determined between the three groups. Other mechanisms for the control of BAT activity, or specifically mitochondrial oxygen consumption in BAT, must be in place. It is likely, that SIRT1 and PGC-1α play a role in the adaptations due to resveratrol treatment and exercise in BAT. Future work will aim to shed light on the mechanisms that led to the reported adaptations in BAT.

Taken together, I demonstrated for the first time that resveratrol and exercise can influence the metabolism in brown adipose tissue on a cellular and mitochondrial level and elucidation of the underlying mechanisms will certainly help to better understand regulation of metabolism in brown adipose tissue and may also uncover potential targets for the development of new treatments in our battle against obesity and obesity related conditions.

Future Work and Acknowledgements

Chapter 9

9 Future work

Knock-out of UCP1 and UCP2 result in increased mGPDH abundance and enzyme complex activity. It would be very interesting to investigate whether this phenotype also shows in UCP3 knock-out mice. To that end, the mechanisms that lead to the adaption of UCP knock-out need to be explored. Further experiments should be aimed to clarify the role of mGPDH in the adaption to UCP ablation. In addition, UCP knock-out mice should be examined for phenotypes of elevated mGPDH activity as was described for certain diseases, like the increased development of cancer. Maybe the presence of UCPs favours a more fatty-acid oriented metabolism and abolishment of UCPs therefore places the cells in need for alternative energy sources and the utilisation of glycolysis derived reduction equivalents becomes more important. Therefore, cells and mitochondria of UCP knock-out animals should be tested for their ability to utilise different substrates for metabolism. Effects of UCP knock-out on the other respirator chain complexes should also be investigated to identify any other adaptations to UCP ablation.

I was able to show a significant effect of resveratrol on mitochondrial function in brown adipose tissue and on noradrenaline stimulation of brown adipose tissue cells. A further investigation as to how these effects were mediated is very important to understand the mechanism underlying the function of resveratrol in BAT. Resveratrol is known to increase SIRT1 and PGC-1α activity and hence it is important to explore the role of SIRT1 and PGC-1α in mediating the observed changes in BAT. Moreover, the mediated effects in mitochondria may be controlled by the state of phosphorylation and future experiments should concentrate on identifying the role of phosphorylation in resveratrol and exercise mediated changes in BAT as mitochondrial preparations were done in the presence of phosphatase inhibitors.

Acknowledgements

First of all I would like to thank Richie. You were a great supervisor and your door was always open for me. Sorry for all the headaches I gave you, Richie (and I am sure there was more than one). I will always remember the great times we had, specifically the conferences! Stay as you are, "a lean, mean, biochemical typing machine".

Special thanks to Alison, Orlagh and Kieran. You guys adopted me to your lab and gave me a very warm introduction to the Irish way of life. Thank you also for loads of help and input concerning the science side of life. However, I am glad the times of constant Lady Gaga terror on the radio are over! Alison, your baking skills kept us all in good spirits, and buns now and then really were a shining light in the daily business. Together with Orlagh you were also incredible hosts of various wine receptions and parties, thank you. Kieran, it is your fault that I am now addicted to Vodka 7up drinks. You were a fantastic help and good council both in the lab and in "normal" life.

I also want to thank Audrey and the rest of the teaching lab staff for providing numerous chemicals and loads of help in optimizing experiments. You always helped with a smile and without any hassle what so ever. Thanks as well to the school's administrative staff Mary-Pat, Miriam, Noel, Liam, David and Kieran in stores and Liam. Many thanks also to the Bioresources staff Anne, Sylvie, Peter, Brian, Mairead, Monica, Mark, David and Kieran and Tania.

After the move to the brand new Trinity Biomedical Sciences Institute in July 2012 my new lab partners were also a great source of motivation and merriment. Thank you Emma, Kasia, Jenny, Sandra, Trevor, Luisa, Kim, Anna, Lisa, Seema, Tania, Ciaran, Claire, Vinnie and Sreeja for the great times, constructive discussions and input.

Special thanks also to Rosalind, who provided the Resveratrol treated and exercised rats for the results in the last chapter. It was great fun working with you and thanks for the inspiring conversations during the dissections.

My parents and my brother Bert supported me all this time both with good advice, motivation and also some cash infusions here and there. You made me the person I am

today and made this incredible experience possible by laying the foundations! I will never forget how much you have done for me! Thank you.

Finally, I'd like to thank Anna. Words can hardly describe what she had to go through with me, specifically in the end phase of this thesis. Stress, long hours and Jameson were challenging for both of us, but together we got through it. I wouldn't have been able to do this without you and your never-ending support and motivation. My sincerest apologies for taking so long!

I acknowledge funding from the Health Research Board Ireland (HRB RP/2008/61).

Bibliography

10 References

Abbas, A. K., A. H. Lichtman, et al. (2007). Cellular and molecular immunology. Philadelphia, Saunders Elsevier.

Adams, A. E., A. M. Carroll, et al. (2008a). "Mitochondrial uncoupling protein 1 expression in thymocytes." Biochimica et biophysica acta **1777**(7-8): 772-776.

Adams, A. E., O. Hanrahan, et al. (2008b). "Images of mitochondrial UCP 1 in mouse thymocytes using confocal microscopy." Biochimica et biophysica acta **1777**(2): 115-117.

Adams, A. E., O. M. Kelly, et al. (2010). "Absence of mitochondrial uncoupling protein 1 affects apoptosis in thymocytes, thymocyte/T-cell profile and peripheral T-cell number." Biochimica et biophysica acta **1797**(6-7): 807-816.

Aggarwal, S., N. Ghilardi, et al. (2003). "Interleukin-23 promotes a distinct CD4 T cell activation state characterized by the production of interleukin-17." The Journal of biological chemistry **278**(3): 1910-1914.

Akira, S., S. Uematsu, et al. (2006). "Pathogen recognition and innate immunity." Cell **124**(4): 783-801.

Alfadda, A., R. A. DosSantos, et al. (2004). "Mice with deletion of the mitochondrial glycerol-3-phosphate dehydrogenase gene exhibit a thrifty phenotype: effect of gender." Am J Physiol Regul Integr Comp Physiol **287**(1): R147-156.

Amat, R., G. Solanes, et al. (2007). "SIRT1 is involved in glucocorticoid-mediated control of uncoupling protein-3 gene transcription." The Journal of biological chemistry **282**(47): 34066-34076.

Andrews, Z. B., Z. W. Liu, et al. (2008). "UCP2 mediates ghrelin's action on NPY/AgRP neurons by lowering free radicals." Nature **454**(7206): 846-851.

Arciero, P. J., M. I. Goran, et al. (1993). "Resting metabolic rate is lower in women than in men." J Appl Physiol **75**(6): 2514-2520.

Arrigo, A. P. (1999). "Gene expression and the thiol redox state." Free Radic Biol Med **27**(9-10): 936-944.

Arsenijevic, D., H. Onuma, et al. (2000). "Disruption of the uncoupling protein-2 gene in mice reveals a role in immunity and reactive oxygen species production." Nat Genet **26**(4): 435-439.

Azzu, V., C. Affourtit, et al. (2008). "Dynamic regulation of uncoupling protein 2 content in INS-1E insulinoma cells." Biochimica et biophysica acta **1777**(10): 1378-1383.

Azzu, V., S. A. Mookerjee, et al. (2010). "Rapid turnover of mitochondrial uncoupling protein 3." The Biochemical journal **426**(1): 13-17.

Babior, B. M., R. S. Kipnes, et al. (1973). "Biological defense mechanisms. The production by leukocytes of superoxide, a potential bactericidal agent." J Clin Invest **52**(3): 741-744.

Bai, Y., H. Onuma, et al. (2005). "Persistent nuclear factor-kappa B activation in Ucp2-/- mice leads to enhanced nitric oxide and inflammatory cytokine production." The Journal of biological chemistry **280**(19): 19062-19069.

Baolin, L., Y. Inami, et al. (2004). "Resveratrol inhibits the release of mediators from bone marrow-derived mouse mast cells in vitro." Planta Med **70**(4): 305-309.

Barger, J. L., T. Kayo, et al. (2008). "A low dose of dietary resveratrol partially mimics caloric restriction and retards aging parameters in mice." PLoS One **3**(6): e2264.

Baur, J. A. and D. A. Sinclair (2006). "Therapeutic potential of resveratrol: the in vivo evidence." Nat Rev Drug Discov **5**(6): 493-506.

Behrens, W. A. and J. Himms-Hagen (1977). "Alteration in skeletal muscle mitochondria of cold-acclimated rats: association with enhanced metabolic response to noradrenaline." J Bioenerg Biomembr **9**(1): 41-63.

Berard, J. L., K. Wolak, et al. (2010). "Characterization of relapsing-remitting and chronic forms of experimental autoimmune encephalomyelitis in C57BL/6 mice." Glia **58**(4): 434-445.

Berardi, M. J., W. M. Shih, et al. (2011). "Mitochondrial uncoupling protein 2 structure determined by NMR molecular fragment searching." Nature **476**(7358): 109-113.

Bhattacharya, S. K., J. H. Thakar, et al. (1991). "Isolation of skeletal muscle mitochondria from hamsters using an ionic medium containing ethylenediaminetetraacetic acid and nagarse." Anal Biochem **192**(2): 344-349.

Bienengraeber, M., K. S. Echtay, et al. (1998). "H+ transport by uncoupling protein (UCP-1) is dependent on a histidine pair, absent in UCP-2 and UCP-3." Biochemistry **37**(1): 3-8.

Biron, C. A. and L. Brossay (2001). "NK cells and NKT cells in innate defense against viral infections." Curr Opin Immunol **13**(4): 458-464.

Blander, G. and L. Guarente (2004). "The Sir2 family of protein deacetylases." Annu Rev Biochem **73**: 417-435.

Borra, M. T., B. C. Smith, et al. (2005). "Mechanism of human SIRT1 activation by resveratrol." The Journal of biological chemistry **280**(17): 17187-17195.

Boss, O., T. Hagen, et al. (2000). "Uncoupling proteins 2 and 3: potential regulators of mitochondrial energy metabolism." Diabetes **49**(2): 143-156.

Boss, O., S. Samec, et al. (1998). "Uncoupling protein-3 expression in rodent skeletal muscle is modulated by food intake but not by changes in environmental temperature." The Journal of biological chemistry **273**(1): 5-8.

Boss, O., S. Samec, et al. (1997). "Uncoupling protein-3: a new member of the mitochondrial carrier family with tissue-specific expression." FEBS Lett **408**(1): 39-42.

Brand, M. D. (1977). "The stoicheiometric relationships between electron transport, proton translocation and adenosine triphosphate synthesis and hydrolysis in mitochondria." Biochem Soc Trans **5**(5): 1615-1620.

Brand, M. D. (1995). Measurement of mitochondrial proton motive force. Bioenergetics - a Practical Approach**:** 39-62.

Brand, M. D. (2000). "Uncoupling to survive? The role of mitochondrial inefficiency in ageing." Exp Gerontol **35**(6-7): 811-820.

Brand, M. D., C. Affourtit, et al. (2004a). "Mitochondrial superoxide: production, biological effects, and activation of uncoupling proteins." Free radical biology & medicine **37**(6): 755-767.

Brand, M. D., J. A. Buckingham, et al. (2004b). "Mitochondrial superoxide and aging: uncoupling-protein activity and superoxide production." Biochem Soc Symp(71): 203-213.

Brand, M. D., L. F. Chien, et al. (1994). "The causes and functions of mitochondrial proton leak." Biochimica et biophysica acta **1187**(2): 132-139.

Brand, M. D., N. Parker, et al. (2010). "Mitochondrial uncoupling protein 2 in pancreatic beta-cells." Diabetes Obes Metab **12 Suppl 2**: 134-140.

Brandes, M., K. Willimann, et al. (2005). "Professional antigen-presentation function by human gammadelta T Cells." Science **309**(5732): 264-268.

Brookes, P. S., N. Parker, et al. (2008). "UCPs--unlikely calcium porters." Nat Cell Biol **10**(11): 1235-1237; author reply 1237-1240.

Brown, G. C. and M. D. Brand (1986). "Changes in permeability to protons and other cations at high proton motive force in rat liver mitochondria." The Biochemical journal **234**(1): 75-81.

Brown, L. J., R. A. Koza, et al. (2002). "Lethal hypoglycemic ketosis and glyceroluria in mice lacking both the mitochondrial and the cytosolic glycerol phosphate dehydrogenases." The Journal of biological chemistry **277**(36): 32899-32904.

Brunet, A., L. B. Sweeney, et al. (2004). "Stress-dependent regulation of FOXO transcription factors by the SIRT1 deacetylase." Science **303**(5666): 2011-2015.

Brustovetsky, N., T. Brustovetsky, et al. (2002). "Calcium-induced cytochrome c release from CNS mitochondria is associated with the permeability transition and rupture of the outer membrane." J Neurochem **80**(2): 207-218.

Buetler, T. M., A. Krauskopf, et al. (2004). "Role of superoxide as a signaling molecule." News Physiol Sci **19**: 120-123.

Bukowiecki, L., A. J. Collet, et al. (1982). "Brown adipose tissue hyperplasia: a fundamental mechanism of adaptation to cold and hyperphagia." Am J Physiol **242**(6): E353-359.

Butterfield, R. J., J. D. Sudweeks, et al. (1998). "New genetic loci that control susceptibility and symptoms of experimental allergic encephalomyelitis in inbred mice." J Immunol **161**(4): 1860-1867.

Buttgereit, F., A. Grant, et al. (1994). "The effects of methylprednisolone on oxidative phosphorylation in Concanavalin-A-stimulated thymocytes. Top-down elasticity analysis and control analysis." Eur J Biochem **223**(2): 513-519.

Cadenas, S., J. A. Buckingham, et al. (1999). "UCP2 and UCP3 rise in starved rat skeletal muscle but mitochondrial proton conductance is unchanged." FEBS Lett **462**(3): 257-260.

Cadenas, S., K. S. Echtay, et al. (2002). "The basal proton conductance of skeletal muscle mitochondria from transgenic mice overexpressing or lacking uncoupling protein-3." The Journal of biological chemistry **277**(4): 2773-2778.

Campfield, L. A., F. J. Smith, et al. (1998). "Strategies and potential molecular targets for obesity treatment." Science **280**(5368): 1383-1387.

Cannon, B. and J. Nedergaard (2004). "Brown adipose tissue: function and physiological significance." Physiol Rev **84**(1): 277-359.

Carroll, A. M., L. R. Haines, et al. (2004a). "Immunodetection of UCP1 in rat thymocytes." Biochem Soc Trans **32**(Pt 6): 1066-1067.

Carroll, A. M. and R. K. Porter (2004b). "Starvation-sensitive UCP 3 protein expression in thymus and spleen mitochondria." Biochimica et biophysica acta **1700**(2): 145-150.

Carroll, A. M., R. K. Porter, et al. (2008). "Identification of serine phosphorylation in mitochondrial uncoupling protein 1." Biochimica et biophysica acta **1777**(7-8): 1060-1065.

Catalgol, B., S. Batirel, et al. (2012). "Resveratrol: French paradox revisited." Front Pharmacol **3**: 141.

Chappell, J. B. (1972). IN SUBCELLULAR COMPONENTS: PREPARATION AND FRACTIONATION. London, Buttersworths.

Chowdhury, S. K., Z. Drahota, et al. (2000). "Activities of mitochondrial oxidative phosphorylation enzymes in cultured amniocytes." Clin Chim Acta **298**(1-2): 157-173.

Chowdhury, S. K., A. Gemin, et al. (2005). "High activity of mitochondrial glycerophosphate dehydrogenase and glycerophosphate-dependent ROS

production in prostate cancer cell lines." Biochemical and biophysical research communications **333**(4): 1139-1145.
Chretien, D., P. Rustin, et al. (1994). "Reference charts for respiratory chain activities in human tissues." Clin Chim Acta **228**(1): 53-70.
Clapham, J. C., J. R. Arch, et al. (2000). "Mice overexpressing human uncoupling protein-3 in skeletal muscle are hyperphagic and lean." Nature **406**(6794): 415-418.
Clarke, K. J. (2011). "An investigation into the role and regulation of uncoupling protein 1 (UCP 1)." PhD Thesis **1**.
Clarke, K. J., A. E. Adams, et al. (2012). "A role for ubiquitinylation and the cytosolic proteasome in turnover of mitochondrial uncoupling protein 1 (UCP1)." Biochimica et biophysica acta.
Commins, S. P., P. M. Watson, et al. (1999). "Induction of uncoupling protein expression in brown and white adipose tissue by leptin." Endocrinology **140**(1): 292-300.
Comuzzie, A. G. and D. B. Allison (1998). "The search for human obesity genes." Science **280**(5368): 1374-1377.
Considine, M. J., M. Goodman, et al. (2003). "Superoxide stimulates a proton leak in potato mitochondria that is related to the activity of uncoupling protein." The Journal of biological chemistry **278**(25): 22298-22302.
Crawford, M. P., S. X. Yan, et al. (2004). "High prevalence of autoreactive, neuroantigen-specific CD8+ T cells in multiple sclerosis revealed by novel flow cytometric assay." Blood **103**(11): 4222-4231.
Cua, D. J., J. Sherlock, et al. (2003). "Interleukin-23 rather than interleukin-12 is the critical cytokine for autoimmune inflammation of the brain." Nature **421**(6924): 744-748.
Cunningham, O., A. M. McElligott, et al. (2003). "Selective detection of UCP 3 expression in skeletal muscle: effect of thyroid status and temperature acclimation." Biochimica et biophysica acta **1604**(3): 170-179.
Cutting, W., H. Mehrtens, et al. (1933). "Actions and uses of dinitrophenol: Promising metabolic applications." JAMA: The Journal of the American Medical Association **101**(3): 193-195.
Cypess, A. M., S. Lehman, et al. (2009). "Identification and importance of brown adipose tissue in adult humans." N Engl J Med **360**(15): 1509-1517.
Dawson, A. G. (1979). "Oxidation of cytosolic NADH formed during aerobic metabolism in mammalian cells." Trends Biochem Sci **4**: 171-176.
de Bilbao, F., D. Arsenijevic, et al. (2004). "Resistance to cerebral ischemic injury in UCP2 knockout mice: evidence for a role of UCP2 as a regulator of mitochondrial glutathione levels." J Neurochem **89**(5): 1283-1292.
Dirks Naylor, A. J. (2009). "Cellular effects of resveratrol in skeletal muscle." Life Sci **84**(19-20): 637-640.
Dlaskova, A., T. Spacek, et al. (2006). "Certain aspects of uncoupling due to mitochondrial uncoupling proteins in vitro and in vivo." Biochim Biophys Acta **1757**(5-6): 467-473.
DosSantos, R. A., A. Alfadda, et al. (2003). "Evidence for a compensated thermogenic defect in transgenic mice lacking the mitochondrial glycerol-3-phosphate dehydrogenase gene." Endocrinology **144**(12): 5469-5479.
Drahota, Z., S. K. Chowdhury, et al. (2002). "Glycerophosphate-dependent hydrogen peroxide production by brown adipose tissue mitochondria and its activation by ferricyanide." Journal of bioenergetics and biomembranes **34**(2): 105-113.
Dulloo, A. G. and S. Samec (2001). "Uncoupling proteins: their roles in adaptive thermogenesis and substrate metabolism reconsidered." Br J Nutr **86**(2): 123-139.

Dummler, K., S. Muller, et al. (1996). "Regulation of adenine nucleotide translocase and glycerol 3-phosphate dehydrogenase expression by thyroid hormones in different rat tissues." The Biochemical journal **317 (Pt 3)**: 913-918.

Dumont, A., S. P. Hehner, et al. (1999). "Hydrogen peroxide-induced apoptosis is CD95-independent, requires the release of mitochondria-derived reactive oxygen species and the activation of NF-kappaB." Oncogene **18**(3): 747-757.

Durmaz, R., M. Inal, et al. (1999). "The effects of MK-801 and U-83836E on post-ischemic reperfusion injury in rat brain." Acta Neurobiol Exp (Wars) **59**(2): 99-104.

Ebers, G. C., A. D. Sadovnick, et al. (1995). "A genetic basis for familial aggregation in multiple sclerosis. Canadian Collaborative Study Group." Nature **377**(6545): 150-151.

Echtay, K. S., T. C. Esteves, et al. (2003). "A signalling role for 4-hydroxy-2-nonenal in regulation of mitochondrial uncoupling." Embo J **22**(16): 4103-4110.

Echtay, K. S., D. Roussel, et al. (2002). "Superoxide activates mitochondrial uncoupling proteins." Nature **415**(6867): 96-99.

Echtay, K. S., E. Winkler, et al. (2001). "Uncoupling proteins 2 and 3 are highly active H(+) transporters and highly nucleotide sensitive when activated by coenzyme Q (ubiquinone)." Proc Natl Acad Sci U S A **98**(4): 1416-1421.

Elliott, P. J. and M. Jirousek (2008). "Sirtuins: novel targets for metabolic disease." Curr Opin Investig Drugs **9**(4): 371-378.

Emre, Y., C. Hurtaud, et al. (2007a). "Role of uncoupling protein UCP2 in cell-mediated immunity: how macrophage-mediated insulitis is accelerated in a model of autoimmune diabetes." Proc Natl Acad Sci U S A **104**(48): 19085-19090.

Emre, Y., C. Hurtaud, et al. (2007b). "Mitochondria contribute to LPS-induced MAPK activation via uncoupling protein UCP2 in macrophages." The Biochemical journal **402**(2): 271-278.

Emre, Y. and T. Nubel (2010). "Uncoupling protein UCP2: when mitochondrial activity meets immunity." FEBS Lett **584**(8): 1437-1442.

Estabrook, R. W. and B. Sacktor (1958). "alpha-Glycerophosphate oxidase of flight muscle mitochondria." The Journal of biological chemistry **233**(4): 1014-1019.

Fernandez-Marcos, P. J. and J. Auwerx (2011). "Regulation of PGC-1alpha, a nodal regulator of mitochondrial biogenesis." Am J Clin Nutr **93**(4): 884S-890.

Finkel, T. (1998). "Oxygen radicals and signaling." Curr Opin Cell Biol **10**(2): 248-253.

Finkel, T. (2003). "Oxidant signals and oxidative stress." Curr Opin Cell Biol **15**(2): 247-254.

Fisler, J. S. and C. H. Warden (2006). "Uncoupling proteins, dietary fat and the metabolic syndrome." Nutr Metab (Lond) **3**: 38.

Fleury, C., M. Neverova, et al. (1997). "Uncoupling protein-2: a novel gene linked to obesity and hyperinsulinemia." Nat Genet **15**(3): 269-272.

Foster, D. O. and M. L. Frydman (1978). "Nonshivering thermogenesis in the rat. II. Measurements of blood flow with microspheres point to brown adipose tissue as the dominant site of the calorigenesis induced by noradrenaline." Can J Physiol Pharmacol **56**(1): 110-122.

Friese, M. A. and L. Fugger (2009). "Pathogenic CD8(+) T cells in multiple sclerosis." Ann Neurol **66**(2): 132-141.

Furlan, R., E. Brambilla, et al. (2001). "Intrathecal delivery of IFN-gamma protects C57BL/6 mice from chronic-progressive experimental autoimmune encephalomyelitis by increasing apoptosis of central nervous system-infiltrating lymphocytes." J Immunol **167**(3): 1821-1829.

Garlid, K. D., D. E. Orosz, et al. (1996). "On the mechanism of fatty acid-induced proton transport by mitochondrial uncoupling protein." The Journal of biological chemistry **271**(5): 2615-2620.

Garrib, A. and W. C. McMurray (1986). "Purification and characterization of glycerol-3-phosphate dehydrogenase (flavin-linked) from rat liver mitochondria." The Journal of biological chemistry **261**(17): 8042-8048.

Garruti, G. and D. Ricquier (1992). "Analysis of uncoupling protein and its mRNA in adipose tissue deposits of adult humans." Int J Obes Relat Metab Disord **16**(5): 383-390.

Giardina, T. M., J. H. Steer, et al. (2008). "Uncoupling protein-2 accumulates rapidly in the inner mitochondrial membrane during mitochondrial reactive oxygen stress in macrophages." Biochimica et biophysica acta **1777**(2): 118-129.

Gimeno, R. E., M. Dembski, et al. (1997). "Cloning and characterization of an uncoupling protein homolog: a potential molecular mediator of human thermogenesis." Diabetes **46**(5): 900-906.

Golozoubova, V., E. Hohtola, et al. (2001). "Only UCP1 can mediate adaptive nonshivering thermogenesis in the cold." FASEB journal : official publication of the Federation of American Societies for Experimental Biology **15**(11): 2048-2050.

Gong, D. W., Y. He, et al. (1997). "Uncoupling protein-3 is a mediator of thermogenesis regulated by thyroid hormone, beta3-adrenergic agonists, and leptin." The Journal of biological chemistry **272**(39): 24129-24132.

Gong, D. W., S. Monemdjou, et al. (2000). "Lack of obesity and normal response to fasting and thyroid hormone in mice lacking uncoupling protein-3." The Journal of biological chemistry **275**(21): 16251-16257.

Gordon, J. A. (1991). "Use of vanadate as protein-phosphotyrosine phosphatase inhibitor." Methods Enzymol **201**: 477-482.

Graier, W. F., M. Trenker, et al. (2008). "Mitochondrial Ca2+, the secret behind the function of uncoupling proteins 2 and 3?" Cell Calcium **44**(1): 36-50.

Gregori, S., K. S. Goudy, et al. (2012). "The cellular and molecular mechanisms of immuno-suppression by human type 1 regulatory T cells." Front Immunol **3**: 30.

Grivennikova, V. G., A. V. Kareyeva, et al. (2010). "What are the sources of hydrogen peroxide production by heart mitochondria?" Biochimica et biophysica acta **1797**(6-7): 939-944.

Grundlingh, J., P. I. Dargan, et al. (2011). "2,4-dinitrophenol (DNP): a weight loss agent with significant acute toxicity and risk of death." J Med Toxicol **7**(3): 205-212.

Guerrero, J. E., D. P. Pacheco, et al. (2003). "Characterizing T-cell receptor gamma-variable gene in Aotus nancymaae owl monkey peripheral blood." Tissue Antigens **62**(6): 472-482.

Hanak, P. and P. Jezek (2001). "Mitochondrial uncoupling proteins and phylogenesis--UCP4 as the ancestral uncoupling protein." FEBS Lett **495**(3): 137-141.

Happel, K. I., M. Zheng, et al. (2003). "Cutting edge: roles of Toll-like receptor 4 and IL-23 in IL-17 expression in response to Klebsiella pneumoniae infection." J Immunol **170**(9): 4432-4436.

Harper, M. E., R. Dent, et al. (2002). "Decreased mitochondrial proton leak and reduced expression of uncoupling protein 3 in skeletal muscle of obese diet-resistant women." Diabetes **51**(8): 2459-2466.

Hayday, A. C. (2000). "[gamma][delta] cells: a right time and a right place for a conserved third way of protection." Annu Rev Immunol **18**: 975-1026.

Hayday, A. C. (2009). "Gammadelta T cells and the lymphoid stress-surveillance response." Immunity **31**(2): 184-196.

Heaton, G. M., R. J. Wagenvoord, et al. (1978). "Brown-adipose-tissue mitochondria: photoaffinity labelling of the regulatory site of energy dissipation." Eur J Biochem **82**(2): 515-521.

Henry, J. A., K. J. Jeffreys, et al. (1992). "Toxicity and deaths from 3,4-methylenedioxymethamphetamine ("ecstasy")." Lancet **340**(8816): 384-387.

Hesselink, M. K. and P. Schrauwen (2005). "Towards comprehension of the physiological role of UCP3." Horm Metab Res **37**(9): 550-554.

Hofmann, W. E., X. Liu, et al. (2001). "Effects of genetic background on thermoregulation and fatty acid-induced uncoupling of mitochondria in UCP1-deficient mice." The Journal of biological chemistry **276**(15): 12460-12465.

Hong, J., N. Li, et al. (2005). "Induction of CD4+CD25+ regulatory T cells by copolymer-I through activation of transcription factor Foxp3." Proc Natl Acad Sci U S A **102**(18): 6449-6454.

Honzik, T., Z. Drahota, et al. (2006). "Specific properties of heavy fraction of mitochondria from human-term placenta - glycerophosphate-dependent hydrogen peroxide production." Placenta **27**(4-5): 348-356.

Horvath, T. L., S. Diano, et al. (2003). "Uncoupling proteins-2 and 3 influence obesity and inflammation in transgenic mice." Int J Obes Relat Metab Disord **27**(4): 433-442.

Houstek, J., B. Cannon, et al. (1975). "Gylcerol-3-phosphate shuttle and its function in intermediary metabolism of hamster brown-adipose tissue." Eur J Biochem **54**(1): 11-18.

Howitz, K. T., K. J. Bitterman, et al. (2003). "Small molecule activators of sirtuins extend Saccharomyces cerevisiae lifespan." Nature **425**(6954): 191-196.

Hunter, D. R. and R. A. Haworth (1979). "The Ca2+-induced membrane transition in mitochondria. I. The protective mechanisms." Archives of biochemistry and biophysics **195**(2): 453-459.

Hurtaud, C., C. Gelly, et al. (2006). "Translation control of UCP2 synthesis by the upstream open reading frame." Cell Mol Life Sci **63**(15): 1780-1789.

Huseby, E. S., D. Liggitt, et al. (2001). "A pathogenic role for myelin-specific CD8(+) T cells in a model for multiple sclerosis." J Exp Med **194**(5): 669-676.

Ibrahim, S. M., E. Mix, et al. (2001). "Gene expression profiling of the nervous system in murine experimental autoimmune encephalomyelitis." Brain **124**(Pt 10): 1927-1938.

Idahl, L. A. and N. Lembert (1995). "Glycerol 3-phosphate-induced ATP production in intact mitochondria from pancreatic B-cells." The Biochemical journal **312 (Pt 1)**: 287-292.

Ivanov, II, G. E. Diehl, et al. (2006a). "Lymphoid tissue inducer cells in intestinal immunity." Curr Top Microbiol Immunol **308**: 59-82.

Ivanov, II, B. S. McKenzie, et al. (2006b). "The orphan nuclear receptor RORgammat directs the differentiation program of proinflammatory IL-17+ T helper cells." Cell **126**(6): 1121-1133.

Jaburek, M., M. Varecha, et al. (1999). "Transport function and regulation of mitochondrial uncoupling proteins 2 and 3." The Journal of biological chemistry **274**(37): 26003-26007.

Janeway, C. A., Jr., B. Jones, et al. (1988). "Specificity and function of T cells bearing gamma delta receptors." Immunol Today **9**(3): 73-76.

Janeway, C. A., Jr. and R. Medzhitov (2002). "Innate immune recognition." Annu Rev Immunol **20**: 197-216.

Jeffery, C. J. (2003). "Moonlighting proteins: old proteins learning new tricks." Trends Genet **19**(8): 415-417.

Jung, C. H. and W. W. Wells (1997). "Ascorbic acid is a stimulatory cofactor for mitochondrial glycerol-3-phosphate dehydrogenase." Biochem Biophys Res Commun **239**(2): 457-462.

Kawamoto, R. M. and A. H. Caswell (1986). "Autophosphorylation of glyceraldehydephosphate dehydrogenase and phosphorylation of protein from skeletal muscle microsomes." Biochemistry **25**(3): 657-661.

Keegan, B. M. and J. H. Noseworthy (2002). "Multiple sclerosis." Annu Rev Med **53**: 285-302.

Kelly, O. M., Y. M. McNamara, et al. (2011a). "The preservation of in vivo phosphorylated and activated uncoupling protein 3 (UCP3) in isolated skeletal muscle mitochondria following administration of 3,4-methylenedioxymethamphetamine (MDMA aka ecstasy) to rats/mice." Mitochondrion.

Kelly, O. M. and R. K. Porter (2011b). "Absence of mitochondrial uncoupling protein 3: effect on thymus and spleen in the fed and fasted mice." Biochimica et biophysica acta **1807**(9): 1064-1074.

Kizaki, T., K. Suzuki, et al. (2002). "Uncoupling protein 2 plays an important role in nitric oxide production of lipopolysaccharide-stimulated macrophages." Proc Natl Acad Sci U S A **99**(14): 9392-9397.

Klingenberg, M. (1970). "Localization of the glycerol-phosphate dehydrogenase in the outer phase of the mitochondrial inner membrane." Eur J Biochem **13**(2): 247-252.

Klingenberg, M. (1984). "Characteristics of the uncoupling protein from brown-fat mitochondria." Biochem Soc Trans **12**(3): 390-393.

Klingenberg, M. (1988). "Nucleotide binding to uncoupling protein. Mechanism of control by protonation." Biochemistry **27**(2): 781-791.

Klingenberg, M. and T. Buecher (1961). "[Glycerin-1-phosphate and flight muscle mitochondria.]." Biochem Z **334**: 1-17.

Klingenberg, M. and S. G. Huang (1999). "Structure and function of the uncoupling protein from brown adipose tissue." Biochimica et biophysica acta **1415**(2): 271-296.

Klingenberg, M. and E. Winkler (1985). "The reconstituted isolated uncoupling protein is a membrane potential driven H+ translocator." Embo J **4**(12): 3087-3092.

Korshunov, S. S., O. V. Korkina, et al. (1998). "Fatty acids as natural uncouplers preventing generation of O2.- and H2O2 by mitochondria in the resting state." FEBS Lett **435**(2-3): 215-218.

Kourie, J. I. (1998). "Interaction of reactive oxygen species with ion transport mechanisms." Am J Physiol **275**(1 Pt 1): C1-24.

Koza, R. A., S. M. Hohmann, et al. (2000). "Synergistic gene interactions control the induction of the mitochondrial uncoupling protein (Ucp1) gene in white fat tissue." The Journal of biological chemistry **275**(44): 34486-34492.

Koza, R. A., U. C. Kozak, et al. (1996). "Sequence and tissue-dependent RNA expression of mouse FAD-linked glycerol-3-phosphate dehydrogenase." Archives of biochemistry and biophysics **336**(1): 97-104.

Krauss, S., C. Y. Zhang, et al. (2002). "A significant portion of mitochondrial proton leak in intact thymocytes depends on expression of UCP2." Proc Natl Acad Sci U S A **99**(1): 118-122.

Krauss, S., C. Y. Zhang, et al. (2005). "The mitochondrial uncoupling-protein homologues." Nat Rev Mol Cell Biol **6**(3): 248-261.

Krauss, S., C. Y. Zhang, et al. (2003). "Superoxide-mediated activation of uncoupling protein 2 causes pancreatic beta cell dysfunction." J Clin Invest **112**(12): 1831-1842.

Kroenke, M. A., T. J. Carlson, et al. (2008). "IL-12- and IL-23-modulated T cells induce distinct types of EAE based on histology, CNS chemokine profile, and response to cytokine inhibition." J Exp Med **205**(7): 1535-1541.

Kumagai, H. and H. Sakai (1983). "A porcine brain protein (35 K protein) which bundles microtubules and its identification as glyceraldehyde 3-phosphate dehydrogenase." J Biochem **93**(5): 1259-1269.

Laemmli, U. K. (1970). "Cleavage of structural proteins during the assembly of the head of bacteriophage T4." Nature **227**(5259): 680-685.

Lafaille, J. J., F. V. Keere, et al. (1997). "Myelin basic protein-specific T helper 2 (Th2) cells cause experimental autoimmune encephalomyelitis in immunodeficient hosts rather than protect them from the disease." J Exp Med **186**(2): 307-312.

Lagouge, M., C. Argmann, et al. (2006). "Resveratrol improves mitochondrial function and protects against metabolic disease by activating SIRT1 and PGC-1alpha." Cell **127**(6): 1109-1122.

Laloi, M., M. Klein, et al. (1997). "A plant cold-induced uncoupling protein." Nature **389**(6647): 135-136.

Lalor, S. (2010). "T cells in experimental autoimmune encephalomyelitis." PhD Thesis **1**.

Lambert, A. J. and M. D. Brand (2004). "Superoxide production by NADH:ubiquinone oxidoreductase (complex I) depends on the pH gradient across the mitochondrial inner membrane." The Biochemical journal **382**(Pt 2): 511-517.

Lambert, A. J. and M. D. Brand (2009). "Reactive oxygen species production by mitochondria." Methods Mol Biol **554**: 165-181.

Lambeth, J. D. (2002). "Nox/Duox family of nicotinamide adenine dinucleotide (phosphate) oxidases." Curr Opin Hematol **9**(1): 11-17.

Landsberg, L., J. B. Young, et al. (2009). "Is obesity associated with lower body temperatures? Core temperature: a forgotten variable in energy balance." Metabolism **58**(6): 871-876.

Langrish, C. L., Y. Chen, et al. (2005). "IL-23 drives a pathogenic T cell population that induces autoimmune inflammation." J Exp Med **201**(2): 233-240.

Lanier, L. L. (2005). "NK cell recognition." Annu Rev Immunol **23**: 225-274.

Lardy, H. and E. Shrago (1990). "Biochemical aspects of obesity." Annu Rev Biochem **59**: 689-710.

Larrouy, D., P. Laharrague, et al. (1997). "Kupffer cells are a dominant site of uncoupling protein 2 expression in rat liver." Biochem Biophys Res Commun **235**(3): 760-764.

Ledesma, A., M. G. de Lacoba, et al. (2002). "Modeling the transmembrane arrangement of the uncoupling protein UCP1 and topological considerations of the nucleotide-binding site." J Bioenerg Biomembr **34**(6): 473-486.

Leiro, J., J. A. Arranz, et al. (2004). "In vitro effects of the polyphenols resveratrol, mangiferin and (-)-epigallocatechin-3-gallate on the scuticociliate fish pathogen Philasterides dicentrarchi." Dis Aquat Organ **59**(2): 171-174.

Liblau, R. S., S. M. Singer, et al. (1995). "Th1 and Th2 CD4+ T cells in the pathogenesis of organ-specific autoimmune diseases." Immunol Today **16**(1): 34-38.

Lin, S. J., P. A. Defossez, et al. (2000). "Requirement of NAD and SIR2 for life-span extension by calorie restriction in Saccharomyces cerevisiae." Science **289**(5487): 2126-2128.

Lin, S. J., M. Kaeberlein, et al. (2002). "Calorie restriction extends Saccharomyces cerevisiae lifespan by increasing respiration." Nature **418**(6895): 344-348.

Lin, W., S. L. Bailey, et al. (2007). "The integrated stress response prevents demyelination by protecting oligodendrocytes against immune-mediated damage." J Clin Invest **117**(2): 448-456.

Liu, H., R. Colavitti, et al. (2005). "Redox-dependent transcriptional regulation." Circulation research **97**(10): 967-974.

Lochner, M., L. Peduto, et al. (2008). "In vivo equilibrium of proinflammatory IL-17+ and regulatory IL-10+ Foxp3+ RORgamma t+ T cells." J Exp Med **205**(6): 1381-1393.

Lockhart, E., A. M. Green, et al. (2006). "IL-17 production is dominated by gammadelta T cells rather than CD4 T cells during Mycobacterium tuberculosis infection." J Immunol **177**(7): 4662-4669.

Lombardi, A., R. A. Busiello, et al. (2010). "UCP3 translocates lipid hydroperoxide and mediates lipid hydroperoxide-dependent mitochondrial uncoupling." The Journal of biological chemistry **285**(22): 16599-16605.

Lombardi, A., E. Silvestri, et al. (2002). "Skeletal muscle mitochondrial free-fatty-acid content and membrane potential sensitivity in different thyroid states: involvement of uncoupling protein-3 and adenine nucleotide translocase." FEBS Lett **532**(1-2): 12-16.

Los, M., W. Droge, et al. (1995). "Hydrogen peroxide as a potent activator of T lymphocyte functions." Eur J Immunol **25**(1): 159-165.

MacDonald, M. J. (1981). "High content of mitochondrial glycerol-3-phosphate dehydrogenase in pancreatic islets and its inhibition by diazoxide." The Journal of biological chemistry **256**(16): 8287-8290.

MacDonald, M. J., J. Tang, et al. (1996). "Low mitochondrial glycerol phosphate dehydrogenase and pyruvate carboxylase in pancreatic islets of Zucker diabetic fatty rats." Diabetes **45**(11): 1626-1630.

MacDonald, M. J., T. F. Warner, et al. (1990). "High activity of mitochondrial glycerol phosphate dehydrogenase in insulinomas and carcinoid and other tumors of the amine precursor uptake decarboxylation system." Cancer Res **50**(22): 7203-7205.

Mailloux, R. J., E. L. Seifert, et al. (2011). "Glutathionylation acts as a control switch for uncoupling proteins UCP2 and UCP3." The Journal of biological chemistry **286**(24): 21865-21875.

Mao, W., X. X. Yu, et al. (1999). "UCP4, a novel brain-specific mitochondrial protein that reduces membrane potential in mammalian cells." FEBS Lett **443**(3): 326-330.

Martin, W. and K. V. Kowallik (1999). "Annotated English translation of Mereschkowsky's 1905 paper." European Journal of Phycology **34**(03): 287-295.

Matthias, A., K. B. Ohlson, et al. (2000). "Thermogenic responses in brown fat cells are fully UCP1-dependent. UCP2 or UCP3 do not substitute for UCP1 in adrenergically or fatty scid-induced thermogenesis." The Journal of biological chemistry **275**(33): 25073-25081.

McCrady-Spitzer, S. K. and J. A. Levine (2012). "Nonexercise activity thermogenesis: a way forward to treat the worldwide obesity epidemic." Surg Obes Relat Dis **8**(5): 501-506.

McDonald, W. I. and T. A. Sears (1970). "Effect of a demyelinating lesion on conduction in the central nervous system studied in single nerve fibres." J Physiol **207**(2): 53P-54P.

McKeown, L. P., A. P. Porter-Armstrong, et al. (2003). "The needs and experiences of caregivers of individuals with multiple sclerosis: a systematic review." Clin Rehabil **17**(3): 234-248.

McLennan, H. R. and M. Degli Esposti (2000). "The contribution of mitochondrial respiratory complexes to the production of reactive oxygen species." J Bioenerg Biomembr **32**(2): 153-162.

Medzhitov, R. (2001). "Toll-like receptors and innate immunity." Nat Rev Immunol **1**(2): 135-145.

Meyer-Siegler, K., D. J. Mauro, et al. (1991). "A human nuclear uracil DNA glycosylase is the 37-kDa subunit of glyceraldehyde-3-phosphate dehydrogenase." Proc Natl Acad Sci U S A **88**(19): 8460-8464.

Mills, E. M., M. L. Banks, et al. (2003). "Pharmacology: uncoupling the agony from ecstasy." Nature **426**(6965): 403-404.

Mitchell, P. and J. Moyle (1967). "Chemiosmotic hypothesis of oxidative phosphorylation." Nature **213**(5072): 137-139.

Miwa, S. and M. D. Brand (2003). "Mitochondrial matrix reactive oxygen species production is very sensitive to mild uncoupling." Biochem Soc Trans **31**(Pt 6): 1300-1301.

Modlin, R. L. and P. A. Sieling (2005). "Immunology. Now presenting: gammadelta T cells." Science **309**(5732): 252-253.

Mori, S., N. Yoshizuka, et al. (2008). "Expression of uncoupling proteins in human skin and skin-derived cells." The Journal of investigative dermatology **128**(8): 1894-1900.

Mosmann, T. R., H. Cherwinski, et al. (1986). "Two types of murine helper T cell clone. I. Definition according to profiles of lymphokine activities and secreted proteins." J Immunol **136**(7): 2348-2357.

Mracek, T., P. Jesina, et al. (2005). "Time-course of hormonal induction of mitochondrial glycerophosphate dehydrogenase biogenesis in rat liver." Biochimica et biophysica acta **1726**(2): 217-223.

Mracek, T., A. Pecinova, et al. (2009). "High efficiency of ROS production by glycerophosphate dehydrogenase in mammalian mitochondria." Archives of biochemistry and biophysics **481**(1): 30-36.

Nedergaard, J. and B. Cannon (2003). "The 'novel' 'uncoupling' proteins UCP2 and UCP3: what do they really do? Pros and cons for suggested functions." Exp Physiol **88**(1): 65-84.

Negre-Salvayre, A., C. Hirtz, et al. (1997a). "A role for uncoupling protein-2 as a regulator of mitochondrial hydrogen peroxide generation." Faseb J **11**(10): 809-815.

Negre-Salvayre, A., C. Hirtz, et al. (1997b). "A role for uncoupling protein-2 as a regulator of mitochondrial hydrogen peroxide generation." FASEB journal : official publication of the Federation of American Societies for Experimental Biology **11**(10): 809-815.

Nicholls, D. G. (1974). "Hamster brown-adipose-tissue mitochondria. The control of respiration and the proton electrochemical potential gradient by possible physiological effectors of the proton conductance of the inner membrane." Eur J Biochem **49**(3): 573-583.

Nicholls, D. G. (2006). "The physiological regulation of uncoupling proteins." Biochimica et biophysica acta **1757**(5-6): 459-466.

Nicholls, D. G. and R. M. Locke (1984). "Thermogenic mechanisms in brown fat." Physiol Rev **64**(1): 1-64.

Nicholls, D. G. and E. Rial (1989). "Measurement of proton leakage across mitochondrial inner membranes and its relation to protonmotive force." Methods Enzymol **174**: 85-94.

O'Connor, R. A., C. T. Prendergast, et al. (2008). "Cutting edge: Th1 cells facilitate the entry of Th17 cells to the central nervous system during experimental autoimmune encephalomyelitis." J Immunol **181**(6): 3750-3754.

Oelkrug, R., M. Kutschke, et al. (2010). "Uncoupling protein 1 decreases superoxide production in brown adipose tissue mitochondria." The Journal of biological chemistry **285**(29): 21961-21968.

Okamoto, K. and J. M. Shaw (2005). "Mitochondrial morphology and dynamics in yeast and multicellular eukaryotes." Annu Rev Genet **39**: 503-536.

Panitch, H. S., R. L. Hirsch, et al. (1987). "Treatment of multiple sclerosis with gamma interferon: exacerbations associated with activation of the immune system." Neurology **37**(7): 1097-1102.

Papa, S. and V. P. Skulachev (1997). "Reactive oxygen species, mitochondria, apoptosis and aging." Mol Cell Biochem **174**(1-2): 305-319.

Pebay-Peyroula, E., C. Dahout-Gonzalez, et al. (2003). "Structure of mitochondrial ADP/ATP carrier in complex with carboxyatractyloside." Nature **426**(6962): 39-44.

Pecqueur, C., M. C. Alves-Guerra, et al. (2001). "Uncoupling protein 2, in vivo distribution, induction upon oxidative stress, and evidence for translational regulation." The Journal of biological chemistry **276**(12): 8705-8712.

Pecqueur, C., T. Bui, et al. (2008). "Uncoupling protein-2 controls proliferation by promoting fatty acid oxidation and limiting glycolysis-derived pyruvate utilization." FASEB journal : official publication of the Federation of American Societies for Experimental Biology **22**(1): 9-18.

Picard, F., M. Kurtev, et al. (2004). "Sirt1 promotes fat mobilization in white adipocytes by repressing PPAR-gamma." Nature **429**(6993): 771-776.

Plecita-Hlavata, L., M. Lessard, et al. (2008). "Mitochondrial oxidative phosphorylation and energetic status are reflected by morphology of mitochondrial network in INS-1E and HEP-G2 cells viewed by 4Pi microscopy." Biochimica et biophysica acta **1777**(7-8): 834-846.

Porter, R. K. and J. F. Andrews (1998). "Effects of leptin on mitochondrial 'proton leak' and uncoupling proteins: implications for mammalian energy metabolism." Proc Nutr Soc **57**(3): 455-460.

Puigserver, P. (2005). "Tissue-specific regulation of metabolic pathways through the transcriptional coactivator PGC1-alpha." Int J Obes (Lond) **29 Suppl 1**: S5-9.

Pulendran, B. and R. Ahmed (2006). "Translating innate immunity into immunological memory: implications for vaccine development." Cell **124**(4): 849-863.

Quinlan, C. L., A. L. Orr, et al. (2012). "Mitochondrial complex II can generate reactive oxygen species at high rates in both the forward and reverse reactions." The Journal of biological chemistry **287**(32): 27255-27264.

Rajan, A. J., Y. L. Gao, et al. (1996). "A pathogenic role for gamma delta T cells in relapsing-remitting experimental allergic encephalomyelitis in the SJL mouse." J Immunol **157**(2): 941-949.

Rajan, A. J., J. D. Klein, et al. (1998). "The effect of gammadelta T cell depletion on cytokine gene expression in experimental allergic encephalomyelitis." J Immunol **160**(12): 5955-5962.

Ravussin, E., S. Lillioja, et al. (1988). "Reduced rate of energy expenditure as a risk factor for body-weight gain." N Engl J Med **318**(8): 467-472.

Renaud, S. and M. de Lorgeril (1992). "Wine, alcohol, platelets, and the French paradox for coronary heart disease." Lancet **339**(8808): 1523-1526.

Rhee, S. G., S. W. Kang, et al. (2005). "Intracellular messenger function of hydrogen peroxide and its regulation by peroxiredoxins." Curr Opin Cell Biol **17**(2): 183-189.

Ricquier, D., F. Bouillaud, et al. (1986). "Expression of uncoupling protein mRNA in thermogenic or weakly thermogenic brown adipose tissue. Evidence for a rapid beta-adrenoreceptor-mediated and transcriptionally regulated step during activation of thermogenesis." The Journal of biological chemistry **261**(30): 13905-13910.

Ritter (1992). structure and development in: the thymus, IRL press and oxford university press.

Robbins, A. R., R. D. Ward, et al. (1995). "A mutation in glyceraldehyde 3-phosphate dehydrogenase alters endocytosis in CHO cells." J Cell Biol **130**(5): 1093-1104.

Robinson, A. J., C. Overy, et al. (2008). "The mechanism of transport by mitochondrial carriers based on analysis of symmetry." Proc Natl Acad Sci U S A **105**(46): 17766-17771.

Rodgers, J. T., C. Lerin, et al. (2005). "Nutrient control of glucose homeostasis through a complex of PGC-1alpha and SIRT1." Nature **434**(7029): 113-118.

Rogina, B. and S. L. Helfand (2004). "Sir2 mediates longevity in the fly through a pathway related to calorie restriction." Proc Natl Acad Sci U S A **101**(45): 15998-16003.

Rolfe, D. F., A. J. Hulbert, et al. (1994). "Characteristics of mitochondrial proton leak and control of oxidative phosphorylation in the major oxygen-consuming tissues of the rat." Biochimica et biophysica acta **1188**(3): 405-416.

Rolfe, D. F., J. M. Newman, et al. (1999). "Contribution of mitochondrial proton leak to respiration rate in working skeletal muscle and liver and to SMR." Am J Physiol **276**(3 Pt 1): C692-699.

Roth, S. and W. Droge (1987). "Regulation of T-cell activation and T-cell growth factor (TCGF) production by hydrogen peroxide." Cell Immunol **108**(2): 417-424.

Rousset, S., M. C. Alves-Guerra, et al. (2004). "The biology of mitochondrial uncoupling proteins." Diabetes **53 Suppl 1**: S130-135.

Rousset, S., Y. Emre, et al. (2006). "The uncoupling protein 2 modulates the cytokine balance in innate immunity." Cytokine **35**(3-4): 135-142.

Rousset, S., J. Mozo, et al. (2007). "UCP2 is a mitochondrial transporter with an unusual very short half-life." FEBS Lett **581**(3): 479-482.

Rutter, G. A., W. F. Pralong, et al. (1992). "Regulation of mitochondrial glycerol-phosphate dehydrogenase by Ca2+ within electropermeabilized insulin-secreting cells (INS-1)." Biochimica et biophysica acta **1175**(1): 107-113.

Saikumar, P., Z. Dong, et al. (1999). "Apoptosis: definition, mechanisms, and relevance to disease." Am J Med **107**(5): 489-506.

Samec, S., J. Seydoux, et al. (1998). "Role of UCP homologues in skeletal muscles and brown adipose tissue: mediators of thermogenesis or regulators of lipids as fuel substrate?" Faseb J **12**(9): 715-724.

Sanchis, D., C. Fleury, et al. (1998). "BMCP1, a novel mitochondrial carrier with high expression in the central nervous system of humans and rodents, and respiration uncoupling activity in recombinant yeast." The Journal of biological chemistry **273**(51): 34611-34615.

Scarpace, P. J., B. S. Bender, et al. (1991). "Escherichia coli peritonitis activates thermogenesis in brown adipose tissue: relationship to fever." Can J Physiol Pharmacol **69**(6): 761-766.

Scholz, T. D., S. L. Koppenhafer, et al. (1997). "Developmental regulation of the alpha-glycerophosphate shuttle in porcine myocardium." J Mol Cell Cardiol **29**(6): 1605-1613.

Schuh, R. A., K. C. Jackson, et al. (2012). "Measuring mitochondrial respiration in intact single muscle fibers." Am J Physiol Regul Integr Comp Physiol **302**(6): R712-719.

Shabalina, I. G., J. Hoeks, et al. (2010). "Cold tolerance of UCP1-ablated mice: a skeletal muscle mitochondria switch toward lipid oxidation with marked UCP3 up-regulation not associated with increased basal, fatty acid- or ROS-induced uncoupling or enhanced GDP effects." Biochimica et biophysica acta **1797**(6-7): 968-980.

Shabalina, I. G., A. Jacobsson, et al. (2004). "Native UCP1 displays simple competitive kinetics between the regulators purine nucleotides and fatty acids." The Journal of biological chemistry **279**(37): 38236-38248.

Shabalina, I. G. and J. Nedergaard (2011). "Mitochondrial ('mild') uncoupling and ROS production: physiologically relevant or not?" Biochem Soc Trans **39**(5): 1305-1309.

Shabalina, I. G., N. Petrovic, et al. (2006). "UCP1 and defense against oxidative stress. 4-Hydroxy-2-nonenal effects on brown fat mitochondria are uncoupling protein 1-independent." The Journal of biological chemistry **281**(20): 13882-13893.

Shakibaei, M., K. B. Harikumar, et al. (2009). "Resveratrol addiction: to die or not to die." Mol Nutr Food Res **53**(1): 115-128.

Shibata, K., H. Yamada, et al. (2007). "Resident Vdelta1+ gammadelta T cells control early infiltration of neutrophils after Escherichia coli infection via IL-17 production." J Immunol **178**(7): 4466-4472.

Shin, H. C., N. Benbernou, et al. (1999). "Expression of IL-17 in human memory CD45RO+ T lymphocytes and its regulation by protein kinase A pathway." Cytokine **11**(4): 257-266.

Sinclair, D. A. (2005). "Toward a unified theory of caloric restriction and longevity regulation." Mech Ageing Dev **126**(9): 987-1002.

Singh, R. and M. R. Green (1993). "Sequence-specific binding of transfer RNA by glyceraldehyde-3-phosphate dehydrogenase." Science **259**(5093): 365-368.

Skulachev, V. P. (1996). "Role of uncoupled and non-coupled oxidations in maintenance of safely low levels of oxygen and its one-electron reductants." Q Rev Biophys **29**(2): 169-202.

Skulachev, V. P. (1998). "Uncoupling: new approaches to an old problem of bioenergetics." Biochimica et biophysica acta **1363**(2): 100-124.

Slater, A. F., C. Stefan, et al. (1995). "Signalling mechanisms and oxidative stress in apoptosis." Toxicol Lett **82-83**: 149-153.

Smith, P. K., R. I. Krohn, et al. (1985). "Measurement of protein using bicinchoninic acid." Anal Biochem **150**(1): 76-85.

Soos, J. M., O. Stuve, et al. (2002). "Cutting edge: oral type I IFN-tau promotes a Th2 bias and enhances suppression of autoimmune encephalomyelitis by oral glatiramer acetate." J Immunol **169**(5): 2231-2235.

Sospedra, M. and R. Martin (2005). "Immunology of multiple sclerosis." Annu Rev Immunol **23**: 683-747.

Speakman, J. R. and S. E. Mitchell (2011). "Caloric restriction." Mol Aspects Med **32**(3): 159-221.

Sprague, J. E., X. Yang, et al. (2007). "Roles of norepinephrine, free Fatty acids, thyroid status, and skeletal muscle uncoupling protein 3 expression in sympathomimetic-induced thermogenesis." J Pharmacol Exp Ther **320**(1): 274-280.

Sriram, G., J. A. Martinez, et al. (2005). "Single-gene disorders: what role could moonlighting enzymes play?" Am J Hum Genet **76**(6): 911-924.

Starkov, A. A., G. Fiskum, et al. (2004). "Mitochondrial alpha-ketoglutarate dehydrogenase complex generates reactive oxygen species." J Neurosci **24**(36): 7779-7788.

Stock, D., C. Gibbons, et al. (2000). "The rotary mechanism of ATP synthase." Curr Opin Struct Biol **10**(6): 672-679.

Stromnes, I. M., L. M. Cerretti, et al. (2008). "Differential regulation of central nervous system autoimmunity by T(H)1 and T(H)17 cells." Nat Med **14**(3): 337-342.

Stuart, J. A., J. A. Harper, et al. (2001). "A mitochondrial uncoupling artifact can be caused by expression of uncoupling protein 1 in yeast." The Biochemical journal **356**(Pt 3): 779-789.

Suzuki, J., M. Gao, et al. (1997). "Chronic cold exposure stimulates microvascular remodeling preferentially in oxidative muscles in rats." Jpn J Physiol **47**(6): 513-520.

Tainter, M., A. Stockton, et al. (1933). "Use of dinitrophenol in obesity and related conditions: A progress report." JAMA: The Journal of the American Medical Association **101**(19): 1472-1475.

Tisdale, E. J. (2001). "Glyceraldehyde-3-phosphate dehydrogenase is required for vesicular transport in the early secretory pathway." The Journal of biological chemistry **276**(4): 2480-2486.

Trenker, M., R. Malli, et al. (2007). "Uncoupling proteins 2 and 3 are fundamental for mitochondrial Ca2+ uniport." Nat Cell Biol **9**(4): 445-452.

Tretter, L., K. Takacs, et al. (2007). "Stimulation of H(2)O(2) generation by calcium in brain mitochondria respiring on alpha-glycerophosphate." J Neurosci Res **85**(15): 3471-3479.

Umemura, M., A. Yahagi, et al. (2007). "IL-17-mediated regulation of innate and acquired immune response against pulmonary Mycobacterium bovis bacille Calmette-Guerin infection." J Immunol **178**(6): 3786-3796.

Valenzano, D. R., E. Terzibasi, et al. (2006). "Resveratrol prolongs lifespan and retards the onset of age-related markers in a short-lived vertebrate." Curr Biol **16**(3): 296-300.

Vidal-Puig, A. J., D. Grujic, et al. (2000). "Energy metabolism in uncoupling protein 3 gene knockout mice." The Journal of biological chemistry **275**(21): 16258-16266.

Vogler, S., R. Goedde, et al. (2005). "Association of a common polymorphism in the promoter of UCP2 with susceptibility to multiple sclerosis." J Mol Med (Berl) **83**(10): 806-811.

Vogler, S., J. Pahnke, et al. (2006). "Uncoupling protein 2 has protective function during experimental autoimmune encephalomyelitis." Am J Pathol **168**(5): 1570-1575.

Weber, M. S., R. Hohlfeld, et al. (2007). "Mechanism of action of glatiramer acetate in treatment of multiple sclerosis." Neurotherapeutics **4**(4): 647-653.

Weiss, H. A., J. M. Millward, et al. (2007). "CD8+ T cells in inflammatory demyelinating disease." J Neuroimmunol **191**(1-2): 79-85.

Willenborg, D. O., S. Fordham, et al. (1996). "IFN-gamma plays a critical down-regulatory role in the induction and effector phase of myelin oligodendrocyte glycoprotein-induced autoimmune encephalomyelitis." J Immunol **157**(8): 3223-3227.

Willenborg, D. O., S. A. Fordham, et al. (1999). "IFN-gamma is critical to the control of murine autoimmune encephalomyelitis and regulates both in the periphery and in the target tissue: a possible role for nitric oxide." J Immunol **163**(10): 5278-5286.

Winkler, E. and M. Klingenberg (1994). "Effect of fatty acids on H+ transport activity of the reconstituted uncoupling protein." The Journal of biological chemistry **269**(4): 2508-2515.

Wood, J. G., B. Rogina, et al. (2004). "Sirtuin activators mimic caloric restriction and delay ageing in metazoans." Nature **430**(7000): 686-689.

Wucherpfennig, K. W., J. Newcombe, et al. (1992). "Gamma delta T-cell receptor repertoire in acute multiple sclerosis lesions." Proc Natl Acad Sci U S A **89**(10): 4588-4592.

Youssef, S., O. Stuve, et al. (2002). "The HMG-CoA reductase inhibitor, atorvastatin, promotes a Th2 bias and reverses paralysis in central nervous system autoimmune disease." Nature **420**(6911): 78-84.

Zamvil, S. S. and L. Steinman (1990). "The T lymphocyte in experimental allergic encephalomyelitis." Annu Rev Immunol **8**: 579-621.

Zhou, M., B. Z. Lin, et al. (2000). "UCP-3 expression in skeletal muscle: effects of exercise, hypoxia, and AMP-activated protein kinase." Am J Physiol Endocrinol Metab **279**(3): E622-629.

Hooke Laboratories, protocol for induction of EAE with different MOG/CFA kits.

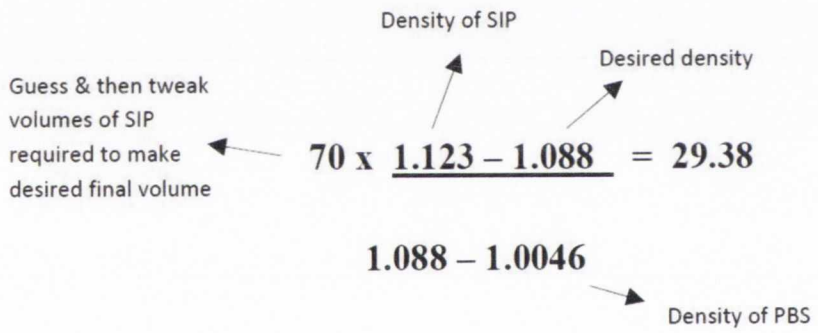
http://hookelabs.com/protocols/eaeAI_C57BL6/eaeAI_C57BL6.html

Appendix

A. Appendix

Stock Isotonic Percoll

Percoll is made isotonic by diluting 9:1 with 10X PBS (Sigma). The different density gradients can be calculated using the equations described in the Percoll Manual (Sigma website). Briefly, for 1.088 g/ml: if you require ~100 ml,



Therefore, 70 ml SIP + 29.38 ml 1X PBS = 99.38 ml 1.088 g/ml Percoll.

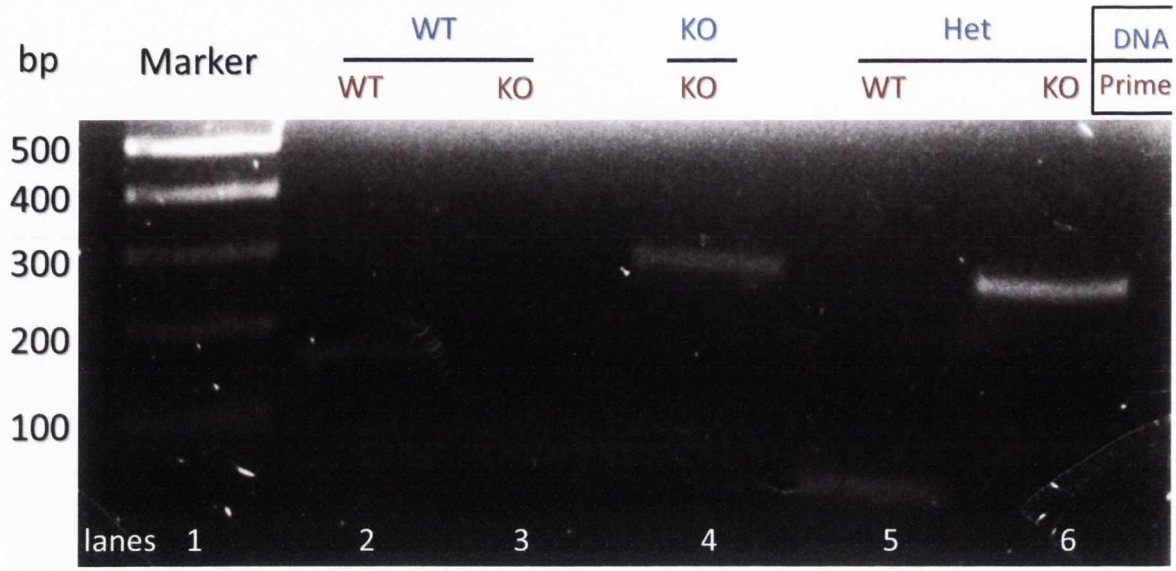


Figure A-1: UCP2 genotyping PCR agarose gel

Genotyping PCR with DNA isolated from earpunches of alleged UCP2+/+ (WT), UCP2-/- (KO) and UCP2+/- (Het) mice (proposed genotype of DNA on top). PCR reactions were performed with primers for WT or KO allele detection (primers used for PCR reactions on bottom). PCR product size indicated WT (156bp) or KO (280bp) as assessed with marker (100bp DNA ladder, Invitrogen).

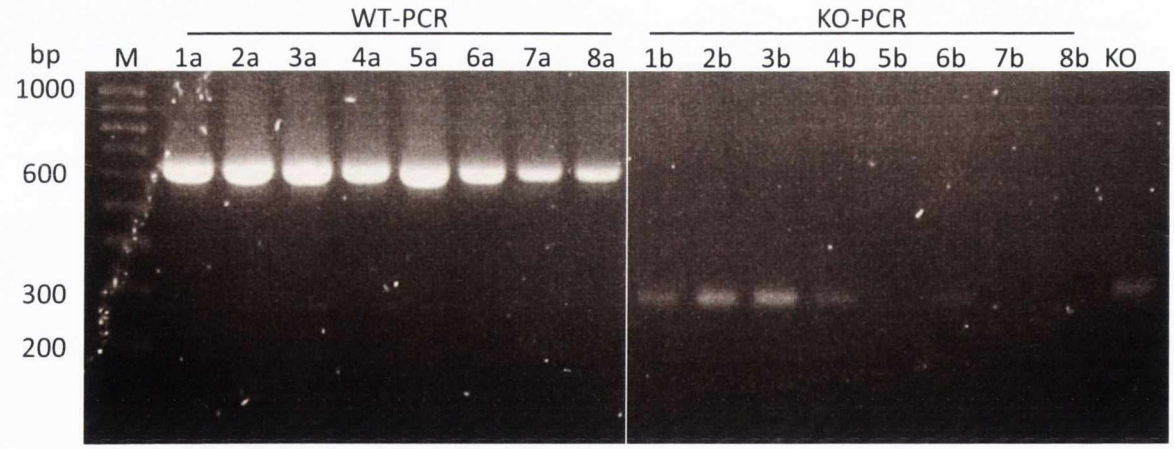


Figure A-2: UCP3 genotyping PCR agarose gel

Genotyping PCR with DNA isolated from earpunches of litters (individuals 1-8) of a UCP3+/+ and UCP3+/- breeding pair. Individual PCR reactions were performed with primers for WT (WT-PCR, 1-8a) or KO (KO-PCR, 1-8b) allele detection. PCR product size indicated WT (600bp) or KO (300bp) as assessed with marker (100bp DNA ladder, Invitrogen)

Table A-1: Seahorse XF24-3 program intact muscle fibers

Command	time (min)	port	repeat
Calibrate			
Mixing	3		
Waiting	2		8x
Mixing	3		
Waiting	2		
Measuring	5		3x
Injecting		A	
Mixing	3		
Waiting	2		
Measuring	5		3x
Injecting		B	
Mixing	3		
Waiting	2		
Measuring	5		3x
Injecting		C	
Mixing	3		
Waiting	2		
Measuring	5		3x
Injecting		D	
Mixing	3		
Waiting	2		
Measuring	5		3x

Table A-2: T-cell frequencies in UCP knock-out mice

Single and double positive and double negative CD4 and CD8 lymphocyte subsets (in % of total lymphocytes) in spleen, thymus and ILN of WT and UCP-KO mice (UCP1-/-, UCP2-/- and UCP3-/- respectively). Data presented as means ± SEM of three separate experiments performed at least in triplicate.

		$CD4^+$		$CD8^+$		$CD4^+ CD8^+$		$CD4^- CD8^-$	
		WT	UCP-/-	WT	UCP-/-	WT	UCP-/-	WT	UCP-/-
UCP1	spleen	21.1 ± 0.7	23.2 ± 0.6	1.5 ± 0.1	1.8 ± 0.1	9.2 ± 0.0	13.1 ± 0.5	61.1 ± 0.6	54.8 ± 0.9
	thymus	14.1 ± 0.4	29.8 ± 9.3	1.1 ± 0.1	1.3 ± 0.1	81.1 ± 1.1	60.6 ± 5.3	1.91 ± 0.4	5.84 ± 1.5
UCP2	spleen	13.6 ± 3.1	14.4 ± 4.9	11.5 ± 2.5	11.4 ± 2.0	0.2 ± 0.1	0.2 ± 0.0	74.8 ± 5.6	74.0 ± 6.8
	thymus	7.9 ± 1.0	9.3 ± 1.1	3.4 ± 0.6	3.2 ± 0.6	86.9 ± 1.6	86.3 ± 1.5	1.8± 0.2	1.2 ± 0.2
	ILN	36.3 ± 1.4	42.8 ± 1.6	40.2 ± 1.3	35.3 ± 2.1	0.5 ± 0.1	1.7 ± 1.2	23.0 ± 2.5	20.2 ± 4.3
UCP3	spleen	20.6 ± 1.6	24.2 ± 0.7	7.7 ± 0.4	10.9 ± 0.3	0.1 ± 0.0	0.1 ± 0.0	71.6 ± 1.2	64.7 ± 0.4
	thymus	7.7 ± 0.1	9.4 ± 0.3	3.0 ± 0.3	3.9 ± 0.2	88.0 ± 0.3	86 ± 0.4	1.2 ± 0.0	0.7 ± 0.1

Table A-3: Apoptotic potential in UCP2 knock-out mice

Means ± SEM of frequencies (in % of total lymphocytes) of early and late apoptotic, necrotic and viable cells in WT and UCP2-/- spleen and thymus following treatment with staurosporin (induced) or vehicle alone (spontaneous) over night at 37°C.

			early apoptotic	late apoptotic	necrotic	viable
spontaneous	Spleen	WT	8.21 ± 1.09	22.59 ± 3.47	0.33 ± 0.13	68.87 ± 4.03
		UCP2-/-	7.76 ± 0.54	14.91 ± 1.32	0.55 ± 0.19	76.87 ± 1.55
	Thymus	WT	12.66 ± 0.96	12.43 ± 1.84	1.40 ± 0.32	73.50 ± 2.99
		UCP2-/-	12.15 ± 0.74	11.62 ± 1.39	1.51 ± 0.22	74.97 ± 2.23
induced	Spleen	WT	8.04 ± 0.79	37.52 ± 6.34	0.79 ± 0.20	53.50 ± 6.37
		UCP2-/-	13.04 ± 0.85	24.51 ± 3.35	0.26 ± 0.10	62.08 ± 3.75
	Thymus	WT	26.52 ± 3.30	34.39 ± 7.58	3.93 ± 1.50	35.16 ± 11.35
		UCP2-/-	22.41 ± 4.54	25.45 ± 5.77	13.79 ± 4.15	40.59 ± 8.60

Table A-4: T-cells in EAE

Overview of frequencies of CD4, CD8 and γδ single positive T-cells in spleen, ILN and brain of WT compared to UCP2-/- mice in EAE

	$CD4^+$		$CD8^+$		$\gamma\delta^+$	
	WT	UCP2-/-	WT	UCP2-/-	WT	UCP2-/-
spleen	40.9 ± 1.5	44.4 ± 1.4	21.1 ± 2.3	21.7 ± 3.0	3.4 ± 0.6	4.2 ± 0.6
ILN	51.4 ± 1.2	53.0 ± 2.4	34.8 ± 2.9	26.7 ± 3.3	2.6 ± 0.3	5.6 ± 2.7
brain	20.2 ± 3.6	29.5 ± 6.0	20.3 ± 6.3	8.8 ± 3.0	4.1 ± 1.0	6.1 ± 1.4

Table A-5: IL-17 positive T-cells in EAE

Overview of frequencies (%) of IL-17 positive $CD4^+$, $CD8^+$ and $\gamma\delta^+$ T-cells in spleen, ILN and brain of WT and UCP2-/- mice in EAE.

	$CD4^+$ IL-17$^+$		$CD8^+$ IL-17$^+$		$\gamma\delta^+$ IL-17$^+$	
	WT	UCP2-/-	WT	UCP2-/-	WT	UCP2-/-
spleen	3.1 ± 0.4	2.9 ± 0.5	1.8 ± 0.2	2.2 ± 0.3	29.4 ± 5.8	30.9 ± 5.2
ILN	2.0 ± 0.2	2.8 ± 0.8	1.2 ± 0.2	1.0 ± 0.3	36.3 ± 7.0	33.4 ± 5.9
brain	13.1 ± 3.1	11.1 ± 2.6	10.0 ± 2.8	9.9 ± 3.3	18.8 ± 4.7	13.2 ± 2.6

Table A-6: IFNγ positive T-cells in EAE

Overview of frequencies of IFNγ positive CD4, CD8 and γδ positive T-cells in spleen, ILN and brain of WT compared to UCP2-/- mice in EAE

	$CD4^+$ IFNγ^+		$CD8^+$ IFNγ^+		$\gamma\delta^+$ IFNγ^+	
	WT	UCP2-/-	WT	UCP2-/-	WT	UCP2-/-
spleen	14.2 ± 6.3	6.2 ± 1.6	20.5 ± 5.8	9.8 ± 2.4	10.0 ± 3.3	5.0 ± 1.7
ILN	1.3 ± 0.1	2.2 ± 0.9	8.8 ± 0.9	7.6 ± 1.5	4.2 ± 1.0	3.0 ± 0.7
brain	18.2 ± 3.7	18.0 ± 3.3	45.5 ± 9.4	38.9 ± 9.0	5.6 ± 1.5	4.7 ± 1.5

Table A-7: Oxygen consumption rates in WT and UCP2 knock-out mice

Oxygen consumption rates ($nmolO_2*min^{-1}*mg$ mitochondrial $protein^{-1}$) of WT and UCP2-/- liver and kidney mitochondria in the presence of 0.1% BSA, Rotenone, Atractyloside and Oligomycin. Mitochondrial oxygen consumption rates were measured in State 4 respiring on succinate or G3P (with 0.5mM $CaCl_2$ present) and following treatment with GDP, palmitate and FCCP. All data are presented as mean ± SEM of at least three independent experiments in triplicate. P values ≤ 0.05 on unpaired student's t-test were deemed significant (*P ≤ 0.05 and **P ≤ 0.01). Statistics were done comparing genotpyes.

Substrate	Tissue	Geno-type	State 4	GDP	Palmitate	FCCP
Succinate	Liver	WT	37.92 ± 2.34	37.87 ± 2.38	39.60 ± 4.30	157.37 ± 15.40
		KO	38.01 ± 3.80	38.30 ± 4.40	38.94 ± 5.24	113.34 ± 9.07
	Kidney	WT	60.92 ± 4.80	56.67 ± 4.68	65.33 ± 9.00	160.75 ± 15.18
		KO	66.36 ± 9.54	63.44 ± 9.38	69.81 ± 7.80	151.62 ± 18.61
G3P	Liver	WT	4.99 ± 1.19	4.82 ± 1.31	5.14 ± 0.98	5.13 ± 0.99
		KO	12.76 ± 3.52	12.86 ± 3.44	14.83 ± 4.24	15.73 ± 4.44
	Kidney	WT	6.91 ± 2.14	6.70 ± 2.24	6.72 ± 1.78	6.65 ± 1.64
		KO	17.16 ± 4.19	17.27 ± 4.19	19.57 ± 4.81	20.61 ± 4.50